Caractérisation des rôles de l'Anilline durant la cytokinèse

Amel Kechad

Département de Pathologie et Biologie Cellulaire

Faculté de Médecine

Thèse présentée à la Faculté des études supérieures

en vue de l'obtention du grade de

Doctorat en Pathologie et Biologie Cellulaire

23 Avril 2018

Université de Montréal

Faculté de Médecine

Cette thèse intitulée :

Caractérisation des rôles de l'Anilline durant la cytokinèse

Présentée

Par

Amel Kechad

Sera évaluée par un jury composé des personnes suivantes

Dr Gilles Hickson, directeur de recherche

Dr Gregory Emery, président-rapporteur

Dr Jean-Claude Labbé, membre du jury

Dre Sabine Elowe, éxaminatrice externe

RÉSUMÉ

La cytokinèse est un processus conservé par lequel une cellule se sépare physiquement en deux. Le fuseau mitotique fournit les signaux au niveau du cortex afin de positionner le sillon de clivage. Ensuite, un anneau contractile riche en acto-myosine (AC) est assemblé et va permettre la fermeture de la cellule à son équateur. Au fur et à mesure que l'AC se contracte, la zone médiane du fuseau mitotique va se compacter pour former le midbody (MB) et un anneau du midbody (AM) se forme pour stabiliser le pont intercellulaire jusqu'à l'abscission. Des défauts à l'une de ces étapes peuvent provoquer un échec de la cytokinèse et générer des cellules tétraploïdes binucléées, souvent observées dans des conditions pathologiques telles que le cancer. Des criblages génétiques et biochimiques ont identifié les protéines clés conservées qui constituent la machineriede la cytokinèse, cependant, on ignore comment la fermeture de l'AC est couplée à la formation du midbody et de l'AM; ni comment l'ancrage de la membrane plasmique est maintenu durant ces événements de transition clés. L'Anilline est une composante essentielle de cette machinerie qui échaffaude de nombreuses protéines telles que l'actine, la myosine et les septines, mais **on ignore comment l'Anilline agit avec ses nombreux partenaires dans le temps et l'espace pour guider la cytocinèse.**

Afin d'adresser ces questions, nous avons effectué une analyse de structure/fonction de l'Anilline par microscopie en temps réel de cellules S2 de *Drosophila.* L'Anilline se localise à l'AC et l'AM et sa déplétion n'affecte pas l'assemblage de l'AC, mais bloque plutôt la cytokinèse à un stade plus tardif. Nous avons trouvé que l'Anilline est nécessaire pour la stabilité de l'AC et la formation de l'AM. L'analyse de mutants tronqués a révélé que l'extrémité N-terminale de l'Anilline se lie à l'AC et supporte la formation de structures stables semblables à l'AM, mais celles-ci ne pouvaient pas maintenir l'ancrage de la membrane plasmique. Inversement, l'extrémité C-terminale ne localise ni à l'AC ni à l'AM, mais recrute la septine Peanut à des structures ectopiques au niveau du cortex équatorial et régit l'ancrage de l'AM à la membrane plasmique.

Ensuite, nous avons entrepris de caractériser cette transition plus en profondeur et nous montrons que la transition de l'AM à l'AC passe par un processus de maturation non caractérisé auparavant, qui nécessite des mécanismes opposés de rétention vs élimination de

l'Anilline à l'équateur. La kinase Citron/Sticky agit sur l'extrémité N-terminale de l'Anilline pour la retenir à l'AM mature, alors que les septines agissent sur l'extrémité C-terminale de l'Anilline pour éliminer localement l'excès de membrane de l'AM naissant par internalisation, extrusion et excrétion de la membrane plasmique et des protéines qui y sont associées.

Finalement, notre analyse structure/fonction de l'Anilline a également révélé son rôle durant la maturation du MB via son extrémité C-terminale qui régit le recrutement des septines et se lie à Tumbleweed / RacGAP50C (Tum). Tum est une protéine activatrice de la GTPase (GAP) requise au début de la cytocinèse pour la formation du fuseau central et l'initiation du sillon, puis pour l'ancrage du MB à la membrane plasmique. Cependant, il n'y a pas de consensus sur le rôle de son activité GAP et aucune fonction connue pour son interaction avec l'Anilline. Notre étude de structure/fonction par microscopie en temps réel de Tum a révélé que l'activité GAP de Tum et son domaine central sont requis pour la formation et la fermeture de l'AC. De plus, nous montrons que sa région de liaison à l'Anilline contribue au recrutement cortical de Tum et à la maturation MB / MR d'une manière dépendante de l'Anilline. Enfin, nous dévoilons une interaction génétique entre Tum et l'Anilline qui intervient dans l'initiation du sillon. Ces résultats suggèrent que l'interaction entre l'Anilline et Tum relie la transition de l'AC en AM à la maturation du fuseau central en MB tout au long de la cytokinèse.

Ensemble, les résultats présentés dans cette thèse montrent qu'à travers ses multiples interactions l'Anilline est une protéine clé impliquée tout au long de la cytokinèse de l'initiation du sillon à la formation de l'AC, sa stabilisation et sa maturation en AM ainsi que son ancrage à la memebrane plasmique.

Mots clés: Anilline, cytokinèse, Anneau contractile, Anneau du midbody, Midbody, Tum, Tumbleweed/ RacGAP50C, septines, Peanut, Citron Kinase, Sticky, pont intercellulaire.

ABSTRACT

Cytokinesis is a multi-step conserved process by which a cell physically separates into two. First, signalling between the mitotic spindle and the cortex provides cues to position the cleavage furrow. Then, an acto-myosin contractile ring (CR) is assembled and will constrict the cell at its equator. As the CR constricts the mitotic spindle's midzone will mature to form the midbody (MB) and a stable midbody ring (MR) forms to stabilize the intercellular bridge until abscission**.** Defects at any of these steps can cause cytokinesis failure and generate binucleate polyploid cells, often observed in pathological conditions such as cancer. Genetic and biochemical screens have identified the key, conserved proteins that constitute the cytokinetic machinery, however, it remains unclear how CR closure is coupled to MB and MR formation and how plasma membrane anchoring is maintained at this key transition events. Anillin is a core and essential component that scaffolds many other cytokinesis proteins such as actin, myosin and septins, but **it remains unclear how Anillin acts with its numerous partners in time and space to guide progress through cytokinesis.**

To address these questions we performed a structure- function analysis of Anillin by time**-**lapse microscopy in Drosophila S2 cells. Anillin localizes to the CR and the MR and its depletion does not affect CR assembly, but rather blocks cytokinesis at a mid**-**late furrowing stage. We have found that Anillin is required for the stability of the CR, formation of the MR and the maturation of the MB. Truncation analysis revealed that Anillin N-terminus connected with the actomyosin CR and supported formation of stable MR-like structures, but these could not maintain anchoring of the plasma membrane. Conversely, Anillin C-terminus failed to connect with the CR or MR but recruited the septin Peanut to the equatorial cortex and together mediated anchorage of the MR to the membrane.

Next, we further characterized this CR to MR transition and show that it proceeds via a previously uncharacterized maturation process that requires opposing mechanisms of removal and retention of Anillin at the equator. The Citron kinase Sticky acts on the N-terminus of Anillin to retain it at the mature MR, whereas the septin cytoskeleton acts on the C-terminus of Anillin to locally trim away excess membrane from the nascent MR via internalization,extrusion, and shedding of the plasma membrane and associated proteins.

Our structure function analysis of Anillin also revealed a requirement for Anillin in MB maturation via its C-terminus that mediates the recruitment of septins and binds to the microtubule associated protein Tumbleweed/RacGAP50C (Tum). Tum is a GTPase activating protein (GAP) required early during cytokinesis for central spindle formation and furrow initiation and later for anchorage of the MB to the plasma membrane. However, there is no consensus on the role of its GAP activity and no known functions for its interaction with Anillin. Our structure function study by real-time microscopy of Tum revealed that the GAP activity of Tum and its central domain are required for CR formation and closure. Furthermore, we found that the putative Anillin binding region of Tum contributes to Tum cortical recruitment and MB/MR maturation later during cytokinesis in an Anillin-dependant manner. Finally, we unveil a genetic interaction between Tum and Anillin that mediates furrow initiation. These results suggest that the interaction between Anillin and Tum links the CR\MR to the spindle/MB throughout cytokinesis.

Together, the results presented in this thesis show that through its multiple interactions Anillin is a key protein involved throughout cytokinesis from initiation of the cleavage furrow to the formation of the CR, its stabilization and maturation to a MR as well as its anchoring to the plasma membrane.

Key words: Anillin, cytokinesis, Contractile ring, Midbody ring, Midbody, Tum, Tumbleweed / RacGAP50C, septin, Peanut, Citron Kinase, Sticky, Intercellular bridge.

VULGARISATION

La division cellulaire est un processus fondamental essentiel pour le développement, la croissance et la survie de tout organisme. Elle se produit en deux étapes: D'abord, pendant la mitose, l'ADN se duplique en deux ensembles qui se déplacent aux pôles opposés de la cellule; ensuite, au cours de la cytokinèse, la cellule se divise physiquement en deux cellules contenant chacune un ensemble d'ADN. La cytokinèse a été decrite depuis plus d'un siècle, cependant nous commençons à peine à comprendre les mécanismes qui la régule.

La recherche sur la cytokinèse suscite de plus en plus d'interêt car l'échec de la cytokinèse a été associé au cancer. L'hypothèse la plus étudiée est que l'échec de la cytokinèse, qui produit une cellule avec un excédent d'ADN, conduirait à une instabilité génomique et pourrait promouvoir le cancer. Il a également été rapporté que les protéines impliquées dans la cytokinèse se trouvent mutées dans de nombreux cancer.

L'objectif de nos travaux est de comprendre comment la cytokinèse se produit normalement, les mécanismes qui la régulent au niveau moléculaire et comment son dysfonctionnement peut conduire au cancer. De nombreuses études ont identifié les protéines clées qui constituent la machinerie de la cytokinèse. Parmi ces composantes, L'Anilline est présente tout au long de la cytokinèse et se lie à de nombreuses protéines impliquées dans ce processus. Mon objectif principal est de comprendre comment l'Anilline à travers ces multiples interactions guide la progression de la cytokinèse.

L'échec de la cytokinèse est considéré comme un événement précoce dans le cancer. Il est donc important d'identifier les mécanismes clés qui régissent ce processus , ce qui nous permettra de cibler la cytokinèse et ses composants pour la prévention ou le traitement du cancer. Il est donc possible d'exploiter la détection de tels défauts pour la détection précoce du cancer, ce qui permettrait d'améliorer les traitements thérapeutiques.

Table des matières

LISTE DES TABLEAUX

LISTE DES FIGURES

Chapitre 1:

Chapitre 3

Chapitre 4

Chapitre 5

LISTE DES SIGLES ET ABBRÉVIATIONS

AC: Anneau Contractile

AM: Anneau du Midbody

AHD : Anillin Homology Domain

ALIX: Apoptosis-Linked gene 2-Interacting protein

APC: Anaphase Promoting Complexe

ARNi: ARN interférent

ARN: Acide Ribonucléique

CDK: Cyclin-Dependent Kinase

CR: Contractile Ring

CS : Central Spindle

CPC: Chromosomal Passenger Complex

Dia : Diaphanous

ESCRT: Endosomal Sorting Complex Required for Transport

Feo: Fascetto

GAP : GTPase activating protein

GEF : Guanine Nucleotide Exchange Factor

INCENP: inner centromere protein

KIF: Kinesin Family Member

LatA : Latruncuilin A

MKLP1: Mitotic Kinesin-Like Protein 1

MR: Midbody Ring

MRLC: non muscle myosin regulatory light chain

OCRL1: ortholog of human oculocerebrorenal syndrome of Lowe 1

Pav: Pavarotti

PH: Pleckstrin Homology

Pbl: Pebble

PIPS : Phosphatidyl inositol phosphate

PI(4, 5) P2: Phosphatidylinositol-4, 5-bisphosphate

Plk1: Polo-Like Kinase

PNUT: Peanut

PRC1: Protein Required for Cytokinesis 1

Rho GAP: Rho Guanine Activating Protein

Rho GEF: Rho Guanine Nucleotide Exchange Factor

RNAi: RNA interference

RNA: Ribonucleic Acid

ROCK: Rho-associated Protein Kinase

Sqh: Spaghetti Squash

Tum: Tumbleweed

REMERCIEMENTS

Je remercie tout d'abord les membres du Jury qui ont accepté de lire et évaluer ma thèse.

Dr Gregory Emery, d'avoir accepté de présider ce jury.

Dre Sabine Elowe, d'avoir accepté d'être examinatrice externe.

Dr Jean Claude Labbé, d'avoir accepté d'être membre du jury.

Je remercie également **Dr Sébastien Carréno, Dre Alisa Piekny et Dr Jean Claude Labbé** qui ont été membres de mon comité de parrainage et jury de mon examen prédoctoral. Merci pour votre feedback, vos commentaires constructifs et vos encouragements tout au long de mon cursus doctoral.

Je remercie infiniment mon directeur de recherche, le **Dr Gilles Hickson**. Merci de m'avoir accueillie au sein de ton équipe et de m'avoir encouragée et donné l'opportunité de poursuivre un doctorat. Nos discussions et nos réunions qui duraient des heures m'ont permises d'affiner mon esprit critique et mes capacités d'analyse et de devenir une meilleure scientifique. Merci pour ta confiance, l'autonomie que tu m'as accordée et ton soutien constant. Merci également pour ta compréhension face aux aléas de la vie de maman; je t'en suis grandement reconnaissante.

Je remercie tous les membres du laboratoire Hickson que j'ai côtoyé pour leur support, leur aide et tous les moments partagés ensembles.

Silvana Jananji, au fil des ans, nous avons partagés succès et échecs professionnels ou personnels. Nous avons eu nos différents mais au final nous avons toujours été présentes l'une pour l'autre. Je te souhaite beaucoup de réussite dans ton doctorat et que tu puisses accomplir de grands projets, à la hauteur de ton ambition.

Nour El amine, nous avons tant appris l'un de l'autre. Merci de m'avoir challengée, soutenue, contredite et aidée pendant notre cursus. Lab meetings were never the same after you left. No one to shout : 'I understand what you mean, but you are wrong' or critisize my 'double of nothing' phenotypes or have a great scientific fight between Anilln and Citron.

Yvonne Ruella, my little miss sunshine. Ta bonne humeur contagieuse, tes mots toujours positifs, tes woot woot que tu m'envoies au quotidien ont fait que tu es devenue bien plus qu'une collègue ou une amie mais une petite sœur pour moi. Merci de faire partie de ma vie tout simplement.

Denise Wernike, your arrival at the lab was a breath of fresh air. You are an example of hard work and efficiency, but also of generosity and attention to others. I am glad to have stayed longer in the lab because it allowed me to know you and count you today among my dear friends.

Sabrya Karim, Je ne t'ai pas connu longtemps mais assez pour apprécier grandement la scientifique et la personne que tu es. Merci pour tes encouragements, ton support, et tes attentions au cours des derniers mois.

Miguel Larivière, Merci d'endurer nos conversations de filles et nos taquineries au quotidien.

Je voudrais également remercier **Assila Belounis**. Merci de toujours trouver les bons mots pour m'encourager, me motiver, et me soutenir. Merci de partager mes bonheurs et mes peines et d'avoir été une amie précieuse au cours des ans.

Melanie Diaz, Merci d'être l'amie douce et attentionnée que tu es. C'est un bonheur de te voir prendre confiance en tes capacités et de te voir évoluer professionnellement et personnellement.

À la plus précieuse des amies, **Yasmine Benkara**. Merci pour ton affection, ton soutien et tes encouragements. Merci de partager le meilleur et le pire et d'être si présente au quotidien, même à 6000 Km.

À mes sœurs **Kenza** et **Wafa** et mon frère **Abdelhadi**, Merci d'être mon support system. Je sais que je peux toujours compter sur vous pour tout.

À mon mari, **Amine Djelouadji**, merci pour ton support constant et ton amour. Merci d'avoir soutenu notre famille et de m'avoir permise de compléter mes études. À présent nous pouvons écrire ensemble, les prochains chapitres de notre vie.

Plus que tout, je remercie mes parents **Boualem et Houria** qui ont toujours cru en moi et soutenu inconditionnellement. Il n'y a pas d'accomplissements assez grands pour égaler une fraction des sacrifices que vous avez fait et faites encore pour nous; ni de mots assez justes pour vous exprimer mon amour et ma gratitude. J'espère avoir été digne de ce que vous m'avez enseignée. Je vous dédie cette thèse et espère vous avoir rendus fiers.

À mon fils, **Manil,**

Tu es et tu seras pour toujours mon plus bel accomplissement

et ma plus grande fierté

1 INTRODUCTION

Tous les organismes proviennent d'une seule cellule par division. Les organismes multicellulaires dépendent de la division cellulaire pour leur développement, croissance et survie. Durant la phase embryonnaire, la division cellulaire est à son apogée et assure principalement la croissance. Ensuite, elle permet la spécification de cellules en tissus et en organes qui assurent différentes fonctions dans l'organisme. À l'âge adulte, le taux de division cellulaire est plus faible et sert principalement à remplacer les cellules perdues, endommagées ou usées. Par ailleurs, la division cellulaire est un processus hautement régulé par de multiples points de contrôles et son dérèglement peut conduire à la destruction de l'organisme. C'est entre autre le cas des cancers, qui ont souvent pour origine une altération de la division cellulaire. La division anarchique et incontrôlée de certaines cellules est responsable de l'amplification de la masse tumorale et de l'apparition de cellules métastasiques, qui propagent le cancer dans tout l'organisme.

1.1 LE CYCLE CELLULAIRE

Il y aurait chez l'homme adulte 20 millions de cellules qui se divisent toutes les secondes. La durée de la division cellulaire peut varier d'un jour à un an en fonction du type cellulaire, cependant, elle se fait toujours a travers un cycle précisément orchestré qui implique deux phases majeures: l'interphase et la phase mitotique**.**

1.1.1 L'interphase

L'interphase qui constitue 90% du cycle cellulaire, est divisée en trois phases: les intervalles G1 et G2 et la phase de synthèse S. L'intervalle G1 est une phase de croissance durant laquelle la cellule augmente sa production de protéines, d'organelles cytoplasmique, d'ARN messagers et de protéines en même temps qu'elle augmente son volume. Le contenu cellulaire est dupliqué à l'exception de l'ADN. S'ensuit la phase S, durant laquelle les chromosomes sont répliqués. S'ensuit une autre phase de croissance l'intervalle G2 durant

laquelle la cellule se prépare à la division. En G2, la cellule vérifie que tout son ADN est répliqué et qu'aucun dommage n'est détecté **(Figure 1.1)**. La cellule est capable d'arrêter sa progression dans G2 à ce point de contrôle afin de corriger de telles erreurs (Alberts et al., 2014).

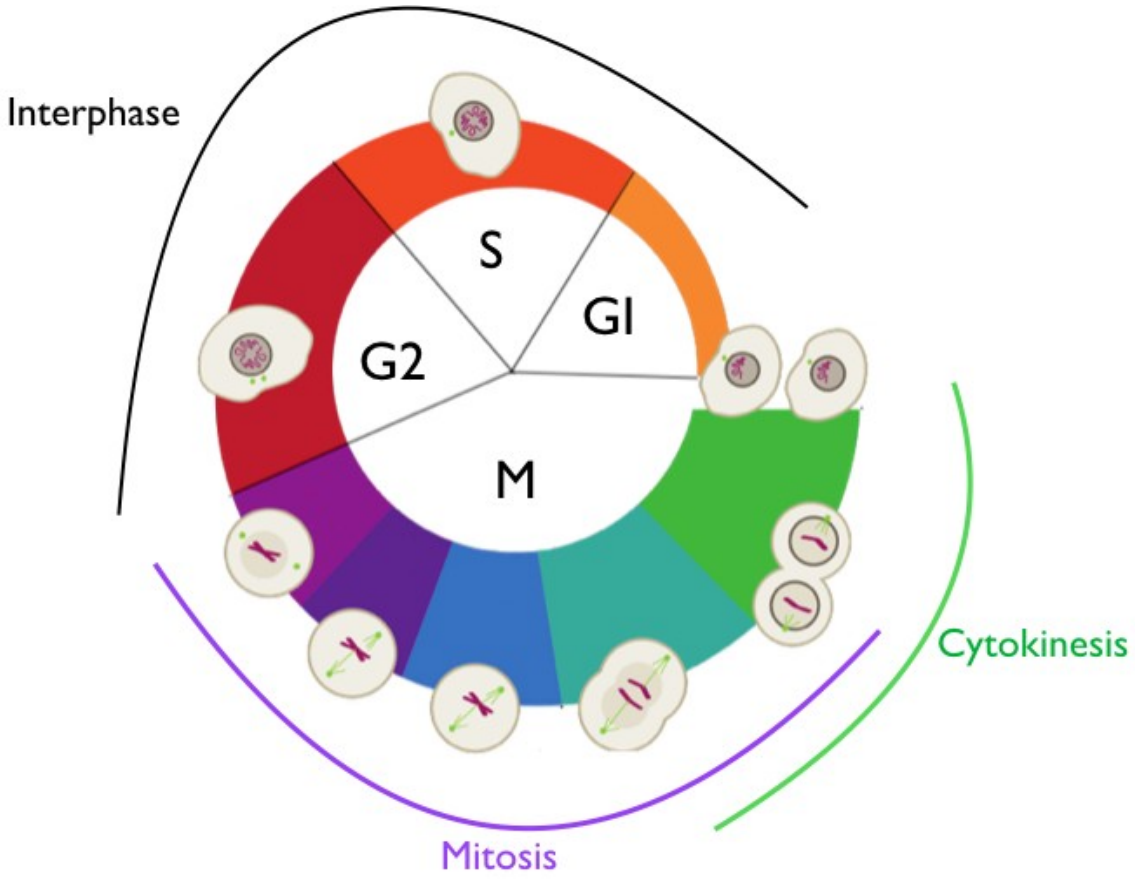

Figure 1.1: Le cycle cellulaire

Schématisation simplifiée de l'enchainement des différentes phases du cycle cellulaire.

1.1.2 La phase mitotique

La phase mitotique consiste en deux processus étroitement couplés: la mitose au cours de laquelle les chromosomes sont divisés également entre les deux cellules filles en formation (Mitchison and Salmon, 2001) et la cytokinèse, le processus par lequel le cytoplasme est divisé et deux cellules distinctes sont formées (Glotzer, 2005). Toutes ces phases se déroulent dans un ordre strict et hautement régulé par de nombreux points de contrôles **(Figure 1.2)**.

1.1.2.1 La mitose

La mitose commence en prophase, lorsque l'enveloppe nucléaire qui séquestre le matériel génétique se rompt et le contenu génétique de la cellule forme un complexe appelé chromatine, constitué de protéines et de chromosomes spécifiques. À ce stade, les fibres de chromatine sont étroitement enroulées et condensées en chromosomes distincts. Chaque chromosome se compose de deux chromatides sœurs liées ensemble au centromère. Une structure appelée le centrosome se duplique et chaque centrosome migre à un des deux pôles de la cellule (Alberts et al., 2014).

En **prométaphase**, Les centrosomes servent de centre nucléateur de la Tubuline. Des microtubules (MTs) astraux et polaires vont polymériser à partir de ces centrosomes formant le fuseau mitotique.

S'ensuit la **métaphase**, l'étape d'alignement des chromosomes. Chaque chromatide est ancrée au niveau du kinétochore par un faisceau de MTs formant ainsi la plaque équatoriale. Cette étape est hautement régulée notamment par le point de contrôle de l'assemblage du fuseau mitotique (mitotic spindle assembly checkpoint) et l'anaphase ne peut être initiée tant que l'alignement n'est pas atteint.

L'**anaphase** est l'étape la plus rapide de la mitose et peut être divisée en deux parties. Durant l'anaphase A, les chromatides sœurs sont tirées vers les pôles opposés de la cellule par un mécanisme de dépolarisation/rétraction des MTs du kinétochore. Ensuite, en anaphase B, des MTs apparaissent entre les deux lots de chromatides sœurs et repoussent, par polymérisation, les chromatides en directions opposées. Ces MTs composent le fuseau central (Glotzer, 2009; Maiato and Lince-Faria, 2010). Les MTs astraux interviennent eux dans la

stabilisation de la géométrie cellulaire et l'orientation du fuseau mitotique, en interagissant entre autre avec le cortex de la cellule.

Finalement, pendant la **télophase**, l'enveloppe nucléaire se forme autour de chaque série de chromatides sœurs séparées et à la fin de cette phase, deux cellules filles sont formées mais demeurent connectées par un pont intercellulaire.

1.1.2.2 La Cytokinèse

La séparation totale des deux cellules filles en deux entités distinctes est réalisée par une ultime phase, la cytokinèse. La cytokinèse se produit parallèlement à la mitose et débute en anaphase. C'est la dernière étape de la division cellulaire qui sépare physiquement les cellules filles afin d'assurer l'héritage approprié des contenus nucléaires et cytoplasmiques.

1.2 LA CYTOKINÈSE

Historiquement la cytokinèse était considérée comme une étape accessoire de la mitose; aujourd'hui elle représente une phase entière du cycle cellulaire, très complexe et hautement régulée. Elle est décrite en détail dans les prochaines sections.

La cytokinèse, a été décrite il y a plus de cent ans par des biologistes qui examinaient des cellules en division et de nombreuses théories ont été proposées pour décrire son mécanisme. On connaissait peu de choses sur la constitution moléculaire des cellules en général et de la machinerie de la cytokinèse en particulier. Par conséquent, pendant longtemps, peu de progrès avaient été réalisés dans la compréhension de la cytokinèse. Cela a changé au cours des vingt dernières années avec plusieurs avancées importantes, notamment grâce à des criblages génétiques à grande échelle qui ont permis de définir l'ensemble des protéines nécessaires à la cytokinèse dans différents organismes (Eggert et al., 2006; Glotzer, 2005). Ces travaux couplés aux progrès technologiques de micromanipulation, d'imagerie à haute résolution, et de modélisation informatique ont permis d'approfondir nos connaissances sur la cytokinèse.

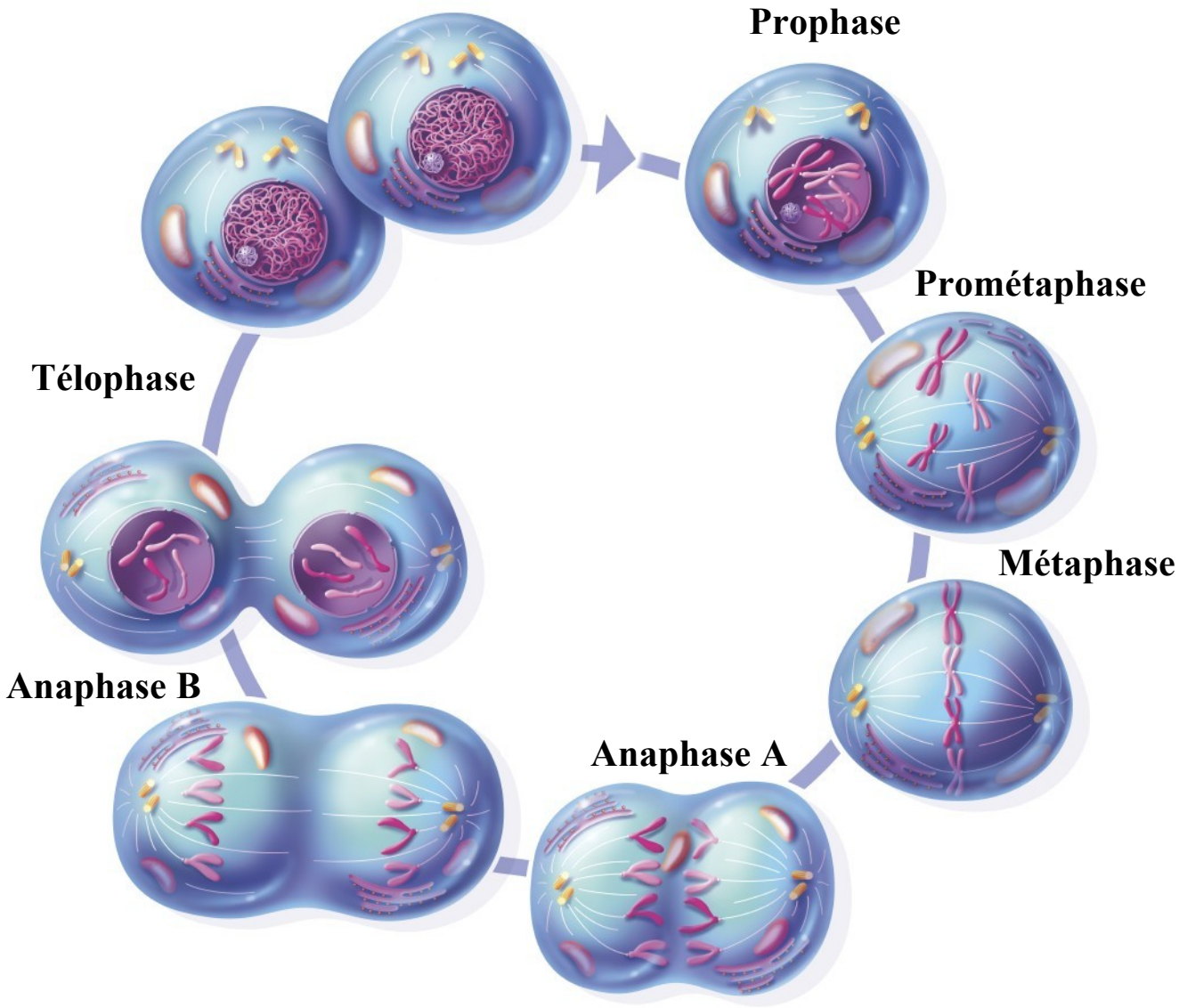

Figure 1.2: La mitose

Schématisation simplifiée de l'enchainement des différentes phases de la mitose.

Voir texte pour plus de détails.

Modifié de :https://aandpsource.files.wordpress.com/2013/10/mitosis-1.jpg

Les mécanismes de cytokinèse varient selon les organismes mais conservent quatre caractéristiques communes **(Figure 1.3**):

- l'assemblage du fuseau central en anaphase qui va dicter la formation d'un anneau contractile (AC) à l'équateur de la cellule et sa constriction.
- La maturation du fuseau central afin de former le midbody.
- La stabilisation d'un pont intracellulaire composé du midbody ainsi que l'anneau du midbody (AM) qui l'entoure.
- la séparation finale des cellules filles, l'abscission.

Dans les sections suivantes, je vais fournir un résumé de l'état actuel des connaissances dans le domaine de la cytokinèse, mettant l'accent sur la cytokinèse dans les cellules animales.

1.2.1 Assemblage du fuseau central

Au début de l'anaphase, la dynamique des MTs change drastiquement. Alors que les chromosomes sont tirés de part et d'autre vers les pôles opposés de la cellule, il se forme entre eux un réseau de MTs antiparallèles qui ont leurs extrémités négatives aux pôles alors que leurs extrémités positives se chevauchent à l'équateur de la cellule. Cette zone de chevauchement est définie comme le fuseau central ou le midzone (Glotzer, 2009). Les MTs qui le composent sont issus principalement des MTs polaires mais également suite à une polymérisation *de novo* a partir de points de nucléation non centrosomique et de complexes d'Augmine (Uehara and Goshima, 2009; Uehara et al., 2009). En plus des MTs, le fuseau central regroupe des protéines associées aux MTs; principalement des kinésines et des kinases qui sont essentielles à sa formation et sa stabilité mais aussi lors des étapes subséquentes de la cytokinèse.

PRC 1 (Protein requlator of cytokinesis 1; Fascetto chez *Drosophila*) est une protéine de fasciculation des MTs qui agit sous forme d'homodimère afin d'ancrer les extrémités positives des MTs antiparallèles en position équatoriale. PRC1 est essentielle pour polariser les MTs du fuseau central et organiser le recrutement et la concentration des protéines responsables de l'assemblage du sillon de clivage **(Figure 1.4)**.

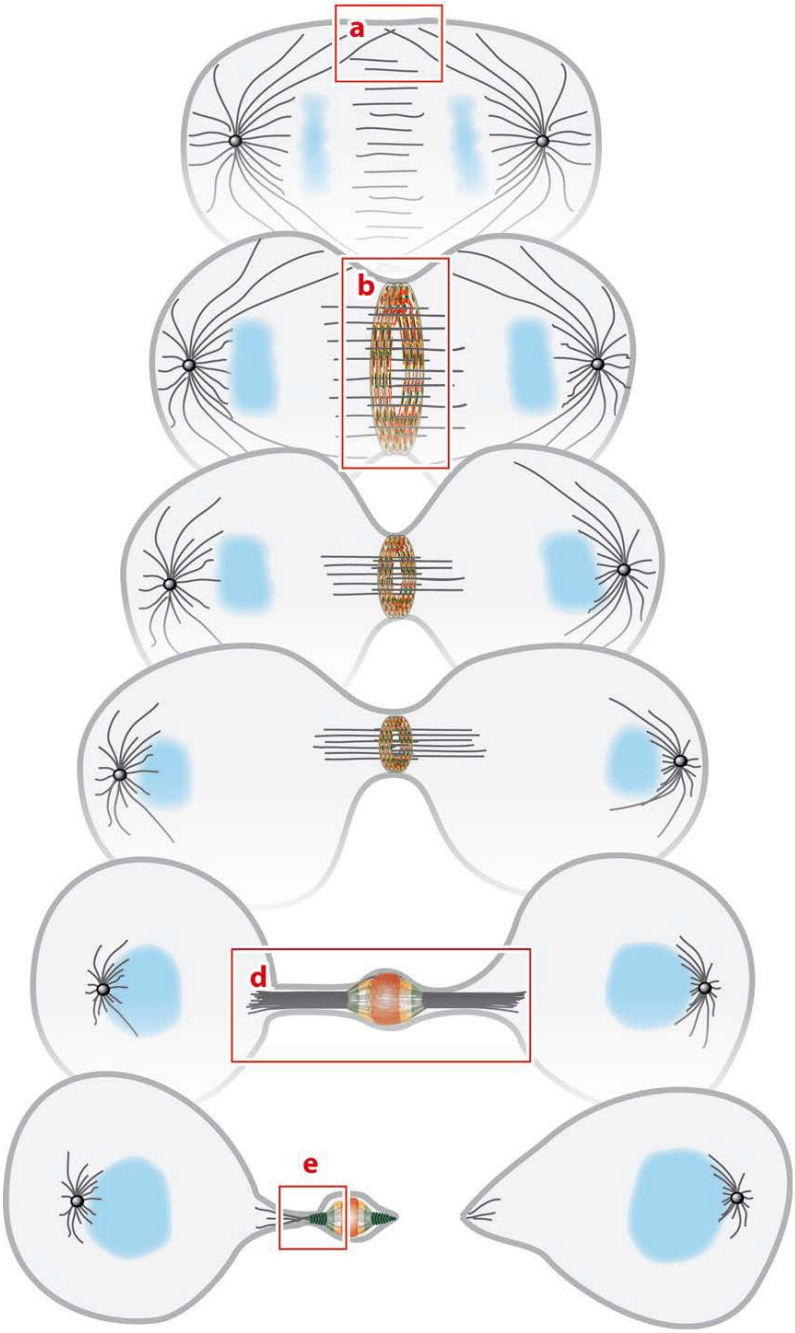

Figure 1.3: La cytokinèse

a- En métaphase, la définition d'un plan de clivage déterminera le site de positionnement et d'assemblage d'un anneau contractile (AC). **b-** La constriction de l'AC aboutira à la formation d'un anneau du midbody. **c-** En parallèle, il y a compaction du fuseau central et sa maturation pour former une structure dense nommée le midbody. **d-**L e midbody et l'anneau du midbody forment le pont intercellulaire entre les deux cellules filles. **e-** Cette structure régit l'abscission aboutissant à la séparation complète des deux cellules filles. Adapté d'après (Green et al., 2012).

Les cellules déplétées en PRC1 sont incapables de former un réseau de MTs antiparallèles et fusionnent au lieu d'achever la cytokinèse (Mollinari et al., 2002). Son activité est régulée par les kinases cycline dépendante 1 (CDK1) et Polo Like Kinase 1 (PLK1, Polo chez *Drosophila*) qui l'empêchent de s'accumuler aux MTs et de les fasciculer avant le début de l'anaphase (Hu et al., 2012; Zhu and Jiang, 2005). PLK1 n'est pas essentielle à la formation du fuseau central; par contre, sa déplétion cause une élongation de la zone de chevauchement des MTs (Brennan et al., 2007; Petronczki et al., 2007).

La kinésine **KIF4** est recruté par PRC1 aux extrémités positives des MTs pour moduler la longueur de la région de chevauchement des MTs antiparallèles. Elle agit en réduisant le taux de croissance des MTs (Hu et al., 2011). In vitro PRC1 et KIF4 sont suffisantes pour assembler un réseau de faisceaux de MTs où la longueur de la région de chevauchement est inversement proportionnelle à la concentration de KIF4 (Bielinget al., 2010; Subramanian et al., 2010). Notons aussi la kinésine **KIF-14** (Nebbish chez *Drosophila*), qui interagit avec PRC1 et régit la localisation de plusieurs autres composantes de la cytokinèse (Bassi et al., 2013; Gruneberg et al., 2006b).

Un complexe protéique nommé **centralspindlin** est également essentiel pour la formation du fuseau central. Centralspindlin est un hétéro tétramère composé de deux molécules de la kinésine, Mitotic Kinesin Like Protein 1 (**MKLP1**, Pavarotti chez *Drosophila*) et deux molécules de la protéine activatrice des Rho GTPases, **MgcRacGAP** (hCyk-4, RacGAP50C or Tumbleweed chez *Drosophila*) (Mishima et al., 2002; Pavicic-Kaltenbrunner et al., 2007). MgcRacGAP et son partenaire de liaison, MKLP1 se lient directement *in vivo* et *in vitr*o, sont interdépendants pour leur localisation au fuseau mitotique et sont nécessaires pour la formation du fuseau central, la formation du sillon de clivage et le succès global de la cytokinèse (Mishima et al., 2002). La formation de ce complexe est régulée par le **choromosome passenger complex** (**CPC)**, un tétramère composé de la kinase **Aurora B** ainsi que trois autres sous-unités qui régulent son activité. Avant l'anaphase, MKLP1 est liée à la protéine 14-3-3, qui empêche son oligomérisation. Durant l'anaphase, la phosphorylation de MKLP1 par Aurora B antagonise la fixation de 14-3-3 et lève son inhibition sur la dimérisation de MKLP1 et la formation du complexe centralspindlin (Douglas et al., 2010). Ce faisant, centralspindlin localise aux extrémités

positives des MTs antiparallèles où il initie la fasciculation des MTs et l'assemblage du fuseau central (Mishima et al., 2002; Mishima et al., 2004). Ni MKLP1 ou MgcRacGAP seul ne peut fasciculer les MTs, mais le complexe centralspindlin intact peut induire la fasciculation des MTs *in vitro* et sa déplétion bloque la formation du fuseau central dans de nombreux organismes (Adams et al., 1998; Mishima et al., 2002; White and Glotzer, 2012).

1.2.2 Spécification du plan de clivage

La spécification du plan de clivage se fait durant l'anaphase et assure le couplage entre l'invagination de la membrane au site défini par le plan de clivage et la ségrégation des chromatides sœurs. La nature et l'origine du signal qui détermine le plan de clivage reste à définir clairement; cependant le moment de la formation du fuseau mitotique, sa composition ainsi que sa position au sein de la cellule en ont fait un candidat de choix qui agirait comme une source des signaux activateurs ou inhibiteurs nécessaires à l'établissement du sillon de clivage. Les premières indications sur le rôle des MTs dans le positionnement du plan de clivage sont venues des expériences de Rappaport qui ont montré que le déplacement du fuseau mitotique vers de nouvelles positions induit rapidement l'apparition d'un sillon dans une nouvelle région de la membrane plasmique (Rappaport and Ebstein, 1965). Même si la nature des MTs qui fournissent le signal est sujette à débat, deux signaux semblent capitaux pour le bon positionnement spatial de cette zone de clivage: l'un venant du fuseau central, le second du fuseau astral (Bringmann and Hyman, 2005; Werner et al., 2007). À un extrême, les embryons de *C. elegans* mutants pour spd-1, un membre d'une famille de protéines qui localise spécifiquement les MTs du fuseau central, peuvent se diviser en l'absence complète du fuseau central (Verbrugghe and White, 2004). À l'autre extrême, les spermatocytes de *Drosophila* mutants pour Asterless, un composant du centriole qui est nécessaire pour la fonction du centrosome, peuvent se diviser en l'absence complète de MTs astraux (Bonaccorsi et al., 1998).

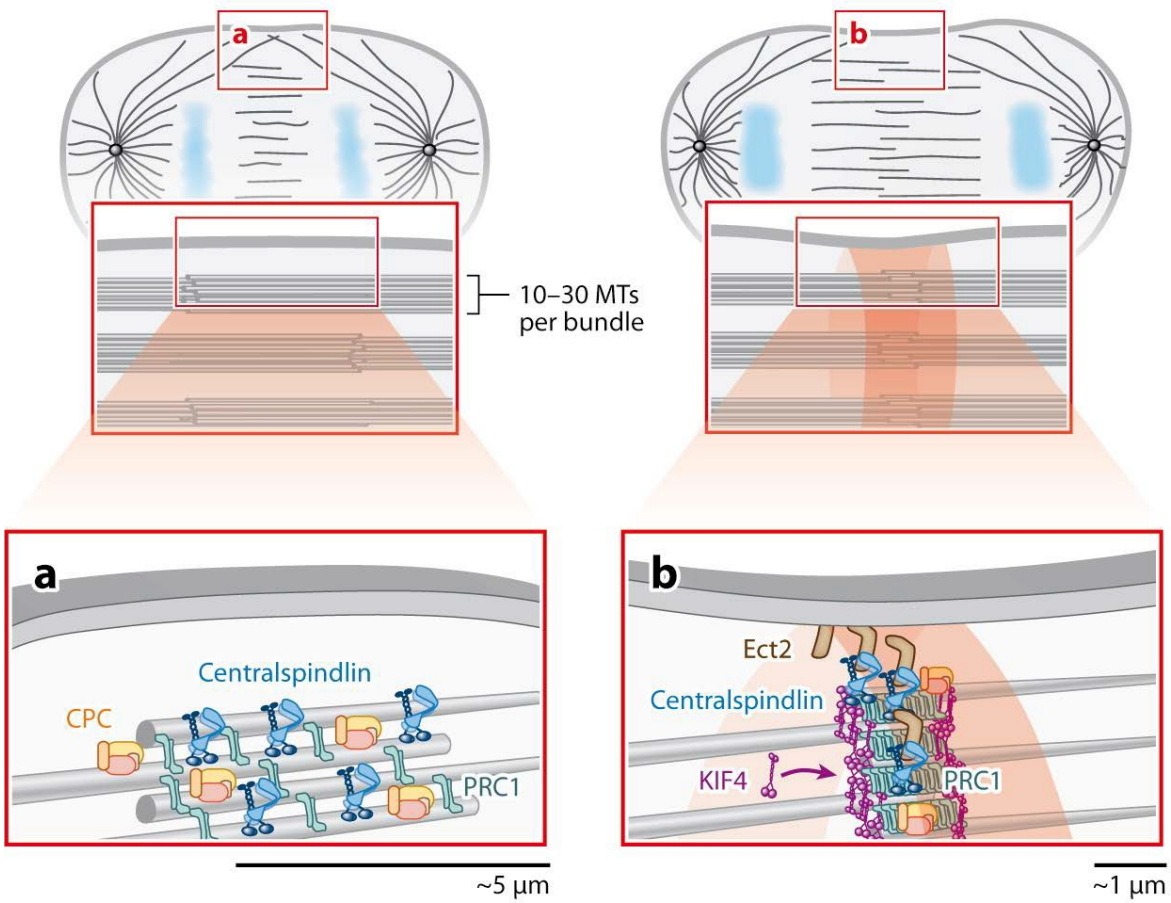

Figure 1.4: Assemblage du fuseau central

a- PRC1 régit la fasciculation des MTs antiparallèles. Le CPC et centralspindlin sont recrutés à la région de chevauchement des MTs et sont nécessaires à leur fasciculation. **b-** PRC1 recrute KIF4 qui limite l'élongation des MTs afin de créer une zone de chevauchement étroite. Adapté de (Green et al., 2012).

Entre ces extrêmes, les cellules utilisent différentes populations de MTs comme sources de signaux complémentaires ou redondants afin de spécifier le plan de clivage (Pour une revue, voir von Dassow, 2009). Outre la source exacte des signaux nécessaires à la spécification du plan de division dans les cellules animales, une autre question qui reste non résolue traite de la nature des forces qui le déterminent. La forme la plus commune de ce débat est entre les concepts de stimulation équatoriale et relaxation polaire **(Figure 1.5)**.

Le modèle de **relaxation polaire** postule que les signaux inhibiteurs délivrés aux pôles par les MTs astraux inhibent la tension corticale localement; en conséquence, la tension devient plus élevée à l'équateur, ce qui conduit à la formation d'un sillon de clivage (Canman et al., 2003; Dechant and Glotzer, 2003; Motegi et al., 2006; Werner et al., 2007). Des travaux récents sur des cellules de *Drosophila* ont également démontré que l'inactivation sélective de protéines nécessaires à la rigidité corticale au niveau des pôles cellulaires est susceptible de contribuer à la relaxation polaire (Kunda et al., 2012).

En revanche, Le modèle de **stimulation équatoriale** postule que le fuseau central en collaboration avec une population stable de MTs astraux liés au cortex équatorial livre des signaux positifs qui initient des forces internes positives et localisées. Suite à de nombreux travaux, il semble aujourd'hui que ces mécanismes ne sont pas mutuellement exclusifs. Dans de nombreux types de cellules, la stimulation équatoriale et la relaxation polaire peuvent contribuer à divers degrés dans différentes conditions (Burgess and Chang, 2005; D'Avino et al., 2005; Oegema and Mitchison, 1997). Alors que les cellules plus larges comme les embryons d'échinoderme, ou *C.elegans*, qui contiennent des astres proéminents et un petit fuseau central dépendent majoritairement des MTs astraux pour le positionnement du plan de division, les plus petites cellules comme les cellules de drosophiles où le fuseau central est étroitement juxtaposé au cortex équatorial dépendent plutôt des voies de stimulation équatoriale.

1.2.3 L'activation de RhoA au cortex équatorial

Indépendamment de l'origine et de la nature du signal qui défnit le plan de clivage, la clé de ce processus est la concentration et l'activation de la GTPase Rho au niveau de l'équateur de la cellule (Bement et al., 2005). Les Rho GTPase ont une faible activité

enzymatique intrinsèque; elles dépendent des facteurs d'échanges de nucléotides guanilyques (GEF) et des protéines activatrices des GTPases (GAP) pour transiter d'un état actif lié au GTP à un état inactif lié au GDP. Bien que tous s'entendent sur l'identité de la GEF responsable de l'activation de Rho, l'identité de la RhoGAP qui régule la cytokinèse reste sujette à débat.

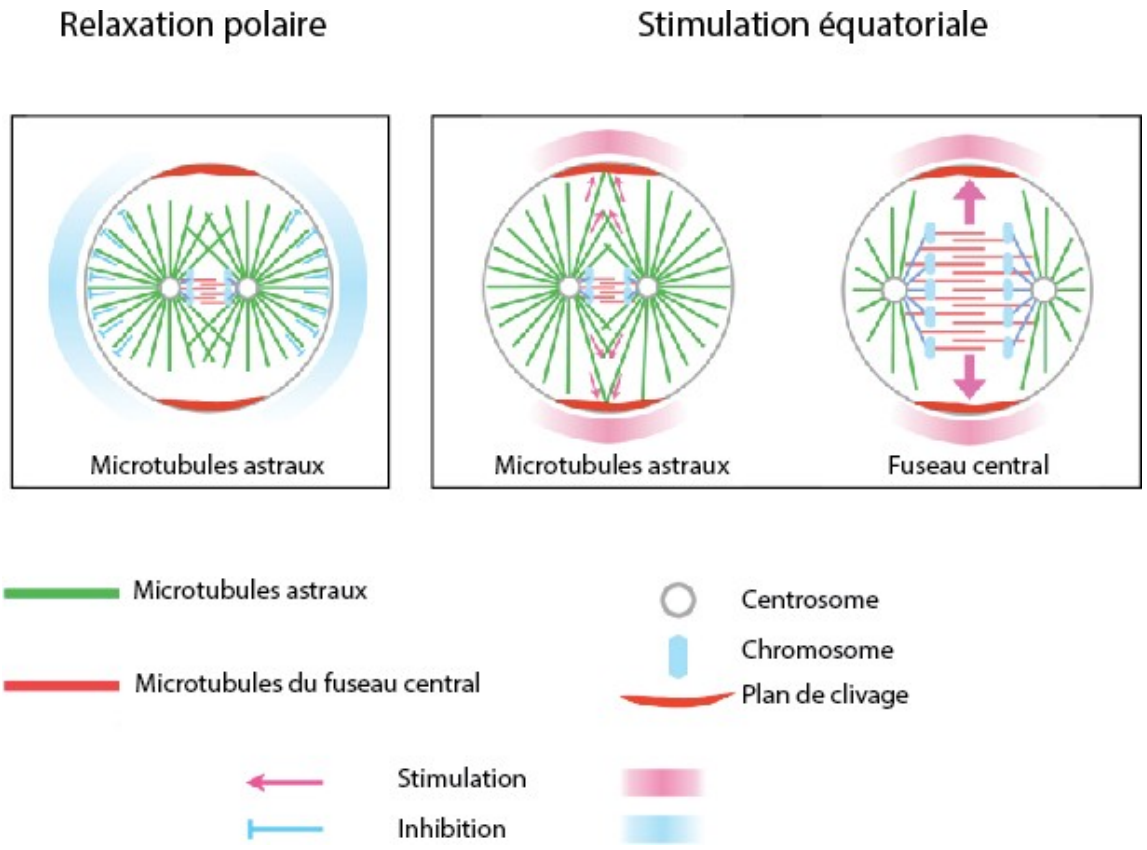

Figure 1.5: Induction du sillon de clivage

Les modèles d'induction du sillon de clivage peuvent être classés en fonction de la source (MTs astraux vs fuseau central) et de la nature (stimulation équatoriale ou relaxation polaire) des signaux de clivage. Adapté de (Mishima, 2016).

1.2.3.1 La voie centralspindlin-ECT2

Le recrutement et l'activation de Rho à l'équateur dépendent du complexe centralspindlin. Suite à l'assemblage du fuseau mitotique, centralspindlin s'accumule à la zone de chevauchement des MTs. Chez les cellules de mammifères et de drosophiles, la sous-unité McgRacGAP lie la RhoGEF ECT2 (Pebble chez *Drosophila*) et la recrute au fuseau central (Somers and Saint, 2003; Yuce et al., 2005). Cette interaction est essentielle durant la cytokinèse puisque des mutations de MgcRacGAP qui bloquent le recrutement de ECT2, bloquent la formation du sillon de clivage. ECT2 lie MgcRacGAP à travers son extrémité C-terminale et la phosphorylation de McgRacGAP par PLK1 est essentielle pour cette interaction (Brennan et al., 2007; Petronczki et al., 2007; Wolfe et al., 2009). ECT2 possède également un domaine PH (Pleckstrin Homology) qui lui permet de lier la membrane et semble être requis pour l'activation de RhoA au cortex et l'assemblage de l'anneau contractile (Chalamalasetty et al., 2006; Su et al., 2011).

1.2.3.2 L'activité GAP de MgcRacGAP

Contre intuitivement, MgcRacGAP qui recrute la RhoGEF ECT2 au fuseau central pour activer Rho, agit également comme RhoGAP durant la cytokinèse. En effet, le domaine GAP de MGCRacGAP est requis durant la cytokinèse dans tous les systèmes ou il a été testé (Loria et al., 2012; Miller and Bement, 2009; Yamada et al., 2006; Zavortink et al., 2005); cependant, la nécessité de l'activité GAP en tant que telle reste moins claire. En effet, L'activité GAP de MgcRacGAP a été impliquée dans la cytokinèse dans plusieurs systèmes, y compris chez la *Xenopus*, les embryons de *C. elegans* et de *Drosophila* ainsi que les cellules de mammifères (Bastos et al., 2012; Canman et al., 2008; Miller and Bement, 2009; Zavortink et al., 2005); alors qu'elle a été jugée dispensable pour la cytokinèse dans les lymphocytes de poulet (Yamada et al., 2006) et les neuroblastes de *Drosophila* (Goldstein et al., 2005).

Différentes études ont également abouti à des conclusions différentes quant à l'identité de la GTPase ciblée par l'activité GAP de MgcRacGAP ; à savoir si elle agit sur la GTPase Rho ou Rac durant la cytokinèse (Discuté dans Basant and Glotzer, 2017). D'une part un groupe propose que MgcRacGAP agisse sur Rac. En effet, son domaine GAP a une affinité et une activité accrue envers Rac et CDC42 comparé à Rho *in vitro* (Bastos et al., 2012; Jantsch-Plunger et al., 2000; Toure et al., 1998) et inactive Rac et

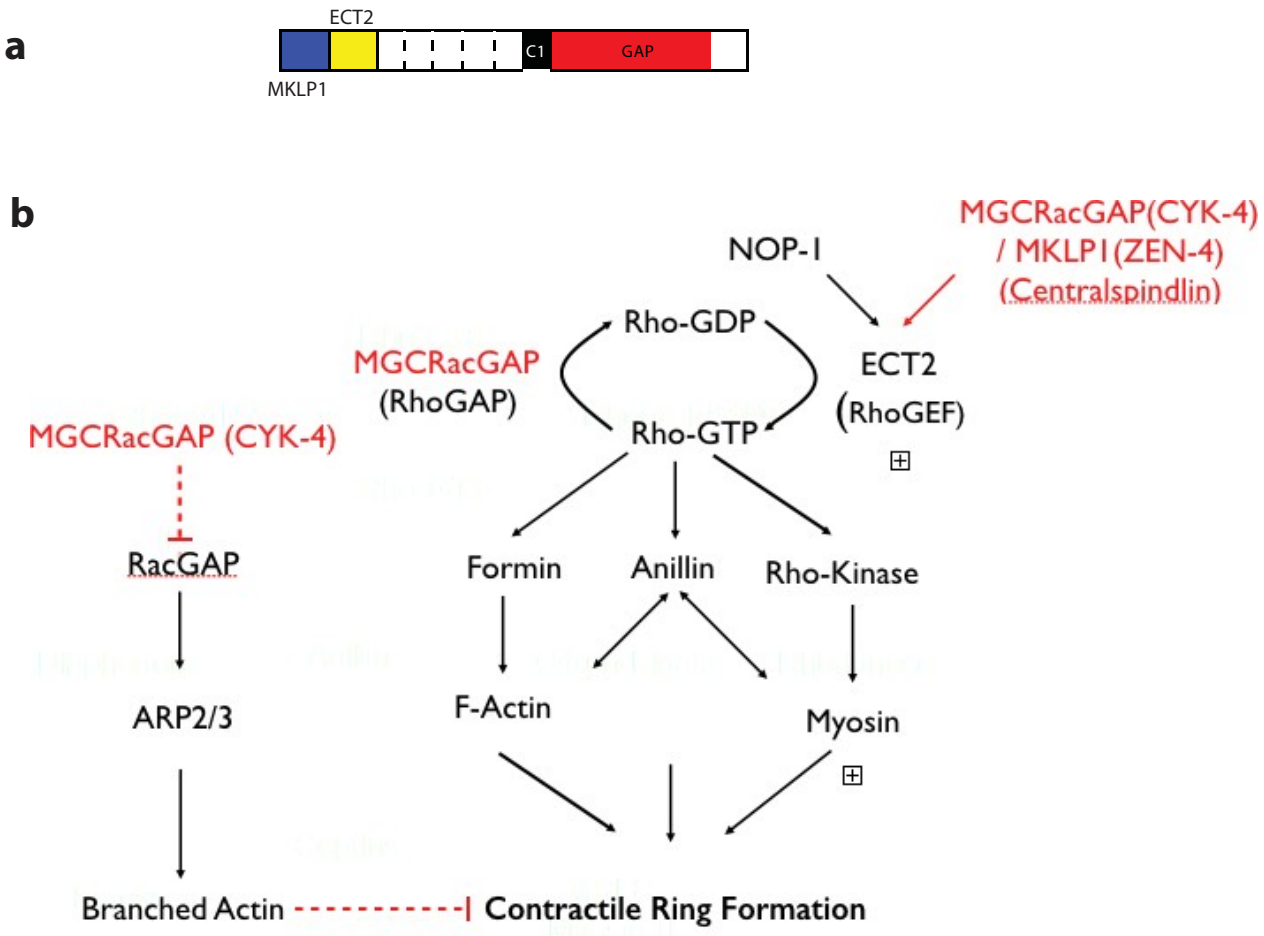

Figure 1.6: les rôles de MgcRacGAP dans l'activation de RhoA

a-Schéma des domaines conservés de MGCRacGAP. **b**- Résumé des différentes fonctions de MGCRacGAP et ses homologues durant la cytokinèse. Voir texte pour plus de details. Adapté de (Basant and Glotzer, 2017).

Cdc42 à la zone équatoriale dans les cellules en division (Canman et al., 2008; Jantsch-Plunger et al., 2000). De plus, l'inhibition génétique de Rac supprime les phénotypes de perte de fonction de CYK-4. Cela a conduit à un modèle où RacGAP inactive la GTPase Rac à l'équateur et empêche ainsi la formation de filaments d'actine ramifiés qui peuvent interférer avec la fermeture de l'AC **(Figure 1.6)** (Canman et al., 2008; D'Avino et al., 2004; Zhuravlev et al., 2017). D'autre part, différents groupes proposent que l'activité GAP agisse sur Rho non pour l'inhiber mais pour favoriser son activation. Néanmoins, différents modèles ont été proposées afin d'expliquer ce paradoxe.

Le modèle du Flux de Rho

Le modèle du Flux de Rho est basée sur l'idée qu'au lieu d'être activée au début de la cytokinèse et inhibée à sa fin, RhoA transite continuellement entre un état «on» lié au GTP et un état «off» lié au GDP tout au long de la cytokinèse. Ce cycle continu serait crucial pour l'activation de Rho dans une zone équatoriale étroite et l'établissement d'un sillon de clivage robuste. Cet équilibre serait atteint à travers une coopération entre l'activité GEF de ECT2 et l'activité GAP de MgcRacGAP. Ainsi MgcRacGAP agirait tout au long de la cytokinèse pour empêcher la propagation de la zone active de Rho vers d'autres sites le long du cortex cellulaire, fournissant ainsi un mécanisme pour focaliser la zone d'activité de RhoA et favoriser l'insertion du sillon de clivage **(Figure 1.6)**. En accord avec cette idée, la perte de l'activité GAP de MgcRacGAP chez des embryons de *Xenopus* cause une accumulation de RhoA dans des régions ectopiques le long du cortex, et une augmentation significative de l'échec de la cytokinèse (Miller and Bement, 2009). Initialement basé sur des modèles mathématiques (Bement et al., 2006), ce modèle est supporté par de nombreuses observations expérimentales. En effet, dans ses expériences sur les embryons d'oursins de mer, Rappaport était capable d'induire, à plusieurs reprises, un nouveau sillon en changeant la localisation du fuseau mitotique. De plus, chez les embryons de *Xenopus,* la zone active de RhoA change de position si le fuseau est déplacé, même si la contraction a été initiée (Bement et al., 2005), en accord avec l'idée que RhoA est localement activée et désactivée en réponse aux signaux du fuseau (Rappaport, 1996).

Activation non canonique de RhoA via ECT2

Dans un modèle alternatif et spécifique à *C. elegans*, il a été proposé que la principale foncion du domaine GAP de CYK-4 est d'activer RhoA de façon non canonique en favorisant son activation par ECT2 (Loria et al., 2012; Tse et al., 2012; Zhang and Glotzer, 2015). Les embryons déficients en activité GAP forment un sillon de clivage qui se ferme lentement et finit éventuellement par régresser. Remarquablement, ce phénotype est exacerbé lorsque l'activation de Rho est inhibée suite à la déplétion de NOP-1, un activateur d'ECT-2 (Tse et al., 2012) et supprimé lorsque l'activation de Rho est augmentée suite a la déplétion de MP-GAP/RGA-3/4, une GAP spécifique à RhoA, ou l'expression d'un allèle activé de la RhoGEF ECT-2. Ensemble, ces résultats soutiennent l'hypothèse que le domaine GAP de CYK-4 participe à l'activation de RhoA à travers ECT2. Bien qu'une interaction entre le domaine GEF de ECT2 et le domaine GAP de CYK-4 eut été rapportée (Zhang and Glotzer, 2015), le mécanisme par lequel cette interaction mènerait à l'activation de Rho reste à élucider **(Figure 1.6)**.

1.2.4 Assemblage de l'anneau contractile

À travers les espèces, les ACs sont composés d'une fine couche d'éléments corticaux contenant principalement des filaments d'actine, des filaments bipolaires de myosine, des filaments de septines ainsi que la protéine d'échafaudage Anilline. Ils contiennent également de nombreuses protéines impliquées dans la nucléation, le coiffage, la ramification, la polymérisation et le désassemblage de l'actine et l'activation de la myosine (Eggert et al., 2006). Remarquablement, tous ces éléments sont sous la régulation de la GTPase RhoA, qui une fois activée au cortex équatorial va initier l'activation et le recrutement des protéines clés nécessaires à l'assemblage de l'AC **(Figure 1.7)**.

Les formines, qui catalysent la polymérisation des filaments d'actine linéaires, sont requises pour la cytokinèse des cellules animales (Castrillon and Wasserman, 1994; Severson et al., 2002; Watanabe et al., 2010). Parmi elles, la formine Diaphanous est normalement auto-inhibée par une interaction intramoléculaire. Lorsque RhoA se lie à Diaphanous, cette inhibition est atténuée (Alberts, 2001), lui permettant de se lier aux filaments de Profiline et

d'actine afin de favoriser la polymérisation et la nucléation des filaments d'actine non ramifiés nécessaires à la formation de l'AC (Kovar and Pollard, 2004; Pruyne et al., 2002). Le complexe Arp2/3, responsable de la nucléation des filaments d'actine ramifiés, a également été identifié dans plusieurs cribles, bien que son rôle dans la cytokinèse ne soit pas aussi bien établi que celui des formines (Eggert et al., 2004; Skop et al., 2004).

Suite à l'activation de Rho, l'activation de la myosine se produit par phosphorylation de la chaîne légère régulatrice (Jordan and Karess, 1997; Komatsu et al., 2000; Yamakita et al., 1994) par deux types de kinases, les kinase Rho-dépendante (ROCK) et la kinase Citron **(Figure 1.7)**. ROCK phosphoryle la chaîne légère régulatrice de la myosine II et la libère de son auto-inhibition, favorisant ainsi la formation de filaments de myosine II et la contractilité de l'actomyosine (Uehara et al., 2010). En parallèle, l'activation de ROCK permet également d'inhiber MYPT1, une phosphatase de la myosine II (Amano et al., 1996; Kimura et al., 1996). RhoA recrute et active également la kinase Citron**,** qui possède un domaine kinase serine/thréonine qui phosphoryle la myosine. Cependant, l'importance de cette phosphorylation durant la cytokinèse demeure controversée (Yamashiro et al., 2003).

Rho régit également le recrutement de l'Anilline, une composante essentielle de l'AC (Piekny and Glotzer, 2008; Piekny and Maddox, 2010). L'Anilline est une protéine d'échafaudage nécessaire au recrutement et à l'organisation de plusieurs protéines structurales et de signalisation au niveau de l'AC, notamment RhoA, l'actine, la myosine et les septines. Les septines sont des GTPases formant des filaments impliqués dans la stabilisation de l'AC et limitant la propagation du sillon de clivage (Estey et al., 2010).

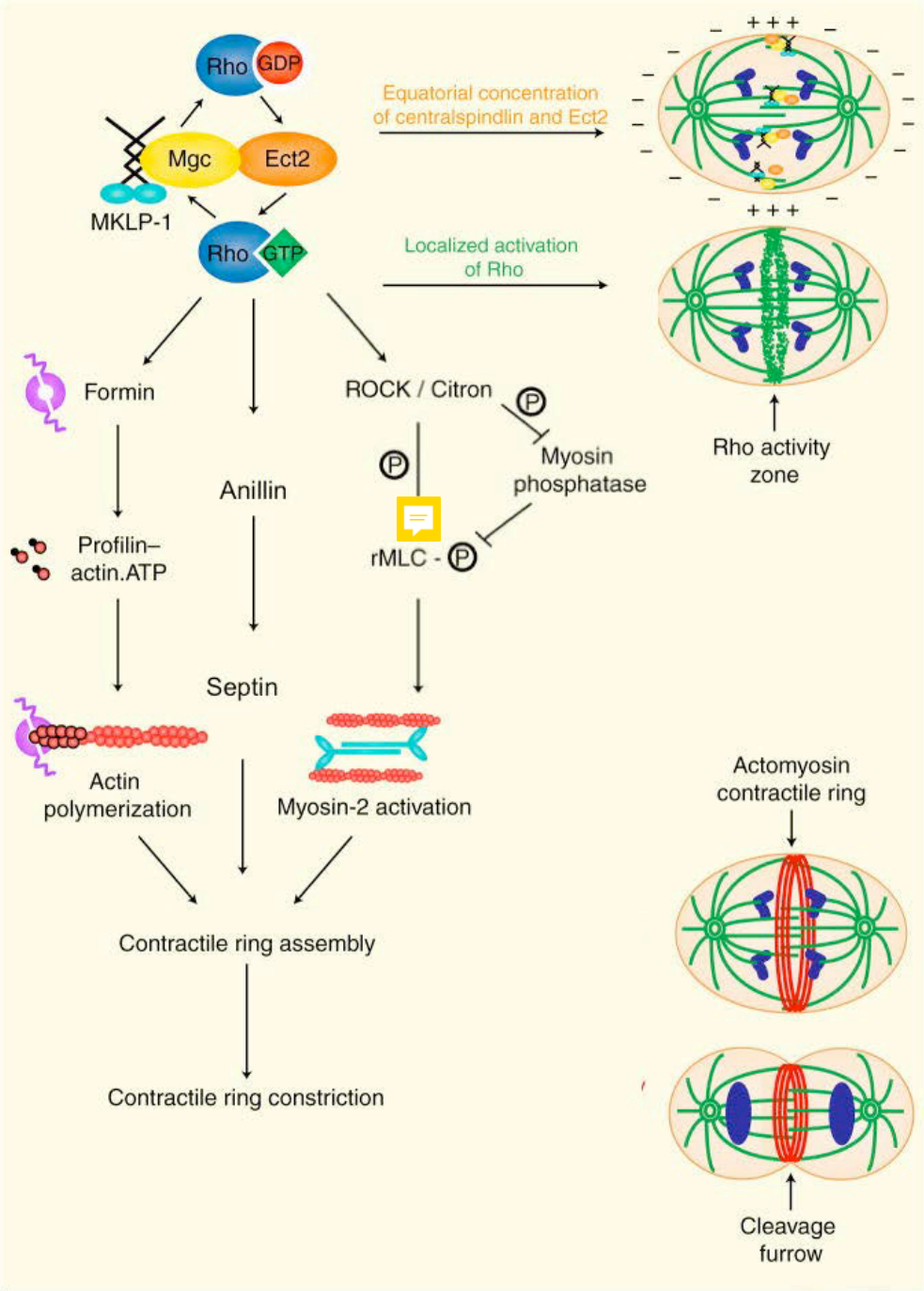

Figure 1.7: Assemblage de l'anneau contractile Voir

texte pour plus de détails. Adapté de (Miller, 2011).

1.2.5 Constriction de l'anneau contractile

Bien que la machinerie de base qui compose l'AC soit connue, son organisation et ses mécanismes de fermeture restent mal définis. En effet, une des questions qui reste sujette à controverse concerne la dynamique des composantes de l'AC pendant la fermeture du sillon de clivage. Comme l'organisation de l'AC ressemblait à celle des filaments d'actine et de myosine-II dans les fibres musculaires, on pensait que les structures d'acto-myosine dans l'AC fonctionnaient de la même façon que les unités sarcomères, en s'appuyant sur l'activité motrice de la Myosine-II. Cependant, cette hypothèse de longue date a été contestée dans une étude montrant que des mutants de myosine incapables de translocation peuvent soutenir pleinement la cytokinèse (Ma et al., 2012). De plus, contrairement aux fibres musculaires qui maintiennent des configurations stables lors de leur contraction, les filaments d'actine et de myosine présentent différentes orientations au sein de l'AC (DeBiasio et al., 1996; Kamasaki et al., 2007). Ces observations suggèrent que c'est la liaison de la myosine à l'actine ainsi que la tension exercée par la myosine sur les filaments d'actine qui est critique pour la cytokinèse (Matsumura et al., 2001). Par ailleurs, à mesure qu'il se ferme, l'AC rétrécit en diamètre mais son épaisseur ne change pas. De plus, des expériences chez *C. elegans* ont montré que des composantes de l'AC sont éliminées au cours de sa fermeture (Carvalho et al., 2009), ce qui suggère que l'AC se ferme par désassemblage des complexes protéiques (Green et al., 2012).

1.2.6 Formation du pont intercellulaire

Le pont intercellulaire est une des premières structures caractéristiques de la cytokinèse à avoir été identifiée et décrite comme une structure dense aux électrons contenant essentiellement des MTs antiparallèles, se chevauchant au centre du pont dans une zone que l'on appelle le « midbody » ou « Flemming body » (Flemming, 1965; Mullins and Biesele, 1973), Depuis, des études de protéomique et de crible d'ARNi ont permis de mieux caractériser cette structure et d'identifier une multitude de facteurs qui la compose (Echard et al., 2004; Skop et al., 2004).

1.2.6.1 Les microtubules

Historiquement le pont intercellulaire a été identifié par son opacité résultant de sa densité

extrême en MTs (McIntosh and Landis, 1971). Ces MTs sont le reliquat du fuseau central qui a été condensé pendant la contraction de l'AC. Ils sont très stables comme le confirme leur acétylation et leur résistance aux drogues dépolymérisantes tel le Nocodazole (Foe and von Dassow, 2008; Piperno et al., 1987; Rosa et al., 2006). Ils se chevauchent à leurs extrémités positives et forment au centre de cette zone, une matrice dense et riche en protéines qui est le midbody **(Figure 1.8a)**. La densité des MTs au sein du midbody est telle qu'il est très difficile de l'étudier par des techniques d'imagerie conventionnelle due à l'incapacité des anticorps d'y pénétrer, créant souvent une zone "noire" caractéristique de l'emplacement du midbody.

1.2.6.2 Le midbody

Quoique dense, le midbody n'est pas statique et subit de nombreux changements au cours de sa maturation tant au niveau de sa morphologie que sa composition. Ainsi, à mesure que l'AC se ferme, les composantes du fuseau central sont divisées en trois groupes qui seront distribués à différents sous compartiments du midbody. Le premier qui contient les kinésines PRC1 et KIF4 est maintenu entre les MTs au cœur du midbody au niveau de la zone noire. Un autre groupe composée de MKLP1 et AuroraB localise sur les MTs de part et d'autres du cœur du midbody et finalement un troisième groupe composé de centralspindlin et ECT2 est relocalisé vers un renflement autour du coeur du midbody nommée l'anneau du midbody (Hu et al., 2012), **(Figure 1.8a)**.

1.2.6.3 L'anneau du midbody

À la fin de sa constriction l'AC mesure environ 1µm et est convertit en une structure plus stable dans un espace compris entre le réseau compact de MTs et le cortex cellulaire, nommée l'anneau du midbody (AM). Plusieurs des composantes de l'AC, incluant RhoA, l'Anilline, les septines et la kinase Citron sont retenues au niveau de l'AM (Gai et al., 2011; Hu et al., 2012; Madaule et al., 1998). Étonnement, l'Actine et la Myosine ne sont pas retenues à l'AM, en accord avec l'idée que ce complexe est désassemblé au cour de la fermeture de l'AC **(Figure 1.8b)**.

En résumé, le midbody, les MTs qui y sont associés et l'AM qui l'entoure forment le pont intracellulaire, une structure stable qui persiste longtemps est sert de plateforme pour le recrutement et l'organisation des nombreuses protéines nécessaires à l'abscission, qui aboutit à

la rupture de la connexion restante entre les cellules filles et finalise le processus de cytokinèse.

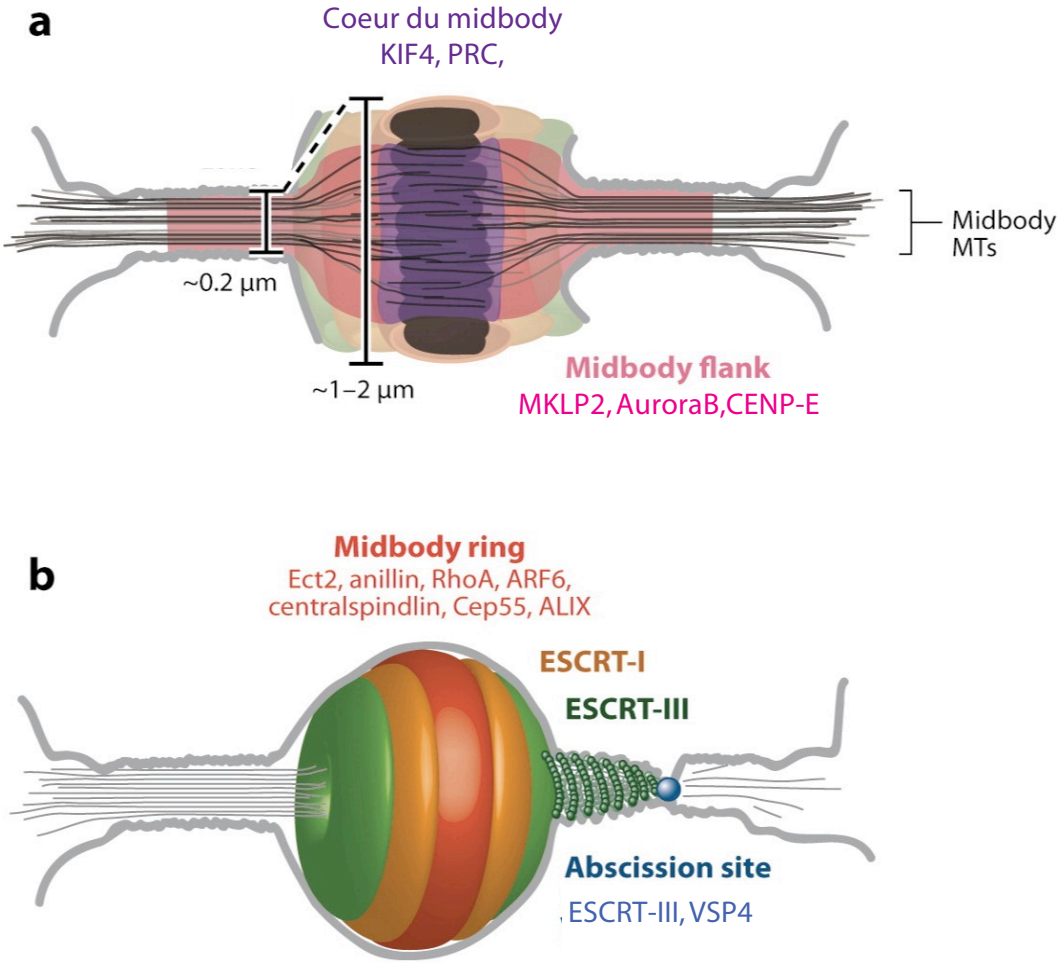

Figure 1.8: Le pont intercellulaire

a-organisation du midbody et des MTsqui composent le pont intercellulaire. **b**-Organisation de l'anneau du midbody et du futur site d'abscission. Adapté de (Green et al., 2012).

1.2.7 L'Abscission

L'étude de l'abscission est relativement récente, notamment car elle nécessite des techniques d'imagerie avancées. Les progrès dans l'utilisation des protéines fluorescentes, de la vidéo microscopie et de la super-résolution ont permis de réaliser les travaux qui ont permis de mieux comprendre ce mécanisme. Au cours de la dernière décennie, différents modèles ont émergés pour expliquer ce processus complexe **(Figure 1.9a)**.

Un premier modèle proposait une rupture physique du pont suivie d'une réparation des extrémités ouvertes (Kanada et al., 2005; LaFlamme et al., 2008). Ce modèle est aujourd'hui peu crédible puisqu'une étude récente a montré que les forces de tension exercés sur le pont ne mènent pas à sa rupture; au contraire, elles semblent plutôt retarder la séparation des cellules filles (Lafaurie-Janvore et al., 2013).

Un deuxième modèle, découle de nombreuses études qui ont clairement établi que le trafic membranaire était un facteur important dans les stades ultérieurs de la cytokinèse (Albertson et al., 2005; Barr and Gruneberg, 2007). Ainsi, Plusieurs études réalisées chez *C. elegans,* la levure fissipare et certaines lignées de cellules humaines ont initialement décrit qu'un blocage de la maturation des vésicules post-Golgi par un composé chimique (Brefeldin A) empêche l'aboutissement de la cytokinèse (Gromley et al., 2005; Skop et al., 2001). Par ailleurs, un complexe macromoléculaire appelé exocyste, responsable de l'ancrage des vésicules à la membrane au cours du transport vésiculaire est également nécessaire à la cytokinèse (Neto et al., 2011). Finalement, plusieurs protéines associées aux vésicules de la famille des RabGTPases sont également requises pour la cytokinèse. Parmi elles, soulignons Rab11 et Rab35 dont la déplétion induit des défauts de cytokinèse majeurs (Kouranti et al., 2006). Ceci dit, bien qu'il soit clairement impliqué dans la cytokinèse, il n'est pas encore clair si le trafic vésiculaire est une partie intégrale de l'abscission ou bien s'il sert uniquement pour le transport des acteurs clés au site d'abscision.

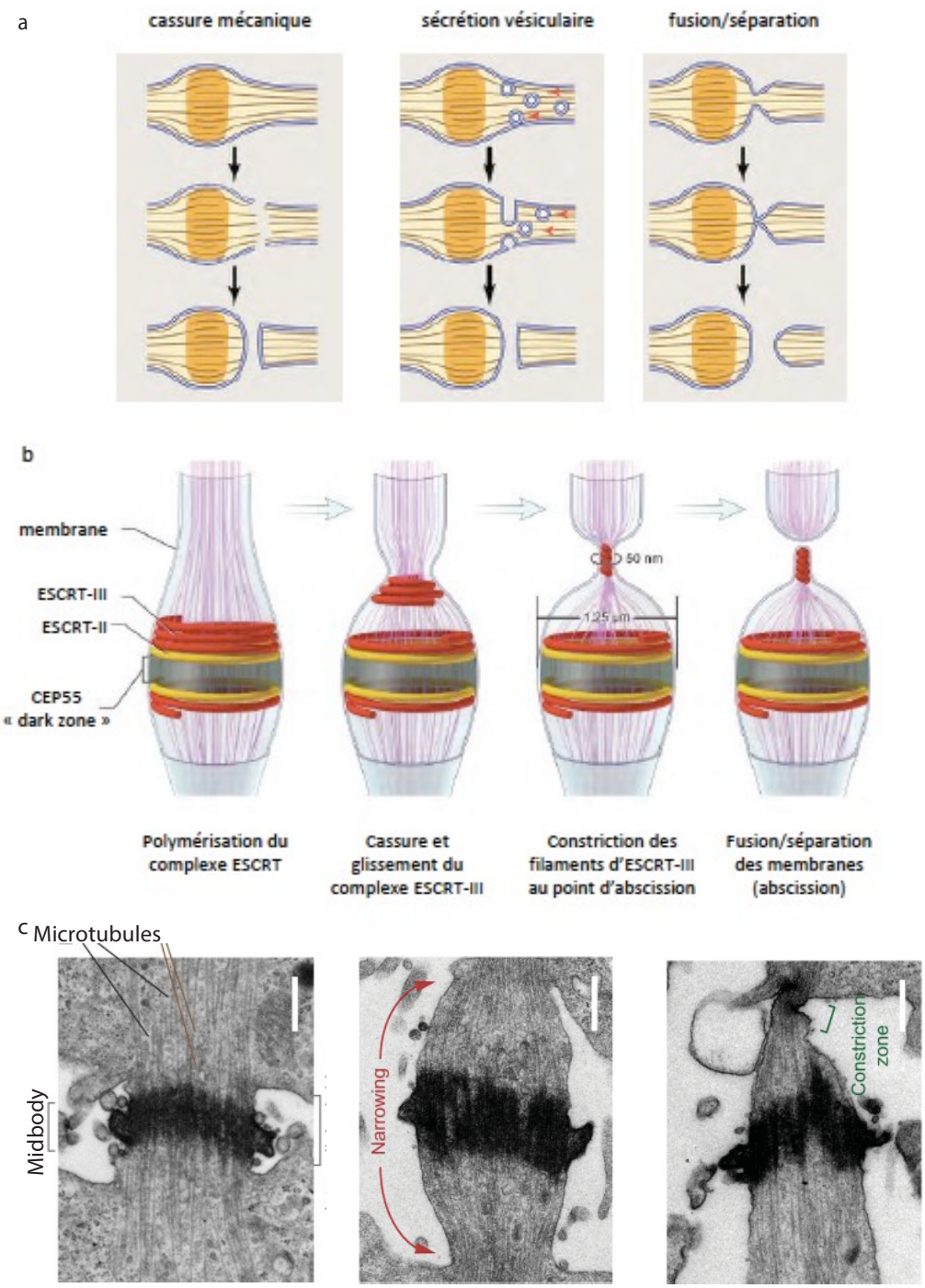

Figure 1.9: L'abscission

a- Différents modèles d'abscission du pont intercellulaire. Adapté d'après (Elia et al., 2011).**b-** Détails du modèle de fusion/séparation des membranes aboutissant à l'abscission.D'après (Elia et al., 2012). **c**-Micrographies électroniques par transmission de ponts intercellulaires de cellules HeLa à différents stades de maturation. Adapté de (Mierzwa and Gerlich, 2014).

Le dernier modèle, et certainement le plus étoffé par la littérature récente stipule que la constriction extrême des membranes en un point du pont intercellulaire permet le rapprochement et **la fusion/séparation** des membranes existantes (Guizetti et al., 2011; Schiel and Prekeris, 2012). Ce modèle repose essentiellement sur la démonstration du recrutement des complexes ESCRT (Endosomal Sorting Complex Required for Transport) au midbody et de leur nécessité pour la cytokinèse (Carlton and Martin-Serrano, 2007). Les protéines ESCRT régissent la fission membranaire au cours du bourgeonnement rétroviral et la formation du corps multivésiculaire (Hurley and Hanson, 2010). Chez les eucaryotes, les composantes du système ESCRT sont au nombre de 5 complexes distincts; ESCRT-0, -I, -II, -III et VPS4 ; avec chacun un rôle précis dans le fonctionnement de cette machinerie. Durant la cytokinèse, le recrutement de ces complexes coïncide avec la perte rapide des MTs associés au midbody et pourrait fournir la force requise pour la constriction et la fusion de la membrane qui conduit à l'abscission finale (Guizetti and Gerlich, 2010). En effet, plusieurs études par imagerie à haute résolution ont démontré que le complexes ESCRTI, ESCRTIII et VPS4 sont recrutés de façon séquentielle au pont intercellulaire. La protéine centrosomale CEP55 recrute la sous unité TSG101 du complexe ESCRT−I et la protéine ALIX (Apoptosis−linked gene-2−interacting protein X) au midbody. À partir de ces complexes CEP55−TSG101 et CEP55−ALIX, le recrutement successif de tous les modules ESCRT−I, ESCRT−II et ESCRT−III va se poursuivre (Elia et al., 2011; Guizetti et al., 2011). ESCRT−III est aujourd'hui le module considéré comme acteur direct de l'abscission **(Figure 1.9b-c)**. En effet, il serait capable de former de manière autonome des filaments de 17nm de diamètre encerclant le pont intercellulaire *in vitro* et *in vivo* juste avant l'abscisison (Guizetti et al., 2011; Henne et al., 2012). Les composants d'ESCRT−III se répartissent au cours de l'abscission en deux régions périphériques du midbody, l'une qui co-localise avec TGS101 au point de recrutement initial, la seconde, à 1µm de la première, qui sera le site précis de clivage final (Elia et al., 2012; Guizetti et al., 2011). Finalement, l'abscission est réalisée soit par un glissement de ces anneaux filamenteux à partir du midbody, soit par une courbure initiée depuis le coeur du pont intercellulaire (Bastos and Barr, 2010; Carlton et al., 2012; Carlton and Martin-Serrano, 2007; Elia et al., 2011; Guizetti et al., 2011; Lafaurie-Janvore et al., 2013).

1.2.8 Le midbody résiduel

Le fait que le pont soit coupé non pas au milieu du midbody; mais d'un coté ou l'autre, génère une division asymétrique où une des cellules filles reste attachée à un résidu du pont intercellulaire, qui formera une structure à part entière nommée le midbody résiduel (MBR) (Chen et al., 2013; Gromley et al., 2005). La composition exacte du MBR reste à déterminer; cependant des analyses par marquages laissent croire qu'il contient les protéines du midbody et de l'anneau du midbody présentes avant l'abscission. On y détecte entre autres, MKLP1, centralspindlin, la kinase Citron, PRC1, KIF14, l'Anilline et CEP55 (Crowell et al., 2014; Dubreuil et al., 2007; Ettinger et al., 2011; Kamasaki et al., 2007; Kechad and Hickson, 2017; Kuo et al., 2011). Le sort du MBR a récemment attiré beaucoup d'attention, car il semble être associé aux cellules souches et la tumorigenèse dans les cellules de mammifères (Chen et al., 2013). En effet, dans les divisions asymétriques de plusieurs tissus, la cellule souche tend à «hériter» du MBR, alors que la cellule différenciée tend plutôt à le rejeter; suggérant que les MBRs pourraient jouer un rôle dans le maintien du potentiel de cellule souche (Ettinger et al., 2011; Kuo et al., 2011). Dans le même ordre d'idées, d'autres études ont démontré que les cellules cancéreuses accumulent des MBRs, contrairement aux cellules normales (Ettinger et al., 2011; Kuo et al., 2011; Pohl and Jentsch, 2009). De plus, les cellules qui accumulent un grand nombre de MBR présentent une tumorigénicité accrue (Kuo et al., 2011). Ainsi, il semble que l'accumulation de résidus du midbody soit associée à une prolifération accrue. Ceci suscite un grand intérêt ces dernières années et plusieurs groupes s'activent à comprendre les mécanismes d'héritage, de rétention et d'élimination du MBR. Deux voies d'héritage du MBR ont été décrites et semblent être spécifiques à différents contextes et types cellulaires. Dans la premiere voie, on rapporte que le MBR est généré par une seule fission d'un côté du midbody. Ce faisant, il reste attaché à une des cellules filles et finit par se rétracter dans le cytoplasme de celle-ci (Chen et al., 2013). Le MBR serait ensuite séquestré dans les autophagosomes et ciblé sur les lysosomes pour la dégradation (Ettinger et al., 2011; Kuo et al., 2011; Pohl and Jentsch, 2009). Dans la seconde voie, le pont serait clivé deux fois de part et d'autre du midbody et relâché dans le milieu extracellulaire (Dubreuil et al., 2007; Ettinger et al., 2011). En accord avec ce scenario, une étude par vidéo microscopie dans laquelle les auteurs ont suivi la diffusion du MBR dans une variété de cellules

cancéreuses et immortalisées, ainsi que dans les cellules souches musculaires, a montré que les MBR sont libérés par des abscissions séquentielles des deux côtés du midbody et ne se rétractent pas dans le cytoplasme. Les MBR libres restent associés à la surface cellulaire pendant plusieurs heures, avant d'être internalisés puis dégradés dans les lysosomes (Crowell et al., 2014). Par ailleurs, ces mêmes auteurs proposent que le MBR ne soit pas seulement hérité par l'une des deux cellules filles mais qu'il peut également être diffusé à plus longue distance et être capté par une autre cellule. Cette diffusion du MBR dans le milieu extracellulaire a également été confirmée récemment *in vivo* chez *C. elegans* et *Drosophila* (Ou et al., 2014; Salzmann et al., 2014). Le MBR pourrait ainsi servir de véhicule pour la signalisation intercellulaire à longue distance.

1.2.9 L'échec de la cytokinèse

Un échec de la cytokinèse peut résulter d'un dysfonctionnement des protéines régulatrices et structurales impliquées dans une des étapes au cours de la progression de la cytokinèse et peut mener à une cytokinèse anormale ou à la multinucléation. Au cours du développement normal, certains processus impliquent des formes spécialisées de la cytokinèse où un échec représente une étape programmée nécessaire pour l'acquisition d'une nouvelle structure ou fonction. Dans ces cas, les pathologies peuvent survenir lorsque la cytokinèse se complète, et non en cas d'échec. Autrement, un échec de la cytokinèse devient problématique et peut avoir de graves conséquences. Je donnerai ici quelques exemples d'échecs de la cytokinèse dans des contextes physiologiques et pathologiques.

1.2.9.1 Variantes de la cytokinèse et polyploidie physiologique

Les cellules germinales présentent un exemple remarquable d'échec de cytokinèse programmée mais qui ne mène pas la binucléation. En effet, ces cellules réalisent une cytokinèse normale mais restent bloquées à l'étape de l'abscission. Ce faisant, elles restent connectées les unes aux autres grâce aux ponts intercellulaires formant ainsi un cyste germinal (Greenbaum et al., 2007). Chez les mammifères, c'est la protéine TEX-14 (Testis expressed 14), exprimée uniquement dans les cellules germinales, qui interagit avec CEP55 au niveau du midbody et prévient le recrutement de TSG-101 et Alix au site de l'abscision (Iwamori et al., 2010). De façon similaire, l'ovogénèse chez *Drosophila* se réalise par 4 cycles de divisions asymétriques

successives suivi d'une cytokinèse incomplète aboutissant à un syncitium de 16 cellules issues du même progéniteur.

La cellularisation, qui se produit pendant le développement des drosophiles est un autre exemple de cytokinèse spécialisée. Le développement embryonnaire chez la drosophile commence par une série rapide de divisions nucléaires mitotiques sans cytokinèse, pour produire un embryon à cellule unique multi nucléée, le blastoderme syncytial. Ce syncytium subit alors un processus de formation cellulaire dans lequel près de 6000 noyaux sont enfermés dans des cellules individuelles. Le processus de cellularisation consiste en l'invagination de la membrane plasmique de l'embryon autour de chacun de ces noyaux pour former une cellule. Initialement, un réseau de cytosquelette hexagonal s'organise sous la membrane plasmique et délimite chaque noyau. Au fur et à mesure que le front de cellularisation franchit les bases des noyaux, les anneaux hexagonaux se résolvent en anneaux discrets qui ressemblent à des anneaux contractiles qui se contracteront ensuite sous les noyaux. Cependant, à la différence de la cytokinèse classique, les cellules ne se ferment pas complètement à leurs bases. Au lieu de cela, chaque cellule conserve un anneau lié à la membrane, entre son cytoplasme et le cytoplasme du vitellus sous-jacent (Mazumdar and Mazumdar, 2002). Remarquablement, ces anneaux rappellent les anneaux contractiles et contiennent de l'actine, de la myosine, de l'Anilline et des septines et des perturbations de l'une ou l'autre de ces composantes causent de défauts de cellularisation (Adam et al., 2000; Field and Alberts, 1995; Field et al., 2005b; Mavrakis et al., 2014; Neufeld and Rubin, 1994).

En règle générale, lorsqu'on parle d'échec de la cytokinèse, on pense à la formation de cellules binuclées polyploides contenant plus que deux ensembles complets de chromosomes. Même si la plupart des cellules somatiques des mammifères sont diploïdes; il existe aussi des cellules polyploïdes dans certains tissus qui sont générées par un échec programmé de la cytokinèse. Dans le foie humain adulte, 30% des hépatocytes sont polyploïdes et constituent 90% de la masse du foie. La binucléation hépatocytaire survient au cours de la maturation postnatale à la suite de défauts de concentration de RhoA au niveau du plan de clivage. En

conséquence, des défauts dans l'organisation de l'actine se produisent et l'anneau contractile n'est pas formé (Gentric et al., 2012). Le but physiologique de cette multinucléation n'est toujours pas clair. Les hépatocytes produisent de nombreuses protéines sériques et de la bile, et détoxiquent la circulation sanguine; la polyploïdie pourrait être nécessaire pour leur métabolisme élevé. Par ailleurs, chez les cellules musculaires lisses vasculaires, la binucléation est associée à la régulation de l'architecture et la motilité des cellules et se produit suite a un phénomène appelé inversion de la cytokinèse. En effet, il semble que les cellules sortent de la mitose malgré des défauts de ségrégation des chromosomes. Ceci a été attribué à un fuseau central aberrant dans ces cellules, résultat de la sous-expression de la Survivine, un membre du complexe CPC (Nagata et al., 2005). Les cardiomyocites se divisent de façon classique au début du développement cardiaque. En revanche, ils ont recours à un échec de la cytokinèse au cours de la vie postnatale pour augmenter leur taille et finaliser la croissance cardiaque. En effet, les cardiomyocytes postnataux perdent leur capacité à compléter la cytokinèse à cause de défauts de localisation de l'Anilline; qui ne parvient pas à se concentrer sur le cortex en anaphase et montre une localisation élargie autour du midbody au cours de la cytokinèse (Engel et al., 2006).

1.2.9.2 Polyploïdie pathologique

Hormis ces situations particulières où un échec de la cytokinèse fait partie du développement normal, des défauts de cytokinèse sont généralement associées à des pathologies, notamment le cancer. En effet, un nombre grandissant d'études supporte l'idée que l'échec de la cytokinèse pourrait promouvoir la tumorigénèse en provoquant la polyploïdie et l'instabilité chromosomique qui en résulte. Théodor Boveri a été le premier à introduire l'idée qu'il pourrait y avoir un lien entre la mitose anormale et les tumeurs malignes. Il a caractérisé le centrosome en 1888 et suggéré qu'une cellule avec plusieurs centrosomes conduirait à l'instabilité génomique et au cancer. Il a proposé que cela pourrait se produire soit à cause d'une division anormale des centrosomes, soit un défaut de la division cellulaire, ce qui conduirait alors à la tétraploïdie (Wunderlich, 2002). Aujourd'hui, il est clairement établi que les cellules polyploïdes sont génétiquement instables et leur présence au sein d'un tissu normalement composé de cellules diploïdes peut être à l'origine de l'apparition de tumeurs (Davoli and de Lange, 2012; Fujiwara et al., 2005). Des défauts de cytokinèse ont été

rapportés dans un bon nombre de cancers (Lacroix and Maddox, 2012). Récemment, il a été démontré directement que les cellules qui avaient échoué un cycle de cytokinèse en culture avaient un plus grand potentiel tumorigènique que leurs homologues diploïdes (Thompson et al., 2010). Dans plusieurs cas, des défauts de la cytokinèse sont la conséquence d'un dérèglement cellulaire propre aux cellules cancéreuses. Cependant, plusieurs études ont démontré un lien causal entre l'échec de la cytokinèse et le développement du cancer (Lacroix and Maddox, 2012; Tormos et al., 2015). Dans les cancers du cerveau que sont les glioblastomes, la présence de cellules aneuploïdes est largement décrite. Une étude récente a rapporté que cette aneuploïdie peut résulter d'un défaut de cytokinèse (Telentschak et al., 2015). Dans le cancer des ovaires, La déplétion du facteur de transcription GATA6 impliqué dans la différentiation des cellules souches, cause un défaut de la cytokinèse, une déformation de l'enveloppe nucléaire et la formation de cellules polyploïdes (Cai et al., 2009). Finalement, plusieurs composantes de la machinerie de la cytokinèse sont surexprimées dans les tumeurs. Notons par exemple la surexpression de la kinésine KIF14 dans les rétinoblastomes (Madhavan et al., 2009). Plusieurs septines sont également mutées chez des patients atteints de leucémie aiguë infantile (Liu et al., 2010). L'Anilline est également impliquée dans la carcinogénèse. En effet, une surexpression de l'Anilline est corrélée au potentiel métastatique de plusieurs tumeurs humaines et l'inhibition de l'Anilline réprime la croissance des cellules de cancers du poumon (Zhang and Maddox, 2010).

Outre le cancer, des défauts de cytokinèse ont été rapportés dans de nombreuses maladies. Le syndrome de Lowe est une maladie causée par une mutation de la protéine OCRL. OCRL agit comme phosphatase des lipides membranaires notamment pour la production du phosphoinositide biphosphate PIP2 qui est nécessaire à la cytokinèse. Chez les cellules de drosophiles, la déplétion d'OCRL mène à l'accumulation de PIP2 sur les membranes de larges vacuoles cytoplasmiques au lieu de l'AC. Cette relocalisation de PIP2 entraine à son tour une relocalisation de l'Anilline et de la myosine vers ces vacuoles et l'échec de la cytokinèse (Ben El Kadhi et al., 2011). De façon similaire, la déplétion d'OCRL dans des cellules humaines cause des défauts de localisation de PIP2, et de l'actine et leur accumulation au pont intercellulaire, bloquant ainsi la cytokinèse. Remarquablement, ces défauts de cytokinèse ont également été observés dans des lignées cellulaires dérivées de

patients atteints du syndrome de Lowe (Dambournet et al., 2011). Par ailleurs, des mutations de la kinase Citron qui causent des défauts de cytokinèse ont été associées à des microencéphalies chez l'humain (Basit et al., 2016; Gai and Di Cunto, 2016; Harding et al., 2016; Shaheen et al., 2016).

Ces nombreux cas de pathologies liées à la cytokinèse ont entrainé un gain d'intérêt pour ce processus, notamment pour le développement de nouveaux traitements qui cibleraient spécifiquement les protéines impliquées uniquement au niveau de la cytokinèse afin de cibler plus spécifiquement les cellules tumorales en division et limiter les effets secondaires sur les cellules somatiques.

1.3 ÉLÉMENTS CLÉS TOUT AU LONG DE LA CYTOKINÈSE

1.3.1 La kinase Citron

La kinase Citron est une protéine multifonctionnelle découverte il y a 20 ans pour son interaction avec les formes activées des Rho GTPases Rho et Rac (Madaule et al., 1998; Madaule et al., 2000). Sticky a ultérieurement été identifiée comme l'orthologue de Citron chez *Drosophila*. Les premières études fonctionnelles de Citron avaient proposé un rôle dans la cytokinèse, notamment du à son enrichissement au niveau de l'AC et l'AM dans des cellules HeLa (Madaule et al., 1998). Depuis, de nombreuses études ont confirmé la localisation de Citron à l'AM ainsi qu'au midbody après la fermeture de l'AC ou elle persiste et sera retenue dans le remnant du midbody après l'abscission (Bassi et al., 2013; D'Avino et al., 2004; D'Avino and Capalbo, 2016; Eda et al., 2001; Gai et al., 2011; Hu et al., 2012; McKenzie and D'Avino, 2016; Naim et al., 2004; Shandala et al., 2004; Watanabe et al., 2013). La surexpression de Citron dans les cellules Hela avait causé des oscillations de l'AC avant sa régression causant un échec de la cytokinèse. Ces résultats ont donné naissance à un modèle où Citron régule la contractilité de l'AC en phosphorylant la myosine. Quelques années plus tard, des études de cribles par RNAi réalisées sur des cellules S2 de *Drosophila* ont montré que la déplétion de Sticky n'affecte pas l'AC mais cause des défauts plus tardifs notamment des défauts d'organisation du pont intercellulaire et une délocalisation de plusieurs protéines de l'AC comme l'Anilline, la septine Peanut et les kinésines KIK14 (Nebbish) et PRC1 (Fascetto) (D'Avino et al., 2004; Echard et al., 2004; Naim et al., 2004).

Des études ultérieures basées sur la protéomique, ainsi que des tests de liaison *in vivo* et *in vitro* ont confirmé une fonction similaire de Citron dans les cellules humaines et ont mis en évidence son rôle dans l'organisation du midbody et l'AM (Bassi et al., 2013; Bassi et al., 2011; Gai et al., 2011; McKenzie et al., 2016; Watanabe et al., 2013).

La kinase Citron a une structure complexe qui contient différents domaines conservés qui régissent ses interactions avec plusieurs protéines clés de la cytokinèse **(Figure 1.10).** Elle possède à son extrémité N-terminale un domaine kinase serine/thréonine dont la seule cible connue est la myosine. Cependant, l'importance de cette phosphorylation durant la cytokinèse demeure controversée (Yamashiro et al., 2003). De plus, Citron interagit avec les kinésines MKLP1 (Pavarroti) and KIF14 (Nebbish,) et le CPC (Bassi et al., 2013; Gruneberg et al., 2006a; McKenzie et al., 2016; Watanabe et al., 2013). Citron et KIF14 sont interdépendants pour leur recrutement mutuel à l'AM et cet interaction est essentielle pour le recrutement de PRC1 (Fascetto) et MKLP1 à l'AM (Bassi et al., 2013) . L'interaction entre Citron et ces protéines associées aux MTs semble être importante pour l'organisation du midbody et du pont intercellulaire (Bassi et al., 2013; Bassi et al., 2011; Watanabe et al., 2010). Citron interagit également avec l'Anilline. En effet, Une fusion de GST avec l'extrémité N-terminale de l'Anilline interagit avec Citron dans des essais de pull down chez les cellules Hela (Gai et al., 2011). Le rôle de cette interaction demeure très peu compris et a été adressée dans les travaux présentés dans cette thèse (voir Chapitre 4).

En résumé, Citron régule la cytokinèse à deux niveaux. D'une part, elle interagit avec plusieurs protéines au midbody et régule leur recrutement , notamment, MKLP1, KIF14 et le CPC. D'autre part, elle relie ces composantes du fuseau central aux composantes de l'AC incluant l'Anilline, la Myosine et RhoA (Bassi et al., 2011; Bassi et al., 2013; Gai et al., 2011; Gruneberg et al. , 2006; McKenzie et al., 2016).

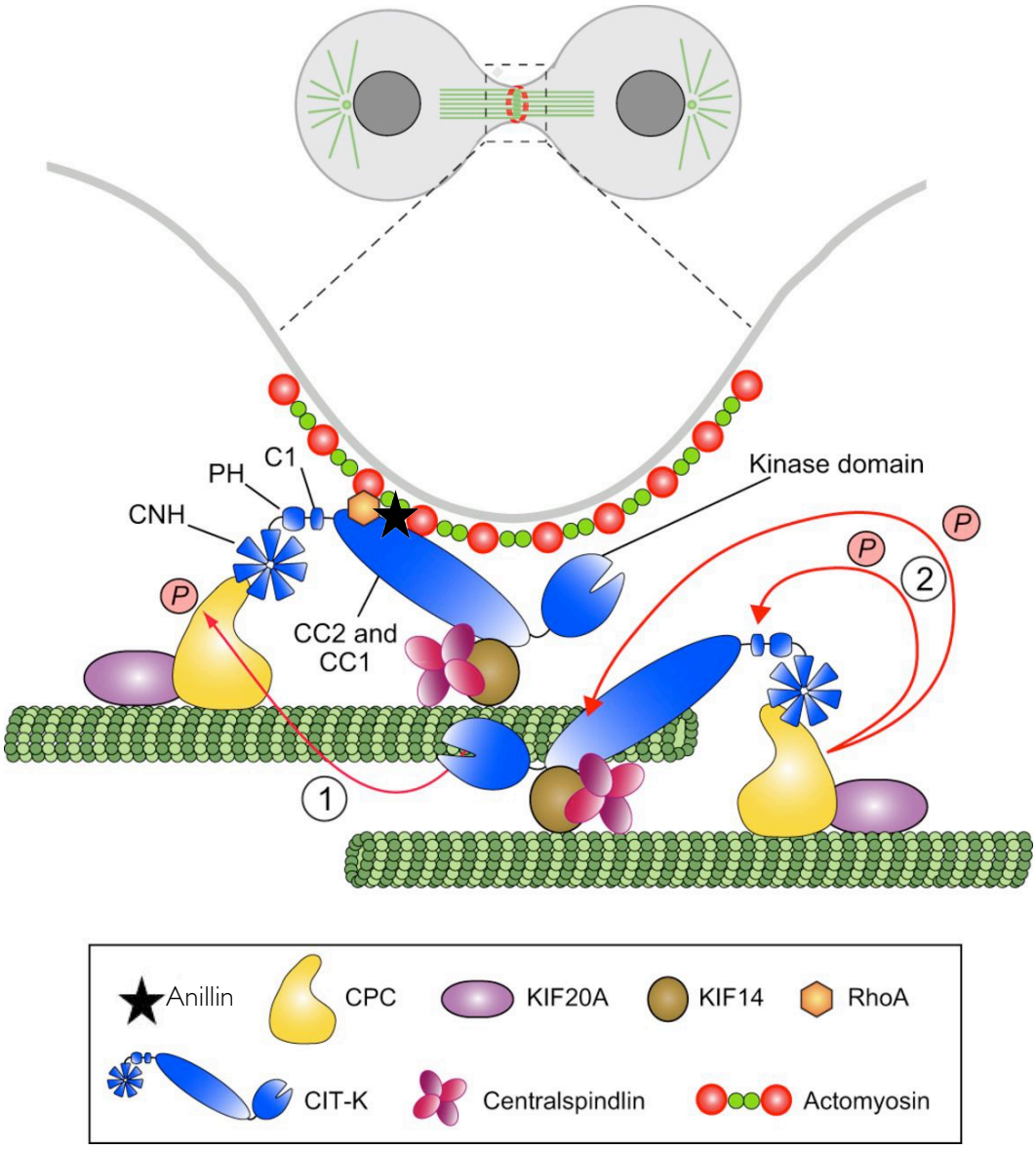

Figure 1.10: Schématisation des interactions de la kinase Citron.

Voir texte pour détails. Adapté de (D'Avino, 2017).

1.3.2 Les Septines

Les Septines ont été découvertes il y a près de 40 ans dans des cribles pour des défauts de division cellulaire dans la levure *Saccharomyces cerevisiae* (Hartwell et al., 1970), et sont depuis reconnues comme des composantes importantes du cytosquelette dans plusieurs espèces. Le nombre de septines présentes varie d'un organisme à l'autre. Par exemple, *Drosophila* a 5 membres (Peanut, Sep1, Sep2, Sep4, Sep5) alors que les humains en ont 13 (Septine 1-12 et Septine 14). Ces GTPases peuvent s'auto-assembler en complexes hétéro et homo oligomériques parfaitement organisés qui peuvent à leur tour se polymériser en filaments non polaires et former des structures d'ordre supérieur telles que des faisceaux, des filaments ou des anneaux **(Figure 1.11)**. Les filaments de Septines se forment par répétition d'une unité hexamèrique ou octamérique composé de 3 ou 4 septines (Versele and Thorner, 2004).

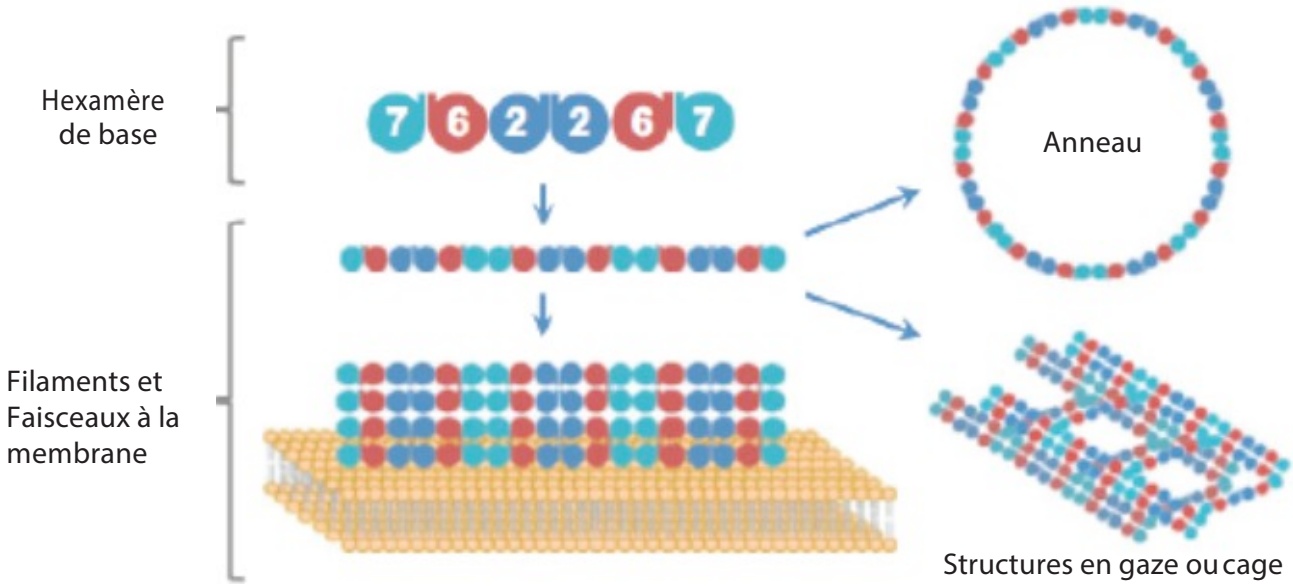

Figure 1.11: Organisation des Septines

Voir texte pour détails. Adapté de (Menon and Gaestel, 2015)

Les septines sont essentielles à la cytokinèse des cellules animales dans de nombreux organismes. Chez *C. elegans*, *Drosophila* et les cellules de mammifères, les septines localisent au sillon de clivage (Fares et al., 1995; Kinoshita et al., 1997; Nguyen et al., 2000) et leur déplétion conduit à la formation de cellules binucléées (Kinoshita et al., 1997; Surka et al., 2002). Chez *Drosophila*, une mutation nulle du gène de la septine Peanut entraine la formation de tissus contenant des amas de cellules multinucléées (Neufeld and Rubin, 1994). Bien que l'on ignore encore comment les septines s'assemblent et interagissent avec d'autres éléments de l'AC, on avait initialement suggéré qu'elles agissent comme des protéines d'échafaudage pour coordonner les changements du cytosquelette et l'organisation membranaire du cytosquelette. En accord avec cette idée, des mutants nuls pour la septine Peanut présentaient des irrégularités au niveaux de l'organisation de l'actine et la myosine dans les canaux annulaire (Ring canals) ainsi que des délais de constriction au cours de la cellularisation (Adam et al., 2000; Mavrakis et al., 2014). Depuis, de plus en plus d'études mettent en évidence l'importance des septines en tant que composantes intégrales de l'AC et pas seulement comme protéines d'échafaudages. Par exemple, la septine de mammifères SEPT2 se lie à la myosine II, et cette association est requise pour l'activation de la myosine pendant la division cellulaire (Joo et al., 2007). De plus, il a été démontré récemment que les septines étaient capables de lier, fasciculer et plier l'actine, ce qui suggère que la liaison des septines à l'Actine est suffisante pour surmonter l'exigence élevée en énergie pour la flexion de l'actine (Mavrakis et al., 2014). Les septines interagissent également avec l'Anilline (Voir section 1.4.3 pour plus de détails) et des mutants de la septine Peanut présentent des défauts de localisation de l'Anilline chez *Drosophila* (Adam et al., 2000).

En plus de lier les composantes de l'AC, les septines peuvent interagir directement avec les lipides, plus particulièrement les phosphatidylinositol phosphates (PIPs) au niveau de la membrane plasmique. En effet, des feuillets de septines ont été observés en étroite apposition à la membrane plasmique (Gilden and Krummel, 2010; Zhang et al., 1999) et semblent jouer un rôle mécanique dans la déformation de la membrane du sillon. La liaison aux PIPs aide au recrutement des septines à la membrane et abaisse également la concentration requise pour leur polymérisation en filaments. Les niveaux élevés de PIPs au niveau du sillon de clivage pourraient agir comme un agent de nucléation pour la formation de filaments de septines.

Dans une étude récente, l'ajout de septines à des liposomes géants a entrainé leur tubulation spontanée *in vitro*, et ce processus a été facilité par la présence de phosphatidylinositol 4-phosphate (PI4P) ou de phosphatidylinositol 4,5-bisphosphate (PIP2) (Takiguchi et al., 2009). Ainsi les septines pourraient orchestrer une synergie en favorisant à la fois la déformation des filaments d'actine, la torsion induite par la myosine et la déformation de la membrane pour permettre un assemblage et une constriction efficace de l'AC.

Enfin, il existe des preuves que les septines régulent le trafic membranaire au cours des derniers stades de la cytokinèse. Dans un modèle proposé de la fonction des septines au cours de la cytokinèse tardive, les septines serviraient à délimiter une zone permissive au milieu du pont intercellulaire où la fusion des vésicules contribue à une abscission réussie (Joo et al., 2007). Par ailleurs, Lorsque les septines ne sont pas recrutées au pont intercellulaire, aucun site de constriction n'est formé et la relocalisation du composant ESCRT III, Chmp4B ne se produit pas, ce qui suggère que les septines sont nécessaires pour la formation du site de constriction (Renshaw et al., 2014).

1.3.3 Les phosphoinositides à la membrane plasmique

La membrane plasmique subit de très importants remodelages au cours de la cytokinèse et sa composition au niveau du sillon de clivage est critique tout au long de ce processus. Les phosphatidylinositol phosphates, ou PIPs représentent certainement la classe de lipides membranaires la plus étudiée avec une contribution claire à la cytokinèse à plusieurs niveaux. Les PIPs sont essentiels pour chaque aspect de la division cellulaire, que ce soit l'arrondissement des cellules mitotiques, l'élongation des cellules, l'orientation des fuseaux, la cytocinèse ou les événements post-cytocinèse (revue dans Brill et al., 2011; Cauvin and Echard, 2015).

Au cours de la cytokinèse, les PIPs jouent un rôle clé dans la régulation de la dynamique du cytosquelette et son association avec les membranes ainsi que le recrutement local de complexes protéiques. En particulier, le phosphatidylinositol (4,5) biphosphate PI(4,5)P2 est un régulateur majeur et conservé au cours de la cytokinèse. Que ce soit chez *S.pombe*, *Drosophila* ou les cellules de mammifères, PI(4,5)P2 s’accumule au sillon de

clivage et est nécessaire pour la cytokinèse. La séquestration de PI(4,5)P2 altère la connexion de l'AC à la membrane du sillon (Field et al., 2005c; Wong et al., 2005) et des drogues qui interfèrent avec l'hydrolyse de PI(4,5)P2 provoquent une instabilité du sillon de clivage et sa régression (Saul et al., 2004). Les PI(4,5)P2 ont des rôles bien documentés dans la régulation de l'actine. En effet, l'activité de plusieurs protéines impliquées dans la dynamique de l'actine-F est régulée par PI(4,5)P2. Ceci inclut les complexes comme la profiline, Arp2/3, N-WASP, la coffiline, la gelsoline ou les protéines de décapsulation (comme CapZ) ou qui sont tous impliqués dans la cytokinèse (Echard et al., 2004; Eggert et al., 2004; Skop et al., 2004; Stock et al., 1999). En plus de l'actine, PI(4,5)P2 au niveau du sillon de clivage interagit et contribue à la localisation de nombreux éléments clés de la cytokinèse (**Figure 1.12**), incluant Rho, la RhoGEF ECT2, MgcRacGAP, les septines, l'Anilline, la myosine II et les protéines de ERM (Ezrin, Radixin, Moesin) (Cauvin and Echard, 2015).

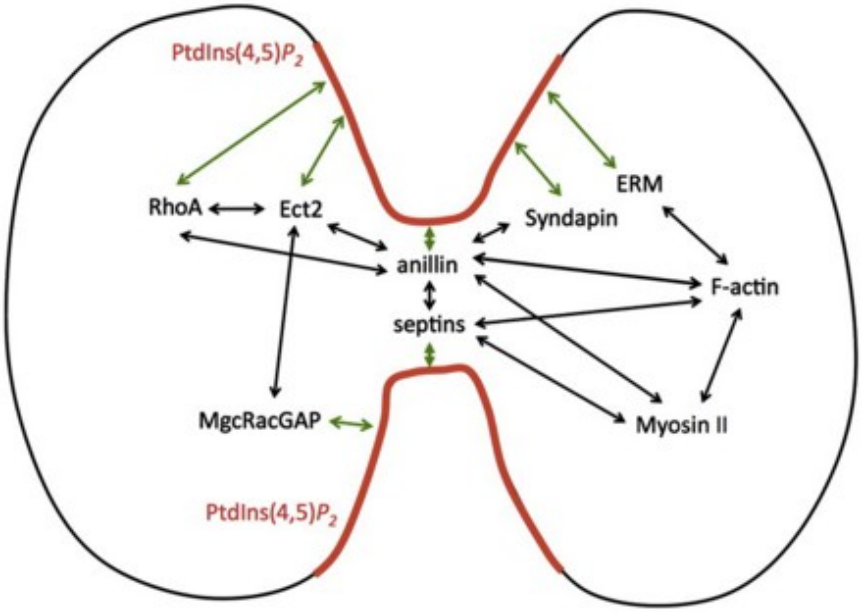

Figure 1.12: Les multiples interactions de PI(4,5)P2 au niveau du sillon de clivage.

PI(4,5)P2 (en rouge) se lie directement et contribue au recrutement ou au maintien de plusieurs protéines clés de la cytokinèse au niveau du sillon de clivage. Adapté de (Cauvin and Echard, 2015).

À travers ces interactions, PI(4,5)P2 joue un rôle critique durant la cytokinèse et contribue à la liaison entre l'AC et le sillon ainsi qu'à la stabilisation du pont intercellulaire. Par ailleurs, des rôles plus tardifs au cours de la cytokinèse ont également été proposés pour le PI(4,5)P2 qui a été impliqué dans l'élimination du remnant du midbody après l'abscission (Crowell et al., 2014).

En plus des PIPs eux mêmes, plusieurs enzymes qui régulent la distribution ou l'état de phosphorylation des phosphatidylinositols ont également été impliqués dans la cytokinèse. Par exemple, une protéine de transfert du phosphatidylinositol codée par le gène vibrator et responsable de l'apport de phosphoinositides à la membrane équatoriale, est essentielle pour la cytokinèse chez la drosophile (Gatt and Glover, 2006; Giansanti et al., 2006). De plus, La phosphatase OCRL, qui déphosphoryle PI(4,5)P2 sur les vésicules d'endocytose et permet son accumulation au sillon de clivage est nécessaire pour la cytokinèse chez les cellules humaines et de drosophiles (Ben El Kadhi et al., 2011; Dambournet et al., 2011). Il a aussi été démontré que les kinases qui agissent sur le phosphoinositol et ses dérivés jouent un rôle direct dans la cytokinèse chez *S. pombe*, *Dictyostelium* et *Drosophila*. Par exemple, la perturbation des PI3 kinases, soit par mutation, soit par des inhibiteurs chimiques, entraine la formation de cellules multinuclées (Brill et al., 2000; Janetopoulos and Devreotes, 2006).

Outres les PIPs, des sous-domaines membranaires, parfois appelés domaines lipidiques (Lipid rafts), enrichis en sphingolipides, en gangliosides et en cholestérol, ainsi qu'en protéines tyrosines phosphorylées semblent également jouer un rôle important dans la division (Ng et al., 2005).

1.4 L'ANILLINE: LE SEIGNEUR DES ANNEAUX

L'Anilline est une protéine d'échafaudage conservée, découverte en 1989 chez *Drosophila* pour ses capacités de lier l'actine filamenteuse (Miller et al., 1989). En 1995, le gène a été cloné et a reçu le nom d'Anillin, dérivé du mot espagnol anillo pour anneau, en raison de sa localisation à l'AC dans les cellules en division (Field and Alberts, 1995). Les allèles de l'Anilline étaient initialement identifiés comme les allèles du gène scraps (scra) dans un crible pour les mutations récessives chez les femelles stériles (Schupbach and Wieschaus, 1989). L'Anilline a ensuite été confirmée comme le produit de scra (Field et al., 2005a) et des homologues de l'Anilline ont été identifiés dans de

nombreux organismes de la levure à l'humain (D'Avino, 2009).

1.4.1 Structure et interactions de l'Anilline

L'Anilline de *Drosophila* contient 1239 acides aminés (Field and Alberts, 1995). Comme ses homologues, elle contient un domaine PH près de l'extrémité C-terminale **(Figure 1.13)**. Une région juste en amont du domaine du PH avec une forte homologie entre les anillines métazoaires est appelée domaine d'homologie de l'Anilline (Anillin Homology Domain ou AHD, Oegema et al., 2000) Ces régions régissent de nombreuses intéractions, notamment avec les septines et RacGAP50C/Tum (D'avino et al., 2008; Gregory et al., 2008). De nombreux motifs de liaison Src-homologie 3 (SH3) et des signaux de localisation nucléaire (NLS) sont prédits à partir de la séquence d'acides aminés. Il a été démontré qu'un NLS situé juste en amont du domaine PH se lie directement aux importines nucléaires (Silverman-Gavrila et al., 2008). À l'extrémité N-terminale réside la région de liaison à l'actine, qui est également responsable de la fasciculation des filaments d'actine (Field et al.,1995; Jananji et al., 2017). Cette région est aussi responsable de l'interaction avec Cindr, homologue de la protéine d'échafaude CD2AP, impliquée dans le remodelage dynamique de l'actine et le trafic membranaire qui se produit au cours de l'endocytose et de la cytokinèse (Haglund et al., 2010). Cette région est hautement conservée entre l'humain, *Xenopus* et *Drosophila* est également responsable de la liaison à la myosine. En effet, il a été démontré que l'Anilline se lie à la myosine II phosphorylée chez *Xenopus laevis* (Straight et al., 2005). Des études par spectrométrie de masse ont également identifié la myosine comme un partenaire de liaison de l'Anilline chez *Drosophila* (D'Avino et al., 2008).

L'Anilline des vertébrés contient 1124 a.a. et est similaire à l'Anilline de drosophiles dans la structure et la fonction. Elle contient également des domaines PH et AHD à son extrémité C-terminale et conserve l'interaction avec les septines (Oegema et al., 2000). Il reste à établir si l'Anilline humaine lie MgcRacGAP; Cependant, il a été rapporté qu'elle interagit à travers son AHD avec d'autres éléments de l'anneau central, notamment la RhoGEF ECT2 (Frenette et al., 2012) et les MTs (van Oostende Triplet et al., 2014). Des interactions supplémentaires ont été révélées entre l'Anilline humaine et RhoA (Piekny and Glotzer, 2008;

Sun et al., 2015) ainsi que P190RhoGAP (Manukyan et al., 2015), impliquant également le domaine AHD. Finalement Le domaine AHD et le domaine PH lient aussi PI(4,5)P2 à la membrane plasmique (Liu et al., 2012; Sun et al., 2015). À son extrémité N-terminale, elle conserve le domaine de liaison à CD2AP (Monzo et al., 2005) et à l'actine (Oegema et al., 2000) et contient en amont de celui-ci un domaine de liaison à la formine mDia 1 (Watanabe et al., 2010). L'extrémité N-terminale interagit également avec la kinase Citron (Gai et al., 2011). Contrairement à l'Anilline de *Drosophila,* trois NLS putatifs sont présents à l'extrémité N- terminale et sont responsables de la localisation nucléaire (Oegema et al., 2000). L'Anilline de mammifères contient également une séquence de boîte de destruction près de l'extrémité N-terminale qui est requise pour l'ubiquitination par APC/C (Zhao and Fang, 2005). L'ubiquitination entraîne la dégradation de l'Anilline à la fin de la division cellulaire.

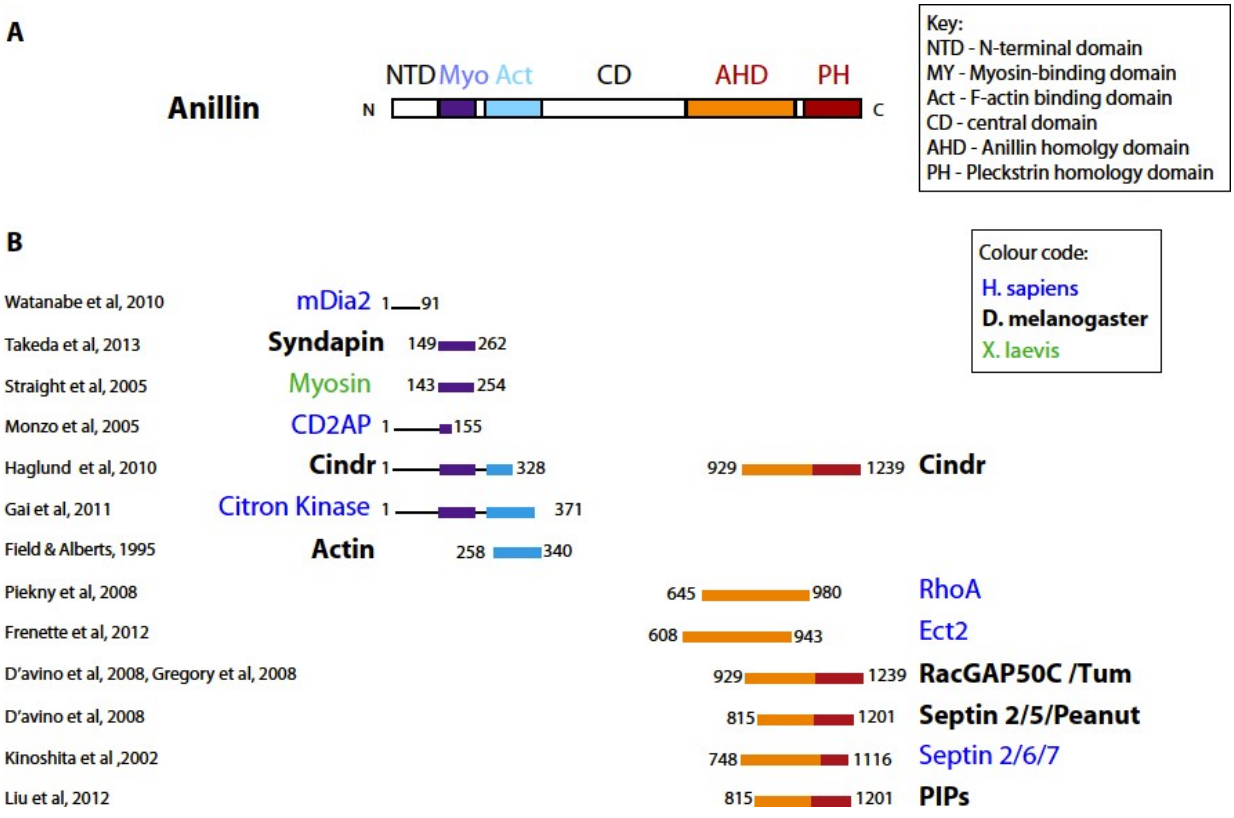

Figure 1.13: l'Anilline, une protéine d'échaffaudage conservée

a- Structure de l'Anilline et ses domaines conservés. **b-** Résumé des protéines interagissant avec l'Anilline à travers les espèces (les différentes expèces sont identifiées par différentes couleurs)

Trois homologues de l'Anilline de *C. elegans*, appelés ANI-1, ANI-2 et ANI-3, contiennent tous un domaine PH et un AHD à leur extrémité C-terminale (Maddox et al., 2005). ANI-1 est la plus proche de la conservation globale de l'Anilline car elle contient des régions présentant des similarités de séquence avec les régions de liaison à l'actine et à la myosine. Aucun domaine ou motif conservé n'a été décrit dans les régions N-terminales de ANI-2 ou ANI-3.

Deux protéines liées à l'Anilline ont été identifiées chez la levure soit Mid1p et Mid2p chez *S. pombe*. Mid1p contient également un domaine PH à son extrémité C-terminale et un domaine AHD qui lie PIP2 (Sun et al., 2015). Mid1p contient un site NLS ainsi que deux signaux de sortie nucléaire, tous deux nécessaires à sa localisation (Paoletti and Chang, 2000) et interagit avec la chaine lourde la myosine-II (Motegi et al., 2006).

1.4.2 Expression et localisation

Chez *Drosophila* et l'humain, l'Anilline est exprimée tout au long du développement et dans une grade variété de tissus ainsi que dans les cellules en culture (Field and Alberts, 1995; Hall et al., 2005). Dans les cellules en division, l'Anilline localise au noyau en interphase; relocalise au cortex cellulaire pendant la métaphase et s'enrichit à l'équateur pendant l'anaphase. Elle marque l'AC et l'AM jusqu'à la fin de la cytokinèse, et est maintenue sur le remnant du midbody après l'abscision **(Figure 1.14)**. À la fin de la division cellulaire, l'Anilline est dégradée et la protéine est synthétisée de nouveau au cours du prochain cycle cellulaire (Hickson and O'Farrell, 2008; Oegema et al., 2000; Straight et al., 2005; Zhao and Fang, 2005).

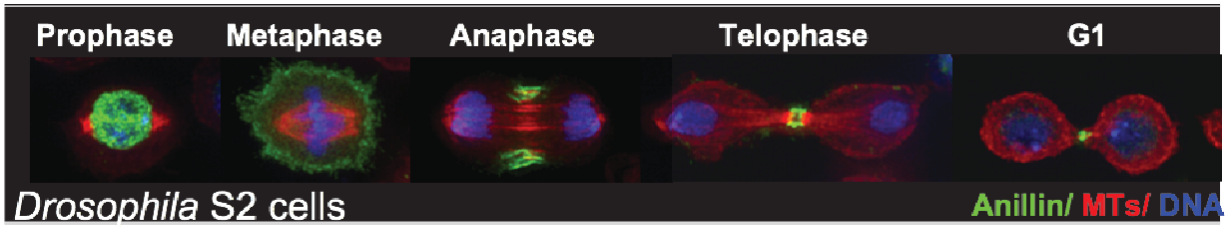

Figure 1.14: Localisation de l'Anilline dans les cellules en division Voir texte pour détails.

Chez *C. elegans*, la localisation de l'Anilline suggère des fonctions spécialisées pour les différents homologues. ANI-1 et ANI-2 sont exprimés dans des tissus et des stades de développement en grande partie non chevauchants (Maddox et al., 2005). ANI-1 est principalement exprimée dans l'embryon et localise au sillon de clivage au cours de la cytokinèse embryonnaire précoce. En revanche, ANI-2 est principalement exprimée chez le ver adulte. Dans le syncytium germinal adulte de *C. elegans*, ANI-1 et ANI-2 s'accumulent sur les ponts intercellulaires stables reliant les cellules. ANI-1 est présente dans toutes les cellules embryonnaires, tandis que ANI-2 est spécifiquement exprimée dans le blastomère P4 au début de l'embryogenèse (Amini et al., 2014; Goupil et al, 2017).

Chez *S. pombe*, il semble qu'une combinaison des deux homologues reproduise la localisation de la protéine humaine. Dans les cellules en interphase, Mid1p se localise principalement au noyau, (Bahler et al.,1998; Paoletti et Chang, 2000; Sohrmann et al., 1996). Après l'entrée en mitose, Mid1p est exporté du noyau et devient la première protéine liée à la cytokinèse détectée à l'équateur (Wu et al., 2003). Elle reste associée à l'équateur jusqu'à la formation du septum, suite à quoi, elle est renvoyée au noyau. Mid2p est recrutée à l'anneau médian beaucoup plus tard que Mid1p et s'associe aux septines (Berlin et al., 2003; Tasto et al., 2003). Une fois la division terminée, Mid2p est ubiquitinée et dégradée (Tasto et al., 2003).

1.4.3 Fonctions de l'Anilline

Vu la multitude de ses partenaires, que ce soit au niveau de l'AC, du midbody ou à la membrane, il n'est pas surprenant que l'Anilline joue un rôle central durant la cytokinèse. Comme sa structure, sa fonction au cours de la cytokinèse semble être hautement conservée. L'Anilline est essentielle à la cytokinèse et sa déplétion par injection d'anticorps ou ARN interférent dans diverses lignées cellulaires conduit à la formation de cellules multinucléées (D'Avino et al., 2008; Echard et al., 2004; Hickson and O'Farrell, 2008; Oegema et al., 2000; Straight et al., 2005; Piekny and Glotzer, 2007; Zhao et al., 2005). Suite à sa découverte, on avait prédit qu'elle serait nécessaire à la formation de l'AC compte tenu de sa localisation précoce dans le sillon et de sa capacité à lier et fasciculer l'actine- F (Field and Alberts, 1995). Cependant, des études plus détaillées ont montré que l'Anilline ne prévient pas la formation de

l'AC mais cause plutôt sa déstabilisation et régression, menant ultimement à un échec de la cytokinèse (D'Avino et al., 2008; Echard et al., 2004; Hickson and O'Farrell, 2008; Oegema et al., 2000; Straight et al., 2005; Piekny and Glotzer, 2007; Zhao et al., 2005). Depuis, beaucoup de progrès ont été réalisés dans notre compréhension des fonctions de l'Anilline. Dans la section qui suit je résumerai les fonctions connues ou prédites pour l'Anilline en fonction de ses différents partenaires. Ma contribution à la compréhension des rôles de l'Anilline durant la cytokinèse sera discutée plus longuement au Chapitre 7.

1.4.3.1 Génération d'une zone active de Rho A

L'Anilline humaine interagit avec RhoA via son domaine AHD et la déplétion de l'Anilline réduit le recrutement de RhoA au cortex équatorial dans les cellules humaines (Piekny and Glotzer, 2008) et les spermatozoïdes chez Drosophila Ainsi, le recrutement de l'Anilline au sillon de clivage dépend de Rho, mais une fois recrutée l'Anilline participe au maintien de Rho au cortex (Hickson and O'Farrell, 2008; Piekny and Glotzer, 2007). En accord avec cette idée, l'Anilline interagit également avec les régulateurs de l'activation de RhoA. Dans les cellules humaines, l'Anilline interagit directement avec la RhoGEF ECT2 via son domaine AHD. Une mutation de ECT2 qui diminue son interaction avec l'Anilline diminue également l'association de ECT2 à la membrane et l'activation de RhoA au cortex équatorial (Frenette et al., 2012). l'Anilline humaine interagit également avec p190 RhoGAP et des mutants de p190 RHOGAP qui sont incapables de lier l'Anilline causent une sur-activation de RhoA et un échec de la cytokinèse (Manukyan et al., 2015)**.** Ainsi en liant Rho A et ses régulateurs l'Anilline pourrait réguler à la fois la production et la stabilisation de Rho au cortex équatorial afin de former un sillon de clivage robuste.

1.4.3.2 Recrutement et échafaudage des composantes de l'AC

La perte de l'Anilline n'empêche pas la formation de l'AC, ni le recrutement de l'actine-F et de la myosine à celui-ci; mais cause plutôt leur délocalisation à l'extérieur de la zone équatoriale. Plusieurs travaux ont montré que l'actine-F, la myosine et l'Anilline sont recrutées de façon indépendante à l'AC dans les cellules humaines et de drosophiles et que leur interaction sert plutôt à renforcer et stabiliser leur recrutement mutuel à l'équateur de la cellule afin de stabiliser l'AC et permettre sa fermeture (Giansanti et al., 1999; Hickson and O'Farrell, 2008; Oegema et al., 2000; Straight et al., 2005). Une étude récente menée dans

notre laboratoire soutient également cette idée. En effet, un mutant d'Anilline qui ne contient pas le domaine de liaison à l'actine est recruté à l'AC et soutient sa fermeture, cependant, il occupe une zone plus étroite au niveau de l'équateur et se montre moins efficace à soutenir la cytokinèse que la protéine sauvage. D'autre part, lorsqu'exprimé seul dans la cellule, le domaine de liaison à l'actine dépend de l'actine pour son recrutement au cortex, ce qui suggère que l'actine contribue également au bon recrutement de l'Anilline. De plus, cette étude a montré que l'Anilline contient trois sites distincts de liaison à l'actine. Individuellement, chacun permet un mode de liaison différent et collectivement ils permettent différentes organisations de l'actine (Jananji et al., 2017). L'Anilline interagit également avec la formine mDia et régule sa localization au cortex (Watanabe et al., 2010). Ainsi, à travers son interaction avec l'actine, et ses nucléateurs, l'Anilline pourrait réguler à la fois la polymérisation et l'organisation de l'actine afin de moduler la rigidité ou la morphologie de l'actine au sein de l'AC. Pour ce qui est de la myosine, l'Anilline pourrait favoriser son interaction avec l'actine au sein de l'AC afin de promouvoir sa contractilité.

L'Anilline lie et recrute les septines. Dans les cellules de mammifères et de drosophiles, l'expression de l'extrémité C-terminale de l'Anilline, qui comprend le domaine PH et une courte séquence en amont, induit la formation de structures corticales ectopiques contenant l'Anilline et la septine SEPT7 / Peanut (Hickson and O'Farrell, 2008; Oegema et al., 2000). Chez Drosophila, une étude par spectrométrie de masse des protéines interagissant avec l'Anilline a identifié trois septines: Peanut, Sep2 et Sep5 (D'Avino et al., 2008; Silverman-Gavrila et al., 2008). *In vivo* des mutations dans le domaine PH de l'Anilline causent des défauts de localisation de Peanut au front de cellularisation (Field et al., 2005a). Dans les spermatozoïdes ou les cellules en culture, la déplétion de l'Anilline cause également des défauts dans le recrutement et l'organisation des septines au niveau de l'AC (Goldbach et al., 2010; Hickson and O'Farrell, 2008). Une fois recrutés par l'Anilline, les septines contribuent également à son maintien au niveau de l'AC. Chez *Drosophila* des mutants nuls pour Peanut sont incapables de maintenir et d'organiser l'Anilline sur les sillons de cellularisation (Adam et al., 2000). Cette relation d'interdépendance entre les septines et l'Anilline semble être conservée. En effet, chez *C. elegans*, ANI-1 est nécessaire pour l'enrichissement des septines dans l'AC, et les septines de *C.elegans* sont

nécessaires pour la localisation asymétrique de l'Anilline (Maddox et al., 2007). De façon similaire, Mid2 chez *S.pombe* dépend des septines pour sa localisation équatoriale (Tasto et al., 2003).

1.4.3.3 Ancrage de l'anneau contractile au sillon de clivage

C'est une hypothèse de longue date que l'Anilline lie la membrane plasmique (Oegema et al., 2000). En accord avec cette idée, l'expression de l'extrémité C-terminale de l'Anilline contenant les domaines AHD-PH est suffisante pour localiser l'Anilline au niveau de la membrane équatoriale et la délétion du domaine PH de l'Anilline empêche son recrutement au cortex chez les cellules humaines (Piekny and Glotzer, 2008). Cependant, les mécanismes régissant cette interaction sont restés peu compris. Récemment, différentes études structurelles et fonctionnelles dont les nôtres (Chapitres 4,5) ont permis de mieux caractériser les différents domaines requis pour cette interaction ainsi que son rôle durant cytokinèse. Nous discuterons en détail de ces travaux dans le chapitre 7.

Par ailleurs, deux études indépendantes ont rapporté une interaction entre RacGAP50C/Tum et l'Anilline chez *Drosophila*. Cette interaction nécessite également le domaine AHD et bien qu'on ignore sa fonction, il a été proposé qu'elle serve à lier le fuseau central à l'AC pour stabiliser le sillon de clivage au début de la cytokinèse (D'Avino et al., 2008; Gregory et al., 2008). Les travaux présentés dans cette thèse menés en parallèle à ces études ont également permis de mieux comprendre les différents rôles de ces interactions de l'Anilline durant la cytokinèse (Chapitre 6 et 7).

1.4.3.4 Interaction avec les microtubules

En plus des interactions entre l'Anilline et les protéines de l'AC, il existe également des évidences que l'Anilline lie les microtubules. L'Anilline a été isolée à partir d'extraits de *Drosophila* sur la base de son affinité pour l'actine-F et les MTs (Field and Alberts, 1995). Chez *C. elegans*, ANI-1 co-sédimente avec des MTs *in vitro* et localise aux MTs astraux qui entrent en contact avec le cortex (Tse et al., 2011). Cette propriété semble être conservée dans les cellules humaines car l'Anilline co-sédimente aussi avec les MTs *in vitro*. Le domaine requis pour cette interaction se situe dans le AHD et chevauche le domaine de liaison à Rho. Dans les cellules Hela, l'Anilline localise sur les MTs astraux et s'enrichit à leurs extrémités

positives après leur stabilisation par un traitement au taxol. Dans des cellules où on a induit une sur-extension des MTs astraux, la déplétion de l'Anilline réduit leur capacité à restreindre le recrutement des protéines corticales comme la myosine à la zone équatoriale. La déplétion de l'Anilline cause également une relocalisation de NuMa, une protéine du cortex polaire, vers le cortex équatorial (van Oostende Triplet et al., 2014). Ainsi, à travers son interaction avec les MTs astraux, l'Anilline pourrait contribuer au bon établissement des domaines équatorial et polaire du cortex sus-jacent, assurant ainsi une formation robuste de l'AC. Chez *Drosophila*, une liaison directe entre l'Anilline et les MTs n'a pas été démontrée. Cependant, des structures riches en Anilline qui se forment à la suite du traitement par la drogue Latrunculine A sont souvent associées avec les extrémités positives des MTs astraux (D'Avino et al., 2008; Hickson and O'Farrell, 2008).

1.4.3.5 Autres fonctions

Récemment, l'Anilline a été impliquée en dehors de la cytokinèse. En autres, l'Anilline semble requise pour le maintien des jonctions intercellulaires. Chez les embryons de *Xenopus*, l'Anilline localise aux jonctions intercellulaires des cellules épithéliales et régule leur intégrité en interagissant avec RhoA, l'actine et la myosine. La déplétion de l'Anilline cause des défauts des jonctions serrées et jonctions adherens et défait l'organisation de l'épithélium (Reyes et al., 2014). Des résultats similaires ont aussi été observées chez l'humain, ou une diminution de l'expression de l'Anilline dans les cellules épithéliales de la prostate, du côlon et du poumon humain cause également le désassemblage des jonctions serrées et adherens et une désorganisation du cytosquelette d'actine et de myosine associé aux jonctions (Wang et al., 2015). Dans le corps humain, l'expression de l'Anilline est plus élevée dans le système nerveux central, ce qui suggère qu'elle peut également être importante pour le développement et/ou la fonction du système nerveux. Comme de fait, plusieurs études ont impliqué l'Anilline dans différents processus au niveau du système nerveux. Chez le poisson zébré, l'Anilline semble jouer un rôle dans les divisons asymétriques des progéniteurs neuronaux. En effet, les progéniteurs de cellules ganglionnaires rétiniennes se divisent de façon asymétriques et positionnent le midbody riche en Anilline au niveau du domaine apical de façon à être hérité par la cellule fille qui va se différencier. Les conditions hypomorphes de l'Anilline perturbent l'hérédité du domaine apical asymétrique et affectent le destin des cellules filles (Paolini et al.,

2015). Chez *C. elegans*, ANI-1 est un régulateur important de la migration des neuroblastes Q et de la formation des neurites, deux processus nécessaires à l'établissement d'un système nerveux fonctionnel (Tian et al., 2015). Ainsi l'Anilline semble réguler plusieurs autres processus à travers des interactions similaires à celles qui régulent la cytokinèse.

1.4.4 Pathologies reliées a l'Anilline

À la lumière des nombreuse interactions et fonctions de l'Anilline durant la cytokinèse, il n'est pas surprenant de voir que l'Anilline a été liée à de nombreuses maladies, plus particulièrement au cancer. En effet, une augmentation progressive de l'expression de l'ARNm de l'Anilline à été corrélée à la progression tumorale dans les tumeurs mammaires, ovariennes, rénales, colorectales, hépatiques, pulmonaires, endométriales et pancréatiques. De plus, les niveaux de l'Anilline sont proportionnels à l'agressivité et au potentiel métastatique des tumeurs (Hall et al., 2005). Une surexpression de l'Anilline est a été rapportée dans plusieurs cancers notamment dans le cancer pancréatique, colorectal et le cancer du sein ou elle est associée à l'invasion tumorale, l'augmentation de la taille des tumeurs et un mauvais pronostic (Magnusson et al., 2016; Olakowski et al., 2009; Wagner and Glotzer, 2016). Ces études sont pour la plupart corrélatives et on ignore si ces observations sont reliées à la fonction de l'Anilline durant la cytokinèse ou à d'autres fonctions non connues de l'Anilline. Dans le cas du cancer du sein, en accord avec le rôle de l'Anilline pendant la cytokinèse, une diminution transitoire de l'expression de l'Anilline dans les lignées cellulaires du cancer du sein a entrainé une augmentation des cellules sénescentes et une accumulation de cellules dans la phase G2 / M du cycle cellulaire avec une morphologie cellulaire modifiée incluant l'apparition de cellules polynucléées. Alternativement, la surexpression de l'Anilline pourrait causer une augmentation des niveaux cytosoliques dans des cellules en interphase ce qui pourrait altérer les cytosquelette d'actine, de septines ou causer des défauts au niveau des jonctions et causer des changements morphologiques favorables au développement des métastases. En accord avec cette idée, la surexpression de l'Anilline dans le cancer des poumons cause une augmentation des niveaux de RhoA et de la motricité cellulaire (Suzuki et al, 2005). Des mutations de l'Anilline ont également été rapportées chez des patients atteints de glomérulosclérose segmentaire focale (FSGS), une forme rare de syndrome néphrotique qui peut causer

l'insuffisance rénale. L'Anilline est surexprimé dans les podocytes (cellules épithéliales du glomérule) dans les échantillons de biopsie rénale chez les individus atteints de FSGS. De plus, ces mutants d'Anilline présentent une liaison réduite à la protéine d'échafaudage CD2AP et leur surexpression dans des podocytes humains immortalisés augmente leur motricité (Gbadegesin et al., 2014)**.** Une meilleure compréhension des fonctions de l'Anilline durant et hors de la cytokinèse et comment un dérèglement de ces fonctions peut mener au cancer est nécessaire. L'Anilline pourrait être la cible de nouvelles thérapies afin de cibler plus spécifiquement les cellules tumorales et minimiser les effets secondaires des traitements.

2 ÉNONCÉ DE LA THÈSE

2.1 CONTEXTE

On a supposé autrefois que la cytokinèse était un processus mécanique relativement simple. Aujourd'hui, ce n'est plus le cas. Plus de 20 ans de travaux ont révélé que la cytokinèse était un processus complexe qui utilise une machinerie moléculaire robuste qui s'assemble avec une grande précision spatio-temporelle. Le défi reste de comprendre précisément comment ces protéines coopèrent dans l'espace et le temps, comment elles interagissent avec les membranes, comment l'ensemble de la machinerie évolue au cours de la cytokinèse et comment cette machinerie s'adapte aux différents contextes développementaux.

2.2 PROBLÉMATIQUE

La cytokinèse des cellules animales passe par la constriction d'un anneau contractile (AC) à base d'acto-myosine. Lorsqu'il atteint un diamètre de ~ 1 µm, un anneau du midbody (AM) se forme pour stabiliser le pont intercellulaire jusqu'à l'abscission. Ces structures partagent la même machinerie mais on ignore comment la fermeture de l'AC est couplée à la formation de l'AM. La protéine d'échafaudage, Anilline, est au coeur de cette machinerie. Elle localise à l'AC et l'AM et sa déplétion n'affecte pas l'assemblage de l'AC, mais bloque plutôt la cytokinèse à un temps plus tardif. Elle permet également d'échafauder de nombreuses autres composantes de la machinerie de la cytokinèse mais on ignore comment l'Anilline agit avec ses nombreux partenaires et les rôles de ses interactions tout au long de la cytokinèse.

2.3 HYPOTHÈSE ET OBJECTIFS

L'objectif principal de cette thèse est de comprendre comment les différents domaines de l'Anilline régulent des étapes spécifiques pendant la cytokinèse. Plus précisément, j'ai voulu :

1) Déterminer comment l'Anilline coordonne la transition de l'AC à l'AM
2) Déterminer comment l'ancrage de la membrane plasmique est maintenu durant la transition de l'AC à l'AM
3) Disséquer comment l'Anilline couple la formation de l'AM à la maturation du midbody

2.4 APPROCHE EXPERIMENTALE

Afin de disséquer les rôles de l'Anilline tout au long de la cytokinèse, nous avons effectué une analyse structure-fonction de l'Anilline par imagerie en temps réel. Pour ce faire, nous avons utilisé les cellules S2 de *Drosophila* comme système modèle. De nombreuses caractéristiques font des cellules S2 un modèle simple mais puissant pour l'étude de la cytokinèse des cellules animales. Premièrement, la plupart des gènes impliqués dans la cytokinèse et leurs fonctions sont conservés des drosophiles aux mammifères. De plus, les drosophiles ont un génome simple qui présente moins de redondance fonctionnelle comparé aux génomes de mammifères, ce qui facilite les études de perte de fonction et l'interprétation des phénotypes observés. Elles présentent également une sensibilité exquise à l'ARNi induit par de longs ARNdb, qui sont à la fois efficaces et simples à générer en laboratoire. Ce système permet ainsi de combiner l'expression de protéines fluorescentes exogènes et la déplétion des protéines endogènes afin d'effectuer des analyses de fonction, des expériences de sauvetage et des analyses de structure fonction dans les cellules vivantes. Finalement, les cellules S2 sont facilement maintenues à température ambiante (20-25 °C) dans des conditions atmosphériques normales (pas de CO2), ce qui les rend idéales pour la microscopie en temps réel et permet ainsi d'extraire des données qualitatives et quantitatives.

2.5 CONTRIBUTION

Les travaux présentés dans cette thèse ont contribué à l'avancement des connaissances dans le domaine de la cytokinèse à plusieurs niveaux :

- **Le chapitre 3** présente un chapitre de livre publié dans lequel je décris les protocoles détaillés utilisés dans notre laboratoire pour l'étude de la cytokinèse par microscopie en temps réel.
- **Le chapitre 4** est un manuscrit publié qui décrit en détail les phénotypes de déplétion de l'Anilline ainsi qu'une étude structure fonction qui a permis de caractériser les rôles des différents domaines de l'Anilline durant la cytokinèse. Un des résultats majeur de cette étude est la caractérisation d'une étape clé durant la cytokinèse que nous avons nommée: la transition de l'AC à l'AM. Auparavant, l'AC et l'AM ont été étudiés

séparément, mais nos travaux montrent que l'AM découle de l'AC via des mécanismes dépendants de l'Anilline. Nous avons également mis à jour les rôles de l'Anilline et des septines comme protéines d'ancrage de l'AM à la membrane.

- **Le chapitre 5** est un manuscrit publié qui représente la suite des travaux présentés dans le chapitre 4. On y présente une caractérisation plus approfondie des mécanismes régulant la transition de l'AC à l'AM ainsi que les rôles de l'Anilline, des septines et de la kinase Citron durant cette transition Entre autre nous décrivons un processus peu connu qui nécessite la perte de la membrane plasmique et des protéines corticales qui y sont associées lors de la maturation de l'AM.
- **Le chapitre 6** est un manuscrit en préparation qui s'intéresse à la relation entre la maturation de l'AC en AM et la maturation du fuseau mitotique en midbody qui se produit en parallèle. J'y décrit une étude structure function de RacGAP50C/Tum qui a révélé son rôle comme protéine clé tout au long de la cytokinèse. Ensuite, je me suis particulièrement intéressée à l'interaction de l'Anilline et RacGAP50C/Tum et présente un rôle de cette interaction durant la transition de l'AC à l'AM.

3 IMAGING CYTOKINESIS OF DROSOPHILA S2 CELLS

Amel Kechad[1,2] & Gilles R. X. Hickson[1,2,3]

[1] Sainte-Justine Hospital Research Center, 3175 Chemin de la Côte Ste-Catherine, Montreal, QC H3T 1C5, Canada.

[2]Département de Pathologie et Biologie Cellulaire, Université de Montréal, P.O. Box 6128, Station Centre-Ville, Montréal, QC H3C 3J7, Canada.

Running title: Cytokinesis of S2 cells

Keywords: *Drosophila* S2 cells; live-cell imaging; RNAi; cytokinesis; midbody; abscission

Manuscript #: 28065320, Epub: 6 mai 2016.

Kechad,A., and G.R Hickson. 2017. Imaging cytokinesis of *Drosophila* S2 cells. *Methods Cell Biol*. 137:47-72

Contributions:

AK et GH ont rédigé le chapitre.

AK a produit les tableaux et les figures.

3.1 ABSTRACT

Animal cell cytokinesis proceeds through three successive stages: a contractile ring stage; an intercellular bridge stage and an abscission stage. Many studies have identified a complex network of key proteins required for successful cytokinesis. While each component interacts with, and depends on, several other components, our understanding of how these proteins cooperate in space and time to ensure faithful progression through the stages of cytokinesis remains incomplete. A full understanding of the complexity of the process and its underlying machinery necessitates experimental systems that allow both genetic manipulation and real-time visualization of the various components throughout the successive stages of cytokinesis. Cultured *Drosophila* S2 cells provide such a system. They are genetically tractable thanks to their exquisite sensitivity to RNA interference mediated by double stranded (ds) RNAs, which can be generated with ease in the laboratory. Furthermore, S2 cells grow well under normal atmospheric conditions, and stable lines expressing fluorescently-tagged proteins can be readily generated, making them ideal for long-term live cell fluorescence microscopy.

Here we describe methodology for exploiting S2 cells for the study of cytokinesis, with an emphasis on live-cell imaging. We describe a variety of fluorescent markers available and their utility for highlighting different structures at different stages of cytokinesis. We describe our experimental set-up that forms the basis for live-cell analysis of loss-of-function RNAi experiments, rescue experiments and structure-function analyses of key regulators of cytokinesis. Finally, we describe the types of phenotypes that one can observe at the different stages of *Drosophila* S2 cell cytokinesis.

3.2 INTRODUCTION

Cytokinesis is the evolutionarily conserved process by which a cell physically separates into two, ensuring the proper partitioning of nuclei and cytoplasmic contents at the end of cell division. It is a highly regulated process that, in animal cells, occurs in three distinct and successive stages: a contractile ring stage; an intercellular bridge stage; and an abscission stage (reviewed in Barr and Gruneberg, 2007; Glotzer, 2009; Gould, 2016; Green et al., 2012; Steigemann and Gerlich, 2009).

Cytokinesis employs robust molecular machinery that assembles with high spatiotemporal precision. Classical genetic studies and genome-wide RNAi screens identified a plethora of evolutionarily conserved proteins necessary for cytokinesis, including cell cycle regulators, cytoskeletal proteins, and membrane trafficking and remodelling proteins. The challenge remains to understand precisely how these proteins co-operate in space and time, how they interact with membranes, how the ensemble of the machinery evolves as cytokinesis progresses, and how that machinery adapts to suit differing developmental contexts.

Traditionally, genes were ascribed cytokinesis functions based on scoring fixed cells for the most obvious outcome for cytokinesis failure following successful mitosis: binucleate cells. However, defective cytokinesis does not always result in binucleation. For example, a failure in abscission will, strictly speaking, generate cells that remain connected by stable intercellular bridges. Furthermore, fixed cells represent snapshots in time. Although informative, they lack temporal information and are inadequate for the proper appreciation and characterization of dynamic phenotypes such as oscillating cleavage furrows, shedding of material from the intercellular bridge and premature abscission, all of which have been documented through live imaging (El Amine et al., 2013; Goldbach et al., 2010; Hickson and O'Farrell, 2008; Kechad et al., 2012; Piekny and Glotzer, 2008; Renshaw et al., 2014; Straight et al., 2005). Here, we describe a simple yet powerful model for studying animal cell cytokinesis using live-cell imaging of *Drosophila* Schneider's line S2 tissue culture cells.

Many features make *Drosophila* tissue culture cells a powerful model system. Firstly, the *Drosophila* genome exhibits less functional redundancy compared to mammalian genomes. This facilitates loss of function studies and interpretation of observed phenotypes.

Secondly, most of the genes involved in cytokinesis and their functions are conserved from flies to mammals (Cabernard, 2012). Crucially, *Drosophila* cells are genetically tractable, thanks to exquisite sensitivity to RNAi elicited by long dsRNAs (Clemens et al., 2000), which are both efficient and simple to generate in the laboratory. For these reasons, *Drosophila* tissue culture cells emerged as a system of choice for RNAi screening efforts (Dean et al., 2005; Echard et al., 2004; Foley and O'Farrell, 2004; Goshima et al., 2007; Kiger et al., 2003; Somma et al., 2002), many of which helped define the repertoire of essential cytokinesis genes. Finally, *Drosophila* cells are simple to work with. They are readily maintained at ambient temperature (20 to 25°C) and normal atmospheric conditions (no CO_2), which makes them ideal for live cell microscopy, as does their amenity for transfection and the availability of genetically encoded fluorescent proteins such as GFP.

Together, these attributes provide a powerful model system in which expression of exogenous fluorescent proteins and depletion of endogenous proteins can be combined to allow reduction of function analyses, rescue experiments and structure-function analyses to be performed in living cells. Here we describe the methodology in practice in our laboratory using S2 cells to study the functions and interdependencies of key regulators of cytokinetic progression in both space and time.

3.3 MATERIALS AND METHODS

3.3.1 Materials and sample preparation

3.3.1.1 S2 cells and culture

Schneider's S2 cells derive from a primary culture of 1 day old Oregon R *Drosophila* embryos (Schneider, 1972). They are spherical, 10-15 µm in diameter, and exhibit hemocyte/macrophage–like cell behaviour and gene expression. We use S2 cells obtained from the University of California San Francisco (UCSF) cell culture facility, but S2 cells can be purchased from *Drosophila* Genome Resource Center (DGRC, Indiana) or Invitrogen/Thermo Fisher Scientific. Methods for culturing S2 cells have been described elsewhere in detail (Bettencourt-Dias and Goshima, 2009; Buster et al., 2010; Goshima, 2010; Pereira et al., 2009; Rogers and Rogers, 2008). Briefly:

1. Culture S2 cells in Schneider's *Drosophila* medium (Life Technologies/Thermo Fisher Scientific, cat#21720-001), supplemented with 10% heat-inactivated foetal calf serum (Invitrogen/Thermo Fisher Scientific, US origin cat#16140-071) and penicillin/streptomycin (Invitrogen/Thermo Fisher Scientific, cat#15140-122). S2 cells are easily maintained under normal ambient temperature (20-25°C) and atmospheric conditions.

2. S2 cells have an approximate 22 h doubling time and should be passaged by simple pipetting every 4 to 7 days at a medium to high density (1:3 to 1:5 dilution) to maintain a good mitotic index and avoid cell death (Goshima, 2010).

NOTES

- Special attention should be given when changing batch lots of cell media or serum as we have observed variation in growth rate and/or dsRNA treatment efficacy. New lots of media or serum should be systematically tested. Cells should be grown in the new media in parallel to the old media for several passages to assess for general cell health, growth rate and RNAi sensitivity. It is recommended that batches that give good results should be purchased in bulk and stockpiled for future use.

- Temperature variability can also cause changes in cell growth rates and the kinetics of RNAi depletions and thus the onset of resulting phenotypes. Temperature should be monitored and kept stable, ideally between 22°C and 25°C.

3.3.1.2 Generation of stable cell lines expressing fluorescently-tagged proteins

S2 cells readily take up DNA and have high transfection rates. It is possible to generate stable cell lines expressing multiple fluorescently tagged proteins of interest (or fragments thereof) and follow their behaviours during cytokinesis in live or fixed cells. Cloning and transfection protocols have been previously described in detail (Bettencourt-Dias and Goshima, 2009; Pereira et al., 2009). Briefly, the following workflow is employed in our laboratory for generating new FP-expressing cell lines:

1. Amplify desired coding sequences of a gene of interest by PCR from cDNA clones obtained, for example, from the DGRC, adding CACC to the 5' end of an initiating ATG.

2. TOPO-clone these into pENTR-D-TOPO Gateway entry plasmid (Thermo Fisher Scientific, cat# k2400-20) and sequence-verify.

3. Recombine coding sequences into expression vectors to form N- or C-terminal fusions with fluorescent proteins (FPs) such as EGFP, mCherry, Venus, Cerulean, Dendra2 using the *Drosophila* Gateway vector collection (https://emb.carnegiescience.edu/drosophila-gateway-vector-collection). We use destination plasmids that employ either the *actin05C* promoter (pAc) for constitutive expression or the *metallothionein* promoter (pMT) for $CuSO_4$-inducible expression. It is good practice to separately place FP tags at both the N- and C-termini, with and without the native stop codon as appropriate, in case the presence of the tag at either end interferes with protein function.

4. Transfect desired expression plasmids into S2 cells in serum-free media using Cellfectin II reagent (Thermo Fisher Scientific, cat#10362-100), together with pCoHygro (Thermo Fisher Scientific) and select stable cell lines using 400 µg/ml hygromycin B (Thermo Fisher Scientific, Cat #10687-010), supplemented to the

growth media for 4 weeks. In our hands, up to 3 transgenes can be expressed simultaneously in the resulting cell lines.

NOTES:

- Transient transfection and selection present challenges to the cells that, from our experience, can compromise normal cell behaviours including division. We therefore do not perform experiments on transiently transfected cells, or until after hygromycin selection has been maintained for 4 weeks and then been discontinued for at least 1 passage.
- In some cases, we find that transgene expression may then be progressively lost after serial passaging. We therefore routinely cryo-preserve aliquots of our newly made cell lines for later thawing, or simply remake lines periodically.

3.3.1.3 Choice of cytokinetic markers

In order to achieve an in depth characterization of cytokinesis dynamics and regulation, one would ideally like to visualize the various components of the cytokinetic machinery that comprise cortical, spindle and membrane-associated proteins at different stages of cytokinesis. The choice of fluorescent marker(s) is important and may vary depending on the experiment in question. As discussed below, there are a number of validated markers that are useful for examining cytokinesis in this system. These are summarized in Table 3. 1, and some are also shown in Figure 3.1.

3.3.1.3.1 General considerations

- When assessing RNAi depletion phenotypes, one should ideally examine a variety of cell lines expressing different FP-tagged cortical and spindle-associated proteins to maximise the chances of observing relevant phenotypes. An example from our own observations, is that the myosin regulatory light chain (MRLC), Spaghetti squash (Sqh-FP), and Anillin-FP are both good markers for the CR and MR, yet only Anillin-FP exhibits shedding from the nascent MR, even when both markers are co-expressed (El Amine et al., 2013). Examining multiple markers can also help mitigate concerns that relevant phenotypes are being masked or enhanced by (over-) expression of a given marker. Alterations in the extent and/or timing of the localization patterns of

different markers following specific experimental manipulations can provide insight into the normal progression of cytokinesis.

- When studying the localization dynamics of a GFP-tagged protein of interest, it is often useful to co-express it with a spindle marker fused to a different FP, e.g. Tubulin-mCherry, or a chromosomal marker, e.g. Histone H2B-mCherry (Hickson et al., 2006). This facilitates the identification of cells in early mitosis, i.e. before the onset of cytokinesis. As both Tubulin-mCherry and Histone H2B-mCherry can be expressed constitutively from the *actin05C* promoter (pAC plasmid), including one of these markers allows the cells to be imaged with and without induction of the second transgene, expressed from the *metallothionein* promoter (pMT plasmid). This is particularly useful in the context of rescue experiments (see below). These markers are also likely to be the least perturbing, especially Histone H2B-FP, which does not even localise to the cytokinesis machinery.

3.3.1.3.2 Specific markers

- Tubulin-FP is an ideal marker for rapid detection of mitotic cells (Goshima and Vale, 2003) and, because it is excluded from the nucleus, binucleate cells. Importantly, it allows visualization of the central spindle, its compaction during furrowing and formation of the midbody, usually identifiable by a characteristic drop in tubulin fluorescence at the center of the midbody (Fig. 1). However, tubulin-FP becomes a poor marker for scoring abscission because the MTsof the intercellular bridge are progressively lost and disappear before abscission (Fig. 1).

- FP-tagged versions of microtubule-associated proteins such as the PRC1 orthologue, Fascetto, and the Aurora B kinase, IAL (Smurnyy et al., 2010; Vale et al., 2009), localize to the central spindle and the early midbody and then rapidly disappear (Fig. 1).

- GFP-Polo kinase, also localises to the central spindle and midbody during cytokinesis (Fig. 1), although it separates into two pools: a MAP205-dependent pool that localizes to the flanking regions of the midbody; and an Aurora B kinase-dependent pool that localises more transiently to the central midbody early during its formation (Kachaner et al., 2014).

- Other Microtubule-associated proteins such as kinesin-6/Pavarotti-FP and its centralspindlin partner, RacGAP50C/Tumbleweed-FP, are reliable markers to visualize the maturation of the central spindle to the midbody and both of these persist in the late MR and MR remnants after abscission (Fig. 1). However, it is not possible to identify early mitotic cells with these markers alone.
- Anillin-FP is an ideal marker because of its localization patterns throughout cytokinesis (Field and Alberts, 1995; Hickson and O'Farrell, 2008). It is nuclear in interphase and becomes cortical upon nuclear envelope breakdown in prophase, allowing easy detection of cells in early mitosis. In anaphase, it becomes enriched at the furrow. Then, it localizes to the CR and MR in telophase and persists in the MR remnant after abscission (Fig. 1).
- LifeAct-FP (El Amine et al., 2013; Riedl et al., 2008) and the formin Diaphanous-FP (Vale et al., 2009) localise to the CR but become undetectable in the late MR. They are also unreliable markers for identifying early mitotic cells.
- Other cortical proteins such as Sqh-FP (MRLC) (Dean et al., 2005; Dean and Spudich, 2006; Hickson et al., 2006; Kechad et al., 2012; Rogers et al., 2004) and Nebbish-FP (KIF-14) (Bassi et al., 2013) and are reliable markers of the CR that persist in the MR and the MR remnant after abscission (Fig. 1). The citron kinase, Sticky-FP, also localises to the MR and MR remnants (Bassi et al., 2013; El Amine et al., 2013), but in our hands, the presence of additional cytoplasmic puncta complicates the use of this as a marker (Fig. 1).

3.3.1.4 dsRNA preparation for RNAi experiments

Exquisite sensitivity to RNAi fuelled the emergence of *Drosophila* S2 cells as a system of choice for genome-wide RNAi screens and it remains one of their major advantages for studying cytokinesis. Unlike mammalian cells that require transfection of carefully designed, expensive small interference RNAs, S2 cells readily take up long dsRNAs, which are easily prepared in the laboratory. Because *Drosophila* lacks an adaptive immune response, long dsRNAs do not trigger an interferon response, but rather the cells take them up and dice them into a pool of siRNAs that lead to efficient degradation of corresponding mRNAs. Detailed, authoritative protocols have been published elsewhere (Bettencourt-Dias and Goshima, 2009;

Buster et al., 2010; Rogers and Rogers, 2008), but briefly we:

1. Amplify target cDNA regions (300 to 700 bp in length) by PCR, incorporating the T7 promoter sequence at both ends.

2. Use PCR products as templates to synthesize complementary RNAs by *in vitro* transcription using T7-ribomax^{TM} Express RNAi System (Promega, Cat #P1300). Digest template DNA with DNAse I and precipitate RNAs with sodium acetate, wash with ethanol, air-dry and resuspend the resulting RNA pellet in water, following the kit instructions. Anneal RNAs in a water bath heated to 90°C and allowed to cool to room temperature. Verify and quantify dsRNAs by agarose gel electrophoresis and adjust concentrations to 1 µg/µl.

NOTES:

- When designing primers for template production, the resulting amplimers should be verified for potential off-target hits, by performing BLAST searches with the parameters set to identify very short sequences of homology in the *D. melanogaster* genome. We aim to avoid stretches of identity of more than 15 bp present in other genes.
- It is also good practice to generate multiple, non-overlapping dsRNAs against the same mRNA target, to provide confidence that any arising phenotypes are indeed specific and not due to off-target effects.
- If antibodies to the target protein are available, the kinetics and efficacy of depletion of a given dsRNA should be monitored by western blot, ideally performed in parallel to live cell imaging. In this way, estimates of depletion efficacy can accompany the phenotypic analysis. We suggest lysing cells at different times post dsRNA treatment and performing SDS-PAGE and immunoblot analysis. Comparing depleted lysates to a serially diluted control lysate will allow estimation of the level of protein depletion over time, and definition of the limits of detection of the antibody. Quantification of protein depletion is particularly important in the absence of observable phenotypes, as few conclusions can be drawn without it.

3.3.2 Live-cell imaging

3.3.2.1 Sample preparation and experimental set-up

1. Under aseptic conditions, seed desired S2 cells at medium density (2 x10^6 /ml, approx. 50% confluency when cells have settled) in 200 µl complete media in 96-well plastic flat-bottomed plates (e.g. Corning, Cat#CS003595). Seed enough wells for duplicates and controls.

NOTE: Limiting cell density is important for RNAi efficiency and to maintain a high mitotic index. For more stable (and/or abundant) targets that require longer incubation with dsRNA for phenotypes to become apparent, cells should be passaged after 4 days with fresh dsRNA added.

2. Where appropriate, add 1 µg of dsRNA (1 µg/µl) per well, mix by pipetting and incubate from 2 to 7 days, depending on the target gene in question. If incubation beyond 4 days is required, split cells 1:2 on day 4 and add 0.5 µg fresh dsRNA.

NOTE: The incubation time required for the onset of phenotypes (e.g. cytokinesis failure) should be determined empirically for each dsRNA and will depend on factors such as the stability of the target protein and any threshold(s) for its requirement.

3. Include negative and positive dsRNA controls:

a. For a negative control, we typically use dsRNAs designed to target the *E. coli LacI* gene, but any other sequence that is not present in the cell line could be used (e.g. kanamycin resistance gene). We also routinely include a control without any dsRNA just to monitor the general density and health of the culture.

b. It is important to include positive controls for every experiment, because of potential variability of the kinetics and/or efficacy of RNAi due to factors such as media, temperature, cell density and cell passage number. We routinely use dsRNA to deplete the RhoGEF, Pebble, or the kinesin-6, Pavarotti, since either of these ordinarily results in rapid and penetrant cytokinesis failure, producing binucleate cells from 2 to 3 days of treatment.

4. When appropriate, induce expression of pMT-driven transgenes with 250 to 500 µM $CuSO_4$ (2.5 to 5 µl of a 100 mM sterile-filtered stock solution per ml of growth media).

NOTE: If performing a simple RNAi loss of function experiment, induction of expression of a relevant marker can be done 12 to 24 h prior to imaging. If performing rescue experiments, induction should be performed at the same time as dsRNA is added, and maintained throughout any subsequent passages, if applicable.

5. 12 to 24 h prior to imaging, gently resuspend dsRNA-treated cells by micro-pipetting and transfer to 8 well chambered coverglass dishes (Lab-tek II, Nunc, cat. #CA43300774) or 96 well glass bottomed plates (Whatman, cat#306180-030) and allow to settle for at least 30 min.

NOTES: Optimal cell density is important for imaging and should be around 2 $x10^6$/ml in a final volume of 400 µl (i.e. pool duplicate wells, or split cells 1:2 into fresh media) for 8 wells dishes and 200 µl in 96 wells dishes. Note also that pipetting may rupture late intercellular bridges, which will need to be considered if abscission events are to be examined. For this reason, we recommend plating the cells 12 to 24 h prior to observing abscission events.

Since S2 cells are only semi-adherent, they can move around and some will leave the field of view during long time-course imaging. Plating S2 cells on the lectin, concanavalin A (ConA), causes them to adhere and flatten out beautifully and this has been exploited in numerous important studies (Rogers et al., 2002; Rogers et al., 2003; Vale et al., 2009). However plating on ConA also blocks the completion of cytokinesis, and is thus not suitable for studying many stages of cytokinesis. S2R+ cells are a more adherent variant line that could alternatively be used.

3.3.2.1.1 Variation: Co-depletion experiments

Another powerful advantage of this system is that two target proteins can be reliably co-depleted in the same cells, allowing genetic interactions to be uncovered, for examples see (El Amine et al., 2013; Hickson et al., 2006). However, such experiments require some additional considerations and controls. First, the incubation times required for each dsRNA need to be determined. If both dsRNAs require the same

incubation time, they can be added to the cells together. However, if the times differ, the dsRNAs should be added sequentially according to their specific schedules. Secondly, individual depletions must also be performed in the presence of control (*lacI*) dsRNAs. This is important since depletion of a given target may be less efficient in the presence of a second dsRNA due to competition effects for components of the RNAi machinery.

An example of a co-depletion experiment is given below (and in Fig. 2B), where dsRNAs targeting the septin gene, *peanut*, which require 7 to 8 day incubations before cytokinesis failures are observed, are to be combined with dsRNAs targeting Anillin, which induce cytokinesis failures by 3 days (Kechad et al., 2012).

1. 7 days prior to imaging seed the cells and add *peanut* dsRNAs to two wells (one will be for a *peanut* only control). In parallel, set up two additional wells incubated only with *lacI* dsRNAs (for *lacI* and *anillin* only controls).

2. 3 to 4 days prior to imaging, split the cells and add *anillin* or *lacI* dsRNAs together with fresh *peanut* or *lacI* dsRNAs, as depicted in Fig. 2B. Incubate for a further 3 days.

3. 12-24 h prior to imaging, split the cells again and re-add both *peanut* and *anillin* dsRNAs before transferring to imaging dishes and proceeding to the microscope system.

3.3.2.1.2 Variation: Rescue experiments

Rescue experiments are invaluable controls for specificity of dsRNA-induced phenotypes and for testing the functionality of FP-tagged proteins. The idea is to specifically deplete an endogenous protein and replace it with an exogenous dsRNA-resistant, FP-tagged version. If the exogenous protein can rescue the defects caused by the dsRNA, it indicates that the RNAi phenotype is specific and that the exogenous protein (i.e. FP-fusion) is functional.

The first task is to generate a dsRNA that will effectively target the endogenous mRNA but not the exogenous one. The simplest method is to generate dsRNAs against the 5' and/or 3'UTRs of the endogenous mRNA. We have successfully performed this

for several genes, including Anillin (Hickson and O'Farrell, 2008).

However, the UTR sequences can sometimes be too short (resulting in weakly penetrant RNAi phenotypes) or their sequences not specific enough for the gene in question. In this case, an alternative strategy is to use a dsRNA that targets the coding sequence and express an engineered mRNA in which codon usage has been changed for the region targeted by the dsRNA. As a result, the expressed transgene still encodes the wild type protein but is not recognized by the dsRNA. We are successfully using this approach for a number of targets, as have others such as for Sqh/MRLC (Dean and Spudich, 2006).

For rescue experiments, we generate cell lines that constitutively express tubulin-mCherry (pAc promoter) and inducibly express the rescue construct (pMT). This then allows the rescue experiments to be imaged live both with and without induction. If the cells successfully progress through cytokinesis only when the transgene is induced, this provides strong confirmation that the RNAi has been effective and that the transgene is indeed rescuing. The pMT promoter can be somewhat leaky, potentially resulting in partial or even complete rescue in the absence of induction. However, this leaky expression will be readily detected on the microscope, aided by the fact that cytokinesis regulators tend to become highly enriched at the division site, and the corresponding levels can be correlated to the phenotype observed. An additional internal control can include subpopulations of cells within the culture that are not detectably expressing the rescuing transgene, even after induction.

3.3.2.2 Time-lapse image acquisition

1. Proceed to your imaging system.

We use an Ultraview Vox spinning disk confocal system (Perkin-Elmer), equipped with a CSU-X1 scanning unit (Yokogawa) fitted to a fully motorized DM16000B inverted microscope (Leica Microsystems). It includes a motorized XY stage with linear encoders for greater positional accuracy and a piezo–electric Z top-plate for fast acquisition of Z-stacks (Applied Scientific Instrumentation). An Orca-R2 charged-coupled device camera

(Hamamatsu) is used for detection. The system is controlled by Volocity 6.3 acquisition software (Improvision/Perkin Elmer).

2. Ensure your cells are protected against dehydration from evaporation for the duration of your experiment.

Since S2 cells are healthy at room temperature and under normal atmospheric conditions, no special conditions or equipment are needed when the cells are on the microscope, provided there are no major fluctuations of ambient temperature. However, you may wish to consider humidity control to counter evaporation of media when imaging over extended periods. Our system is equipped with a stage-top incubator (Pathology Devices) that includes humidity control, although we have found this unnecessary for most of our imaging needs, i.e. up to 24 hours imaging, with 400 µl media per well in 8 well chambered coverslip dishes (Nunc Lab-tek II).

3. Select an appropriate objective for **low-resolution imaging** (e.g. 40x 0.85 NA air).

When imaging a new cell line or assessing the effect of a dsRNA for the first time, we typically perform low resolution time-lapse imaging for 24 h to 48 h, starting 2 to 3 days after dsRNA treatment. This allows cells to be followed through mitosis, cytokinesis, abscission and in many cases to the next mitosis. It also allows us to monitor the onset of any phenotypes and their potential progression as the RNAi takes full effect. A non-immersion, air objective (40x 0.85 NA) is ideal for visiting all wells of an 8-well dish, allowing controls to be imaged in parallel.

4. Set laser power and camera exposure times.

We routinely use two excitation laser lines: 488 nm for GFP and 561 nm for mCherry. To reduce photobleaching and phototoxicity, we limit laser power and exposure times as much as possible, although these will vary depending on protein expression levels and the specific aims of the experiment. We also routinely set camera binning to 2x2 to increase the signal to noise ratio, at the expense of resolution.

5. Select and save 3 to 4 fields of cells per condition and initiate acquisition of two-channel Z-stacks at 4 to 5 min intervals for 12 to 24 h.

When saving the XYZ points, we use the microscope stand's motorised focus drive for setting the Z position. We then typically acquire, at each XYZ position, a Z-stack of 10 µm thickness with a 1 µm Z step size, using the piezo-electric stage. If you are capturing images from two channels consecutively with only one camera (as we are), special consideration should be given to the order of Z stack versus channel acquisition. If the resulting data are to be analyzed for co-localization, for example, camera exposure time should be minimized and both channels should be captured at each Z position before moving to the next Z position. If co-localization in not an issue, the system can be set to collect the full stack images for one channel, before proceeding to the second channel. If emission filters are being employed, this latter configuration will allow for faster acquisition.

6. Perform **high-resolution imaging**, e.g. using a 63x 1.4 NA oil-immersion objective.

Once we have a general characterization of phenotypes from the low-resolution imaging, the time of their onset, success/failure rates etc., we refine our analysis by repeating the experiment using high-resolution (spatial and temporal) time-lapse imaging conditions.

7. Identify and save the positions of cells in prophase/prometaphase.

Inclusion of markers such as tubulin-FP, Histone H2B-FP, or Anillin-FP facilitates this step. Work quickly at this step to be able to initiate the acquisition before cells enter anaphase. We typically select up to 10 XYZ positions (using the microscope focus drive for the Z position), all in the same well. We thus image different conditions consecutively rather than simultaneously.

8. Initiate the acquisition of two-channel Z-stacks at 30 to 60 sec intervals for up to 2 h.

At high resolution, we typically set our Z-stacks with a 0.25-0.5 µm Z step size.

9. Analyze collected datasets using Volocity Analysis software or third-party software (e.g. Imaris, Bitplane).

NOTES:

- Pharmacological inhibitors that disrupt the mitotic spindle (e.g. colchicine, taxol), actin dynamics (e.g. Latrunculin A, jasplakinolide) or cell cycle progression (e.g. MG132, RO3306) can be used to alter cytokinesis dynamics. It is possible to add these directly to the culture medium during image acquisition with a micropipette, although this takes some practice and luck not to disturb the poorly adherent S2 cells. Adherent S2R+ cells may be better suited for these kinds of experiments. It is also worth noting that the myosin-2 inhibitor, blebbistatin, which blocks cytokinesis in a variety of cell types, is ineffective in *Drosophila* cells (Straight et al., 2003).

3.3.2.3 Data analysis and expected phenotypes

3.3.2.3.1 Data analysis:

A- Low-resolution imaging:

From the long-term low-resolution imaging, we routinely analyze at least 50 division attempts from different fields for each condition. For each division attempt, we routinely score the times of anaphase onset, completion of CR closure, mature MR formation, and abscission or regression, as appropriate. This provides a range of temporal information and is very useful for determining the time of phenotypic onset for specific dsRNAs and potentially uncovering different aspects of the phenotype that manifest over time. For example, long time-course imaging revealed that the earliest observable phenotype upon Sticky/Citron kinase depletion is actually premature abscission, which occurs after only 2 days of dsRNA treatment, and which precedes the more obvious cytokinesis failures that occur after 3 to 4 days of dsRNA (El Amine et al., 2013). In a second example, low-resolution live imaging of Anillin-depleted cells helped define two populations of cells exhibiting slightly different phenotypes. In one population, the CR forms, but then rapidly becomes unstable, and oscillates back and forth across the cell equator before regressing 30 minutes after anaphase onset. In the second population, the CR does not oscillate but still fails to ingress to completion and regresses 1 h after anaphase onset (Kechad et al., 2012).

For each experiment, data are compared to both negative and positive controls, performed in parallel under identical conditions. Negative controls (e.g. *lacI* RNAi) are necessary to exclude false positives while positive controls (e.g. *pebble*/RhoGEF RNAi) exclude false negatives by providing confirmation that the cells remain responsive to RNAi. This can be particularly important for rescue experiments.

Additional controls that we often include in the context of rescue experiments are: no induction of the rescuing transgene; and a dsRNA targeting both the endogenous and exogenous forms. If all conditions except the rescue condition show the expected loss of function phenotype, one can then be confident of rescue. Of course, rescue may be partial, showing incomplete penetrance if observed in only a subset of cells. It is also possible that cytokinetic progression be partially rescued, i.e. cytokinesis could still fail, but in a different way or at a later stage. Such rescue experiments using separation-of-function alleles are a powerful means to dissect the requirements for each component of the cytokinetic machinery throughout cytokinetic progression.

B- Hi-resolution imaging:

Once the long-term low-resolution imaging has defined the optimal experimental conditions (i.e. duration of RNAi) and provided an overview of the experimental phenotypes, imaging is performed at higher spatial and temporal resolution to better capture and assess those phenotypes. The resulting datasets are ideal for more quantitative analyses such as intensity measurements, protein co-localization measurements, line profiles, 3D reconstructions to measure the volume of the different structures, all throughout the progression of cytokinesis.

3.3.2.3.2 Expected phenotypes:

Using this live imaging approach, we have identified some common phenotypes that can arise from failure at each stage of progression through cytokinesis and we briefly describe them here (Fig. 3). One limitation of S2 cells is that they do not always divide in a perfectly stereotyped and reproducible way. As noted by others, they often have supernumerary centrosomes, which usually cluster together to form a bipolar spindle, but can also form multipolar spindles (Goshima, 2010). During the furrowing stage of cytokinesis, the cells have a tendency to bleb at the poles and can exhibit variability in furrow morphology. For this

reason it is important to examine sufficient numbers of cells to have confidence in a given phenotype.

A- Early cytokinesis phenotypes:

The first step of cytokinesis is formation of the central spindle in early anaphase. Anaphase onset can readily be scored by observing markers such as histone H2B-FP and tubulin-FP (shortening of kinetochore fibers). The exclusion of cytoplasmic signal that the chromosomes induce can also be used to track the chromosomes with other fluorescent markers (e.g. Anillin-FP), if expression levels are high enough. Failure to form the central spindle results in collapse of the MTscausing rapid failure of furrowing within 15 to 20 minutes after anaphase.

The anaphase spindle delivers positive and negative signals that stimulate local formation and contraction of the cleavage furrow. The limiting event for furrow initiation is the activation of the small GTPase RhoA to a narrow zone that specifies furrow position. Rho activation stimulates local actin filament assembly and myosin recruitment and activation, triggering the formation of the CR. Rho also promotes recruitment and activation, of scaffolding proteins such as Anillin and septins, which help organize and stabilize the CR. Failure to localize Rho or its activators, leads to failure in furrow ingression and rapid regression yielding a binucleated cell.

As the CR ingresses, it brings the equatorial membrane with it. Different scaffolding proteins mediate this process and defects in membrane anchorage result in uncoupling between the plasma membrane and the cell cortex, often leading to an excessive blebbing phenotype. During CR closure, several microtubule-associated proteins will move along the central spindle and accumulate in and around a central region of densely packed interdigitated MTsthat we refer to as the midbody, and which is characterized by a local drop in the tubulin-FP signal (Fig. 1). Cells that fail to form a midbody will often display a thicker central spindle that lacks the central drop in tubulin intensity. They will initiate furrowing, however, the CR will ingress with a delay to ultimately regress resulting in binucleated cells.

Cytokinesis failure during CR closure can also result from aberrant membrane organization. For example, depletion of the inositol 5-phosphtase, dOCRL, results in the ectopic localization of PtdIns(4,5)P(2) and CR components to endomembranes and leads to furrow regression (Ben El Kadhi et al., 2011).

B- Late cytokinesis phenotypes:

In S2 cells, the CR closes until it reaches a diameter of 1-2 μm, then it begins to transition to a stable MR. We have identified a 1 h time window, during which this early MR will undergo further maturation in parallel to midbody maturation that together form the intercellular bridge that connects the two sister cells until abscission. This maturation process is detectable by a gradual thinning of the MR structure accompanied by extrusions and internalization of different ring components such as Anillin, Septins, Rho, Sticky kinase, as well as components of the midbody such as Tumbleweed, Pavarotti and Aurora B. Perturbations at this step can result in excess shedding events and can ultimately cause MR disintegration, causing premature abscission or rapid regression of the membrane (e.g. citron kinase/*sticky* RNAi (El Amine et al., 2013). Conversely, this process can also be blocked resulting in larger MRs that are unable to complete cytokinesis (e.g. *peanut* RNAi, (El Amine et al., 2013).

Throughout this maturation process, the midbody and MR remain anchored to the plasma membrane. Defects in anchorage will cause rapid detachment of the plasma membrane and formation of binucleated cells with internal MR-like structures that can persist for hours (Kechad et al., 2012). Interestingly, many of the late cytokinetic failures that we observe happen soon after this 1h time frame, suggesting that this is a particularly sensitive step during S2 cell cytokinesis.

C- Abscission phenotypes:

Once the intercellular bridge is mature and well anchored to the membrane, the last stage of cytokinesis can proceed: abscission. Abscission is the longest and most variable stage of S2 cell cytokinesis. It can complete from 3 to >12 hours after furrowing. Prior to this stage, the MTsat the intercellular bridge gradually thin until they completely disappear. Sister cells remain linked by the late MR that is now <1 μm in diameter. A defect in abscission can yield sister cells that remain connected even as they undergo the next mitosis (e.g. Shrub/CHMP4 RNAi, (El Amine et al., 2013).

D- Post-abscission MR remnants:

Upon normal completion of abscission of S2 cells, the MR remnant remains associated

with one of the two sister cells. Although we have not systematically tracked the fate of these MR remnants, it is clear that they can persist for some time. MR remnants are readily observed using markers such as Anillin-GFP and they often persist in the cytoplasm of the cells until at least the following mitosis. This cytoplasmic localization suggests that they are engulfed, as has been shown in mammalian cells (Crowell et al., 2014).

3.3.3 Fixed-cell imaging

Although the real power of this system is for live-cell imaging, imaging of fixed cells remains a useful complementary approach. Importantly, immunofluorescence of fixed cells is the only way to localize endogenous proteins implicated in cytokinesis. It is important to confirm that tagged, and often over-expressed, versions of a protein of interest faithfully replicate the localization of the endogenous protein. However, it should be noted that cytokinetic structures such as the midbody and associated MR are densely packed structures and that certain epitopes may be locally masked. For example, it is well known that tubulin antibodies do not label the central region of the midbody (the part that is surrounded by the MR), even though electron micrographs and FP-tubulin fluorescence demonstrate that MTsextend through this region. Thus a lack of an immunofluorescence signal at a particular location may not necessarily indicate a lack of protein localization there.

Here is the protocol that we use for indirect immunofluorescence:

1. Seed the cells at high confluence (6 x10^6 /ml) in an 8 well chambered coverglass (Lab-tek II, cat#CA43300774) or 96 well glass bottomed dishes (Whatman, cat#306180-030). Allow the cells to settle overnight. We recommend setting more than one well for each condition.

Critical: S2 cells are only loosely attached to the glass and many will be lost after the numerous washes. The following steps must be done very carefully to minimize cell loss. We perform all steps (addition and removal) with a standard 200µl micropipette. Using this approach, we find that sufficient cells remain, especially near the edges of the wells. An alternative approach to increase cell numbers may include plating cells for approximately 5-10 min on ConA-coated glass prior to fixation. The cells will begin to adhere, but the pipetting

step may disrupt late intercellular bridges.

2. Remove the medium and fix for 10 min at room temperature in 200 µl Fixation buffer: phosphate buffered saline (PBS) containing 3.7% formaldehyde (Sigma, cat#f1635) and (optional) 0.1 % glutaraldehyde (Sigma.cat# g7651). The inclusion of glutaraldehyde better preserves microtubule morphology. Other fixatives such as methanol or trichloroacetic acid can be used. We recommend testing different fixatives to determine which one is most suitable to preserve epitopes and features of interest.
3. Wash once and permeabilize with PTX buffer: PBS containing 0.1% Triton-X100 (Fisher, cat# bp151500).
4. Block for 1 hour with blocking buffer: PTX containing 5% normal goat serum (Jackson Immuno Research, cat# 005-000-121)
5. Incubate with primary antibodies diluted in 100 µl blocking buffer. We generally perform this step overnight at 4°C.
6. Remove antibodies and carefully wash several times over a 30 min period in blocking buffer.
7. Incubate with appropriate goat secondary antibodies, such as ones coupled to Alexa Fluor (Molecular Probes/ Thermo Fisher Scientific), diluted 1:1000 in blocking buffer for 1 hour at room temperature. Dyes such as Alexa Fluor-phalloidin (Molecular Probes/ Thermo Fisher Scientific) and Hoechst 33258 (Molecular Probes/ Thermo Fisher Scientific, cat#H356) can also be included in this step (1:1000 dilution).
8. Remove antibody and gently wash several times over a 30 min period in PTX buffer.
9. Replace with 100 µl Fluoromount-G mounting medium (Southern Biotech, cat# 0100-01) and proceed to your imaging system as soon as possible. Store at 4°C in the dark.

3.4 CONCLUSION & PERSPECTIVES

Drosophila S2 cells provide a powerful system for dissecting the cell-intrinsic mechanisms underlying the different stages of animal cell cytokinesis: formation of the CR; formation of the intercellular bridge; and abscission. Growth at ambient temperature and atmospheric conditions makes S2 cells ideal for long time course microscopy, and this allows the tracking of individual cells as they progress through cytokinesis. This live-cell imaging approach is essential for properly evaluating phenotypes and for uncovering alterations to the timing of events. S2 cells can be readily manipulated through RNAi-mediated protein depletion and expression of fluorescently tagged proteins, making them ideally suited for loss-of-function analyses and structure-function analyses of important cytokinesis regulators.

The genetic tractability of *Drosophila* tissue culture cells has recently been extended to include CRISPR-mediated genome editing (Bassett et al., 2014; Bottcher et al., 2014), which can be combined with RNAi (Housden et al., 2015). Further refinements include the engineering of related cell lines for integrase-mediated targeted insertions to improve the homogeneity of transgenic lines (Cherbas et al., 2015), and the development of lines expressing a fly-FUCCI system for analysis of cell cycle dynamics (Zielke et al., 2016). Finally, *Drosophila* tissue culture cells also offer a valuable resource for the biochemical purification and identification of protein complexes important during mitosis and cytokinesis (D'Avino et al., 2009). We fully expect this versatile system to continue making important contributions to our understanding of the molecular mechanisms governing cytokinetic progression.

3.5 ACKNOWLEDGEMENTS

We thank members of the Hickson laboratory for discussions and helpful comments, and especially Mélanie Diaz for help with graphical design. We thank the Fonds de Recherche Québec Santé (FRQS) for a Doctoral studentship to A.K. and a Junior 2 scholarship to G.H. Research in the laboratory is supported by an infrastructure award from the Canada Foundation for Innovation and operating grants from the Canadian Institutes for Health Research (MOP97788), the Natural Sciences and Engineering Research Council and the Cole Foundation.

3.6 REFERENCES

Barr, F.A., and U. Gruneberg. 2007. Cytokinesis: placing and making the final cut. *Cell*. 131:847-860.

Bassett, A.R., C. Tibbit, C.P. Ponting, and J.L. Liu. 2014. Mutagenesis and homologous recombination in Drosophila cell lines using CRISPR/Cas9. *Biol Open*. 3:42-49.

Bassi, Z.I., M. Audusseau, M.G. Riparbelli, G. Callaini, and P.P. D'Avino. 2013. Citron kinase controls a molecular network required for midbody formation in cytokinesis. *Proc Natl Acad Sci U S A*. 110:9782-9787.

Ben El Kadhi, K., C. Roubinet, S. Solinet, G. Emery, and S. Carreno. 2011. The inositol 5-phosphatase dOCRL controls PI(4,5)P2 homeostasis and is necessary for cytokinesis. *Curr Biol*. 21:1074-1079.

Bettencourt-Dias, M., and G. Goshima. 2009. RNAi in Drosophila S2 cells as a tool for studying cell cycle progression. *Methods Mol Biol*. 545:39-62.

Bottcher, R., M. Hollmann, K. Merk, V. Nitschko, C. Obermaier, J. Philippou-Massier, I. Wieland, U. Gaul, and K. Forstemann. 2014. Efficient chromosomal gene modification with CRISPR/cas9 and PCR-based homologous recombination donors in cultured Drosophila cells. *Nucleic Acids Res*. 42:e89.

Buster, D.W., J. Nye, J.E. Klebba, and G.C. Rogers. 2010. Preparation of Drosophila S2 cells for light microscopy. *J Vis Exp*.

Cabernard, C. 2012. Cytokinesis in Drosophila melanogaster. *Cytoskeleton (Hoboken)*. 69:791-809.

Cherbas, L., J. Hackney, L. Gong, C. Salzer, E. Mauser, D. Zhang, and P. Cherbas. 2015. Tools for Targeted Genome Engineering of Established Drosophila Cell Lines. *Genetics*. 201:1307-1318.

Clemens, J.C., C.A. Worby, N. Simonson-Leff, M. Muda, T. Maehama, B.A. Hemmings, and J.E. Dixon. 2000. Use of double-stranded RNA interference in Drosophila cell lines to dissect signal transduction pathways. *Proc Natl Acad Sci U S A*. 97:6499-6503.

Crowell, E.F., A.L. Gaffuri, B. Gayraud-Morel, S. Tajbakhsh, and A. Echard. 2014. Engulfment of the midbody remnant after cytokinesis in mammalian cells. *J Cell Sci*. 127:3840-3851.

D'Avino, P.P., V. Archambault, M.R. Przewloka, W. Zhang, E.D. Laue, and D.M. Glover. 2009.

Isolation of protein complexes involved in mitosis and cytokinesis from Drosophila cultured cells. *Methods Mol Biol*. 545:99-112.

Dean, S.O., S.L. Rogers, N. Stuurman, R.D. Vale, and J.A. Spudich. 2005. Distinct pathways control recruitment and maintenance of myosin II at the cleavage furrow during cytokinesis. *Proc Natl Acad Sci U S A*. 102:13473-13478.

Dean, S.O., and J.A. Spudich. 2006. Rho kinase's role in myosin recruitment to the equatorial cortex of mitotic Drosophila S2 cells is for myosin regulatory light chain phosphorylation. *PLoS One*. 1:e131.

Echard, A., G.R. Hickson, E. Foley, and P.H. O'Farrell. 2004. Terminal cytokinesis events uncovered after an RNAi screen. *Curr Biol*. 14:1685-1693.

El Amine, N., A. Kechad, S. Jananji, and G.R. Hickson. 2013. Opposing actions of septins and Sticky on Anillin promote the transition from contractile to midbody ring. *J Cell Biol*. 203:487-504.

Field, C.M., and B.M. Alberts. 1995. Anillin, a contractile ring protein that cycles from the nucleus to the cell cortex. *J Cell Biol*. 131:165-178.

Foley, E., and P.H. O'Farrell. 2004. Functional dissection of an innate immune response by a genome-wide RNAi screen. *PLoS Biol*. 2:E203.

Glotzer, M. 2009. The 3Ms of central spindle assembly: microtubules, motors and MAPs. *Nat Rev Mol Cell Biol*. 10:9-20.

Goldbach, P., R. Wong, N. Beise, R. Sarpal, W.S. Trimble, and J.A. Brill. 2010. Stabilization of the actomyosin ring enables spermatocyte cytokinesis in Drosophila. *Mol Biol Cell*. 21:1482-1493.

Goshima, G. 2010. Assessment of mitotic spindle phenotypes in Drosophila S2 cells. *Methods Cell Biol*. 97:259-275.

Goshima, G., and R.D. Vale. 2003. The roles of microtubule-based motor proteins in mitosis: comprehensive RNAi analysis in the Drosophila S2 cell line. *J Cell Biol*. 162:1003-1016.

Goshima, G., R. Wollman, S.S. Goodwin, N. Zhang, J.M. Scholey, R.D. Vale, and N. Stuurman. 2007. Genes required for mitotic spindle assembly in Drosophila S2 cells. *Science*. 316:417-421.

Gould, G.W. 2016. Animal cell cytokinesis: The role of dynamic changes in the plasma membrane

proteome and lipidome. *Semin Cell Dev Biol*.

Green, R.A., E. Paluch, and K. Oegema. 2012. Cytokinesis in Animal Cells. *Annu Rev Cell Dev Biol*.

Hickson, G.R., A. Echard, and P.H. O'Farrell. 2006. Rho-kinase controls cell shape changes during cytokinesis. *Curr Biol*. 16:359-370.

Hickson, G.R., and P.H. O'Farrell. 2008. Rho-dependent control of anillin behavior during cytokinesis. *J Cell Biol*. 180:285-294.

Housden, B.E., A.J. Valvezan, C. Kelley, R. Sopko, Y. Hu, C. Roesel, S. Lin, M. Buckner, R. Tao, B. Yilmazel, S.E. Mohr, B.D. Manning, and N. Perrimon. 2015. Identification of potential drug targets for tuberous sclerosis complex by synthetic screens combining CRISPR-based knockouts with RNAi. *Sci Signal*. 8:rs9.

Kachaner, D., X. Pinson, K.B. El Kadhi, K. Normandin, L. Talje, H. Lavoie, G. Lepine, S. Carreno, B.H. Kwok, G.R. Hickson, and V. Archambault. 2014. Interdomain allosteric regulation of Polo kinase by Aurora B and Map205 is required for cytokinesis. *J Cell Biol*. 207:201-211.

Kechad, A., S. Jananji, Y. Ruella, and G.R. Hickson. 2012. Anillin acts as a bifunctional linker coordinating midbody ring biogenesis during cytokinesis. *Curr Biol*. 22:197-203.

Kiger, A.A., B. Baum, S. Jones, M.R. Jones, A. Coulson, C. Echeverri, and N. Perrimon. 2003. A functional genomic analysis of cell morphology using RNA interference. *J Biol*. 2:27.

Pereira, A.J., I. Matos, M. Lince-Faria, and H. Maiato. 2009. Dissecting mitosis with laser microsurgery and RNAi in Drosophila cells. *Methods Mol Biol*. 545:145-164.

Piekny, A.J., and M. Glotzer. 2008. Anillin is a scaffold protein that links RhoA, actin, and myosin during cytokinesis. *Curr Biol*. 18:30-36.

Renshaw, M.J., J. Liu, B.D. Lavoie, and A. Wilde. 2014. Anillin-dependent organization of septin filaments promotes intercellular bridge elongation and Chmp4B targeting to the abscission site. *Open Biol*. 4:130190.

Riedl, J., A.H. Crevenna, K. Kessenbrock, J.H. Yu, D. Neukirchen, M. Bista, F. Bradke, D. Jenne, T.A. Holak, Z. Werb, M. Sixt, and R. Wedlich-Soldner. 2008. Lifeact: a versatile marker to visualize F-actin. *Nat Methods*. 5:605-607.

Rogers, S.L., and G.C. Rogers. 2008. Culture of Drosophila S2 cells and their use for RNAi-mediated loss-of-function studies and immunofluorescence microscopy. *Nat Protoc*. 3:606-611.

Rogers, S.L., G.C. Rogers, D.J. Sharp, and R.D. Vale. 2002. Drosophila EB1 is important for proper assembly, dynamics, and positioning of the mitotic spindle. *J Cell Biol*. 158:873-884.

Rogers, S.L., U. Wiedemann, U. Hacker, C. Turck, and R.D. Vale. 2004. Drosophila RhoGEF2 associates with microtubule plus ends in an EB1-dependent manner. *Curr Biol*. 14:1827-1833.

Rogers, S.L., U. Wiedemann, N. Stuurman, and R.D. Vale. 2003. Molecular requirements for actin-based lamella formation in Drosophila S2 cells. *J Cell Biol*. 162:1079-1088.

Schneider, I. 1972. Cell lines derived from late embryonic stages of Drosophila melanogaster. *J Embryol Exp Morphol*. 27:353-365.

Smurnyy, Y., A.V. Toms, G.R. Hickson, M.J. Eck, and U.S. Eggert. 2010. Binucleine 2, an isoform-specific inhibitor of Drosophila Aurora B kinase, provides insights into the mechanism of cytokinesis. *ACS Chem Biol*. 5:1015-1020.

Somma, M.P., B. Fasulo, G. Cenci, E. Cundari, and M. Gatti. 2002. Molecular dissection of cytokinesis by RNA interference in Drosophila cultured cells. *Mol Biol Cell*. 13:2448-2460.

Steigemann, P., and D.W. Gerlich. 2009. Cytokinetic abscission: cellular dynamics at the midbody. *Trends Cell Biol*. 19:606-616.

Straight, A.F., A. Cheung, J. Limouze, I. Chen, N.J. Westwood, J.R. Sellers, and T.J. Mitchison. 2003. Dissecting temporal and spatial control of cytokinesis with a myosin II Inhibitor. *Science*. 299:1743-1747.

Straight, A.F., C.M. Field, and T.J. Mitchison. 2005. Anillin binds nonmuscle myosin II and regulates the contractile ring. *Mol Biol Cell*. 16:193-201.

Vale, R.D., J.A. Spudich, and E.R. Griffis. 2009. Dynamics of myosin, microtubules, and Kinesin-6 at the cortex during cytokinesis in Drosophila S2 cells. *J Cell Biol*. 186:727-738.

Zielke, N., M. van Straaten, J. Bohlen, and B.A. Edgar. 2016. Using the Fly-FUCCI System for the Live Analysis of Cell Cycle Dynamics in Cultured Drosophila Cells. *Methods Mol Biol*. 1342:305-320.

Stages FP-Markers	Easy ID of cells in early mitosis?	CS/CR 	Midbody/ Nascent MR 	Shedding 	Mature MR 	MR remnant 	Comments	Refs
Histone H2B	✓	✗	✗	✗	✗	✗	- Does not localise directly to division site. - Reliable chromosomal marker to identify different steps of mitosis.	Hickson et al., 2006
Tubulin	✓	✓	✓	✓	✗	✗	- Reliable marker for mitosis, the central spindle and midbody. - Unreliable for late MRs and abscission.	Goshima and Vale, 2003
Fascetto (PRC1)	✗	✓	✓	✓	✗	✗	- Reliable central spindle and early midbody marker. - Unreliable for late MRs and abscission.	Hickson lab, unpublished
IAL (Aurora B)	✓	✓	✓	✓	✗	✗	- Localises to inner centromeres in early mitosis. - Reliable central spindle and early midbody marker. - Unreliable for late MRs and abscission.	Vale and Griffis, 2009 Smyrny et al., 2010 El Amine et al., 2013
Polo	✓	✓	✓	✓	✗	✗	- Localises to kinetochores and spindle poles in early mitosis. - Reliable central spindle and midbody marker. - Unreliable for late MRs and abscission.	D'Avino et al., 2007 kachaner et al., 2015
Pavarotti (Kinesin-6)	✓	✓	✓	✓	✗	✗	- Reliable central spindle and midbody marker. - Unreliable for late MRs and abscission.	Echard et al., 2004 Goshima and Vale, 2005
Tum (RacGAP50C)	✗	✓	✓	✓	✗	✗	- Reliable cytokinesis marker, labels the central spindle early. - Relocalises to ring structures later in cytokinesis.	D'avino et al., 2006 Hickson lab, unpublished
LifeAct	✗	✓	✓	✗	✗	✗	- Hard to distinguish mitosis from interphase. - Labels the cortex and early ring structures. - Unreliable for late MRs and abscission.	Riedel et al., 2009 El Amine et al., 2013
Diaphanous	✗	✓	✓	✗	✗	✗	- Labels the cortex and ring structures. - Unreliable for late MRs and abscission.	Vale et al., 2009 Hickson lab, unpublished
Anillin	✓	✓	✓	✓	✓	✓	- Reliable cytokinesis marker. Allows identification of mitotic cells upon nuclear envelope breakdown. - Labels ring structures throughout cytokinesis.	Hickson and O'Farrell, 2008 Kechad et al., 2012 El Amine et al., 2013
Nebbish (KIF14)	✗	✓	✓	✓	✓	✓	- Reliable cytokinesis marker. - Labels ring structures throughout cytokinesis.	Bassi et al., 2013 Hickson lab, unpublished
Sticky (Citron kinase)	✗	✓	✓	✓	✓	✓	- Labels ring structures throughout cytokinesis. - Other puncta also present that can be hard to distinguish from late MR.	Bassi et al., 2013 El Amine et al, 2013
Septin2	✗	✓	✓	✓	✗	✗	- Labels the CR and nascent MR - Unreliable for late MRs and abscission.	Hickson lab, unpublished
Sqh (MRLC)	✗	✓	✓	✗	✓	✓	- Reliable cytokinesis marker. - Labels ring structures throughout cytokinesis.	Rogers et al. 2004 Dean et al. 2005 Hickson & O'Farrell, 2006 Kechad et al. 2012

3.7 FIGURES & TABLES

Table 3.1: Summary of localization patterns of a selection of validated markers for examining S2 cell cytokinesis.

Localization patterns of fluorescently tagged cytokinetic markers expressed in *Drosophila* S2 cells. Each marker is assessed for its reliability in identifying cells in early mitosis (i.e. before anaphase onset) and labeling the different MTsand/or cortical structures throughout cytokinesis: Central spindle (CS), contractile ring (CR), midbody, midbody ring (MR), shedding events and remnants that persist after abscission.✓or ✗ marks indicate reliability or unreliability, respectively, of each fluorescently tagged marker for labeling the indicated structure.

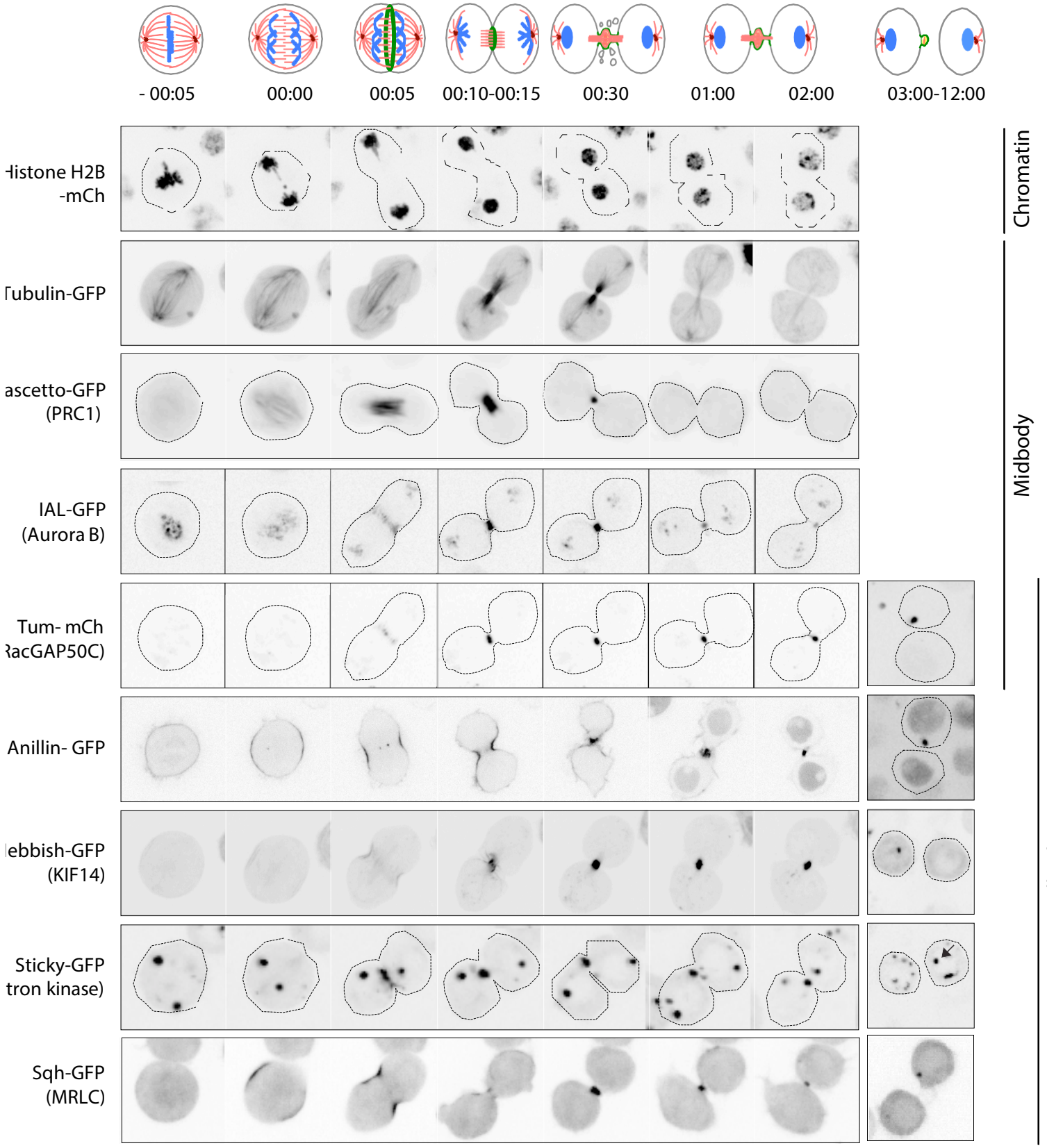
- 00:05
00:00
00:05
00:10-00:15
00:30
01:00
02:00
03:00-12:00
Histone H2B -mCh
Tubulin-GFP
Pascetto-GFP (PRC1)
IAL-GFP (Aurora B)
Tum- mCh RacGAP50C)
Anillin- GFP
Pebbish-GFP (KIF14)
Sticky-GFP tron kinase)
Sqh-GFP (MRLC)
Chromatin
Midbody
Midbody Ring & Remnant

Figure 3.1: Localization patterns of specific cytokinetic markers

Time-lapse sequences of a selection of S2 cell lines, expressing different FP-tagged markers that exhibit distinct localization patterns at the different stages of cytokinesis. All were expressed from the copper-inducible pMT promoter except Histone H2B-mCherry (mCh) and Tubulin-GFP, which were constitutively expressed from the pAc promoter. Dotted lines represent cell outlines. The arrow in the Sticky-GFP panel marks the MR remnant after abscission. Spinning disk confocal images were acquired using a 63X 1.4 NA plan-apochromat oil-immersion objective. Single Z confocal images, with look up tables inverted using Adobe Photoshop CS6, are shown. Times are in h: min, scale bar is 5 µm.

A)

- 3 days

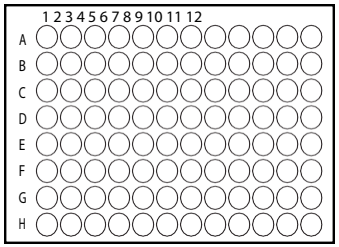

- Seed cells and add dsRNA.
- Include +ve and -ve controls.
- Induce expression with CuS04 if necessary.

Split + re-add dsRNA

- 12 to 24 hours

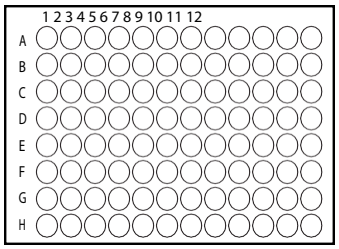

Transfer to glass bottomed imaging dish
(96 well plate or 8 well chambered coverslips)

Time 0

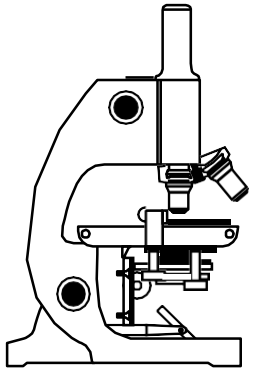

Spinning disk confocal microscopy

Low Resolutic
40X air objecti
4 XY positions per c
Multi-well visiting
4-5 min interva
12-24 h tota

High Resolutic
63X 1.4 NA C
5-10 XY positions p
30-60s intervals
2h total imaging

B)

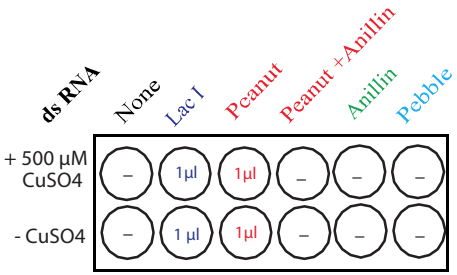

- 7 days

- Seed S2 cells in plastic 96 wells plate.
- Add 1 µg (1µg/µl) of Peanut dsRNA.
- Include negative controls: no dsRNA and Lac I.
- If rescue experiment, add CuSO4
- Include duplicate wells in which expression will not be induced.

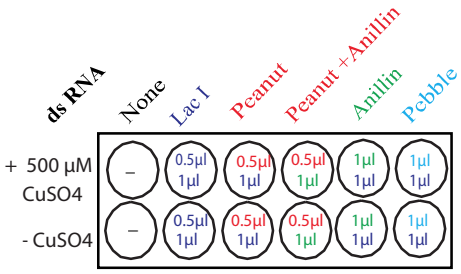

- 3 days

- Split S2 cells 1:2 in plastic 96 wells plate.
- Re-add fresh LacI and Peanut dsRNAs.
- Introduce Anillin and Pebble dsRNA.
- If rescue experiment, maintain [CuSO4].
- Adjust [dsRNA] to 2µg in all wells with LacI dsRNA

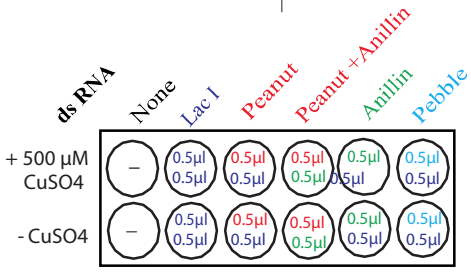

- 12 to 24 hours

- Split S2 cells 1:2 in glass bottomed imaging dish
- Re-add fresh ds RNA as required.
- If loss of function experiments add CuSO4, as appr

Figure 3.2: Typical experimental set-up and workflow.

A) General overview of a simple RNAi loss-of-function experiment: 3 days prior to imaging, plate the cells in a 96 well plastic plate and incubate with dsRNA along with positive (typically *pebble* ds RNA) and negative (typically *lacI dsRNA* and no dsRNA) controls. If a rescue experiment, induce expression with $CuSO_4$. 12 to 24 hours prior to imaging, split cells, re-add fresh dsRNA and transfer to glass bottomed imaging dish. If a loss of function experiment, induce expression with $CuSO_4$. At Day 0, proceed to your imaging system.

B) A specific example of a co-depletion experiment using dsRNAs that require different incubation times. First add dsRNAs that need the longest incubation time; here *peanut* dsRNA (7 days incubation), along with negative controls (*lacI dsRNA* and no dsRNA). Then split the cells and add dsRNAs that require a shorter incubation time; here *anillin* dsRNA (3 days incubation) along with positive control, *pebble* dsRNA (3 days incubation). 12 to 24 hours prior to imaging, split cells, re-add fresh dsRNA and transfer to a glass bottomed imaging dish. At Day 0, proceed to your imaging system. Adjust dsRNA concentration in each well as indicated. Include a non-induced duplicate experiment, where appropriate, to confirm RNAi efficacy.

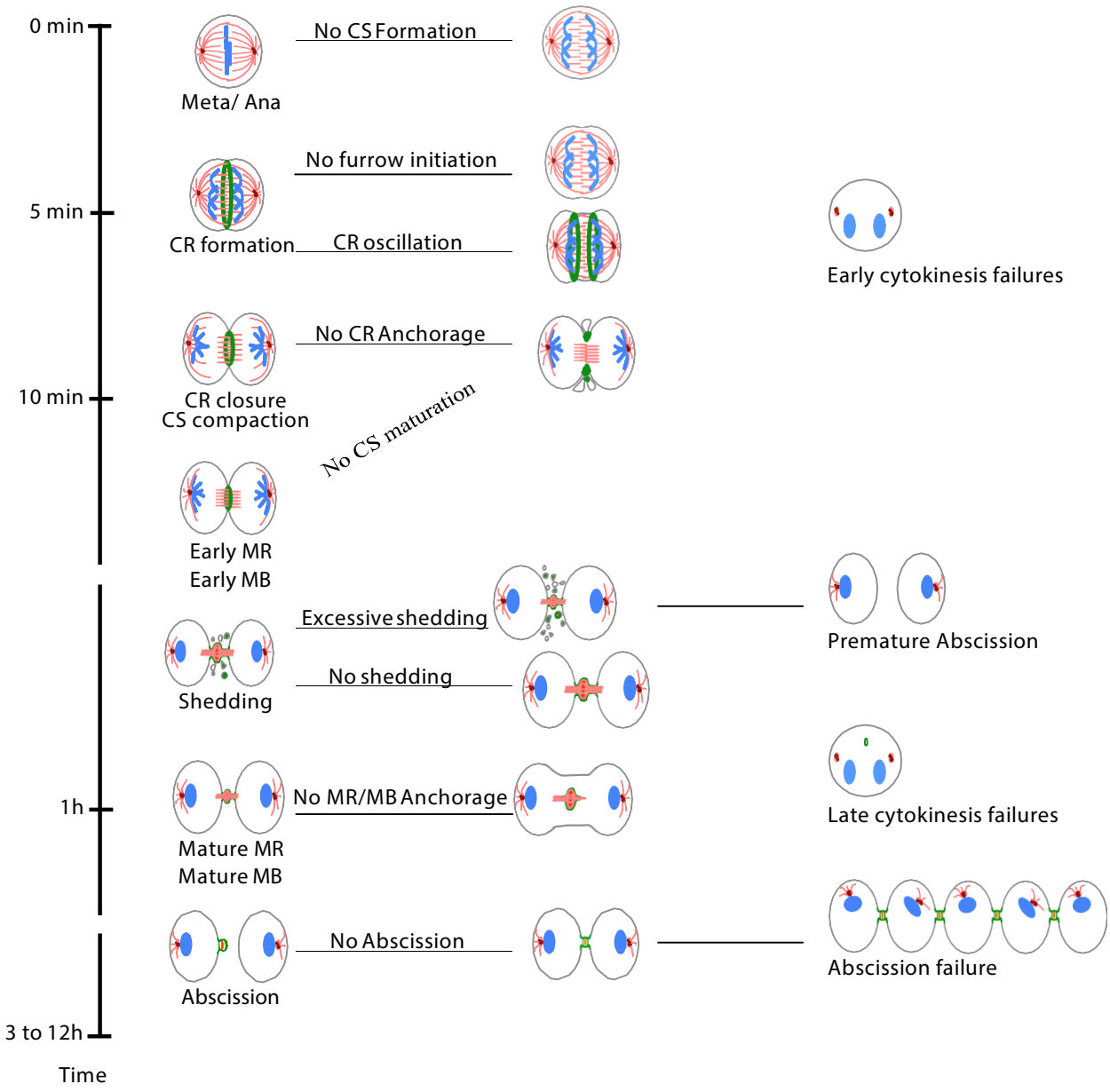
Normal progression
Defects
Possible outcomes
0 min
5 min
10 min
1h
3 to 12h
Time
Meta/ Ana
No CS Formation
No furrow initiation
CR formation
CR oscillation
Early cytokinesis failures
No CR Anchorage
CR closure
CS compaction
No CS maturation
Early MR
Early MB
Excessive shedding
Shedding
No shedding
Premature Abscission
Late cytokinesis failures
No MR/MB Anchorage
Mature MR
Mature MB
No Abscission
Abscission
Abscission failure

Figure 3.3: The progression of cytokinesis in S2 cells and possible phenotypic outcomes.

Cartoons describing the key steps during the normal progression of cytokinesis. These steps are highly regulated and prone to failure under certain experimental conditions. Here, we summarize some of the possible defects at each step and how they result in different phenotypes of cytokinesis failure.

4 ANILLIN ACTS AS A BIFUNCTIONAL LINKER COORDINATING MIDBODY RING BIOGENESIS DURING CYTOKINESIS.

Amel Kechad[1], Silvana Jananji[1], Yvonne Ruella[1,2] and Gilles R. X. Hickson[1,2,#]

[1]CHU Sainte-Justine Centre de Recherche, Centre de Cancérologie Charles Bruneau,

3175 Chemin de la Côte Ste-Catherine, Montréal, Québec, H3T 1C5, Canada.

[2]Départment de Pathologie et Biologie Cellulaire, Université de Montréal, Montréal, Québec, Canada.

Running title: Anillin in midbody ring biogenesis.

Keywords: Anillin, cytokinesis, contractile ring, midbody ring, septins.

Manuscript #: 22226749, Epub 5 janvier 2012

Kechad, A., S. Jananji, Y. Ruella, and Hickson G.R. 2012. Anillin acts as a bifunctional linker coordinating midbody ring biogenesis during cytokinesis. *Curr Biol.* 22: 197-203.

Contributions:

AK et GH ont conçu le projet

AK et GH ont rédigé l'article.

Les expériences ont été effectués par:

AK dans Fig. 1, 2, 3F-G, 4A-I, S1D, S2, S4,

GH dans Fig. 3 A-D, 4-I, S3

YR dans Fig S1C

SJ dans Fig S1B et la productions des constructions utilisées dans l'article

4.1 ABSTRACT

Animal cell cytokinesis proceeds via constriction of an actomyosin-based contractile ring (CR), (Eggert et al., 2006; Pollard, 2010). Upon reaching a diameter of ~1 µm (Mullins and Biesele, 1977), a midbody ring (MR) forms to stabilize the intercellular bridge until abscission (Barr and Gruneberg, 2007; Schweitzer and D'Souza-Schroey, 2004; Steigmann and Guerlich, 2009). How MR formation is coupled to CR closure and how plasma membrane anchoring is maintained at this key transition is unknown.

Time-lapse microscopy of *Drosophila* S2 cells depleted of the scaffold protein, Anillin (D'Avino, 2009; Hickson and O'Farrell, 2008; Piekny and Maddox, 2010), revealed that Anillin is required for complete closure of the CR and formation of the MR. Truncation analysis revealed that Anillin N-termini connected with the actomyosin CR and supported formation of stable MR-like structures, but these could not maintain anchoring of the plasma membrane. Conversely, Anillin C-termini failed to connect with the CR or MR but recruited the septin, Peanut, to ectopic structures at the equatorial cortex. Peanut depletion mimicked truncation of the Anillin C-terminus, resulting in MR-like structures that failed to anchor the membrane.

These data demonstrate that Anillin coordinates the transition from CR to MR, and that it does so by linking two distinct cortical cytoskeletal elements. One apparently acts as the core structural template for MR assembly, while the other ensures stable anchoring of the plasma membrane beyond the CR stage.

4.2 RESULTS AND DISCUSSION

4.2.1 The transition from the CR to mature MR requires Anillin

Anillin localizes to the CR and MR (Field and Alberts, 1995), and has conserved N-terminal domains shown in *Drosophila* to bind F-actin (Field and Alberts, 1995) and Cindr (Haglund et al., 2010), and in vertebrates to bind myosin II (Straight et al., 2005) and the formin, mDia2 (Watanabe et al., 2008). Conserved C-terminal AH/PH domains can also bind RacGAP50c/Tum in *Drosophila* (D'Avino et al., 2008; Gregory et al., 2008), and septins (Kinoshita et al., 2002; Oegema et al., 2000) and Rho (Piekny and Glotzer, 2008) in mammals. Because loss of Anillin blocks cytokinesis during late furrowing (Echard et al., 2004; Goldbach et al., 2008; Hickson and O'Farrell, 2008b; Piekny and Glotzer, 2008; Somma et al., 2002; Straight et al., 2005; Zhao and Fang, 2005) we sought to test whether Anillin might play a role in MR formation. We re-examined Anillin depletion phenotypes in *Drosophila* cells. Each of 3 distinct dsRNAs (Fig. S1A) depleted Anillin by 80% at 72 h (Fig. S1B), and produced penetrant and similar phenotypes, captured by time-lapse spinning disc confocal microscopy > of cells stably expressing myosin-GFP (Fig. 1) or GFP-tubulin (Fig. S1D). Images acquired every 4-5 min over several days revealed that cells failed their first division 30-72 h after dsRNA administration. Myosin-GFP recruitment and furrow initiation appeared normal, but cells blebbed excessively and failed cytokinesis via two similar yet distinct phenotypes. In one population, classed as oscillating failures, furrows ingressed to approximately 50% before oscillating laterally (Fig. 1B,D) as described previously in *Drosophila* (Hickson and O'Farrell, 2008b) and human cells (Piekny and Glotzer, 2008; Straight et al., 2005; Zhao and Fang, 2005), yielding binucleate cells 68±10 min after anaphase. In the second population, furrows ingressed beyond 50% and reached a semi-stable state (albeit with minor oscillations) that persisted for ~20 min before reopening (Fig. 1C and Movie S1), yielding binucleate cells 1h21±16 min after anaphase. These late furrow failures were the more prevalent (Fig. 1D). Images acquired at 30-60 sec intervals revealed that control (LacI RNAi) CRs closed within 12 ±2 min (mean±sd, n=10) of anaphase, producing MR structures of ~1 µm in diameter (Fig. 1E).

Initial closure rates of Anillin-depleted CRs were comparable to controls but they progressively slowed such that maximal ingression was reached 25 min post anaphase with a mean diameter of ~3 μm (Fig. 1E). While total myosin-GFP intensity declined sharply in control furrows, the decline slowed markedly in Anillin-depleted furrows, resulting in elevated levels of myosin at the time of maximal ingression (Fig.1C and Fig. S1C). In addition, Anillin-depleted cells failed to display a thinning of the center of the intercellular bridge (marked by GFP-tubulin, Fig. S1D), an event that normally accompanies MR formation.Thus, in addition to its role in preventing cleavage furrow oscillations, Anillin is required to maintain the normal rate and extent of CR closure and to allow formation of the MR, even when furrows do not oscillate.

4.2.2 C-terminally truncated Anillin supports formation of MR-like structures that fail to stably anchor the plasma membrane

Towards functionally dissecting Anillin, we generated stable cell lines inducibly expressing Anillin amino acids 1-758 fused to GFP or mCherry (Anillin-ΔC-FP, Fig. 2). In cells co-expressing endogenous Anillin and/or full-length Anillin-FP (Fig. 2A and Movie S2, upper cell), Anillin-ΔC-FP localized to nuclei during interphase (not shown) and to the cell cortex at metaphase (Fig. 2A). However, it was poorly recruited to the furrow cortex during ingression (Fig. 2A), indicating that although the Anillin N-terminus can localize to the cortex, the deleted AH/PH region must play a major role in recruiting Anillin during furrowing. Although barely detectable at the furrow apex at CR closure (Fig. 2A, 00:06:00), Anillin-ΔC-FP was still recruited to the MR during the following 10-20 min (Fig. 2A) and remained there until after abscission (not shown).

In Anillin-depleted cells, Anillin-ΔC-FP localized to the cell cortex at metaphase, became enriched at the equatorial cortex during early anaphase, and remained cortical throughout furrowing (Fig. 2B). Furrowing was slowed to a similar extent to cells depleted of all sources of Anillin, blebbing of the plasma membrane persisted and cytokinesis failed almost exclusively with the late furrow phenotype (Fig. 2B-D and Movie S2, lower cell). At the close of the prolonged furrowing, Anillin-ΔC-FP localized robustly to a structure resembling a MR, although its diameter was generally greater than a *bona fide* MR (Fig. 2B-

C). With a mean time of 40 min after anaphase (n=10), the plasma membrane lost attachment to the rings and regressed, resulting in binucleate cells harboring internal MR-like structures (Fig. 2B and Movie S2, lower cell), whose diameters decreased over ~20 min to that approaching control MRs (Fig. 2C). These MR-like structures persisted for many hours and were observed in 75% of failed division attempts, captured by time-lapse microscopy (n>50). Myosin-GFP provided an independent marker of these ring structures (Fig. S2B,C). Fromtimelapse recordings, 80-95% of cells co-expressing Anillin-ΔC-mCherry and myosin-GFP failed cytokinesis with internal MR-like structures (n>50, Fig. 2E and Fig. S2A), when depleted of endogenous Anillin. Conversely, only 18-25% (depending on dsRNA used) of cells expressing only myosin-GFP, depleted of Anillin, displayed such internal rings after failure: 12-30% displayed puncta (Fig. 2E and Fig. S2A); while 50-75% exhibited no persistent structures (Fig. 2E and Fig. S2A), even though myosin had been present at elevated levels during furrowing (Fig. 1D and Fig. S1C). Thus Anillin-ΔC-FP promoted the recruitment or stabilization of myosin-GFP to the structures. Myosin is a *bona fide* MR marker, consistent with these structures being analogous to MRs. Additional support includes reduced accessibility of both structures to Anillin antibodies (Fig. S2D,E), reduced levels of phalloidin-staining of both structures (Fig. S2F,G), and shared resistance of both structures to 1µg/ml of the inhibitor of actin polymerization, Latrunculin A (not shown).

4.2.3 N-terminally truncated Anillin localizes to cortical material that is disconnected from ring structures.

The reciprocal truncation, comprising only the AH/PH region, (Anillin-ΔN-FP) was cytoplasmic at metaphase (unlike full-length Anillin) and robustly recruited to the equatorial cortex during anaphase (Fig. 3A and Movie S3, upper cell), consistent with the above experiments and an analogous human truncation (Piekny and Glotzer, 2008). However, during furrowing, when Anillin-FP and myosin-FP normally colocalize (Fig. 3B), Anillin-ΔN-FP localized to cortical protrusions that extended outwards beyond co-expressed myosin-FP (Fig 3C) and endogenous Anillin (Fig. S3B), appearing as puncta that trailed the apex of the closing CR (Fig. 3A and Movie S3, middle cell). Anillin-ΔN-FP partially colocalized with a plasma membrane probe during furrowing (mCherry-PLCδ-PH, Fig. S3A) but was

excluded from the nascent MR marked by endogenous Anillin (Fig. 3D-E), rather displaying a peri-MR localization that was progressively lost by 60-90 min post-furrowing (not shown). Anillin-ΔN-GFP puncta colocalized poorly with phalloidin-labeled F-actin (Fig. S3C-E). Cells overexpressing Anillin-ΔN-FP furrowed with normal kinetics and completed cytokinesis (Fig. 3F-G). However, upon depletion of endogenous Anillin (using dsRNA2 or dsRNA3), 90% of division attempts failed (n=50) in a manner similar to Anillin-depleted control cells (Fig. 3F-G). Anillin-ΔN-FP was still recruited to the equatorial cortex and formed puncta that were associated with protrusions. Some of these protrusions clearly extended outwards for several μm (Fig. 3H-H' and Movie S3, middle cell), reminiscent of the microvillus-like projections that emanate from CRs of sea urchin embryos (Schroeder, 1972). Spatial segregation of Anillin-ΔN-FP and myosin-GFP was striking after endogenous Anillin depletion. While both FPs were simultaneously recruited to the equatorial cortex (Fig. 3I and Movie S3, lower cell), Anillin-ΔN-mCherry abruptly appeared in puncta external to the myosin-GFP. Myosin-GFP then oscillated back and forth across the equator, while Anillin-ΔN-mCherry remained equatorial (see Fig. S3F for additional example). Anillin-ΔN-FP presumably remained anchored via additional membrane and/or cytoskeletal components such as microtubules (D'Avino et al., 2008; Gregory et al., 2008; Hickson and O'Farrell, 2008b) or septins (see below). Anillin-ΔN-FP localized to the extreme cell periphery, even in cells treated with 1 μg/ml LatA to disrupt the cortical actin cytoskeleton (Fig. S3G). Given that the puncta were external to actomyosin, we interpret them as representing plasma membrane-associated material that was inappropriately disconnected from the underlying actomyosin cytoskeleton.

Collectively, these data show that the Anillin N-terminus localizes to the CR and is sufficient to allow its transformation into an MR structure, while the C-terminal domains of Anillin are required for robust recruitment during furrowing, timely closure of the CR and, crucially, for stable anchoring of the plasma membrane by the MR.

We also co-expressed Anillin-ΔN-FP and Anillin-ΔC-FP in the same cells. Each truncation localized to the same distinct cortical structures as when expressed alone, and co-expression did not rescue loss of Anillin, indicating that the N- and C-termini need to be physically linked to faithfully coordinate the transition from CR to MR (data not shown).

4.2.4 The septin, Peanut, acts with the Anillin C-terminus to anchor the plasma membrane to cytokinetic rings.

The Anillin C-terminus binds septins (Oegema et al., 2000) and Anillin recruits septins to the CR (Field et al., 2005; Hickson and O'Farrell, 2008b; Maddox et al., 2005) and to actin filaments *in vitro* (Kinoshita et al., 2002). We tested whether septins were constituents of the cortical material to which Anillin-ΔN-FP localized. Immunofluoresence confirmed Pnut colocalization with Anillin-ΔN-FP during cytokinesis (Fig. 4A), and also in cortical linear structures in interphase cells (Fig. S4), similar to those reported for a human Anillin C-terminal fragment (Oegema et al., 2000), and that we interpret as being plasma-membrane associated. Conversely, Pnut was undetectable in the Anillin-ΔC-FP-dependent MR-like structures that formed when endogenous Anillin was depleted (Fig. 4B, the localization of Pnut to tubular cytoplasmic structures is normal for S2 cells. Hickson and O'Farrell, 2008b).

Live imaging of Anillin-GFP expressing cells following 7-8 day incubation with Pnut dsRNAs (Fig. 4 C) revealed a 34% cytokinesis failure rate (n>80, Fig. 4F). In 87% of these failed attempts (n>20), Anillin-GFP localized to persistent MR-like structures that failed to anchor the plasma membrane (Fig. 4C,G and Movie S4), indicating that Pnut depletion phenocopies truncation of the Anillin C-terminus. Parallel depletions of Pnut in control cells marked only by GFP-tubulin resulted in a markedly higher cytokinesis failure rate (71%, n>50, Fig. 4F), suggesting that Anillin-GFP overexpression can partially rescue loss of Pnut.

In Anillin-ΔC-FP-expressing cells, Pnut depletion induced an 89% failure rate (n>40), predominantly with a late furrow phenotype (Fig. 4D,F). In 91% of failed cells, Anillin-ΔC-FP localized to internal MR-like structures following furrow regression (Fig. 4G). In Anillin-ΔN-FP-expressing cells, Pnut depletion induced a 93% failure rate (n>50), predominantly with an oscillating furrow phenotype (Fig. 4F). Pnut depletion also diminished recruitment of Anillin-ΔN-FP to the cleavage furrow, where it no longer formed puncta (Fig. 4E,H), and abolished the ectopic structures in interphase cells (Fig. S4E).

Thus the C-terminus of Anillin and Pnut are each dispensable for forming stable MR-like structures, but they cooperate to form ectopic structures and each is required for the MR to anchor the plasma membrane. Determining the precise mechanism of membrane anchoring requires further study. However, given that Anillin can localize to the MR independently of Pnut (Fig. 4), yet is insufficient to tether the membrane in the absence of Pnut, it seems likely that Anillin organizes a septin-dependent membrane anchor (Gilden et al., 2010) .

In summary, we show that Anillin is required for complete CR closure and concomitant MR formation. The Anillin N-terminus (Anillin-ΔC-FP), recruited to CRs, was sufficient to form stable structures that bore hallmarks of bona fide MRs but that failed toanchor the plasma membrane. The Anillin C-terminus (Anillin-ΔN-FP) was independently targeted to the equatorial cortex where it formed septin-dependent structures that were excluded from the actomyosin CR and the nascent MR.

These observations suggest that the MR derives directly from the CR, rather than forming as a separate entity, and lead to a model (Fig. 4I) in which Anillin N-termini guide the transformation of the CR into a stable core MR structure, while the Anillin C-termini simultaneously organize septins to form a robust membrane anchor. The data support early suggestions that Anillin might link the plasma membrane to the CR (Field and Alberts, 1995; Giansanti et al., 1999), but suggest that Anillin organizes a redundant membrane anchor at the CR stage that becomes essential at the MR stage. Further studies of these Anillin-dependent structures will likely yield deeper insight into the architecture of the cortical cytokinetic machinery.

4.3 MATERIAL AND METHODS

Constructs, cell lines and RNAi.

mCherry-tubulin and myosin-GFP (gifts from R. Vale), and Anillin-GFP have been described previously (Eggert et al., 2006). Functional Anillin-mCherry was generated by recombining Anillin pENTR-D-topo clone with the constitutive expression vector pAC-ChW (*actin05C* promoter). UAS-mCherry-PLCδ1-PH and its constitutive driver pAc-Gal4 were obtained from A. Kiger (UCSD).

For Anillin-ΔC-FP, and Anillin-ΔN-FP constructs, respectively, the first 2405 bp and the last 1334 bp of the coding sequence from clone LD23793 was PCR amplified and cloned into pENTR-D-TOPO (Invitrogen), following the manufacturer's recommendations. After sequence verification, these were recombined using LR Clonase into the copper inducible expression vectors pMT-WG and pMT-WCh, to generate fusions to the 5' ends of GFP and mCherry, respectively. Drosophila Schneider's S2 cells were transfected using Cellfectin reagent (Invitrogen) with relevant plasmids, together with pCoHygro, to generate stable, hygromycin-resistant cell lines following established protocols (Invitrogen).

Double-stranded RNAs (dsRNAs) were designed as described in (Mullins and Biesele, 1977) and generated using Ribomax kits (Promega). Anillin dsRNA1, Anillin dsRNA2 (against 3' UTR), Pnut dsRNA were previously described (Eggert et al., 2006), Anillin dsRNA3 was generated using the following primer sequences: 5'- atggacccgtttactcagc-3' and 5'-tcgactggacaaatgcggtttc-3'.

RNAi experiments were performed as follows: cells were plated in 96 well dishes and incubated with ~1 µg/ml dsRNA. 12-24 h prior to imaging or fixation, cells were transferred to 8-well chambered coverglass dishes (Labtek, Nunc). Live imaging was performed between 30 and 72 hours for Anillin RNAi, and between 7 and 9 days for Pnut RNAi, in which case cells were split and fresh dsRNA added at day 4.

Immunoblotting

S2 cells were grown in 12 well dishes, treated with indicated dsRNAs, and harvested by centrifugation. Cells were lysed in lysis buffer (50 mM Tris-HCl, pH7.5, 150 mM NaCl, 1% Triton-X-100), and total cell lysates were subjected to SDS-PAGE (8% polyacrylamide). Proteins were transferred to a nitrocellulose membrane and blocked with 5% milk in Tris-buffered saline containing 0.2% Tween-20 (TBST). The membrane was cut at the 80 kDa molecular weight marker with the upper molecular weight part immunoblotted with rabbit anti-Anillin antibodies (1:1000, a gift from J. Brill) while the lower molecular weight part was blotted with mAb anti-tubulin antibody (Sigma-Aldrich, clone DM1A, 1:1000). The blots were washed in TBST, incubated with horseradish peroxidase-coupled donkey anti- rabbit or anti-mouse secondary antibodies (1:5000, GE healthcare) and washed again prior to detection of signals using ECL reagent (Perkin Elmer).

Live cell microscopy

Live cell imaging of Drosophila S2 cells was performed in 8-well chambered coverglass dishes (Labtek, Nunc) at room temperature (20-23°C) using an Ultraview Vox spinning disc confocal system (Perkin Elmer), employing a CSU-X1 scanning unit (Yokogawa) and an Orca-R2 CCD camera (Hamamatsu) fitted to a Leica DMI6000B inverted microscope equipped with a motorized piezo-electric stage (Applied Scientific Instrumentation). Image acquisition and quantitation was performed using Volocity 5 software (Improvision/ PerkinElmer). Routine and long time-course imaging was performed using Plan Apo 40x (0.85 NA) air objectives with camera binning set to 2x2, high-resolution imaging was ession of FP-fusions under the control of the metallothionien promoter (pMT plasmids) were induced with 250 µM $CuSO_4$ when cells were transferred to imaging dishes, 12-24 h prior to the start of imaging in cases where there was no RNAi, or at the time of final dsRNA addition for rescue and Pnut RNAi experiments.

For FM4-64-FX imaging, living cells of interest were identified using the relevant GFP channel, and 5µg/ml freshly prepared FM4-64-FX (Invitrogen) was added directly to the culture medium 2-10 min prior to the start of image acquisition.

Immunofluorescence & fixed cell microscopy

Cells were transferred to either 8-well chambered coverglass dishes (Labtek, Nunc) or 96-well glass bottomed plates (Whatman) at least 2 h prior to fixation for 5 min in 4% formaldehyde/ 0.1% glutaraldehyde in phosphate-buffered saline (PBS). After permeabilisation and blocking in PBS containing 0.1% triton-X100 (PTX buffer) and 5% normal goat serum, cells were incubated with primary antibodies (rabbit anti-Anillin, a gift from C. Field, used at 1:1000; concentrated mAb 4C9H4 anti-peanut, from Developmental Studies Hybridoma Bank, used at 1:400) at 4°C overnight, washed with PTX buffer and incubated for 1 h with Alexa-488 or Alexa-546-conjugated goat anti-mouse or anti-rabbit secondary antibodies (1:500, Molecular Probes/ Invitrogen), as appropriate. Where appropriate, Hoechst 33258 (1:500) and rhodamine-phalloidin (1:500, Molecular Probes) were added at the same time. Cells were washed in PTX and mounted in Fluoromount-G (SouthernBiotech). Images were acquired using either the Ultraview Vox system described above or a Deltavision RT deconvolution system (Applied Precision) using Plan Apo 63x or 100x 1.4NA objectives.

Image analysis

Quantitation of 4D datasets (x,y,z, time) was performed using Volocity 5 Quantitation. Furrow diameters were measured using the line tool. Intensity measurements of myosin-GFP (Fig. S1C) were performed using the "select objects by % intensity" tool. Optimal percentage values were determined empirically for each cell and the resulting sum intensity values were then expressed as percentages relative to the highest value within the given time series. Datasets were background-corrected and photobleaching-corrected, the latter estimated empirically from nearby interphase cells whose intensity values do not ordinarily fluctuate during the sampling times used. Intensity measurements of Anillin-ΔC-GFP (Fig. 4H) are sum values expressed as percentages from time 0, obtained by selecting the cell equator as a boxed region of interest and subtracting from each voxel the background signals empirically determined from nearby dark spaces between cells. Images were processed for publication using Adobe Photoshop and assembled as figures using Adobe Illustrator. Movie files were exported from Volocity as Quicktime movies.

4.4 ACKNOWLEDGEMENTS

We are indebted to Patrick O'Farrell in whose lab this work was initiated (NIH grant R01-GM037193). We thank Christine Field, Julie Brill and the Developmental Studies Hybridoma Bank for antibodies, Ron Vale for myosin(Sqh)-GFP and mCherry-tubulin constructs. We thank Amy Maddox, Sébastien Carreno, Ekat Kritikou, Alisa Piekny, Catherine Sheppard and Nour El Amine for helpful discussions and comments on the manuscript.

GRXH is a Special Fellow of the Leukemia & Lymphoma Society and holder of *Fonds de la Recherche en Santé du Québec* (FRSQ) junior 1 salary award. This work is supported by grants from the Canadian Institutes of Health Research (MOP-97788), the Canadian Fund for Innovation and the FRSQ.

4.5 REFERENCES

Barr, F. A., and Gruneberg, U. 2007. Cytokinesis: placing and making the final cut. *Cell*. 131:847-860.

D'Avino, P.P., Takeda, T., Capalbo, L., Zhang, W., Lilley, K.S., Laue, E.D., and Glover, D.M. 2008. Interaction between Anillin and RacGAP50C connects the actomyosin contractile ring with spindle microtubules at the cell division site. *J Cell Sci.* 121:1151-1158.

D'Avino, P.P. 2009. How to scaffold the contractile ring for a safe cytokinesis - lessons from Anillin-related proteins. *J. Cell.Sci*. 122: 1071-1079.

Echard, A., Hickson, G.R., Foley, E., and O'Farrell, P.H. 2004. Terminal cytokinesis events uncovered after an RNAi screen. *Curr Biol*. 14:1685-1693.

Eggert, U.S., Mitchison, T.J., and Field, C.M. 2006. Animal cytokinesis: from parts list to mechanisms. *Annu Rev Biochem* . 75:543-566.

Field, C.M., and Alberts, B.M. 1995. Anillin, a contractile ring protein that cycles from the nucleus to the cell cortex. *J Cell Biol*.131:165-178.

Field, C.M., Coughlin, M., Doberstein, S., Marty, T., and Sullivan, W. 2005. Characterization of Anillin mutants reveals essential roles in septin localization and plasma membrane integrity. *Development*. 132:2849-2860.

Giansanti, M.G., Bonaccorsi, S., and Gatti, M. 1999. The role of anillin in meiotic cytokinesis of Drosophila males. *JCell Sci*. 112:2323-2334.

Gilden, J., and Krummel, M.F. 2010. Control of cortical rigidity by the cytoskeleton: emerging roles for septins. *Cytoskeleton*. 67:477-486.

Goldbach, P., Wong, R., Beise, N., Sarpal, R., Trimble, W.S., and Brill, J.A. 2010. Stabilization of the actomyosin ring enables spermatocyte cytokinesis in *Drosophila*. *Mol Biol Cell.* 21:1482-1493.

Gregory, S.L., Ebrahimi, S., Milverton, J., Jones, W.M., Bejsovec, A., and Saint, R. 2008. Cell division requires a direct link between microtubule-bound RacGAP and Anillin in the contractile ring. *Curr Biol*. 18:25-29.

Haglund, K., Nezis, I.P., Lemus, D., Grabbe, C., Wesche, J., Liestol, K., Dikic, I., Palmer, R., and Stenmark, H. 2010. Cindr interacts with anillin to control cytokinesis in Drosophila melanogaster. *Curr Biol*.20: 944-950.

Hickson, G.R., and O'Farrell, P.H. 2008. Anillin: a pivotal organizer of the cytokinetic machinery. *Biochem Soc Trans*. 36: 439-441.

Hickson, G.R., and O'Farrell, P.H. 2008. Rho-dependent control of anillin behavior during cytokinesis. *J Cell Biol*. 180: 285-294.

Kinoshita, M., Field, C.M., Coughlin, M.L., Straight, A.F., and Mitchison, T.J. 2002. Self-andactin-templated assembly of Mammalian septins. *Dev Cell*. 3:791-802.

Maddox, A.S., Habermann, B., Desai, A., and Oegema, K. 2005. Distinct roles for two *C. elegans* anillins in thegonad and early embryo. *Development*.132:2837-2848.

Mullins, J. M., andBiesele, J.J. 1977.Terminal phase of cytokinesis in D-98s cells. *J Cell Biol*. 73:672-684.

Oegema, K., Savoian, M.S., Mitchison, T.J., and Field, C.M. 2000. Functional analysis of a human homologue of the Drosophila actin binding protein anillin suggests a role in cytokinesis. *J Cell Biol*. 150:539-552.

Piekny, A.J., and Glotzer, M. 2008. Anillin is a scaffold protein that links RhoA, actin, and myosin during cytokinesis. *Curr Biol.* 18:30-36.

Piekny, A.J., and Maddox, A.S. 2010. The myriad roles of Anillin during cytokinesis. *Semin Cell Dev Biol*. 21: 881-891.

Pollard,T. D. 2010. Mechanics of cytokinesis in eukaryotes. *Curr Opin Cell Biol*. *22*: 50-56.

Schroeder, T.E. 1972. The contractile ring. II. Determining its brief existence, volumetric changes,andvital role in cleaving *Arbacia* eggs. *J Cell Biol.* 53: 419-434.

Schweitzer, J.K., and D'Souza-Schorey, C. 2004. Finishing the job: cytoskeletalandmembrane events bring cytokinesis to an end. *Exp Cell Res. 295*:1-8.

Somma, M.P., Fasulo, B., Cenci, G., Cundari, E., and Gatti, M. 2002. Molecular dissection of cytokinesis by RNA interference in *Drosophila* cultured cells. *Mol Biol Cell.* 13:2448-2460.

Steigemann, P., and Gerlich, D.W. 2009. Cytokinetic abscission: cellular dynamics at the midbody. *Trends Cell Biol*. *19*: 606-616.

Straight, A.F., Field, C.M., and Mitchison, T.J. 2005. Anillin binds non muscle myosin II and regulates the contractile ring. *Mol Biol Cell*. 16:193-201.

Watanabe, S., Ando, Y., Yasuda, S., Hosoya, H., Watanabe, N., Ishizaki, T., and Narumiya, S. 2008. mDia2 induces the actin scaffold for the contractile ring and stabilizes its position during cytokinesis in NIH 3T3 cells. *Mol Biol Cell.* 19:2328-2338.

Zhao, W.M., and Fang, G. 2005. Anillin is a substrate of anaphase-promoting complex/cyclosome (APC/C) that controls spatial contractility of myosin during late cytokinesis. *J Biol Chem*. 280: 33516-33524.

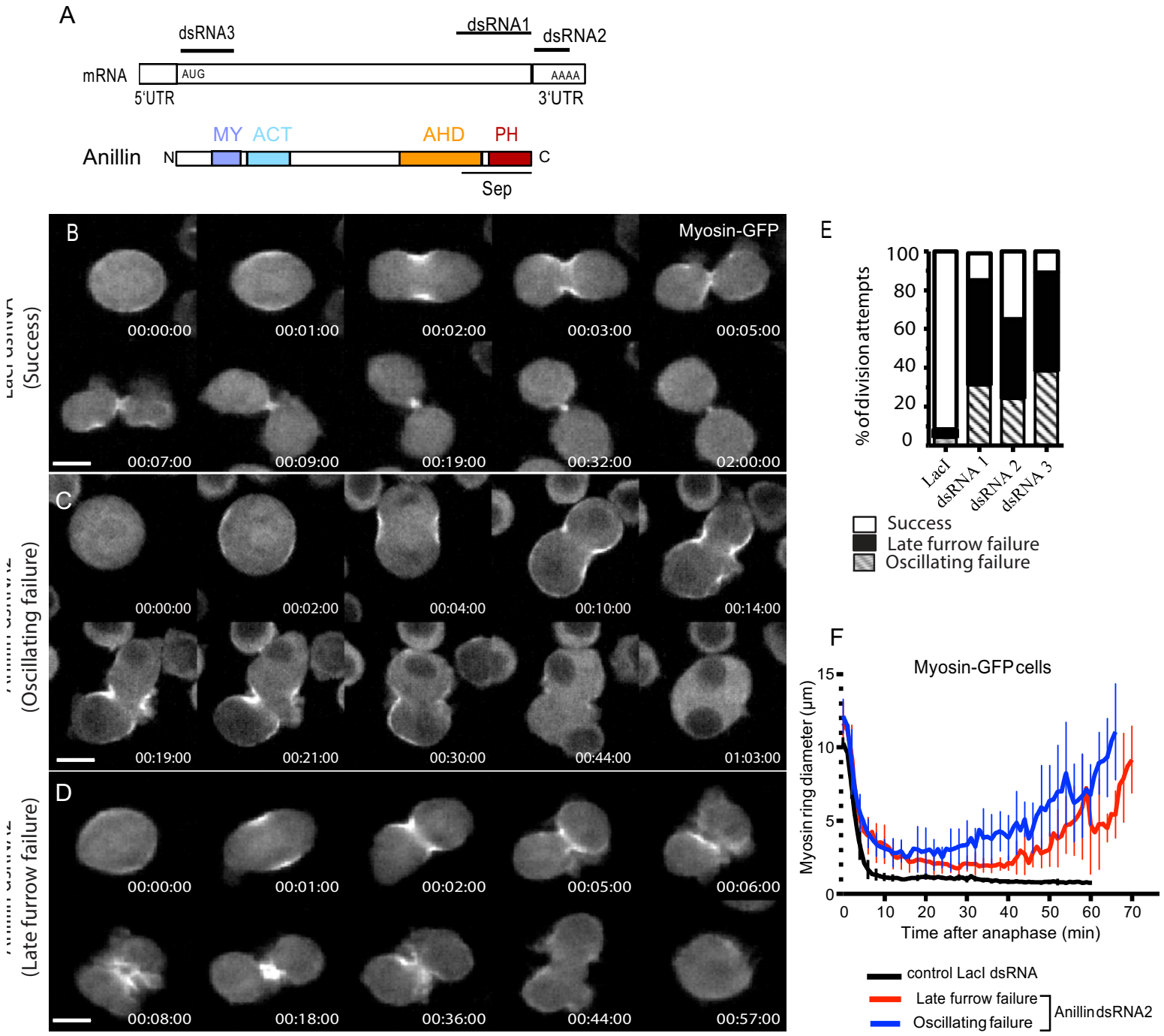
A
dsRNA3
dsRNA1
dsRNA2
mRNA
AUG
AAAA
5'UTR
3'UTR
MY ACT
AHD
PH
Anillin
N
C
Sep
B
Myosin-GFP
00:00:00
00:01:00
00:02:00
00:03:00
00:05:00
00:07:00
00:09:00
00:19:00
00:32:00
02:00:00
(Success)
C
00:00:00
00:02:00
00:04:00
00:10:00
00:14:00
00:19:00
00:21:00
00:30:00
00:44:00
01:03:00
(Oscillating failure)
D
00:00:00
00:01:00
00:02:00
00:05:00
00:06:00
00:08:00
00:18:00
00:36:00
00:44:00
00:57:00
(Late furrow failure)
E
% of division attempts
100
80
60
40
20
0
LacI
dsRNA 1
dsRNA 2
dsRNA 3
Success
Late furrow failure
Oscillating failure
F
Myosin-GFP cells
Myosin ring diameter (µm)
15
10
5
0
0
10
20
30
40
50
60
70
Time after anaphase (min)
control LacI dsRNA
Late furrow failure
Oscillating failure
Anillin dsRNA2

4.6 FIGURES AND LEGENDS

Figure 4.1: Complete closure of the CR and formation of the MR requires Anillin.

A Time-lapse sequence of control myosin-GFP cell undergoing cytokinesis after incubation with control (LacI) dsRNA. See movie S1, left hand cell. **B** Anillin-depleted myosin-GFP expressing cell failing cytokinesis via an oscillating furrow phenotype. **C** Anillin-depleted myosin-GFP expressing cell failing cytokinesis via a late furrow phenotype. See movie S1, right hand cell. **D** Quantification of phenotypic classes of cells succeeding or undergoing their first failed division following 30-72 h incubation with each dsRNA (n=50 each). **E** Diameters of myosin-GFP rings from the 3 phenotypic classes plotted over time (mean ± sd, n=10 per condition). See also Fig. S1. Scale bars, 5 μm.

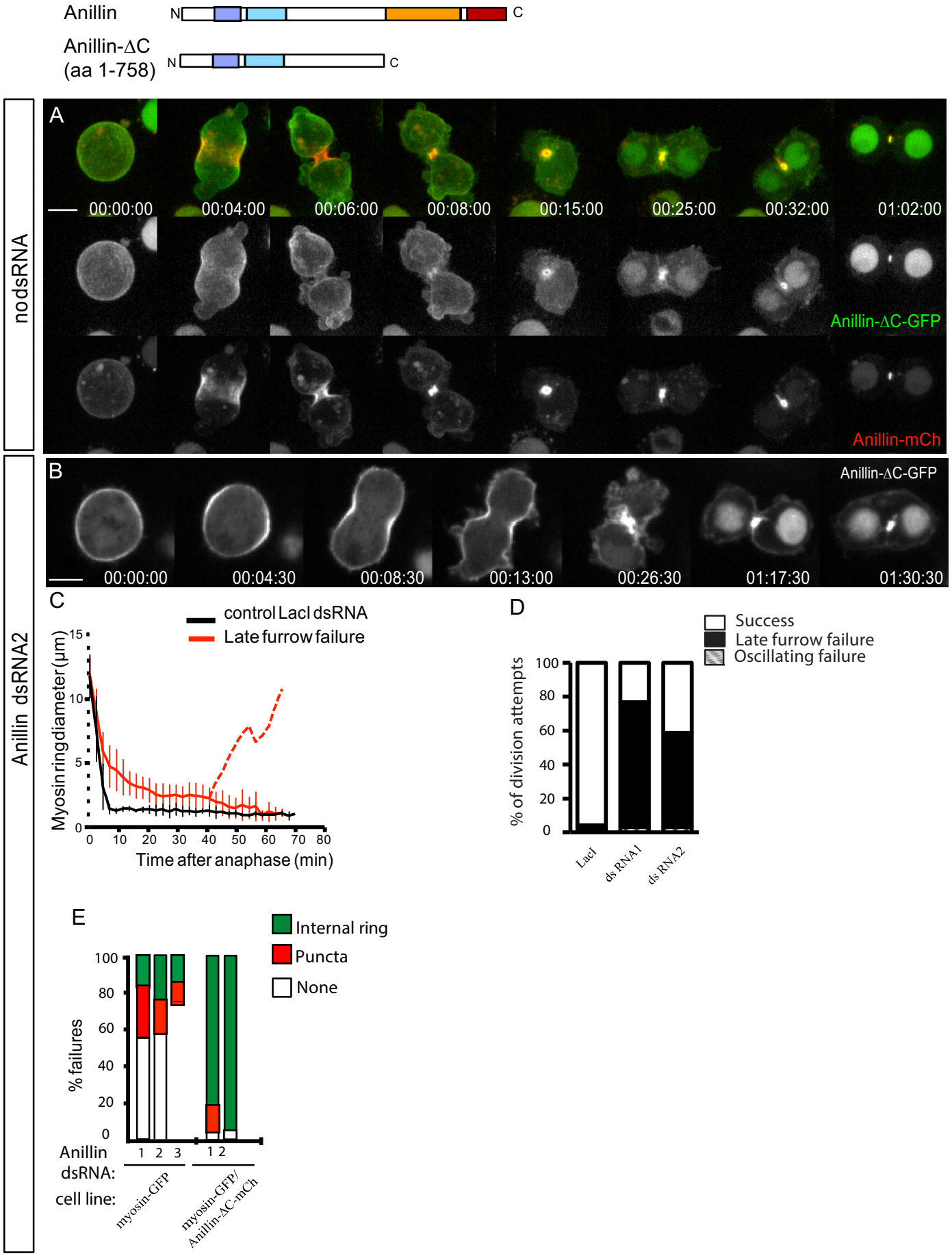
Anillin
N
C
Anillin-ΔC
(aa 1-758)
N
C
no dsRNA
A
00:00:00
00:04:00
00:06:00
00:08:00
00:15:00
00:25:00
00:32:00
01:02:00
Anillin-ΔC-GFP
Anillin-mCh
Anillin dsRNA2
B
Anillin-ΔC-GFP
00:00:00
00:04:30
00:08:30
00:13:00
00:26:30
01:17:30
01:30:30
C
control LacI dsRNA
Late furrow failure
Myosin ring diameter (μm)
Time after anaphase (min)
D
Success
Late furrow failure
Oscillating failure
% of division attempts
LacI
ds RNA1
ds RNA2
E
Internal ring
Puncta
None
% failures
Anillin dsRNA:
cell line:
myosin-GFP
myosin-GFP/ Anillin-ΔC-mCh

Figure 4.2: Anillin-ΔC supports formation of midbody ring-like structures but not their anchoring to the plasma membrane.

A Time-lapse sequence of a typical cell expressing Anillin-mCh (lower panels, red in merged) and Anillin-ΔC-GFP (middle panels, green in merged) undergoing furrowing and MR formation. See also movie S2, upper cell. **B** Timelapse sequence of a typical cell depleted of endogenous Anillin and expressing Anillin-ΔC-GFP. See also movie S2, lower cell. **C** Myosin-GFP ring diameters plotted over time from cells co-expressing Anillin-ΔC-mCh following control or endogenous Anillin RNAi (mean ± sd, n=10 per condition). Dotted line represents the equatorial diameter from mean time of furrow regression. **D** Quantification of phenotypic classes observed in Anillin-ΔC-GFP-expressing cells succeeding or undergoing their first failed division following 30-72 h control (LacI) or Anillin RNAi (n=50 per condition). **E** quantification from time-lapse records of each terminal binucleate phenotype (shown in Fig. S2A) for the indicated cell lines depleted of endogenous Anillin using the indicated dsRNAs (n≥30 failed division attempts per condition). See also Fig. S2. Scale bars, 5 μm.

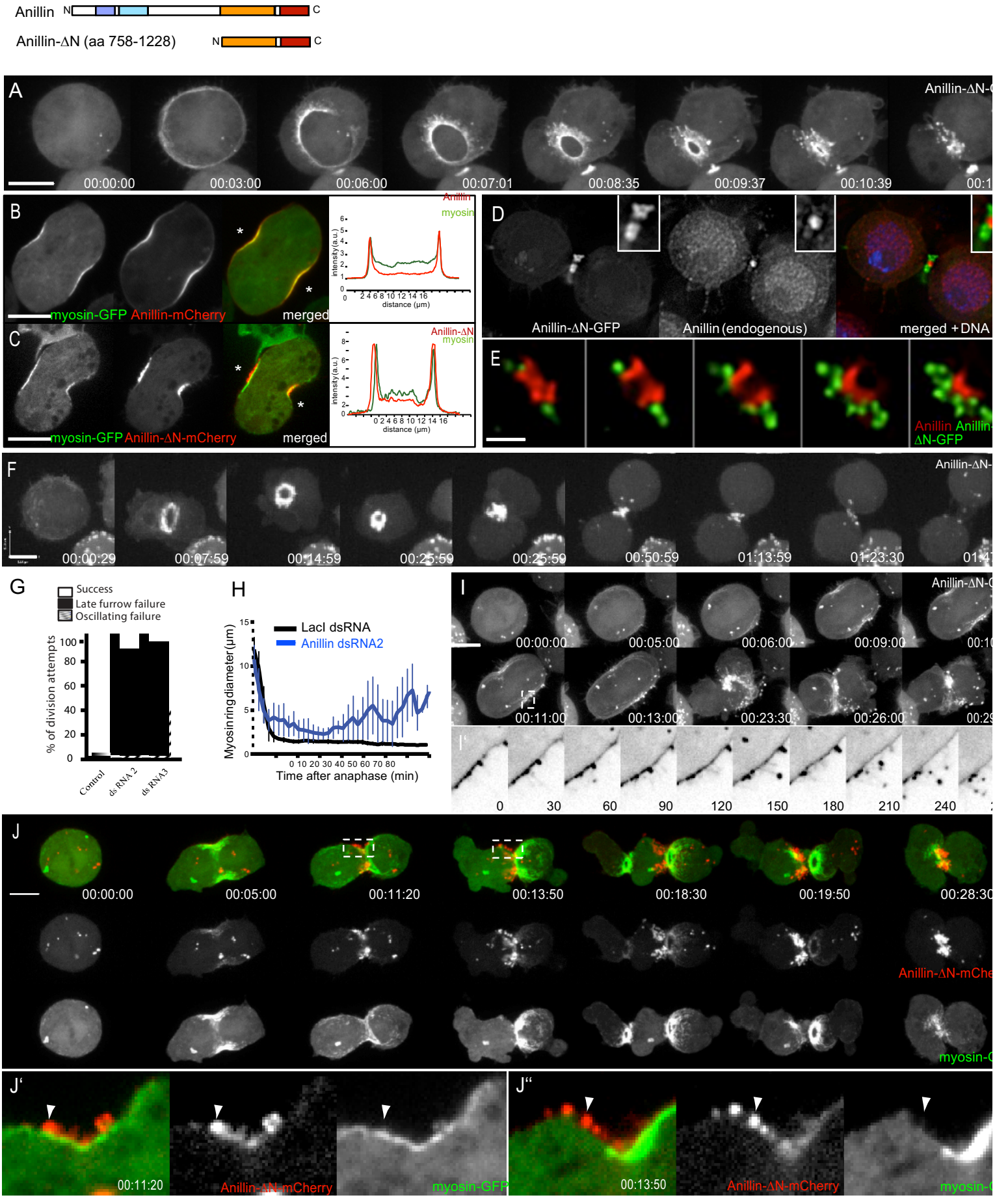
Anillin N C
Anillin-ΔN (aa 758-1228) N C
A
Anillin-ΔN-
00:00:00
00:03:00
00:06:00
00:07:01
00:08:35
00:09:37
00:10:39
B
myosin-GFP Anillin-mCherry
merged
Anillin
myosin
intensity (a.u.)
distance (μm)
C
myosin-GFP Anillin-ΔN-mCherry
merged
Anillin-ΔN
myosin
D
Anillin-ΔN-GFP
Anillin (endogenous)
merged + DNA
E
Anillin Anillin-ΔN-GFP
F
Anillin-ΔN-
00:00:29
00:07:59
00:14:59
00:25:59
00:25:59
00:50:59
01:13:59
01:23:30
G
Success
Late furrow failure
Oscillating failure
% of division attempts
Control
ds RNA 2
ds RNA3
H
LacI dsRNA
Anillin dsRNA2
Myosin ring diameter (μm)
Time after anaphase (min)
I
Anillin-ΔN-
00:00:00
00:05:00
00:06:00
00:09:00
00:11:00
00:13:00
00:23:30
00:26:00
I'
0
30
60
90
120
150
180
210
240
J
00:00:00
00:05:00
00:11:20
00:13:50
00:18:30
00:19:50
00:28:30
Anillin-ΔN-mChe
myosin-
J'
00:11:20
Anillin-ΔN-mCherry
myosin-GFP
J''
00:13:50
Anillin-ΔN-mCherry
myosin-

Figure 4.3: Anillin-ΔN forms cortical material that is disconnected from ring structures

A Time-lapse sequence of a cell expressing Anillin-ΔN-GFP and mCh-tubulin (not shown). See also movie S3, upper cell. **B-C** Cell co-expressing myosin-GFP and Anillin-mCh (B) or Anillin-ΔN-mCh (C) during early furrowing. Intensity profiles along a line drawn between the asterisks are shown. **D-E** Deconvolved single Z planes (or montage of Z planes, E) of MRs fixed and stained for endogenous Anillin (red in merged) in cells co-expressing Anillin-ΔN-GFP (green). **F** Quantification of phenotypic classes observed in Anillin-ΔN-GFP-expressing cells succeeding or undergoing their first failed division following 30-72 h control (LacI) or Anillin RNAi (n=50 per condition). **G** Myosin-GFP ring diameters plotted over time in cells co-expressing Anillin-ΔN-mCh following control or endogenous Anillin RNAi (late furrow failures only, mean±sd, n=10 per condition). **H** Time-lapse sequence of a typical cell depleted of endogenous Anillin and expressing Anillin-ΔN-GFP and mCh-tubulin (not shown). Maximum intensity projection of 6 Z planes. See also movie S3, middle cell. **H'** Inverted LUT of single optical section of boxed region in **H**, enlarged and with higher temporal resolution as indicated (sec). **I** Time-lapse sequence of a typical cell depleted of endogenous Anillin and expressing Anillin-ΔN-mCh (red) and myosin-GFP (green) attempting cytokinesis (maximum intensity projection). See also movie S3, lower cell. **I'-I"** Magnified views of single z planes from boxed regions in I. See also Fig. S3. Scale bars, 5 μm.

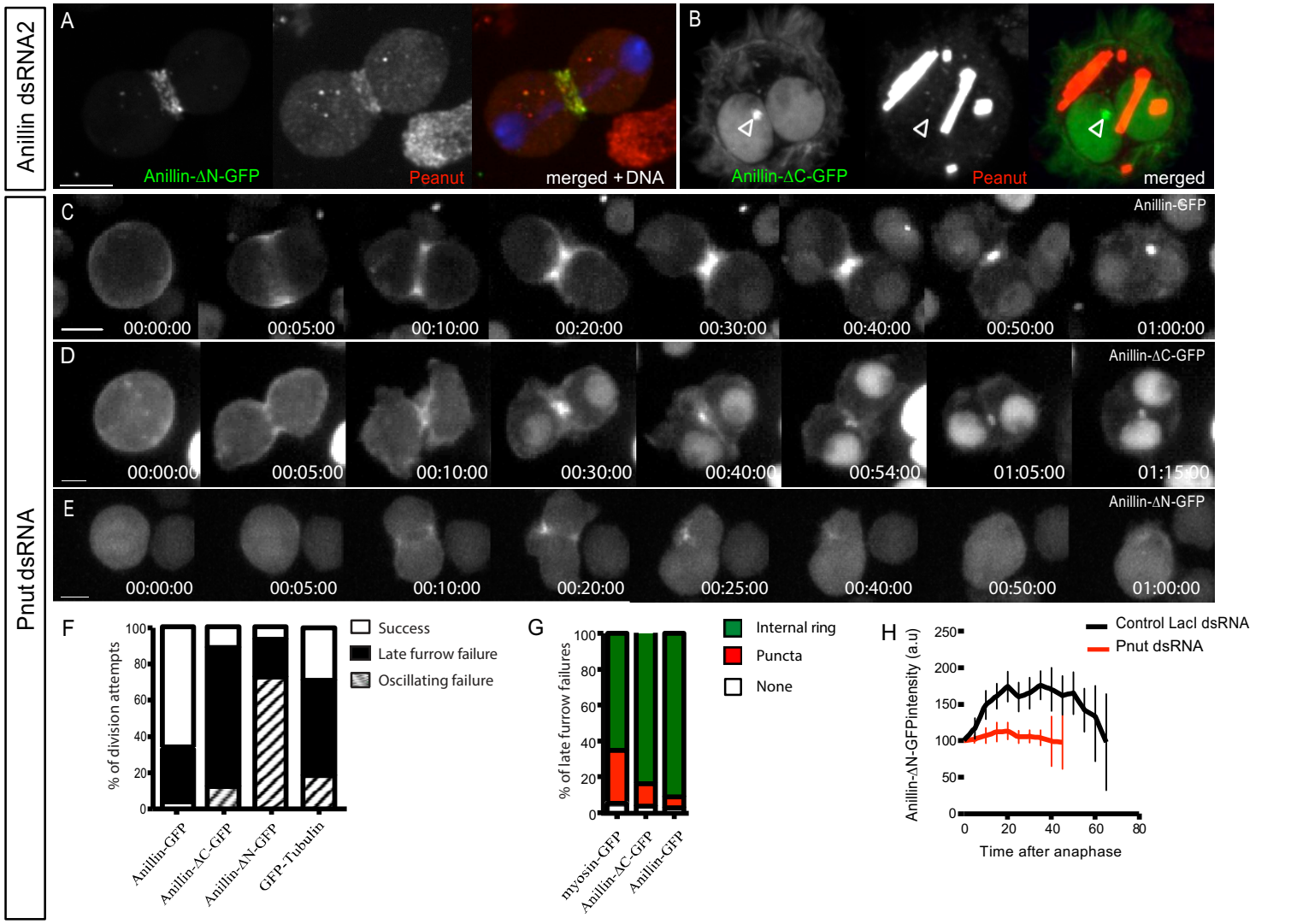
Anillin dsRNA2
Pnut dsRNA
A
Anillin-ΔN-GFP
Peanut
merged + DNA
B
Anillin-ΔC-GFP
Peanut
merged
C
Anillin-GFP
00:00:00
00:05:00
00:10:00
00:20:00
00:30:00
00:40:00
00:50:00
01:00:00
D
Anillin-ΔC-GFP
00:00:00
00:05:00
00:10:00
00:30:00
00:40:00
00:54:00
01:05:00
01:15:00
E
Anillin-ΔN-GFP
00:00:00
00:05:00
00:10:00
00:20:00
00:25:00
00:40:00
00:50:00
01:00:00
F
% of division attempts
Success
Late furrow failure
Oscillating failure
Anillin-GFP
Anillin-ΔC-GFP
Anillin-ΔN-GFP
GFP-Tubulin
G
% of late furrow failures
Internal ring
Puncta
None
myosin-GFP
Anillin-ΔC-GFP
Anillin-GFP
H
Anillin-ΔN-GFP intensity (a.u)
Control LacI dsRNA
Pnut dsRNA
Time after anaphase

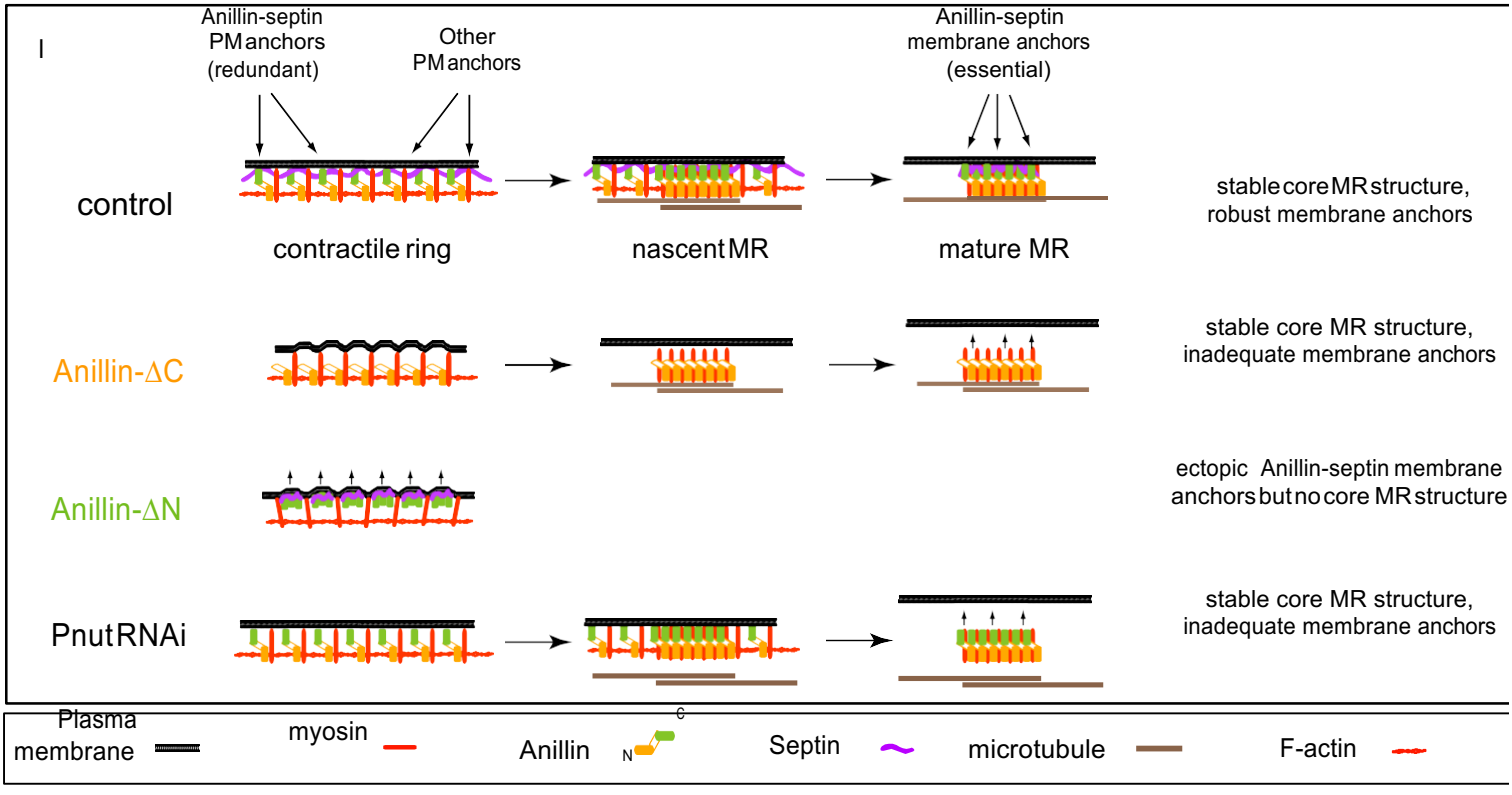
I
Anillin-septin PM anchors (redundant)
Other PM anchors
Anillin-septin membrane anchors (essential)
control
contractile ring
nascent MR
mature MR
stable core MR structure, robust membrane anchors
Anillin-ΔC
stable core MR structure, inadequate membrane anchors
Anillin-ΔN
ectopic Anillin-septin membrane anchors but no core MR structure
Pnut RNAi
stable core MR structure, inadequate membrane anchors
Plasma membrane
myosin
Anillin
N
C
Septin
microtubule
F-actin

Figure 4.4: The septin, Peanut, acts with the Anillin Cterminus to anchor theplasma membrane to the MR.

A Pnut immunofluorescence of a cell expressing Anillin‐ΔN‐GFP during furrowing. **B** Pnut immunofluorescence in a cell expressing Anillin-ΔC-GFP following Anillin RNAi. Open arrowhead marks an Anillin-ΔC-FP-positive MR-like structure that does not label with Pnut antibody. Note that the localization of Pnut to tubular cytoplasmic structures is normal for S2 cells [21]. **C-E** Time-lapse sequences of cells expressing Anillin-GFP (C), Anillin-ΔC-GFP (D) and Anillin-ΔN-GFP (E) following a 7- day incubation with Pnut dsRNA. See also movie S8. **F** Quantification from timelapse records of each phenotypic class for the indicated cell lines depleted of pnut (n=30 division attempts per condition). **G** Percentages of failures that resulted in GFP localizing to persistent internal midbody ring-like structures in the indicated cell lines. **H** Quantitation over time of total Anillin-ΔN-GFP intensities at the cytokinetic apparatus following control or Pnut RNAi. **I** Cartoon summary of results and model for Anillin and septin action during the transition from CR to MR. Scale bars, 5 μm.

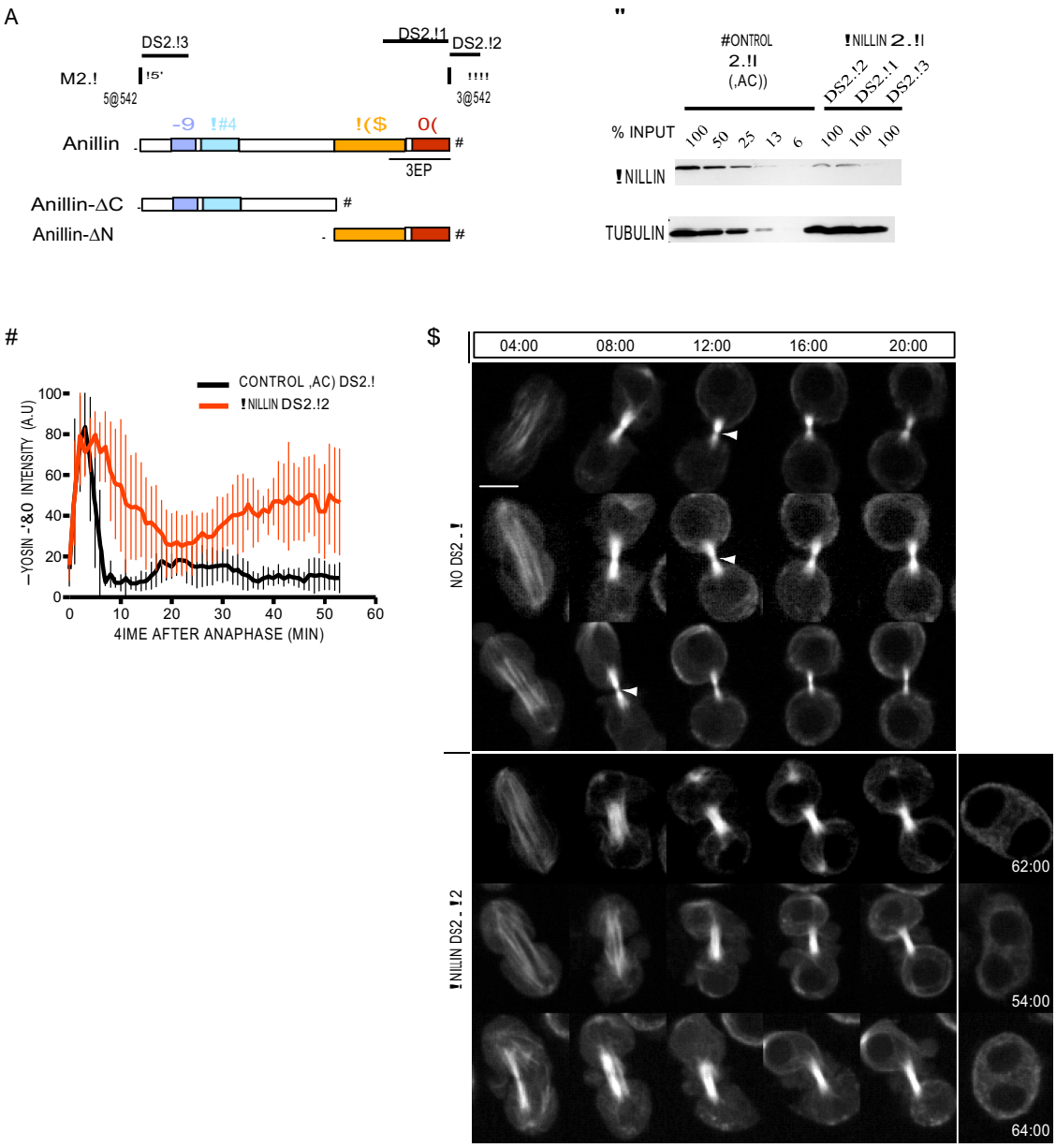
A
DS2.!3
DS2.!1
DS2.!2
M2.!
!5'
!!!!
5@542
3@542
-9 !#4
!($ 0(
Anillin
#
3EP
Anillin-ΔC
#
Anillin-ΔN
#
"
#ONTROL
2.!!
(,AC))
!NILLIN 2.!!
DS2.!2
DS2.!1
DS2.!3
% INPUT
100 50 25 13 6 100 100 100
!NILLIN
TUBULIN
#
CONTROL ,AC) DS2.!
!NILLIN DS2.!2
—YOSIN -'&O INTENSITY (A.U)
100
80
60
40
20
0
0 10 20 30 40 50 60
4IME AFTER ANAPHASE (MIN)
$
04:00 08:00 12:00 16:00 20:00
NO DS2.!
!NILLIN DS2.!2
62:00
54:00
64:00

Figure S4.1: Anillin- depleted late furrows have elevated levels of myosin and the intercellular bridge fails to display the characteristic narrowed region that normally accompanies MR formation

A Cartoons of Anillin mRNA, showing regions targeted by dsRNAs used in this study, and of domain organization of Anillin including myosin-binding (MY), actin binding (ACT), Anillin homology (AHD), pleckstrin homology (PH) domains and septin interacting region (Sep). Truncations used in this study are also depicted. **B** Immunoblot analysis of untransfected S2 cells treated for 72 h with control (LacI) or Anillin dsRNAs. A serial dilution of the control lysate was run alongside Anillin-depleted lysates. After transfer, the blot was cut in two and each half probed for Anillin or tubulin as shown. **C** Quantitation over time of total myosin-GFP intensities at the cytokinetic apparatus following 48-58 h incubation with control or Anillin dsRNAs. The precipitous decline in myosin-GFP that normally occurs during furrowing is less apparent upon Anillin depletion. **D** Stills from time-lapse sequences of cells expressing GFP-tubulin following 48-58 h incubation with or without Anillin dsRNA2. The center of the intercellular bridge, which narrows where the MR forms in controls (arrowheads), does not narrow in Anillin-depleted cells. Scale bar, 5 μm.

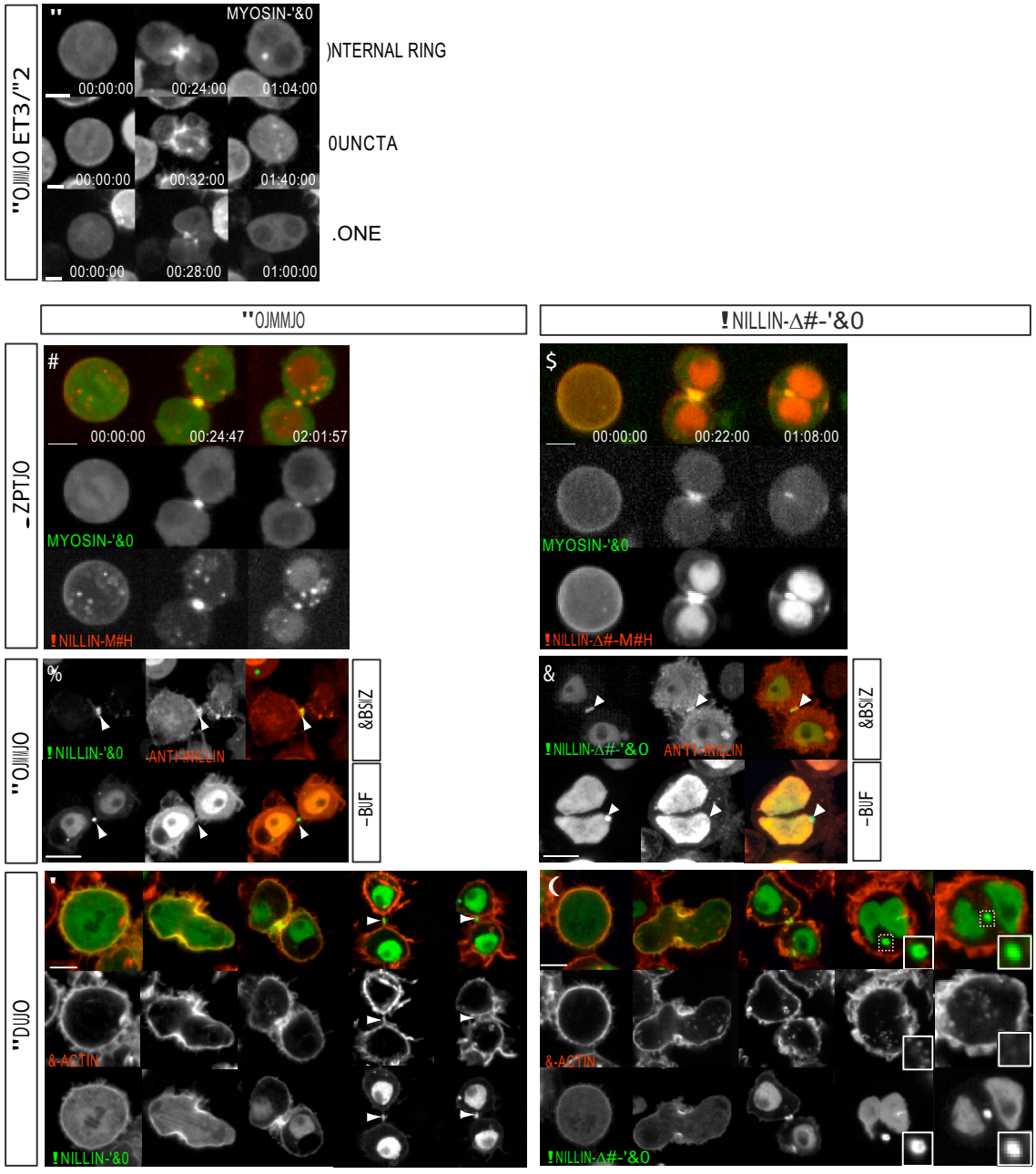
MYOSIN-'&0
00:00:00
00:24:00
01:04:00
00:00:00
00:32:00
01:40:00
00:00:00
00:28:00
01:00:00
)NTERNAL RING
0UNCTA
.ONE
00:00:00
00:24:47
02:01:57
MYOSIN-'&0
!NILLIN-M#H
00:00:00
00:22:00
01:08:00
MYOSIN-'&0
!NILLIN-Δ#-M#H
!NILLIN-'&0
ANTI-NILLIN
!NILLIN-Δ#-'&0
ANTI-NILLIN
&BS\Z
-BUF
&-ACTIN
!NILLIN-'&0
&-ACTIN
!NILLIN-Δ#-'&0

Figure S4.2: **Anillin-dependent MRs and Anillin-ΔC-dependent MR-like structures each recruit myosin and show reduced Anillin antibody accessibility and reduced F-actin staining**

A Time-lapse images of Anillin-depleted, myosin-GFP expressing cells failing via a late furrow phenotype, giving rise to the three indicated terminal binucleate phenotypes. **B-C** Time-lapse sequences of cells co-expressing myosin-GFP and Anillin-mCherry (B) or Anillin-ΔC-mCherry (C) depleted of endogenous Anillin (dsRNA2 for 48-72 h). **D-E** Cells expressing Anillin-GFP (D) or Anillin-ΔC-GFP (E) (green in merged) fixed and stained with anti-Anillin antibody (red in merged) at the early nascent MR stage (upper panels) and at a later stage (lower panels). Images represent single confocal sections that were acquired and contrasted identically. Arrowheads point to MRs and MR-like structures. **F-G** Montage of cells depleted of endogenous Anillin (dsRNA2 for 48-72 h) and expressing Anillin-GFP (F) or Anillin-ΔC-GFP (G), fixed and stained for F-actin (red in merged). Arrowheads point to MRs in F, boxed regions are magnified in G. Scale bars, 5 μm.

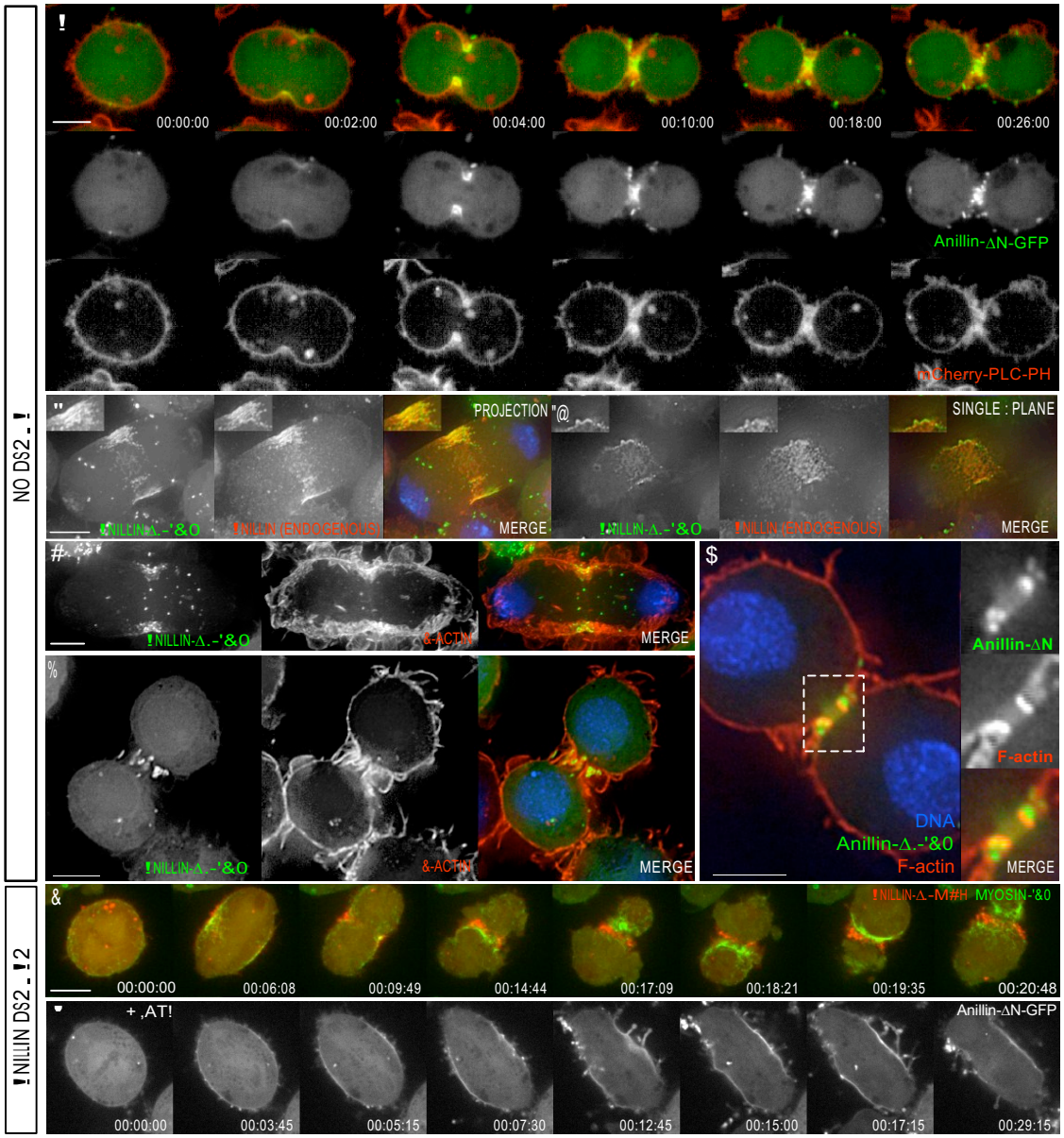
NO DS2_!
!NILLIN DS2_!2
00:00:00
00:02:00
00:04:00
00:10:00
00:18:00
00:26:00
Anillin-ΔN-GFP
mCherry-PLC-PH
PROJECTION "@
SINGLE : PLANE
MERGE
&-ACTIN
Anillin-ΔN
F-actin
DNA
Anillin-Δ.-'&0
00:00:00
00:06:08
00:09:49
00:14:44
00:17:09
00:18:21
00:19:35
00:20:48
+ ,AT!
00:00:00
00:03:45
00:05:15
00:07:30
00:12:45
00:15:00
00:17:15
00:29:15

Fig. S4.3 Anillin-ΔN localizes to the cortex independently of actomyosin and endogenous Anillin (Related to Fig. 3).

A Cell co-expressing Anillin-ΔN-GFP (green in merged) and mCherry-PLCδ1-PH (red in merged) **B** Cell expressing Anillin-ΔN-GFP (green in merged), stained for endogenous Anillin (red in merged) and DNA (blue). A is a maximum intensity projection of 20 deconvolved Z planes; B' is a single plane near the coverslip; insets show magnified regions of the adjacent cortex. **C-E** Cells expressing Anillin-ΔN-GFP (green in merged), stained for F-actin (red in merged) and DNA (blue). C, E are maximum intensity projections of 5 deconvolved Z planes; D is a single optical section. Note the lack of colocalization of Anillin-ΔN-GFP and F-actin. **F** Time-lapse sequence of a cell co-expressing Anillin-ΔN-GFP (red) and myosin-GFP (green), depleted of endogenous Anillin following 48 h incubation with dsRNA2. Although both FPs are recruited to the equatorial cortex at the same time, they do not remain colocalized. **G** Time-lapse sequence of an Anillin-depleted cell expressing Anillin-ΔN-GFP, in the presence of 1 µg/ml LatA added 30-60 min before filming. Scale bars, 5 µm

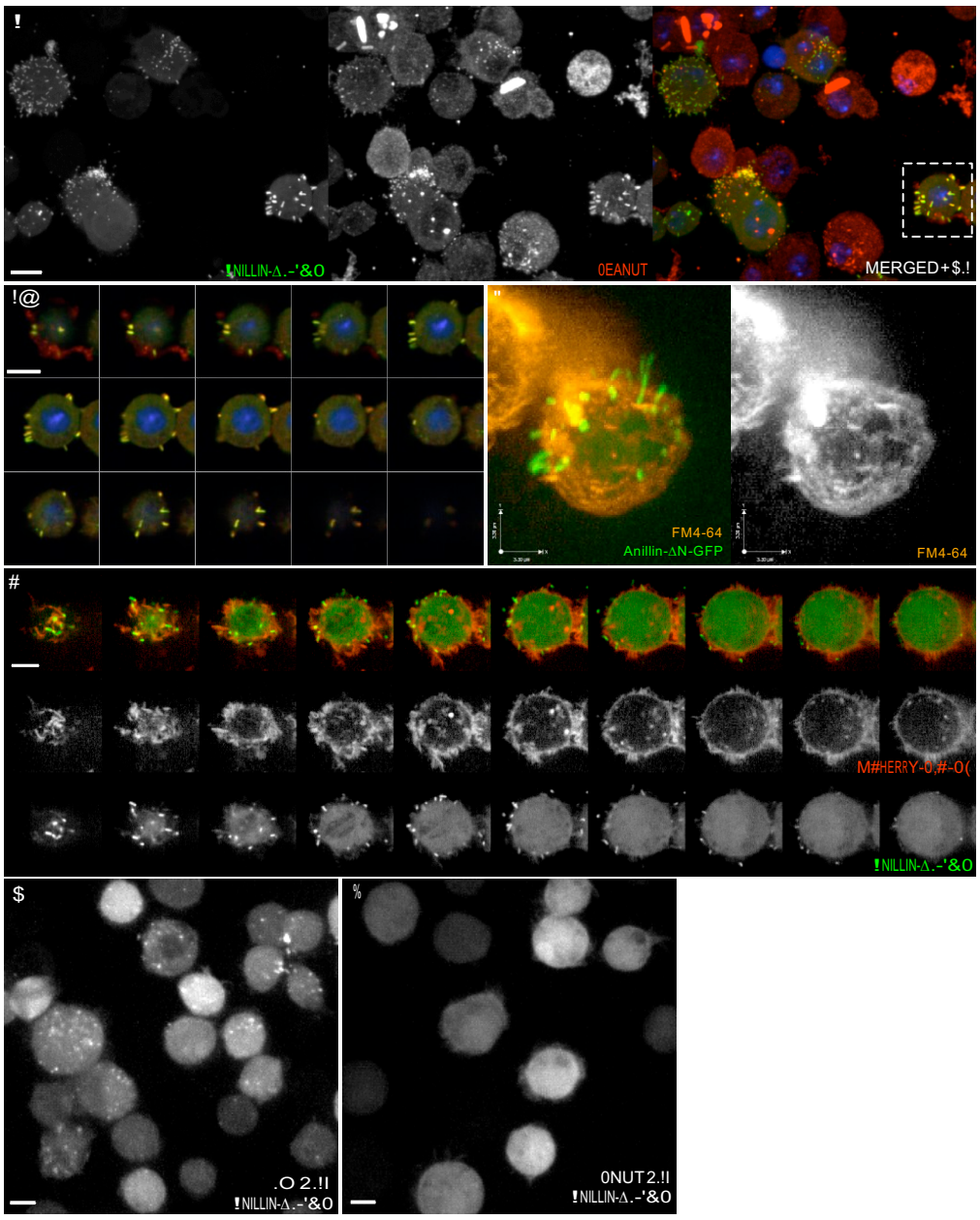
!
!NILLIN-Δ.-'&O
0EANUT
MERGED+$.!
!@
"
FM4-64
Anillin-ΔN-GFP
FM4-64
#
M#HERRY-0,#-0(
!NILLIN-Δ.-'&O
$
.O 2.!I
!NILLIN-Δ.-'&O
%
0NUT2.!I
!NILLIN-Δ.-'&O

Fig. S4.4 Peanut and Anillin-ΔN form cortical structures in interphase cells (Related to Fig. 4).

A Cells expressing Anillin-ΔN-GFP (left panel, green in merged) fixed and stained with an antibody against Peanut (centre, red in merged). Anillin-ΔN-GFP and Peanut colocalize in ectopic structures of many interphase cells. Note that Peanut also localizes strongly to cylindrical cytoplasmic structures (devoid of Anillin) that are found in untransfected S2 cells, as described in [1]. **A'** Montage of optical sections of boxed cell in (**A**), showing cell surface localization of ectopic structures. **B** Maximum intensity projection of an interphase cell expressing Anillin-ΔN-GFP, incubated with lipophylic dye FM4-64FX 5 min prior to imaging. The Anillin-ΔN-GFP structures protrude from the cell surface, but do not label with the dye. **C** Montage of optical sections of an interphase cell co-expressing Anillin-ΔN-GFP and mCherry-PLCδ1-PH. The Anillin-ΔN-GFP structures protrude from the cell surface, but do not colocalize with mCherry-PLCδ1-PH. **D-E** Anillin-ΔN-GFP-expressing cells after 6-day incubation with control (D) or Pnut dsRNAs (E). Anillin-ΔN-GFP no longer localizes to ectopic structures, indicating that they are Pnut-dependent. Scale bars, 5 μm.

5 OPPOSING ACTIONS OF SEPTINS AND STICKY ON ANILLIN PROMOTE THE TRANSITION FROM CONTRACTILE TO MIDBODY RING.

Nour El Amine[1,2], Amel Kechad[1,2], Silvana Jananji[1] and Gilles R. X. Hickson[1,2,#]

[1]CHU Sainte-Justine Centre de Recherche, Centre de Cancérologie Charles Bruneau, 3175 Chemin de la Côte Ste- Catherine, Montréal, Québec, H3T 1C5, Canada.

[2]Départment de Pathologie et Biologie Cellulaire, Université de Montréal, Montréal, Québec, H3C 3J7, Canada.

Running title: midbody ring biogenesis.

Keywords: Anillin, citron kinase, sticky , spetins, cytokinesis, contractile ring, midbody ring.

Manuscript #:201305053, 28 Aout 2013.
El Amine, N., A. Kechad, S. Jananji, and G.R. Hickson. 2013. Opposing actions of septins and Sticky on Anillin promote the transition from contractile to midbody ring. *The journal of Cell Biology*. 203:487-504.

Contributions:

NE, AK et GH ont conçu le projet

NE, AK et GH ont rédigé l'article.

Les expériences ont été effectués par

NE dans Fig. 1, 2, 6, 7, 8, S2, S3, S4, S5

AK dans Fig. 4, 5, S1

GH dans Fig. 3, 9

SJ dans la production de certaines constructions utilisées dans l'article

5.1 ABSTRACT

During cytokinesis, closure of the actomyosin contractile ring (CR) is coupled to the formation of a midbody ring (MR), through poorly understood mechanisms. Using time-lapse microscopy of *Drosophila* S2 cells, we show that the transition from the CR to the MR proceeds via a previously uncharacterized maturation process that requires opposing mechanisms of removal and retention of the scaffold protein, Anillin. The septin cytoskeleton acts on the C-terminus of Anillin to locally trim away excess membrane from the late CR/nascent MR via internalization, extrusion and shedding, whereas the citron kinase, Sticky, acts on the N-terminus of Anillin to retain it at the mature MR. Simultaneous depletion of septins and Sticky not only disrupted MR formation but also caused earlier CR oscillations, uncovering redundant mechanisms of CR stability that can partly explain the essential role of Anillin in this process. Our findings highlight the relatedness of the CR and MR and suggest that membrane removal is coordinated with CR disassembly.

5.2 INTRODUCTION

During cytokinesis of animal cells, an actomyosin-based contractile ring (CR) forms and drives the ingression of a cleavage furrow that bisects the cell at the midpoint of the microtubule-based spindle (Barr and Gruneberg, 2007; Eggert et al., 2006; Glotzer, 2005; Green et al., 2012; Pollard, 2010). The CR is a dynamic, membrane-bound structure that requires continuous Rho-dependent signaling (Bement et al., 2005) and contains many cytoskeletal proteins including actin, myosin II, Anillin, septins, and their regulators. CR closure occurs via disassembly and proceeds until reaching a diameter of 1-2 μm (Carvalho et al., 2009; Schroeder, 1972). The CR then transforms itself into the midbody ring (MR), a long-lived, dense structure that forms around the center of the midbody as it matures from the anti-parallel midzone microtubules that become compacted during CR closure (Hu et al., 2012; Mullins and Biesele, 1977). The MR is essential for cementing the efforts of the CR and for specifying where, and presumably when, abscission ultimately occurs (Green et al., 2012; Steigemann and Gerlich, 2009).

Our prior work showed that the transition from the CR to the MR requires the scaffold protein, Anillin (Kechad et al., 2012). Anillin depleted CRs are unstable and oscillate back and forth across the equator (Goldbach et al., 2010; Hickson and O'Farrell, 2008b; Piekny and Glotzer, 2008; Straight et al., 2005; Zhao and Fang, 2005), but even CRs that do not oscillate, fail to close completely and fail to form a stable MR (Kechad et al., 2012). Anillin can bind many other cytokinesis proteins including F-actin (Field and Alberts, 1995), myosin (Straight et al., 2005), septins (Field et al., 2005; Liu et al., 2012; Oegema et al., 2000), RacGAP50c (D'Avino et al., 2008; Gregory et al., 2008), among others (reviewed in D'Avino, 2009; Hickson and O'Farrell, 2008a; Piekny and Maddox, 2010). It remains unclear how Anillin acts to dampen the inherent instabilities of cleavage furrows (Dorn and Maddox, 2011; Sedzinski et al., 2011), and how it subsequently guides MR formation following CR closure.

Here we show that the CR gives rise to the MR via a previously uncharacterized maturation process involving opposing mechanisms acting on Anillin: the septin, Peanut, acts with the C-terminus of Anillin to locally remove membrane; while the Citron kinase, Sticky, acts to retain the N-terminus of Anillin at ring structures. Furthermore, Peanut and Sticky redundantly stabilize the earlier CR. The data lead to the proposal that septin-dependent

removal of membrane-associated Anillin during disassembly of the actomyosin ring contributes to CR stability and closure, while Sticky-dependent retention of Anillin also contributes to CR stability and limits the removal of Anillin from the mature MR.

5.3 RESULTS

5.3.1 Maturation of the midbody ring is accompanied by removal and retention of Anillin.

To better define the process of MR formation and maturation, we have monitored the localization of Anillin-GFP (Hickson and O'Farrell, 2008b) using time-lapse spinning disc confocal microscopy. Anillin-GFP localized to the CR and MR throughout cytokinesis and to the MR remnant that remained associated with one of the sister cells after abscission (Fig. 1A). Induced expression of Anillin-GFP under the control of the *metallothionein* promoter resulted in a 4-fold over-expression of Anillin (Fig. S1A-C). This fully rescued for loss of endogenous Anillin (Hickson and O'Farrell, 2008b) and had no consequence on the duration of furrowing or the timing of abscission when compared to other markers such as GFP-tubulin or the myosin regulatory light chain, Spaghetti squash-GFP (myosin-GFP, not shown). However, during formation of the MR, we observed a gradual thinning of the MR structure that was unexpectedly accompanied by extrusion and internalization of Anillin-GFP (Fig. 1A-C). Extrusion originated from blebs or tubules that formed either at late stages of furrowing (Fig. 1B and Video S1) or at the nascent MR soon after furrowing (Fig. 1C). The extruded material persisted for several minutes and in some cases was clearly shed completely from the cell (Fig. 1B and C, arrowheads). During internalization, Anillin-containing structures budded from the cytokinetic apparatus and were internalized into the cytoplasm as punctate vesicular structures (Fig. 1E, and Video S2). At the nascent MR, Anillin-FP sometimes labeled plasma membrane folds that had been gathered up during CR closure (Fig. S1E). Such plasma membrane folds were also evident by electron microscopy (Fig. S1F). Mature MRs, however, were more uniform in shape, had more closely opposed plasma membranes and exhibited a double ring ultrastructure with a more electron dense outer layer and a less dense inner layer (Fig. S1F), similar to that described for intercellular canals in *Drosophila* embryos (Haglund et al., 2011). The extruded structures labeled with a plasma membrane marker, myristoylated-

palmitoylated-GFP (myrpalm-GFP, Fig. S1), although this revealed many additional plasma membrane protrusions associated with the nascent MR that did not contain Anillin-FP (Fig. S1G). These membrane protrusions accumulated during furrowing, but then gradually dissipated during MR maturation, indicating that excess plasma membrane is gathered by the CR and then removed from the nascent MR (Fig. S1H).

Extrusion/shedding and internalization of Anillin occurred during the ~1 h period that followed CR closure, and coincided with a progressive decline in total Anillin-FP intensity measured at the nascent MR (Fig. 1E, n=20). Beyond this time, the appearance and intensity of MRs remained constant until after abscission. We examined the dynamic nature of Anillin-GFP at different stages of MR biogenesis using FRAP. When the entire MR region was bleached within 15 min of CR closure (Fig. 1F, upper panel), 30±13% of Anillin-GFP fluorescence recovered within 4 min (Fig. 1G, n=16). However, when bleached >45 min after CR closure (Fig. 1F, lower panel), only 10±6% recovery was observed within 4 min (Fig. 1G, n=9), indicating that the potential to restore Anillin to the MR declined as it matured. Photoconversion of an Anillin-Dendra2-FP revealed that the recovery occurred preferentially at the flanking regions while less exchange occurred at the central region of the MR (Fig. S1H). We conclude that nascent MRs mature over the course of ~1 h into stable MRs, during which they progressively extrude, shed and internalize Anillin.

5.3.2 Nascent MRs shed numerous cytokinesis proteins, but not F-actin.

We wished to determine whether other cytokinesis proteins were also shed with Anillin during MR maturation. Immunofluorescence analysis revealed that the septin, Peanut (Fig. 2A), and Rho1 (Fig. 2B), were also enriched on the extruded membranes. Similarly the Citron kinase, Sticky-FP, was extruded with Anillin-FP (Fig. 2C), as were the components of the centralspindlin complex, RacGAP50C/Tumbleweed-FP (Tum, Fig. 2D) and the kinesin-6 motor, Pavarotti-FP (Pav, Fig. 2E). Aurora B-GFP, which also localizes primarily to the central spindle and midbody microtubules (Fig. 2F), was also extruded from the center of the midbody soon after CR closure.

Cells expressing myosin-GFP showed no evidence of extrusion, shedding or

internalization (Fig. 2G), unless Anillin-mCh was also co-expressed, in which case some myosin-GFP colocalized with shed Anillin-mCh (Fig. 2H). However, the F-actin probe LifeAct-GFP (Riedl et al., 2008), although enriched at the late CR, did not colocalize with extruded Anillin-FP (Fig. 2I). Phalloidin staining of fixed cells also revealed that the extruded Anillin-positive membranes labeled poorly for F-actin (Fig. 2J). Thus, while numerous key components of the cytokinesis machinery were removed via extrusion and shedding, actin was specifically not. We next designed experiments to further understand the mechanisms of Anillin removal from the late CR/nascent MR.

5.3.3 Shedding from the nascent MR requires Anillin but not ESCRT-III or the proteasome.

Aurora B-GFP and Tum-GFP showed evidence of shedding even when Anillin was not over-expressed (Fig. 3A-B). We therefore used these markers to test whether Anillin was itself required for shedding. In Anillin-depleted cells, Aurora B-GFP was no longer extruded compared to controls, but still disappeared from the cleavage site over a similar time-course to controls (Fig. 3A-B, n>20). Similarly, no evidence of Tum-GFP extrusion was observed from Anillin-depleted late CRs/nascent MRs (Fig. 3C-D, n>20). Thus Anillin is required for extrusion, although we note that this may reflect a direct requirement for Anillin in the extrusion process, or an indirect consequence of the requirement for Anillin in complete CR closure (Kechad et al., 2012), or both.

The membrane topology during extrusion/shedding is the same as the abscission event that occurs later. We therefore tested whether shedding, like abscission, requires ESCRT III complexes. A 3-4 day depletion of Shrub, the *Drosophila* ortholog of CHMP4B, a key ESCRT III component (Carlton et al., 2012; Elia et al., 2011), delayed abscission well beyond the 3h48±1h57 (mean±sd, n=12) observed for untreated controls, although cells never became binucleated. Shrb-depleted cells remained paired for so long that they could not be reliably followed from furrowing to abscission, as the cells, being poorly adherent, would often move out of the imaging field over time. However, we noted that 30% of Shrb-depleted cells initiated cytokinesis while still connected to their sister cells from the previous attempt (Fig. 3E-G, n=110 pairs), whereas control cells had always undergone abscission prior to reaching

the next metaphase (n>55 pairs). Daisy chains of Shrb-depleted cells were sometimes observed, consistent with abscission failure in multiple rounds of division. Even in the most extreme cases, normal MR maturation was observed, including extrusion, shedding and internalization of Anillin-GFP (Fig. 3H and Fig. S2A. See also Video S4). Similar results were obtained upon depletion of dIST1 (not shown), another ESCRT-III component required for cytokinesis (Agromayor et al., 2009). Thus, ESCRT III is required for abscission, as expected, but not for MR maturation.

Human Anillin is subject to APC/C-mediated degradation (Zhao and Fang, 2005). We tested whether degradation of *Drosophila* Anillin might contribute to its decline during MR maturation, by treating cells expressing Anillin-GFP with the proteasome inhibitor, MG132. When added early in mitosis, 5 μM MG132 induced widespread metaphase arrest, as expected. Cells that successfully underwent the metaphase/anaphase transition during the 5 min before or after MG132 addition, however furrowed normally (Fig. S2B). However, while untreated control cells typically exhibited a net loss of Anillin-GFP soon after the end of furrowing, MG132-treated furrows accumulated Anillin-GFP during the subsequent 15-20 min after closure (Fig. S2C, n=14), before exhibiting a profile of net loss that was similar to controls (Fig. S2D, n=20), and that ended with a mature MR that was indistinguishable from controls (Fig. S2E). Extrusion and shedding of Anillin-GFP during MR maturation continued in MG132 (Fig. S2E). We conclude that proteasomal degradation is not required for extrusion/shedding of Anillin and does not provide a major contribution to the loss of Anillin from the MR during its maturation. However, proteasomal degradation, directly or indirectly, appears to limit the extent or accelerate the rate of Anillin-GFP accumulation at the late CR/ nascent MR.

A third population of cells displayed a highly aberrant exit from mitosis that was seen 5-40 min after MG132 addition. Slow and excessive spindle elongation, slow and broad furrows, and a failure of nuclear envelope reformation and/or nuclear import of Anillin-GFP characterized this (Fig. S2F). We interpret these cells as having degraded only a subset of APC/C substrates, resulting in a partial arrest. Remarkably, most of these cells succeed to a midbody-like stage, although they were not followed until completion.

Collectively, these experiments show that cortical extrusion/ shedding during the transition from CR to MR requires Anillin but does not depend on ESCRT-III or the proteasome. We next performed a structure-function analysis of Anillin to further define the requirements for its extrusion and shedding.

5.3.4 Removal of Anillin from the nascent MR is mediated via its C-terminus, while retention at the mature MR is mediated via its N-terminus.

Anillin is a large multi-domain protein (Fig. 4A) that can bind to many other cytokinesis proteins (D'Avino, 2009; Piekny and Maddox, 2010). We analyzed truncation mutants lacking domains to determine which mediate its retention and removal at the nascent MR. Anillin-ΔActBD-GFP, which lacks the actin-binding and bundling domain (ActBD) identified by Field & Alberts (1995), was no longer recruited to the actin-rich cortex in mitosis, similar to the behavior of full length Anillin-GFP in LatA-treated cells (Hickson and O'Farrell, 2008b). However, Anillin-ΔActBD-GFP was still recruited to the furrow, nascent MR and mature MR and exhibited dramatic extrusion and shedding (Fig. S3A). Anillin-ΔMyoBD-GFP, which lacks the region adjacent to the ActBD that is homologous to the *Xenopus* myosin II-binding domain (Straight et al., 2005), still localized to the cortex at metaphase, indicating a functional ActBD, and to the CR and nascent MR during cytokinesis (Fig. S3B). It was also readily extruded and shed and localized to mature MRs, although these appeared smaller than MRs containing full length Anillin-GFP. Anillin-ΔN, in which the entire N-terminus was deleted leaving only the Anillin homology and Pleckstrin homology domains (AHD and PHD, respectively), was still extruded and shed. Constructs expressing only the AHD or PHD were poorly recruited and showed no evidence of shedding, and deletion of either domain blocked extrusion and shedding. Thus the C-terminal AHD and PHD are each required and together sufficient for extrusion and shedding.

Conversely, a mutant comprising only the extreme N-terminal domain (NTD) and the ActBD and MyoBD (Anillin-N) was still recruited to the MR (Fig. S3C) and behaved similarly to the larger Anillin-ΔC (Kechad et al., 2012). The reciprocal mutants lacking these domains (Anillin-ΔN and AnillinΔN+CD) failed to be retained at the mature MR despite localizing to the nascent MR and readily being extruded and shed (Fig. 4B). Thus, the Anillin

N-terminus is both necessary and sufficient for retention at the mature MR.

Co-expressing N- and C-terminal truncations fused to different fluorescent proteins in the same cells did not alter their respective behaviors and made their differences even more apparent. Fig. 4B shows Anillin-ΔC-GFP incorporating into the MR without being extruded or internalized, while Anillin-ΔN+CD-mCh is completely shed from the nascent MR without incorporating into the mature MR (Fig. 4B and Video S5). Taken together, our data indicate that distinct mechanisms of removal and retention act on the C- and N-termini of Anillin, respectively. We next aimed to better understand the removal mechanisms acting on the C-terminus of Anillin.

5.3.5 Maturation of the MR requires septin-dependent removal of Anillin via its C-terminal PH domain.

The Anillin PH domain is known to bind septins (Field and Alberts, 1995; Liu et al., 2012; Oegema et al., 2000) and phosphoinositides (Liu et al., 2012), and septins are required for the recruitment of Anillin-ΔN to the cleavage furrow (Kechad et al., 2012). We further evaluated the requirement for the PH domain and septins in Anillin removal during MR maturation. Anillin-ΔPH-FP localized efficiently to the CR and MR but showed little, if any, evidence of extrusion or internalization from the nascent MR, whether or not endogenous Anillin was depleted (Fig. 5A,C). Anillin-ΔPH-GFP MRs also appeared larger than controls of the same age (Fig 5E). Measuring MR volumes over time revealed that Anillin-ΔPH-GFP MRs did not thin to the same extent as Anillin-GFP controls (Fig. 5F). This effect was dominant, suggesting that the PH domain is autonomously required for Anillin removal. A 7-8 day incubation with dsRNAs targeting the septin, Peanut (Pnut) (Neufeld and Rubin, 1994), which results in >94% depletion in S2 cells (Fig. 5B), also blocked extrusion/ shedding of Anillin-GFP (Fig. 5A) and inhibited the thinning of the MR during its maturation (Fig. 5D-F). Thus, the PH domain of Anillin and Pnut are each required for cortical removal during MR maturation.

In the 30% (Anillin-ΔPH-GFP + Anillin dsRNA, n=75) and 34% (Anillin-GFP + Pnut dsRNA) of attempts at cytokinesis that failed, deletion of the PH domain or depletion of Pnut

produced similar phenotypes: at 1h10 ± 12 min (mean±sd, n=50) and 1h23 ± 33 min (mean±sd, n=50) after anaphase onset, respectively, the plasma membrane regressed leaving internal MR-like structures (Fig. 5G and (Kechad et al., 2012)). However, in the cells that succeeded, Anillin-ΔPH-FP delayed abscission, which occurred 10h42 ± 6h07 (mean±sd, n=50) after furrowing, while Pnut depletion led to premature abscission that occurred 2h19 ± 0h42 (mean ± sd, n=50) after furrowing, compared to 4h54± 1h36 (mean±sd, n=75) for Anillin-FP expressing controls (Fig. 5G). Given that the PH domain binds both the membrane and septins (Liu et al., 2012), this difference in abscission timing could reflect the difference between loss of septin-binding (Pnut-depletion) and the additional loss of PIP2 binding (deletion of the entire PH domain). Accordingly, PIP2 binding by the Anillin PH domain may facilitate abscission.

These experiments show that the PH domain of Anillin and the septin, Pnut, are required for the normal thinning of the nascent MR and the extrusion and shedding of membrane-associated Anillin. We next sought to better understand the mechanism of Anillin retention at the MR.

5.3.6 Sticky acts to limit extrusion and shedding and retains Anillin at the MR.

Citron kinase (Cit-K), Sticky in *Drosophila*, is a conserved Rho-associated kinase required for a late step of cytokinesis (D'Avino et al., 2004; Di Cunto et al., 2002; Di Cunto et al., 2000; Echard et al., 2004; Gruneberg et al., 2006; Naim et al., 2004; Shandala et al., 2004). Human Cit-K and Anillin can be co-immunoprecipitated and Cit-K has been suggested to maintain Anillin at the MR (Gai et al., 2011; Watanabe et al., 2013). Cit-K/Sticky and Anillin depletion phenotypes also bear some similarities, such as plasma membrane blebbing (Echard et al., 2004; Gai et al., 2011; Naim et al., 2004; Somma et al., 2002). However, because the relationship between Anillin and Cit-K/Sticky remains unclear, we re-examined Sticky depletion phenotypes. Immunoblot analysis revealed that 3 day incubation of S2 cells with Sticky dsRNAs led to a >90% depletion of both major migrating forms of Sticky (Fig. S4A), similar to that described previously (D'Avino et al., 2004).

Time-lapse sequences captured at 1 min intervals with a 63x objective revealed that

Sticky-depleted CRs closed with normal kinetics and morphology (Fig. 6A,B; Videos S6 and S7), consistent with previous reports (Bassi et al., 2011; Echard et al., 2004). The midbody microtubules also adopted their characteristic compacted morphology at the close of furrowing (Fig 6A,B), unlike Anillin-depleted cells (Fig. 3B,D, Kechad et al., 2012). However, measuring Anillin-GFP intensities revealed that Anillin levels continued to increase after the close of furrowing, such that the peak intensity of the nascent MR was ~10 min later than that of control cells (Fig. 6C). At the time of normal MR formation and maturation, Anillin-GFP displayed enhanced extrusion and internalization events (Fig. 6D). As in controls, blebs and tubules of Anillin-positive membranes formed and subsequently left the MR region by lateral movement or outright shedding (Fig. 6A-B; Videos S6 and S7). Although we observed clear examples of both internalization and extrusion/shedding in both control and Sticky-depleted cells, it was often difficult to differentiate between the two in any given case, especially as extruded material could subsequently be internalized. We therefore simply quantified removal (by either mechanism). This revealed that more Anillin-GFP was removed from Sticky-depleted nascent MRs, and over a longer period than in controls (Fig. 6D). Removal continued until Anillin-GFP was no longer detectable at the MR site, and furrows either regressed within a few min, or underwent abscission, prematurely (Fig. 6A-B and Videos S6 and S7).

To better define the outcomes of cytokinesis attempts upon Sticky depletion, we acquired time-lapse sequences at 2-4 min intervals over longer periods using a 40x objective. 77% of attempts failed while 23% succeeded (n>65, Fig. 6E). Interestingly, successes occurred earlier and with much less variability than LacI dsRNA-treated controls (Fig 6E), confirming our earlier inference of premature abscission in Sticky-depleted cells obtained from scoring the frequency of paired S2 cells (Echard et al., 2004). These successful divisions probably represent a hypomorphic phenotype, as they were more prevalent at earlier times following dsRNA addition with failures predominating later. Failures resulted from rapid furrow regression 77±15 (mean±sd, n=50) min after CR closure (Fig. 6E). Thus, ~75 min after furrowing, Sticky-depleted nascent MRs either quickly resolved, or regressed and failed. In both cases, a persistent Anillin-GFP-positive MR structure failed to form in more than 90% of division attempts (n>58 per condition, Fig. 6A-B).

Analysis of fixed cells revealed that Pnut (Fig. 6F) and Rho1 (Fig. 6G) were also

enriched in the extruded Anillin-positive membranes, while F-actin was depleted (Fig. 6H), as had been observed for extrusion in cells that were not depleted of Sticky (Fig. 2). Importantly, nascent MRs of Sticky-depleted untransfected cells also revealed markedly enhanced extrusion of endogenous Anillin, compared to controls (Fig. 6I-J), confirming that Sticky limits extrusion and that extrusion is not simply a consequence of Anillin-FP overexpression. We conclude that Sticky acts to retain Anillin at the mature MR.

5.3.7 Sticky acts with the N-terminus of Anillin to promote both MR formation and CR stability

Sticky depletion had no effect on the recruitment or removal of Anillin-ΔN-FP (Fig. 7A), but greatly diminished the localization of Anillin-ΔC-FP to the nascent MR (Fig. 7B) and prevented it from forming stable MR-like structures, whether or not endogenous Anillin was co-depleted (Fig. 7C). Furthermore, a functional Sticky-mCherry localized to internal Anillin-ΔC-GFP-dependent MR-like structures that resulted upon depletion of endogenous Anillin (Fig. 7D), but did not colocalize with Anillin-ΔN-GFP-positive structures that accumulate around the nascent MR when endogenous Anillin is present (Fig. 7E). Thus Sticky is specifically required to retain the N-terminus of Anillin at the mature MR.

Cleavage furrows are inherently unstable (Sedzinski et al., 2011) and oscillate following certain perturbations, including Anillin depletion (Goldbach et al., 2010; Hickson and O'Farrell, 2008b; Piekny and Glotzer, 2008; Straight et al., 2005; Zhao and Fang, 2005) and over-expression of full-length or truncated Cit-K (Gai et al., 2011; Madaule et al., 1998). Remarkably, cells expressing Anillin-ΔC-FP and depleted of endogenous Anillin, which furrow slowly without oscillating and form stable MR-like structures (Kechad et al., 2012), also became prone to oscillate when Sticky was co-depleted (Fig 7F-G). This indicates that Sticky promotes the ability of the Anillin N-terminus to stabilize furrows.

Since Peanut depletion blocked Anillin removal from the MR and Sticky depletion blocked Anillin retention, we tested the effects of co-depleting Sticky and Pnut. Little, if any, evidence of extrusion or internalization of Anillin-GFP was observed indicating that the enhanced extrusion observed upon Sticky depletion was still Pnut-dependent (Fig. 7H, Video

S8). In 39% (n=46) of cells, the formation of stable MR-like structures was abolished, as expected (Fig. 7I). The remaining 61% exhibited an intermediate phenotype whereby Anillin-positive MR structures persisted, but unlike control or Pnut-depleted cells (Fig. S4A-B), these often did not label for myosin (Fig. S4C-D). This partial destabilization of the MR suggests that Sticky acts to retain myosin at the MR. Furthermore, some of the structures were clearly not closed rings, but had less well-defined shapes (e.g. Fig. 7H and Video S8). Persistence of Anillin at these structures may reflect the existence of other Sticky-independent mechanisms that contribute to Anillin retention at the midbody.

Strikingly, cells co-depleted of Sticky and Pnut were prone to oscillate during furrowing (53% oscillations, n=135), whereas singly depleted cells were much less so (<10% oscillations, Fig. 7G-H and Video S8). During oscillations, Anillin-FP migrated laterally in repeated cycles, much like myosin does upon Anillin depletion. The fact that co-depletion of Sticky and Pnut destabilized furrows and caused Anillin to oscillate, suggests that Pnut contributes to a stabilizing influence of the Anillin C-terminus. Anillin-ΔN-FP, comprising only the Anillin C-terminus, failed to rescue oscillations but was completely disconnected from actomyosin (Kechad et al., 2012), underscoring the importance of the linkage to actomyosin. These data show that Anillin stabilizes furrows in part by linking actomyosin to the membrane-associated septin cytoskeleton and in part via a distinct Sticky-dependent action of its N-terminus.

5.3.8 Sticky's essential role during MR formation is as a scaffold.

We next wished to test whether Sticky kinase activity is required to retain Anillin-GFP at the MR. We generated inducible cell lines that co-expressed Anillin-GFP and mCherry-tagged wild type or kinase-dead (KD) versions of Sticky, at roughly endogenous levels (Fig. 8A). Both Sticky-mCh and Sticky-KD-mCh were faithfully recruited to the CR and MR, although both also led to the formation of Anillin-GFP-negative, intracellular aggregates, similar to those described by others (Eda et al. 2001, Fig. 8C and see Video S9). Expression of either Sticky-mCh or Sticky-KD-mCh rescued the widespread failures of cytokinesis induced by depletion of endogenous Sticky using a dsRNA directed against the Sticky 3'UTR (Fig. 8B). That formation of Sticky- and Anillin-positive MRs (Fig. 8C-E and Video S10) were

rescued in Sticky-KD-mCh cells indicates that Sticky kinase activity is dispensable for both MR formation and abscission (Fig. 8B, 8E). However, abscission timing was slightly accelerated for Sticky-KD-mCh MRs (128±49 min, mean±sd, n=28) than for Sticky-mCh MRs (196±67 min, mean±sd, n=26). Furthermore, the majority of cells that failed did not recruit detectable levels of Sticky-mCh (7/8 failures) or Sticky-KD-mCh (18/24 failures) to the CR/MR, consistent with failures reflecting lack of Sticky rather than lack of kinase function (Fig. 8B and Fig. S3B). In addition, excess Sticky-mCh and Sticky-KD-mCh were both also internalized and extruded/shed with Anillin-GFP (Fig. 8C-E and Videos S9 and S10), indicating that Sticky must itself be subject to retention at the midbody. We conclude that the essential role of Sticky in these cells is as a scaffold that serves to retain Anillin and stabilize the MR.

5.4 DISCUSSION

The organization of the cell cortex during closure of the CR and formation of a stable MR remains poorly defined. We show in *Drosophila* S2 cells that the late CR/nascent MR thins via a maturation process that lasts ~1 h and that involves a molecular tug-of-war between stable retention and dynamic removal of the membrane- and cytoskeleton-associated scaffold, Anillin. Retention requires a scaffold function of the Citron kinase, Sticky, and the N-terminus of Anillin, while removal requires septins and the C-terminus of Anillin and includes dramatic extrusion and shedding of membranes. Simultaneous perturbation of these antagonistic processes disrupts not only MR maturation but also CR stability, supporting our prior proposal that the CR and MR represent different stages of the same structure (Kechad et al., 2012). The work provides novel insight into the elusive mechanisms of CR closure and its maturation to the MR (Fig. 9).

Anillin-septin dependent membrane removal.

The extrusion and shedding of membrane from the nascent MR was unexpected, however it is highly reminiscent of Anillin- and prominin-1-positive, membrane-bound particles that shed from apical MRs in the vertebrate neuro-epithelium (Dubreuil et al., 2007). Electron microscopy has also revealed budding of membranous structures from the MR of human D98S cells (Mullins and Biesele, 1977), and prominent membrane “microvilli” in

cleavage stage sea urchin embryos (Schroeder, 1972). We have also observed extrusion of Anillin from the nascent MRs of human HeLa and neuroblastoma cells (unpublished data). Finally, we note that tubules of Anillin and Pnut-positive membranes are shed from the newly formed cells at the close of cellularization of the *Drosophila* embryo, a process mechanistically related to cytokinesis (Adam et al., 2000; Field et al., 2005), and our unpublished data). Thus membrane extrusion may be a universal feature of animal cell cytokinesis.

Is membrane removal cause or consequence of CR closure?

Key questions arise concerning the mechanism of Anillin-septin-membrane extrusion and whether it is a cause or consequence of CR closure, or both. In mammalian interphase cells, membrane blebs recruit septins, after F-actin, to facilitate bleb retraction (Gilden et al., 2012). However, the membrane protrusions/tubules that we describe are enriched in Anillin from their first emergence, they are poor in actin and they never retract. Thus rather than being recruited to or trapped in pre-existing blebs, we favor the model that Anillin directs septin-dependent membrane tubulation. Septins are capable of tubulating membranes (Tanaka-Takiguchi et al., 2009), although the topology of such structures is reversed compared to the extrusions that we describe. However, it remains unclear how Rho1 and Anillin (and potentially other cytokinesis proteins) might alter septin behaviors. Experimentally disconnecting the N-terminus of Anillin from the actomyosin network, either by deleting the N-terminus of Anillin (Kechad et al., 2012), or by disrupting the actin cytoskeleton with LatA (Hickson and O'Farrell, 2008b), triggers the C-terminus of Anillin to induce Pnut-dependent remodeling of the plasma membrane, resulting in either punctate or tubular protrusions that extend outwards from the cell. These data argue that the extrusions at the late CR/nascent MR may simply reflect the local disassembly of actin, thereby liberating Anillin N-termini and allowing Anillin C-termini/septins to tubulate membranes in such a dramatic fashion. Indeed, membrane extrusion is most obvious at the time when the MR is becoming resistant to Latrunculin A (Echard et al., 2004), suggesting coordination with disassembly of the actin ring. Finally, actin and Anillin-ΔC were notably absent from the extruded and shed membranes, indicating that not all CR components are removed in this way.

Can furrow oscillations result from impeding CR disassembly?

The CR closes by disassembly (Carvalho et al., 2009; Schroeder, 1972). Our results suggest that this involves both depolymerization and membrane-associated removal. Accordingly, Anillin and septins may sequester the excess membrane that is liberated upon actomyosin depolymerization. Anillin-depleted CRs fail to close to completion and become unstable and oscillate (Goldbach et al., 2010; Hickson and O'Farrell, 2008b; Piekny and Glotzer, 2008; Straight et al., 2005; Zhao and Fang, 2005). Our findings raise the possibility that this phenotype reflects a failure to sequester membrane (via septins) that impedes the normal disassembly of the actin ring, combined with the loss of an additional Sticky-dependent scaffolding role of the N-terminus of Anillin.

We note that Sticky and Pnut co-depletion did not completely phenocopy Anillin depletion. The latter is more severe with a proportion of cells that undergo wild oscillations that are too unstable to allow ingression beyond 50% closure (Kechad et al., 2012). Sticky and Pnut co-depleted cells, although they oscillated, mostly ingressed to completion and then failed at the MR stage (this study). Thus Anillin likely has additional inputs into furrow stability that are independent of Sticky and Pnut. RacGAP50C/Tum is a strong candidate known to interact with the Anillin AHD (D'Avino et al., 2008; Gregory et al., 2008).

The essential role of Sticky is as a scaffold for the mature MR, but it also functions during furrowing.

We show that Sticky is required to retain the N-terminus of Anillin at the mature MR. Human Cit-K can phosphorylate the myosin regulatory light chain (MRLC) (Yamashiro et al., 2003) and MRLC is another component of the MR in S2 cells (Dean and Spudich, 2006; Kechad et al., 2012). Expression of phosphomimetic MRLC (Spaghetti squash-E20E21) in S2 cells cannot rescue for Sticky depletion, indicating that myosin phosphorylation cannot be the only essential role of Sticky (Dean and Spudich, 2006). Our results further show that kinase activity is completely dispensable for the essential function of Sticky, since a kinase-dead version is still able to form a stable MR and rescue cytokinesis. In agreement with this, the central coiled-coil region of human Cit-K is sufficient to support cytokinesis in HeLa cells (Watanabe et al., 2013). The fact that Sticky was extruded and shed with Anillin suggests that

Sticky itself must be retained by additional, saturable mechanisms at the midbody, likely via KIF14-dependent mechanisms (Bassi et al., 2013; Gruneberg et al., 2006; Watanabe et al., 2013).

Although Cit-K/Sticky localizes to the CR (Bassi et al., 2011; D'Avino et al., 2004; Eda et al., 2001; Madaule et al., 1998), whether it acts there is a long-standing enigma. Our findings confirm that it does, albeit redundantly. Firstly, unlike control furrows, Sticky-depleted furrows continued to accumulate Anillin-GFP for 10 min after closure, indicating that Sticky normally functions at this time. Secondly, Sticky depletion caused furrow oscillations in cells co-depleted of Pnut or in cells expressing Anillin-ΔC and co-depleted of endogenous Anillin. This indicates that Sticky plays a role in furrow stability that is redundant with the C-terminus of Anillin and Pnut. We attempted to test whether kinase activity was required for this role. However, rescuing Sticky depletion in the context of Pnut co-depletion was problematic. The longer induction times required by the fact that Pnut depletion takes many days, resulted in poor recruitment of Sticky-mCh and Sticky-KD-mCh to CRs, with both proteins preferring to form ectopic aggregates. Thus, while kinase activity is dispensable for Sticky's essential role at the MR, it remains possible that its kinase activity contributes to CR stability.

Concluding remarks

Current models for CR closure focus on the cytoskeletal proteins and pay little attention to the plasma membrane to which these elements are anchored. While net membrane addition may be required during furrow ingression (Albertson et al., 2005; McKay and Burgess, 2011; Neto et al., 2011), our findings highlight a need for membrane removal from the furrow apex that must be coordinated with CR disassembly and MR assembly. Extrusion and shedding is one way of achieving this; other potential mechanisms include internalization and lateral outflow within the lipid bilayer. Theoretical and experimental analyses in different systems will be needed to fully test this novel perspective.

5.5 MATERIALS AND METHODS

Constructs, cell lines and RNAi.

All constructs were generated by PCR amplification of the ORF, without stop codons, followed by cloning into pENTR-D-TOPO (Invitrogen), followed by recombination using LR Clonase into appropriate destination vectors (Drosophila Gateway vector collection, T. Murphy, Carnegie). Anillin-GFP (pMT-WG, driven by the *metallothionein* promoter), Anillin-mCherry (pAc-Wch, driven by the constitutive *Act05C* promoter), mCherry-tubulin (pAc-ChW), $MRLC^{Sqh}$-GFP (endogenous *spaghetti squash* promoter), Anillin-ΔC-FP (pMT-WG or pMT-WCh), Anillin-ΔN-FP (pMT-WG or pMT-WCh), Pav-GFP (pMT-WG) have been described previously (Hickson and O'Farrell, 2008b; Kechad et al., 2012) (Echard et al, 2004). Internal deletions and site-directed mutagenesis were performed by PCR by overlap extension, followed by cloning into pENTR-D-TOPO and subsequent recombination into pMT-WG and pMT-WCh. All Anillin constructs derive from clone LD23793 (BDGP Gold collection, *Drosophila* Genomics Resource Center) that encodes the CG2092-RB polypeptide. Note that CG2092-RB has an additional 27 residues within the actin-binding domain that is absent in CG2092-RA (Field and Alberts, 1995), but CG2092-RB is better supported by sequencing data. Anillin-ΔN+CD-FP encodes amino acids 410-1239 and lacks all N-terminal domains up to and including the actin-binding and bundling domain. Anillin-ΔPH-FP encodes amino acids 1-1104 and thus lacks the last 135 residues comprising the entire PH domain. Anillin-ΔActBD encodes amino acids 1-255+410-1239 and lacks the minimal actin binding and bundling domain defined in (Field and Alberts, 1995). Anillin-ΔMyoBD encodes amino acids 1-145+238-1239 and lacks 92 amino acids homologous to the *Xenopus* myosin-binding domain defined in (Straight et al., 2005). The *sticky* (CG10522) ORF was PCR amplified from clone RE26327 (DGC release 2 collection, Drosophila Genomics Resource Center). The Sticky kinase-dead mutant was generated by site directed mutagenesis using primers 5'-GACATATACGCCATGgcggcgATCAAAAAGTCGGTG-3' and 5'-CACCGACTTTTTGAT cgccgcCATGGCGTATATGTC-3' that introduced K142A and K143A mutations in the kinase domain. The Aurora B ORF was amplified by RT-PCR from S2 cell cDNA and was described in (Smurnyy et al., 2010). Myrpalm-GFP (in pAc-WG) was a gift from S. Carreno (Université de Montréal/ IRIC) and encodes the first 16 amino acids of Lyn (MGCIKSKRKDNLNDDE),

including myristoylation and palmitoylation signals, upstream of GFP and driven by the *act05C* promoter. LifeAct-GFP encodes the 17 amino sequence described by (Riedl et al., 2008) cloned upstream of GFP (pMT-WG). The Dendra2 sequence was subcloned from pDendra2-N1 (Clontech) into pAc-WG, replacing GFP, to generate pAc-WD2 and allowing subsequent generation of Anillin-Dendra2 by Gateway recombination. All constructs were verified by sequencing.

Plasmids were used to transfect *Drosophila* Schneider's S2 cells using Cellfectin reagent (Invitrogen), together with pCoHygro, and additional plasmids as needed to generate stable, hygromycin-resistant cell lines following established protocols (Invitrogen). After selection, cells were cultured in Schneider's medium supplemented with 10% foetal calf serum (Invitrogen) and penicillin/streptomycin.

Double-stranded RNAs (dsRNAs) were generated using Ribomax in vitro transcription kits (Promega) and DNA templates generated in a two-step PCR amplification from cDNA or genomic DNA, as described previously (Echard et al., 2004). Briefly, in the first round PCR, gene specific primer sequences included a 5′ anchor sequence (GGGCGGGT), while the second round PCR used a universal T7-anchor primer (TAATACGACTCACTATAGGGAGACCACGGGCGGGT). Gene-specific primer sequences were previously described for *anillin* dsRNA (Echard et al., 2004; Hickson and O'Farrell, 2008b), *anillin* 3' UTR dsRNA (Hickson and O'Farrell, 2008b), *peanut* dsRNA (Hickson and O'Farrell, 2008b), and *sticky* dsRNAs (Echard et al., 2004). *Shrb/CHMP4/CG8055* and *dIST1/CG10103* dsRNAs were generated using primer pairs GGGCGGGTTCGATACAAAGCTAAGACTGCG and GGGCGGGTATGATCCAGACAT GAAGAGCAGC (Shrb), and GGGCGGGTGTTGGTGTTCAGATCCTTCTCC and GGGCGGGTCTACAGAGCGATATAGCCGAGC (dIST1). The *sticky* 3'UTR dsRNA was generated using primer sequences GGGCGGGTGCATATAGATGAAGGATATAT and GGGCGGGTTTTAAAATATTATGCGACTTC.

RNAi experiments were performed as follows: cells were plated in 96 well dishes and incubated with ~1 µg/ml dsRNA. 12-24 h prior to imaging or fixation, cells were transferred to 8-well chambered coverglass dishes (Labtek, Nunc). Live imaging was performed between

30 and 72 hours for Anillin dsRNAs, between 30 and 48 hours for Sticky dsRNAs and between 144 and 192 hr for Pnut dsRNA, in which case cells were split and fresh dsRNA added on the fourth day. These dsRNA incubation times were maintained for co-depletion experiments, but the individual dsRNA incubations were performed in the presence of irrelevant LacI control dsRNAs to control for possible effects of combining dsRNAs.

Live cell microscopy

Live cell imaging of *Drosophila* S2 cells in Schneider's medium was performed at room temperature using an Ultraview Vox spinning disc confocal system (PerkinElmer), employing a CSU-X1 scanning unit (Yokogawa) and an Orca-R2 CCD camera (Hamamatsu) fitted to a Leica DMI6000B inverted microscope equipped with a motorized piezo-electric stage (Applied Scientific Instrumentation). Image acquisition was performed using Volocity versions 5 and 6 (Improvision/Perkin Elmer). Routine and long time-course imaging was performed using a Plan Apo 40x (0.85 NA) air objective with camera binning set to 2x2, high-resolution imaging was performed using Plan Apo 63x or 100x oil immersion objectives (NA 1.4) with camera binning set to 2x2 unless otherwise described in the figure legends.

Expression of FP-fusions under the control of the *metallothionien* promoter (pMT plasmids) were induced with 250 μM $CuSO_4$ at the time of dsRNA addition in the case of rescue experiments, or when cells were transferred to imaging dishes, 12-24 h prior to the start of imaging. Where described, MG132 (Enzo Life Sciences) was added to a final concentration of 5μM directly to the culture medium.

Immunofluorescence microscopy

Cells were transferred to either 8-well chambered coverglass dishes (Labtek, Nunc) or 96-well glass bottomed plates (Whatman) at least 2 h prior to fixation for 5 min in 4% formaldehyde/ 0.1% glutaraldehyde in phosphate-buffered saline (PBS). After permeabilization and blocking in PBS containing 0.1% triton-X100 (PTX buffer) and 5% normal goat serum, cells were incubated with primary antibodies (rabbit anti-Anillin, a gift from Dr. Christine Field, used at 1:1000; concentrated mAb 4C9H4 anti-peanut, from Developmental Studies Hybridoma Bank, used at 1:400) at 4°C overnight, washed with PTX buffer and incubated for 1 h with Alexa-

488, Alexa-546, or Alexa-647-conjugated goat anti-mouse or anti-rabbit secondary antibodies (1:500, Molecular Probes/ Invitrogen), as appropriate. Where appropriate, Hoechst 33258 (1:500) and rhodamine-phalloidin (1:500, Molecular Probes) were added at the same time. Cells were washed in PTX and mounted in Fluoromount-G (SouthernBiotech). Images were acquired using the Ultraview Vox system descried above using oil-immersion Plan Apo 63x or 100x 1.4NA objectives.

FRAP and Image analysis

FRAP was performed using the Photokinesis module (Perkin Elmer), controlled through Volocity software. 5 μm thick stacks of 4 z sections were acquired with 63x objective, 2x2 camera binning. Acquisition was at max speed (exposure time 200 msec) for the first 15 seconds post bleaching (representing cytoplasmic recovery) then at one image per 15 seconds for 5 minutes. % recovery = % (Max intensity post bleach - intensity at bleach)/(Intensity pre bleach - Intensity at bleach). All intensity values in FRAP experiments were normalized to the first time point of acquisition. For statistical analysis, an unpaired t-test was performed using Graphpad Prism.

MR volume measurements were obtained as follows: cells were imaged using 63X 1.4NA objective (12 Z sections, 1 min intervals) during at least one hour after furrowing using Volocity acquisition. Datasets were then exported as openlab liff files and analyzed using IMARIS 7 quantification module as follows: a surface around the MR was selected using intensity threshold and the volume of this surface was determined empirically for each MR. These values were then expressed as percentages relative to the value of MR volume at the end of furrowing (the first time-point of analysis). Relative fold differences in MR volume were calculated relative to the volume of control Anillin-GFP MRs for each given time point post-furrowing. The same process was applied for intensity measurements of each extrusion, internalization or shedding (Fig. 6D).

Intensity measurements of MRs were performed using the Volocity "select objects by % intensity" tool. Optimal percentage values were determined empirically for each MR and the resulting sum intensity values were then expressed as percentages relative to the highest value within the given time series (usually, t=0). Datasets were background-corrected.

Quantification of the Anillin-GFP loss in Fig. 6C was performed using Imaris 7 following export from Volocity as openlab liff files. Individual shedding events were selected by creating surfaces using variable thresholds between different cells. Intensity values of individual shedding events were expressed as percentages relative to the total intensity associated with the MR at the start of the given time series. Images were processed for publication using Adobe Photoshop CS and assembled as figures using Adobe Illustrator CS. Video files were exported from Volocity as Quicktime movies.

Immunoblotting

S2 cells were grown in 12 well dishes, treated with indicated dsRNAs, and harvested by centrifugation. Cells were lysed in lysis buffer (50 mM Tris-HCl, pH7.5, 150 mM NaCl, 1% Triton-X-100 completed with protease inhibitor cocktail (Roche)), and total cell lysates were subjected to SDS-PAGE (8-15% polyacrylamide). Proteins were transferred to a nitrocellulose membrane and blocked with 5% milk in Tris-buffered saline containing 0.2% Tween-20 (TBST). The membrane was cut at the appropriate molecular weight marker with the upper molecular weight part immunoblotted with affinity purified anti-Anillin antibodies (1:1000, a gift from J. Brill, generated in rabbits against amino acids 1-409 of Anillin fused to GST (Goldbach et al., 2010)) or anti-Sticky antiserum (1:3000, generated in rabbits against a fragment of the STI protein (amino acids 531–742) fused to a carboxy-terminal 6XHis tag, a gift from P. D'avino (D'Avino et al., 2004)) while the lower molecular weight part was blotted with mAb anti-tubulin antibody (Sigma-Aldrich, clone DM1A, 1:1000). For anti-Peanut (1:1000, concentrated supernatant from clone 4C9H4 (Neufeld and Rubin, 1994), Developmental Studies Hybridoma Bank, Iowa) immunoblotting was performed in duplicate where one membrane was immunoblotted with anti-Peanut and the other with mAb anti-tubulin (as indicated above). The blots were washed in TBST, incubated with horseradish peroxidase-coupled donkey anti-rabbit or anti-mouse secondary antibodies (1:5000, GE healthcare) and washed again prior to detection of signals using Clarity Western ECL Substrate (BioRad).

Electron Microscopy

Drosophila S2 cells were gently pelleted by centrifugation, incubated for an hour at room

temperature in a fixative consisting of 2.5% glutaraldehyde, 4% paraformaldehyde and 5 mM $CaCl_2$ in 0.1M cacodylate buffer pH7.4 (Caco), and in 1% OsO_4 in Caco for postfixation. The pellet was stained in 2% uranyl acetate overnight at 4°C, dehydrated in a graded series of ethanol and embedded in Epon 812. Ultrathin tissue sections were cut using a Reichert Ultracut ultramicrotome and mounted on copper grids. Ultrathin sections were stained with uranyl acetate and lead citrate and examined with a Philips CM100 electron microscope.

5.6 ACKNOWLEDGEMENTS

We thank Patrick O'Farrell, in whose lab this work was initiated (supported by NIH grant R01-GM037193), and for comments on an early version of the manuscript. We thank Christine Field, Julie Brill, Paolo D'Avino and the Developmental Studies Hybridoma Bank for antibodies, Ron Vale, Sébastien Carreno and Yvonne Ruella for constructs, Raphaëlle Cadenas for generating ESCRT dsRNAs and Diane Gingras for help with EM. GRXH thanks the *Fonds de Recherche du Québec — Santé* (FRQS) for a Junior 1 scholarship. AK thanks the *Fondation du CHU Sainte-Justine/Fondation des Étoiles* and the FRQS for graduate fellowships. This work was supported by grants from the Canadian Institutes of Health Research (MOP-97788), the Canadian Fund for Innovation and the FRQS to GRXH.

5.7 REFERENCES

Adam, J.C., J.R. Pringle, and M. Peifer. 2000. Evidence for functional differentiation among Drosophila septins in cytokinesis and cellularization. *Mol Biol Cell*. 11:3123-35.

Agromayor, M., J.G. Carlton, J.P. Phelan, D.R. Matthews, L.M. Carlin, S. Ameer-Beg, K. Bowers, and J. Martin-Serrano. 2009. Essential role of hIST1 in cytokinesis. *Mol Biol Cell*. 20:1374-87.

Albertson, R., B. Riggs, and W. Sullivan. 2005. Membrane traffic: a driving force in cytokinesis. *Trends Cell Biol*. 15:92-101.

Barr, F.A., and U. Gruneberg. 2007. Cytokinesis: placing and making the final cut. *Cell*. 131:847-60.

Bassi, Z.I., M. Audusseau, M.G. Riparbelli, G. Callaini, and P.P. D'Avino. 2013. Citron kinase controls a molecular network required for midbody formation in cytokinesis. *Proc Natl Acad Sci U S A*. 110:9782-7.

Bassi, Z.I., K.J. Verbrugghe, L. Capalbo, S. Gregory, E. Montembault, D.M. Glover, and P.P. D'Avino. 2011. Sticky/Citron kinase maintains proper RhoA localization at the cleavage site during cytokinesis. *J Cell Biol*. 195:595-603.

Bement, W.M., H.A. Benink, and G. von Dassow. 2005. A microtubule-dependent zone of active RhoA during cleavage plane specification. *J Cell Biol*. 170:91-101.

Carlton, J.G., A. Caballe, M. Agromayor, M. Kloc, and J. Martin-Serrano. 2012. ESCRT-III governs the Aurora B-mediated abscission checkpoint through CHMP4C. *Science*. 336:220-5.

Carvalho, A., A. Desai, and K. Oegema. 2009. Structural memory in the contractile ring makes the duration of cytokinesis independent of cell size. *Cell*. 137:926-37.

D'Avino, P.P. 2009. How to scaffold the contractile ring for a safe cytokinesis - lessons from Anillin-related proteins. *J Cell Sci*. 122:1071-9.

D'Avino, P.P., M.S. Savoian, and D.M. Glover. 2004. Mutations in sticky lead to defective

organization of the contractile ring during cytokinesis and are enhanced by Rho and suppressed by Rac. *J Cell Biol*. 166:61-71.

D'Avino, P.P., T. Takeda, L. Capalbo, W. Zhang, K.S. Lilley, E.D. Laue, and D.M. Glover. 2008. Interaction between Anillin and RacGAP50C connects the actomyosin contractile ring with spindle microtubules at the cell division site. *J Cell Sci*. 121:1151-8.

Dean, S.O., and J.A. Spudich. 2006. Rho kinase's role in myosin recruitment to the equatorial cortex of mitotic Drosophila S2 cells is for myosin regulatory light chain phosphorylation. *PLoS ONE*. 1:e131.

Di Cunto, F., S. Imarisio, P. Camera, C. Boitani, F. Altruda, and L. Silengo. 2002. Essential role of citron kinase in cytokinesis of spermatogenic precursors. *J Cell Sci*. 115:4819-26.

Di Cunto, F., S. Imarisio, E. Hirsch, V. Broccoli, A. Bulfone, A. Migheli, C. Atzori, E. Turco, R. Triolo, G.P. Dotto, L. Silengo, and F. Altruda. 2000. Defective neurogenesis in citron kinase knockout mice by altered cytokinesis and massive apoptosis. *Neuron*. 28:115-27.

Dorn, J.F., and A.S. Maddox. 2011. Cytokinesis: cells go back and forth about division. *Curr Biol*. 21:R848-50.

Dubreuil, V., A.M. Marzesco, D. Corbeil, W.B. Huttner, and M. Wilsch-Brauninger. 2007. Midbody and primary cilium of neural progenitors release extracellular membrane particles enriched in the stem cell marker prominin-1. *J Cell Biol*. 176:483-95.

Echard, A., G.R. Hickson, E. Foley, and P.H. O'Farrell. 2004. Terminal cytokinesis events uncovered after an RNAi screen. *Curr Biol*. 14:1685-93.

Eda, M., S. Yonemura, T. Kato, N. Watanabe, T. Ishizaki, P. Madaule, and S. Narumiya. 2001. Rho-dependent transfer of Citron-kinase to the cleavage furrow of dividing cells. *J Cell Sci*. 114:3273-84.

Eggert, U.S., T.J. Mitchison, and C.M. Field. 2006. Animal cytokinesis: from parts list to mechanisms. *Annu Rev Biochem*. 75:543-66.

Elia, N., R. Sougrat, T.A. Spurlin, J.H. Hurley, and J. Lippincott-Schwartz. 2011. Dynamics of endosomal sorting complex required for transport (ESCRT) machinery during cytokinesis and its role in abscission. *Proc Natl Acad Sci U S A*. 108:4846-51.

Field, C.M., and B.M. Alberts. 1995. Anillin, a contractile ring protein that cycles from the nucleus to the cell cortex. *J Cell Biol*. 131:165-78.

Field, C.M., M. Coughlin, S. Doberstein, T. Marty, and W. Sullivan. 2005. Characterization of anillin mutants reveals essential roles in septin localization and plasma membrane integrity. *Development*. 132:2849-60.

Gai, M., P. Camera, A. Dema, F. Bianchi, G. Berto, E. Scarpa, G. Germena, and F. Di Cunto. 2011. Citron kinase controls abscission through RhoA and anillin. *Mol Biol Cell*. 22:3768-78.

Gilden, J.K., S. Peck, Y.C. Chen, and M.F. Krummel. 2012. The septin cytoskeleton facilitates membrane retraction during motility and blebbing. *J Cell Biol*. 196:103-14.

Glotzer, M. 2005. The molecular requirements for cytokinesis. *Science*. 307:1735-9.

Goldbach, P., R. Wong, N. Beise, R. Sarpal, W.S. Trimble, and J.A. Brill. 2010. Stabilization of the actomyosin ring enables spermatocyte cytokinesis in Drosophila. *Mol Biol Cell*. 21:1482-93.

Green, R.A., E. Paluch, and K. Oegema. 2012. Cytokinesis in Animal Cells. *Annu Rev Cell Dev Biol*.

Gregory, S.L., S. Ebrahimi, J. Milverton, W.M. Jones, A. Bejsovec, and R. Saint. 2008. Cell division requires a direct link between microtubule-bound RacGAP and Anillin in the contractile ring. *Curr Biol*. 18:25-9.

Gruneberg, U., R. Neef, X. Li, E.H. Chan, R.B. Chalamalasetty, E.A. Nigg, and F.A. Barr. 2006. KIF14 and citron kinase act together to promote efficient cytokinesis. *J Cell*

Biol. 172:363-72.

Haglund, K., I.P. Nezis, and H. Stenmark. 2011. Structure and functions of stable intercellular bridges formed by incomplete cytokinesis during development. *Commun Integr Biol*. 4:1-9.

Hickson, G.R., and P.H. O'Farrell. 2008a. Anillin: a pivotal organizer of the cytokinetic machinery. *Biochem Soc Trans*. 36:439-41.

Hickson, G.R., and P.H. O'Farrell. 2008b. Rho-dependent control of anillin behavior during cytokinesis. *J Cell Biol*. 180:285-94.

Hu, C.K., M. Coughlin, and T.J. Mitchison. 2012. Midbody assembly and its regulation during cytokinesis. *Mol Biol Cell*. 23:1024-34.

Kechad, A., S. Jananji, Y. Ruella, and G.R. Hickson. 2012. Anillin acts as a bifunctional linker coordinating midbody ring biogenesis during cytokinesis. *Curr Biol*. 22:197-203.

Liu, J., G.D. Fairn, D.F. Ceccarelli, F. Sicheri, and A. Wilde. 2012. Cleavage furrow organization requires PIP(2)-mediated recruitment of anillin. *Curr Biol*. 22:64-9.

Madaule, P., M. Eda, N. Watanabe, K. Fujisawa, T. Matsuoka, H. Bito, T. Ishizaki, and S. Narumiya. 1998. Role of citron kinase as a target of the small GTPase Rho in cytokinesis. *Nature*. 394:491-4.

McKay, H.F., and D.R. Burgess. 2011. 'Life is a highway': membrane trafficking during cytokinesis. *Traffic*. 12:247-51.

Mullins, J.M., and J.J. Biesele. 1977. Terminal phase of cytokinesis in D-98s cells. *J Cell Biol*. 73:672-84.

Naim, V., S. Imarisio, F. Di Cunto, M. Gatti, and S. Bonaccorsi. 2004. Drosophila citron kinase is required for the final steps of cytokinesis. *Mol Biol Cell*. 15:5053-63.

Neto, H., L.L. Collins, and G.W. Gould. 2011. Vesicle trafficking and membrane remodelling in cytokinesis. *Biochem J*. 437:13-24.

Neufeld, T.P., and G.M. Rubin. 1994. The Drosophila peanut gene is required for cytokinesis and encodes a protein similar to yeast putative bud neck filament proteins. *Cell*. 77:371-9.

Oegema, K., M.S. Savoian, T.J. Mitchison, and C.M. Field. 2000. Functional analysis of a human homologue of the Drosophila actin binding protein anillin suggests a role in cytokinesis. *J Cell Biol*. 150:539-52.

Piekny, A.J., and M. Glotzer. 2008. Anillin is a scaffold protein that links RhoA, actin, and myosin during cytokinesis. *Curr Biol*. 18:30-6.

Piekny, A.J., and A.S. Maddox. 2010. The myriad roles of Anillin during cytokinesis. *Semin Cell Dev Biol*. 21:881-91.

Pollard, T.D. 2010. Mechanics of cytokinesis in eukaryotes. *Curr Opin Cell Biol*. 22:50-6.

Riedl, J., A.H. Crevenna, K. Kessenbrock, J.H. Yu, D. Neukirchen, M. Bista, F. Bradke, D. Jenne, T.A. Holak, Z. Werb, M. Sixt, and R. Wedlich-Soldner. 2008. Lifeact: a versatile marker to visualize F-actin. *Nat Methods*. 5:605-7.

Schroeder, T.E. 1972. The contractile ring. II. Determining its brief existence, volumetric changes, and vital role in cleaving Arbacia eggs. *J Cell Biol*. 53:419-34.

Sedzinski, J., M. Biro, A. Oswald, J.Y. Tinevez, G. Salbreux, and E. Paluch. 2011. Polar actomyosin contractility destabilizes the position of the cytokinetic furrow. *Nature*. 476:462-6.

Shandala, T., S.L. Gregory, H.E. Dalton, M. Smallhorn, and R. Saint. 2004. Citron kinase is an essential effector of the Pbl-activated Rho signalling pathway in Drosophila melanogaster. *Development*. 131:5053-63.

Smurnyy, Y., A.V. Toms, G.R. Hickson, M.J. Eck, and U.S. Eggert. 2010. Binucleine 2, an isoform-specific inhibitor of Drosophila Aurora B kinase, provides insights into the mechanism of cytokinesis. *ACS Chem Biol*. 5:1015-20.

Somma, M.P., B. Fasulo, G. Cenci, E. Cundari, and M. Gatti. 2002. Molecular dissection of

cytokinesis by RNA interference in Drosophila cultured cells. *Mol Biol Cell*. 13:2448-60.

Steigemann, P., and D.W. Gerlich. 2009. Cytokinetic abscission: cellular dynamics at the midbody. *Trends Cell Biol*. 19:606-16.

Straight, A.F., C.M. Field, and T.J. Mitchison. 2005. Anillin binds nonmuscle myosin II and regulates the contractile ring. *Mol Biol Cell*. 16:193-201.

Tanaka-Takiguchi, Y., M. Kinoshita, and K. Takiguchi. 2009. Septin-mediated uniform bracing of phospholipid membranes. *Curr Biol*. 19:140-5.

Watanabe, S., T. De Zan, T. Ishizaki, and S. Narumiya. 2013. Citron kinase mediates transition from constriction to abscission through its coiled-coil domain. *J Cell Sci*. 126:1773-84.

Yamashiro, S., G. Totsukawa, Y. Yamakita, Y. Sasaki, P. Madaule, T. Ishizaki, S. Narumiya, and F. Matsumura. 2003. Citron kinase, a Rho-dependent kinase, induces di-phosphorylation of regulatory light chain of myosin II. *Mol Biol Cell*. 14:1745-56.

Zhao, W.M., and G. Fang. 2005. Anillin is a substrate of anaphase-promoting complex/cyclosome (APC/C) that controls spatial contractility of myosin during late cytokinesis. *J Biol Chem*. 280:33516-24.

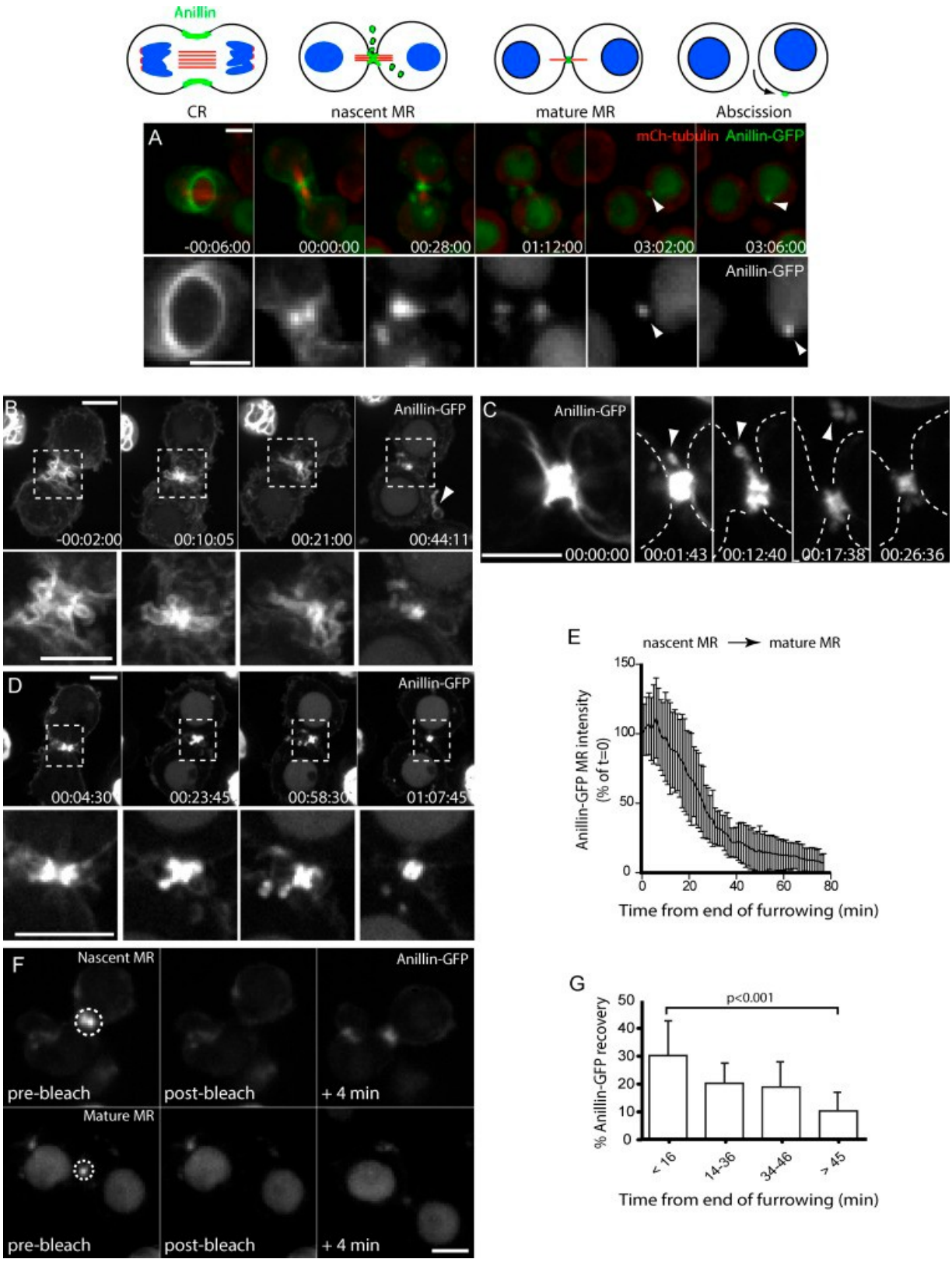
Anillin
CR
nascent MR
mature MR
Abscission
A
mCh-tubulin Anillin-GFP
-00:06:00
00:00:00
00:28:00
01:12:00
03:02:00
03:06:00
Anillin-GFP
B
Anillin-GFP
-00:02:00
00:10:05
00:21:00
00:44:11
C
Anillin-GFP
00:00:00
00:01:43
00:12:40
00:17:38
00:26:36
D
Anillin-GFP
00:04:30
00:23:45
00:58:30
01:07:45
E
nascent MR → mature MR
Anillin-GFP MR intensity (% of t=0)
150
100
50
0
0
20
40
60
80
Time from end of furrowing (min)
F
Nascent MR
Anillin-GFP
pre-bleach
post-bleach
+ 4 min
Mature MR
pre-bleach
post-bleach
+ 4 min
G
p<0.001
% Anillin-GFP recovery
50
40
30
20
10
0
< 16
14-36
34-46
> 45
Time from end of furrowing (min)

5.8 FIGURES AND LEGENDS

Figure 5.1: Maturation of the MR is accompanied by both removal and retention of Anillin.

A Time-lapse sequence of a cell expressing Anillin-GFP and mCh-tubulin (40x objective). Arrowheads mark the mature MR before and after abscission MR release). **B-D** Time-lapse sequence of cells expressing Anillin-GFP and mCh-tubulin (not shown) acquired with 40x objective, showing extrusion and shedding (B-C) and internalization (D). Boxed regions in B and D are shown magnified below; arrowheads mark shed material. **E** Relative Anillin-GFP fluorescence (sum intensity) at nascent MRs measured from the end of furrowing (mean±sd, n=20). **F** FRAP experiments of nascent and mature MRs, showing images acquired immediately before (pre-bleach), after (bleach) and 4 min after high intensity illumination of the outlined ROI (63x objective, 2x2 camera binning). **G** The % recovery of GFP fluorescence within 4 min of bleaching is shown for MRs of different ages (n=9 to 17 each, mean±sd). p value is for an unpaired t-test. Times are h:min:s from the end of furrowing. Scale bars, 5 µm. See also Videos S1 and S2.

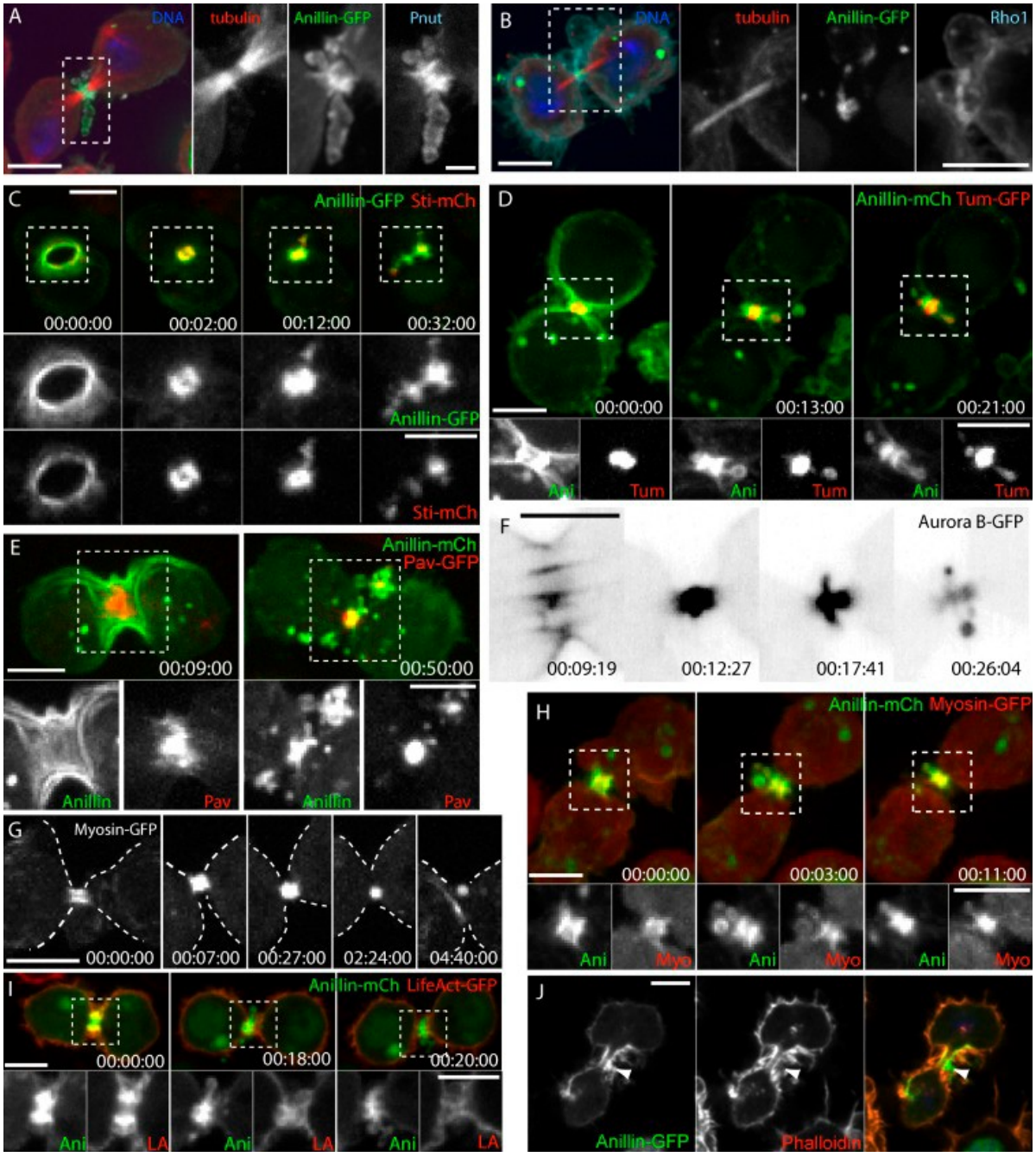
A
DNA
tubulin
Anillin-GFP
Pnut
B
DNA
tubulin
Anillin-GFP
Rho1
C
Anillin-GFP Sti-mCh
00:00:00
00:02:00
00:12:00
00:32:00
Anillin-GFP
Sti-mCh
D
Anillin-mCh Tum-GFP
00:00:00
00:13:00
00:21:00
Ani
Tum
Ani
Tum
Ani
Tum
E
Anillin-mCh
Pav-GFP
00:09:00
00:50:00
Anillin
Pav
Anillin
Pav
F
Aurora B-GFP
00:09:19
00:12:27
00:17:41
00:26:04
G
Myosin-GFP
00:00:00
00:07:00
00:27:00
02:24:00
04:40:00
H
Anillin-mCh Myosin-GFP
00:00:00
00:03:00
00:11:00
Ani
Myo
Ani
Myo
Ani
Myo
I
Anillin-mCh LifeAct-GFP
00:00:00
00:18:00
00:20:00
Ani
LA
Ani
LA
Ani
LA
J
Anillin-GFP
Phalloidin

Figure 5.2: Nascent MRs shed numerous CR components, except F-actin.

A-B Fixed cells expressing Anillin-GFP, tubulin-mCh stained for anti-Pnut (A) and anti-Rho1 (B) by immunofluorescence. Separated channels of boxed regions are shown magnified on the right. **C** Cell expressing Anillin-GFP and Sticky-mCh. Separated channels of boxed regions are shown magnified below. **D** Cell expressing Anillin-mCh and Tum-GFP. Separated channels of boxed regions are shown magnified below. **E** Cell expressing Anillin-mCh and Pavarotti-GFP. Separated channels of boxed regions are shown magnified below. **F** Inverted LUT of the nascent MR of an Aurora B-GFP expressing cell. **G** The nascent MR of a myosin-GFP expressing cell. **H** The nascent MR of a cell expressing myosin-GFP (Myo) and Anillin-mCh (Ani). Separated channels of boxed regions are shown magnified below. **I** The nascent MR of a cell expressing LifeAct-GFP (LA) and Anillin-mCh (Ani). Separated channels of boxed regions are shown magnified below. **J** The nascent MR of a cell expressing Anillin-GFP fixed and stained with rhodamine-phalloidin. Times are h:min:s from the end of furrowng. Scale bars, 5 μm, except magnified region in A, 1μm . See also Videos S3.

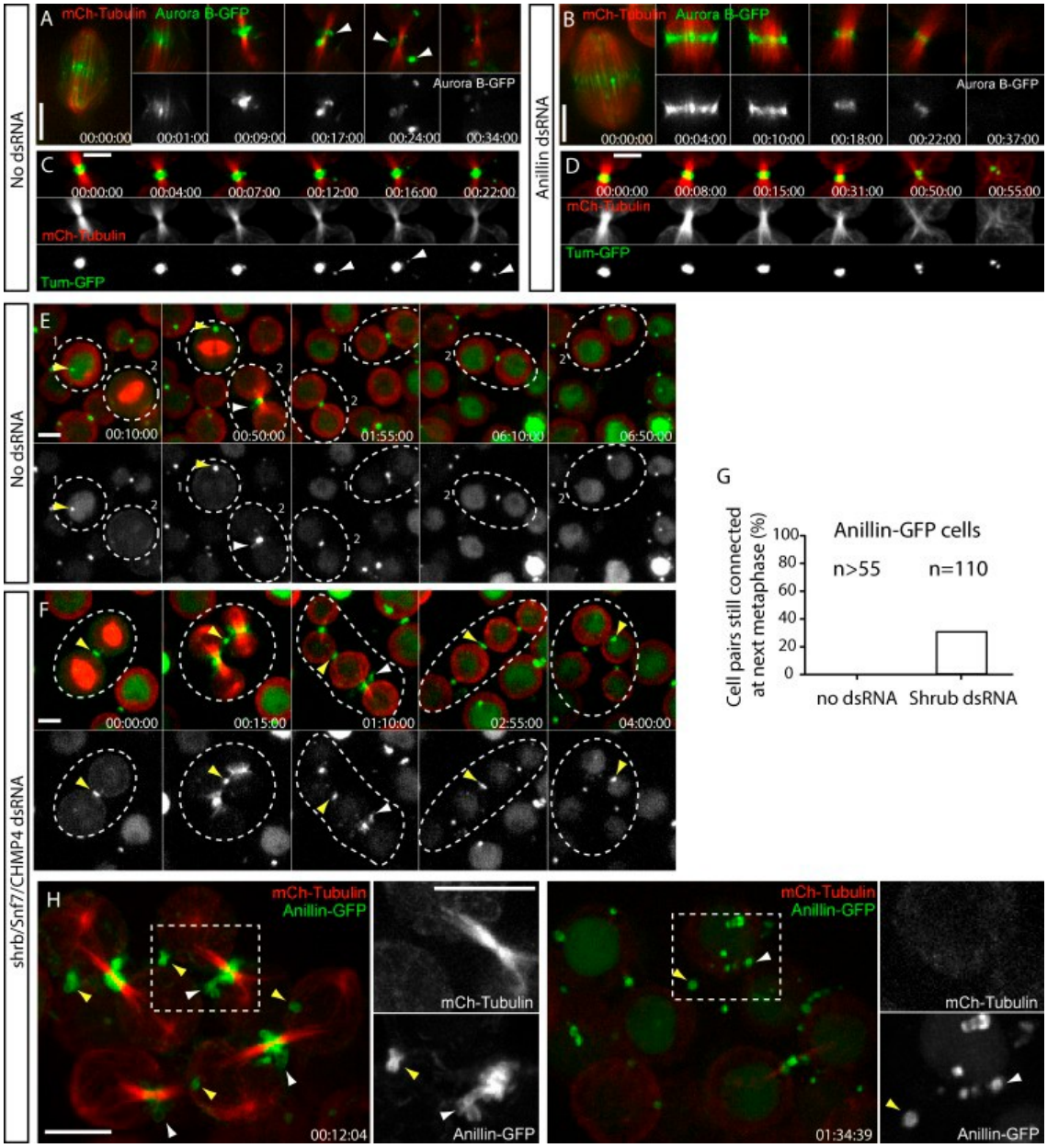
No dsRNA
A
mCh-Tubulin Aurora B-GFP
Aurora B-GFP
00:00:00 00:01:00 00:09:00 00:17:00 00:24:00 00:34:00
Anillin dsRNA
B
mCh-Tubulin Aurora B-GFP
Aurora B-GFP
00:00:00 00:04:00 00:10:00 00:18:00 00:22:00 00:37:00
C
00:00:00 00:04:00 00:07:00 00:12:00 00:16:00 00:22:00
mCh-Tubulin
Tum-GFP
D
00:00:00 00:08:00 00:15:00 00:31:00 00:50:00 00:55:00
mCh-Tubulin
Tum-GFP
No dsRNA
E
00:10:00 00:50:00 01:55:00 06:10:00 06:50:00
shrb/Snf7/CHMP4 dsRNA
F
00:00:00 00:15:00 01:10:00 02:55:00 04:00:00
G
Anillin-GFP cells
n>55 n=110
Cell pairs still connected at next metaphase (%)
100
80
60
40
20
0
no dsRNA Shrub dsRNA
H
mCh-Tubulin
Anillin-GFP
00:12:04
mCh-Tubulin
Anillin-GFP
mCh-Tubulin
Anillin-GFP
01:34:39
mCh-Tubulin
Anillin-GFP

Figure 5.3: Shedding from the nascent MR requires Anillin but not ESCRT III.

A-B Time-lapse sequence of cells expressing Aurora B-GFP and mCherry-tubulin following a 3-day incubation without (A) or with (B) Anillin dsRNAs, acquired with 100x 1.4 NA objective. Arrowheads in A mark shedding events. **C-D** Time-lapse sequence of cells expressing Tum-GFP and mCherry-tubulin following a 3-day incubation without (C) or with (D) Anillin dsRNAs. Arrowheads in C mark shedding events. **E-F** Selected frames from a time-lapse sequence of Anillin-GFP cells following 4-day incubation without (E) or with (F) *Shrub* dsRNAs, acquired with 40x objective. Yellow arrowheads mark mature MRs/MR remnants from previous divisions; white arrowheads mark MRs from the current division. **G** Quantification of Anillin-GFP-expressing cells that have failed to undergo abscission and thus remain paired at metaphase in control and Shrub-depleted cells. Data are from 2 independent experiments. **H** Selected frames from a time-lapse sequence of Anillin-GFP cells, acquired with 100x objective, following 4-day incubation with *Shrub* dsRNAs. Yellow arrowheads mark mature MRs from previous divisions; white arrowheads mark nascent MRs from the current division that are shedding Anillin-GFP. Times are h:min:s. Scale bars, 5 μm. See also Videos S4.

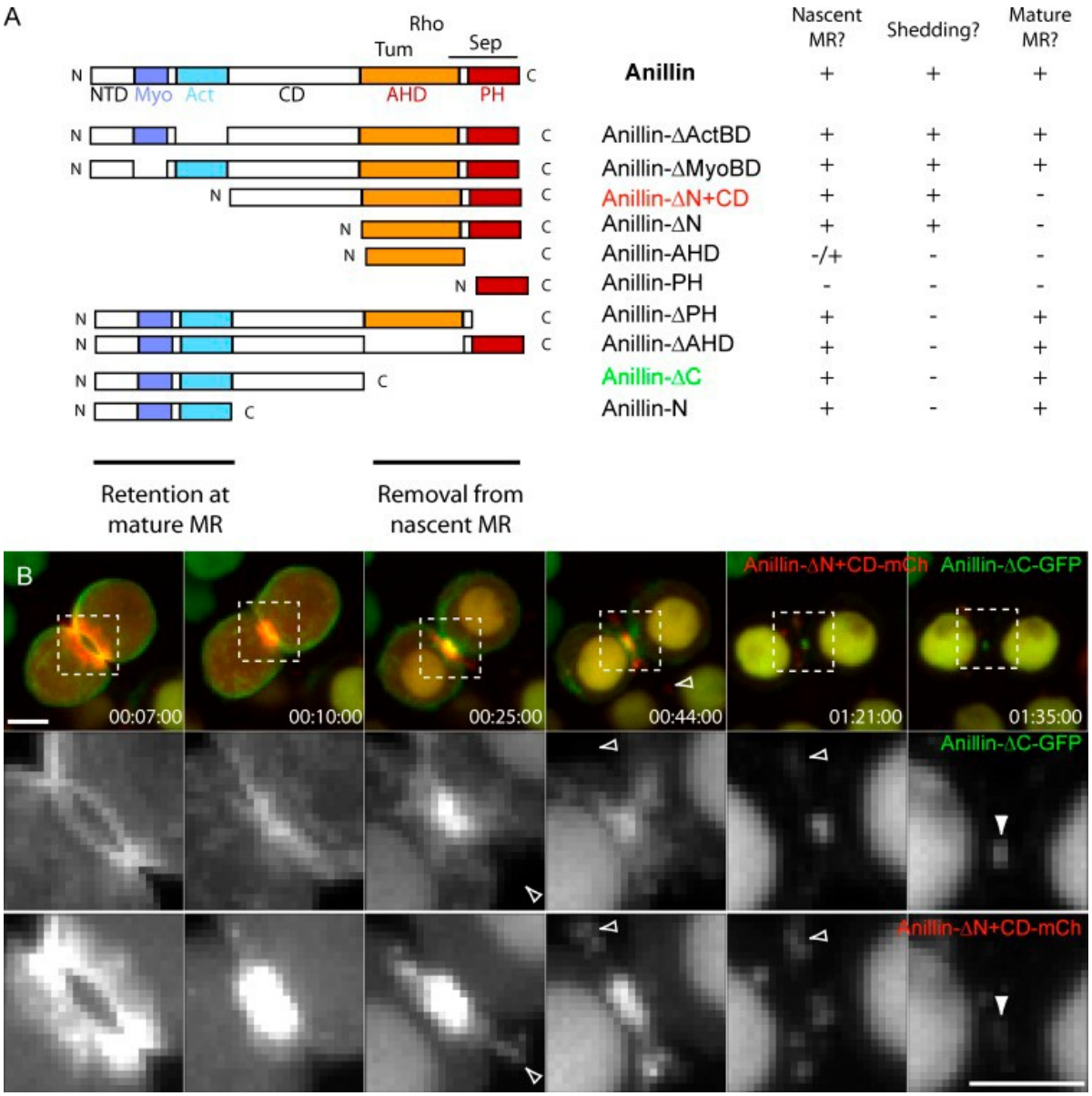
A
Rho
Tum
Sep
N
C
NTD
Myo
Act
CD
AHD
PH
Anillin
Nascent MR?
Shedding?
Mature MR?
Anillin-ΔActBD
Anillin-ΔMyoBD
Anillin-ΔN+CD
Anillin-ΔN
Anillin-AHD
Anillin-PH
Anillin-ΔPH
Anillin-ΔAHD
Anillin-ΔC
Anillin-N
+
-
-/+
Retention at mature MR
Removal from nascent MR
B
00:07:00
00:10:00
00:25:00
00:44:00
01:21:00
01:35:00
Anillin-ΔN+CD-mCh
Anillin-ΔC-GFP

Figure 5.4: Removal of Anillin from the nascent MR is mediated via its C-terminal domains, while retention requires its N-terminal domains.

A Domain organization of Anillin and truncation mutants analyses for their localization to the nascent MR, ability to be extruded and shed and their retention at the mature MR. **B** Time-lapse sequence of a cell co-expressing AnillinΔC-GFP and Anillin-ΔN+CD-mCh. Open arrowheads mark shed material, closed arrowheads mark the mature MR. Separated channels and magnified images of the boxed regions are shown below. Times are h:min:s. Scale bars, 5 μm. See also Video S5.

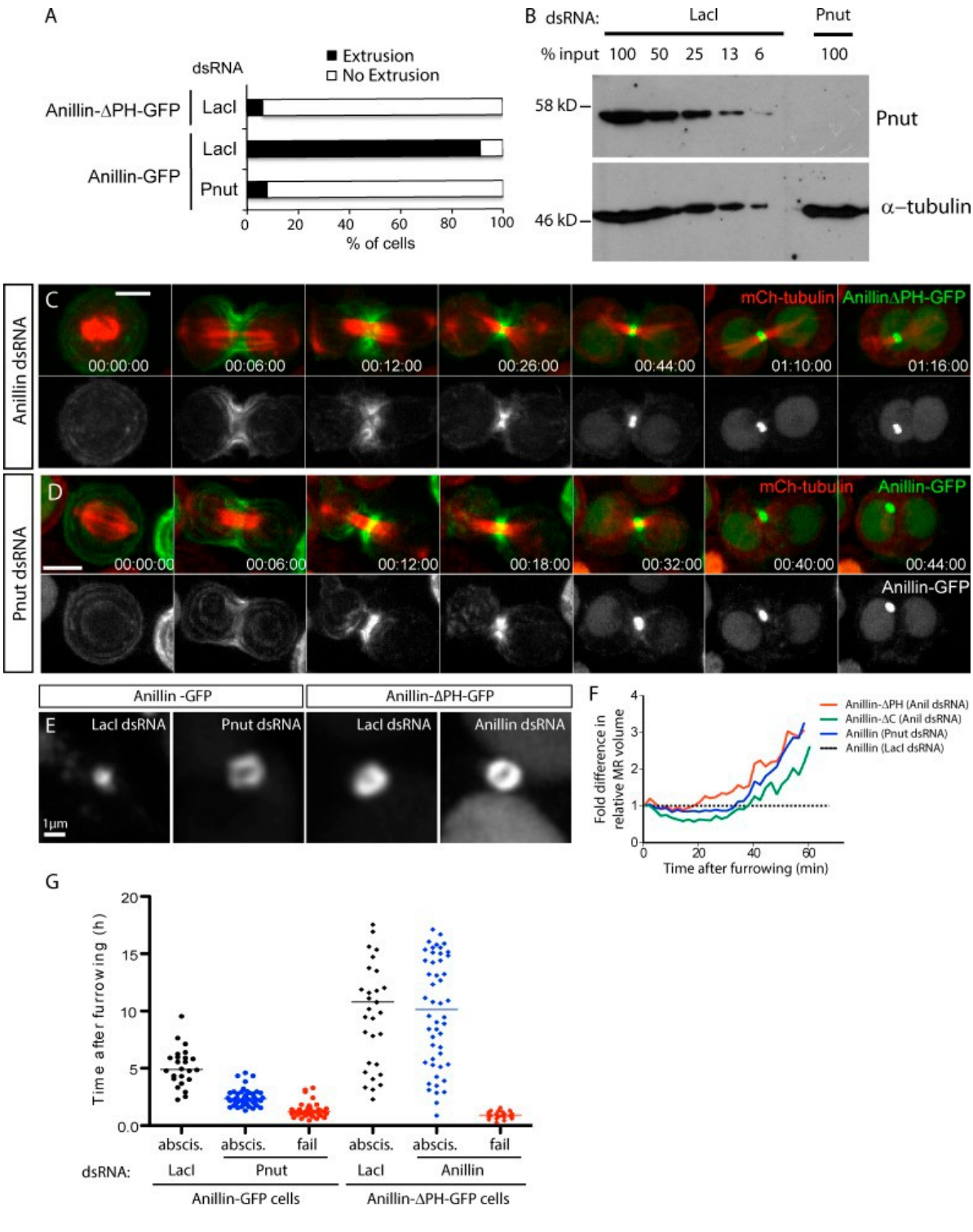
A
dsRNA
Extrusion
No Extrusion
Anillin-ΔPH-GFP
LacI
Anillin-GFP
LacI
Pnut
0
20
40
60
80
100
% of cells
B dsRNA:
LacI
Pnut
% input 100 50 25 13 6
100
58 kD
Pnut
46 kD
α–tubulin
Anillin dsRNA
C
mCh-tubulin
AnillinΔPH-GFP
00:00:00
00:06:00
00:12:00
00:26:00
00:44:00
01:10:00
01:16:00
Pnut dsRNA
D
mCh-tubulin
Anillin-GFP
00:00:00
00:06:00
00:12:00
00:18:00
00:32:00
00:40:00
00:44:00
Anillin-GFP
Anillin -GFP
Anillin-ΔPH-GFP
E
LacI dsRNA
Pnut dsRNA
LacI dsRNA
Anillin dsRNA
1μm
F
Fold difference in relative MR volume
Time after furrowing (min)
Anillin-ΔPH (Anil dsRNA)
Anillin-ΔC (Anil dsRNA)
Anillin (Pnut dsRNA)
Anillin (LacI dsRNA)
G
Time after furrowing (h)
abscis.
abscis.
fail
abscis.
abscis.
fail
dsRNA:
LacI
Pnut
LacI
Anillin
Anillin-GFP cells
Anillin-ΔPH-GFP cells

Figure 5.5: Proper maturation of the MR requires septin-dependent removal of Anillin via its C-terminal PH domain.

A Frequency of extrusion from time-lapse sequences of Anillin-ΔPH-GFP, and of Anillin-GFP following 8 days Pnut RNAi. **B** Anti-Pnut immunoblot of S2 cell lysates serially-diluted following LacI control dsRNA incubation or following Pnut dsRNA incubation; anti-tubulin loading control. **C** Time-lapse sequences of cells expressing Anillin-ΔPH-GFP, depleted of endogenous Anillin. **D** Time-lapse sequence of an Anillin-GFP-expressing cell following 8 days Pnut RNAi. **E** Representative images of age-matched MR structures from Anillin-GFP or Anillin-ΔPH-GFP cells treated with the indicated dsRNAs. **F** Volume measurements of the nascent MR of cells expressing Anillin-ΔPH-GFP, Anillin-ΔC-GFP or Anillin-GFP, treated with indicated dsRNAs, from the end of furrowing, normalized at each time point to equivalently aged Anillin-GFP controls (n=10 per condition from 2 independent experiments). **G** Timing of abscission or furrow regression (failure) of Anillin-GFP cells treated for 7-9 days with LacI (control, n=30) or Pnut dsRNAs (n=75), and of Anillin-ΔPH-GFP cells treated for 3 days with LacI (control, n=30) or Anillin dsRNAs (n=75). Mean values are shown, data are from a single representative experiment out of three repeats. Times are h:min:s, Scale bars, 5 µm, except E, 1 µm.

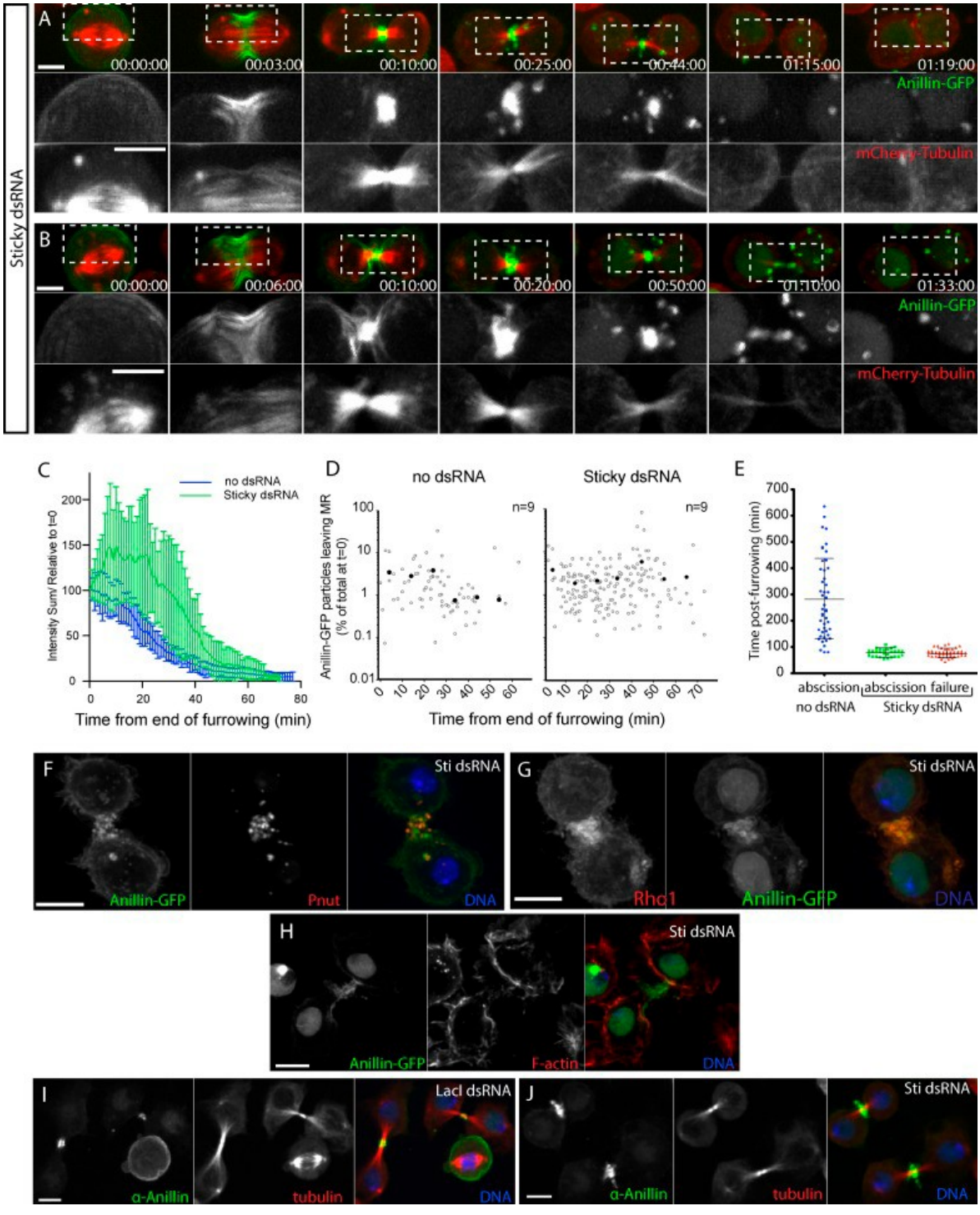
Sticky dsRNA
A
00:00:00
00:03:00
00:10:00
00:25:00
00:44:00
01:15:00
01:19:00
Anillin-GFP
mCherry-Tubulin
B
00:00:00
00:06:00
00:10:00
00:20:00
00:50:00
01:10:00
01:33:00
Anillin-GFP
mCherry-Tubulin
C
no dsRNA
Sticky dsRNA
Intensity Sum/ Relative to t=0
Time from end of furrowing (min)
D
no dsRNA
Sticky dsRNA
n=9
n=9
Anillin-GFP particles leaving MR (% of total at t=0)
Time from end of furrowing (min)
E
Time post-furrowing (min)
abscission
abscission failure
no dsRNA
Sticky dsRNA
F
Sti dsRNA
Anillin-GFP
Pnut
DNA
G
Sti dsRNA
Rhc1
Anillin-GFP
DNA
H
Sti dsRNA
Anillin-GFP
F-actin
DNA
I
LacI dsRNA
α-Anillin
tubulin
DNA
J
Sti dsRNA
α-Anillin
tubulin
DNA

Figure 5.6: Sticky acts to limit extrusion/shedding and retain Anillin at the MR.

A-B Sticky-depleted cells expressing Anillin-GFP and mCh-tubulin failing cytokinesis (A) or prematurely abscising (B) (63x objective). **C** Quantification of relative Anillin-GFP intensities (sum intensity) at the MR from the time of midbody formation in control (n=9) and Sticky-depleted cells (n=17). **D** Quantification of individual extrusion or internalization events (open circles) plotted as a function of time and associated Anillin-GFP $\log_{10}$ intensity (as a measure of total intensity at the close of furrowing, t=0). Closed circles represent mean values for each 10 min interval (n=9 cells each, from one experiment representative of two repeats). **E** Timing of abscission or furrow regression (failure) events of individual Anillin-GFP cells treated for 30-48h with LacI or Sticky dsRNAs. Data are from 2 independent experiments, horizontal lines mark the median times. **F-H** Confocal images of Sticky-depleted cells expressing Anillin-GFP (left, green in merged), stained for Pnut (F, center, red in merged), Rho1 (G, left, red in merged) or F-actin (H, center, red in merged) and DNA (blue in merged). **I-J** Confocal images of untransfected S2 cells treated with LacI control dsRNA (I) or Sticky dsRNA (J) and stained for endogenous Anillin (left, green in merged), tubulin (center (red in merged) and DNA (blue in merged) (63x objective). Times are h:min:s. Scale bars, 5 µm. See also Videos S6 and S7.

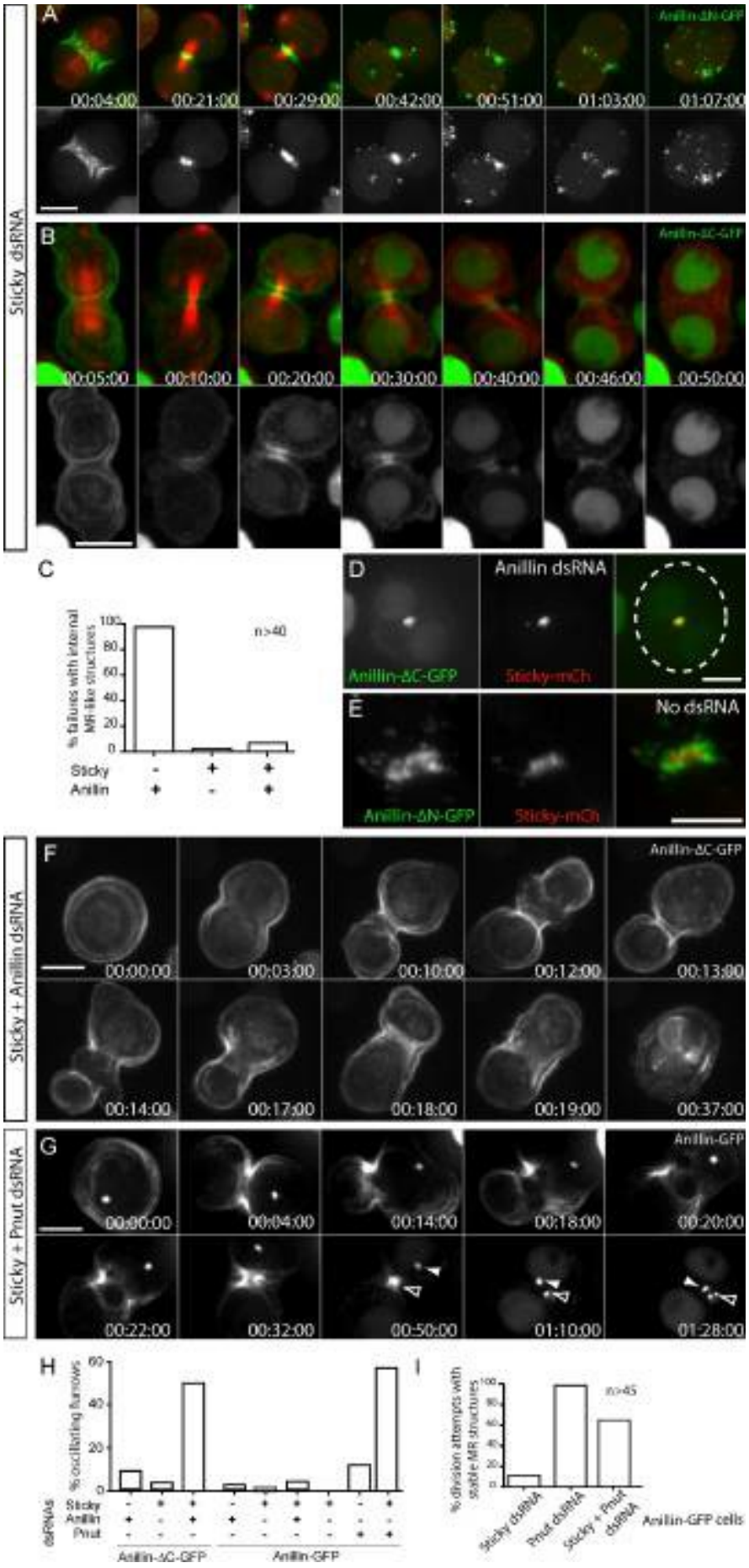
Sticky dsRNA
A
Anillin-ΔN-GFP
00:04:00
00:21:00
00:29:00
00:42:00
00:51:00
01:03:00
01:07:00
B
Anillin-ΔC-GFP
00:05:00
00:10:00
00:20:00
00:30:00
00:40:00
00:46:00
00:50:00
C
% failures with internal MR like structures
n>40
Sticky
Anillin
D
Anillin dsRNA
Anillin-ΔC-GFP
Sticky-mCh
E
No dsRNA
Anillin-ΔN-GFP
Sticky-mCh
Sticky + Anillin dsRNA
F
Anillin-ΔC-GFP
00:00:00
00:03:00
00:10:00
00:12:00
00:13:00
00:14:00
00:17:00
00:18:00
00:19:00
00:37:00
Sticky + Pnut dsRNA
G
Anillin-GFP
00:00:00
00:04:00
00:14:00
00:18:00
00:20:00
00:22:00
00:32:00
00:50:00
01:10:00
01:28:00
H
% oscillating furrows
dsRNAs
Sticky
Anillin
Pnut
Anillin-ΔC-GFP
Anillin-GFP
I
% division attempts with stable MR structures
n>45
Sticky dsRNA
Pnut dsRNA
Sticky + Pnut dsRNA
Anillin-GFP cells

Figure 5.7: Sticky acts with the N-terminus of Anillin to promote both MR formation and CR stability.

A-B Time-lapse sequence of cells expressing mCh-tubulin and Anillin-ΔN-GFP (A) or Anillin-ΔC-GFP (B) after a ~30 h incubation with Sticky dsRNAs (63x objective, 2x2 camera binning). **C** Quantification from time-lapse records of failed attempts at cytokinesis that form internal Anillin-ΔC-FP-positive MR-like structures following incubation with indicated dsRNAs. Data are from 2 independent experiments. **D-E** Confocal images of cells co-expressing Sticky-mCh and Anillin-ΔC-GFP (D) or Anillin-ΔN-GFP (E) following endogenous Anillin depletion. Dotted line in D marks the cell boundary (63x objective, no camera binning). **F** Time-lapse sequence of a cell expressing Anillin-ΔC following co-depletion of Sticky and Anillin. **G** Quantification from time-lapse records (40x objective, 2x2 camera binning) of the percentage of Anillin-GFP and Anillin-ΔC-GFP cells displaying oscillating furrows during CR closure, following incubation with the indicated dsRNAs (n>78 per condition, from 2 independent experiments). **H** Time-lapse sequence of a cell expressing Anillin-GFP following co-depletion of Pnut (144-162 hr RNAi) and Sticky (30-48 hr RNAi), captured with 63x objective with 2x2 camera binning. Closed arrowhead marks a presumed MR remnant from a previous division. Open arrowhead marks failing MR from the current division attempt. **I** Quantification from time-lapse records (40x objective, 2x2 camera binning) of attempts at cytokinesis that result in Anillin-GFP-positive MR structures following incubation with indicated dsRNAs (n>45 per condition, from 2 independent experiments). Times are h:min:s. Scale bars, 5 μm. See also Video S8.

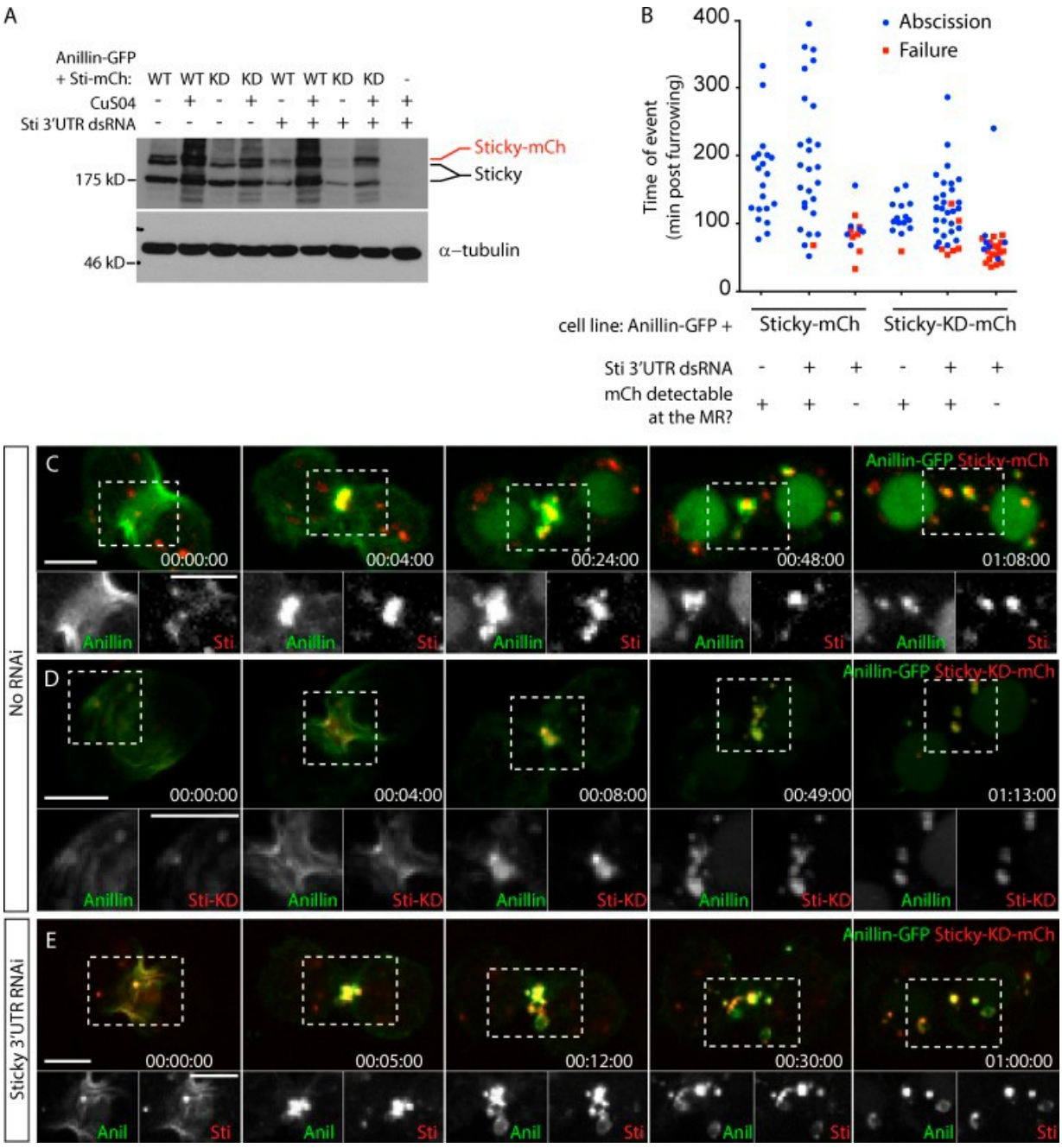
A
Anillin-GFP
+ Sti-mCh: WT WT KD KD WT WT KD KD -
CuS04 - + - + - + - + +
Sti 3'UTR dsRNA - - - - + + + + +
175 kD
46 kD
Sticky-mCh
Sticky
α–tubulin
B
Abscission
Failure
Time of event (min post furrowing)
400
300
200
100
0
cell line: Anillin-GFP + Sticky-mCh Sticky-KD-mCh
Sti 3'UTR dsRNA - + + - + +
mCh detectable at the MR? + + - + + -
No RNAi
C
Anillin-GFP Sticky-mCh
00:00:00
00:04:00
00:24:00
00:48:00
01:08:00
Anillin
Sti
D
Anillin-GFP Sticky-KD-mCh
00:00:00
00:04:00
00:08:00
00:49:00
01:13:00
Anillin
Sti-KD
Sticky 3'UTR RNAi
E
Anillin-GFP Sticky-KD-mCh
00:00:00
00:05:00
00:12:00
00:30:00
01:00:00
Anil
Sti

Figure 5.8: Sticky's essential role during MR formation is as a scaffold**.**

A Anti-Sticky immunoblot of cell lysates from indicated cell lines following Sticky 3'UTR dsRNA or LacI control dsRNA incubation, with anti-tubulin blot as a loading control. **B** Timing of abscission (blue) or furrow regression (failure, red) of cells co-expressing Anillin-GFP and Sticky-mCh or Sticky-KD-mCh, treated for 3-5 days with LacI (control) or Sticky 3'UTR dsRNAs. Data are from 2 independent experiments. **C-D** Time-lapse sequence of a cell co-expressing Anillin-GFP and Sticky-mCh (C) or Sticky-KD-mCh (D). Separated channels of the boxed regions are shown magnified below. **E** Time-lapse sequence of a cell co-expressing Anillin-GFP and Sticky-KD-mCh following depletion of endogenous Sticky. Times are h:min:s, Scale bars, 5 μm. See also Videos S9 and S10.

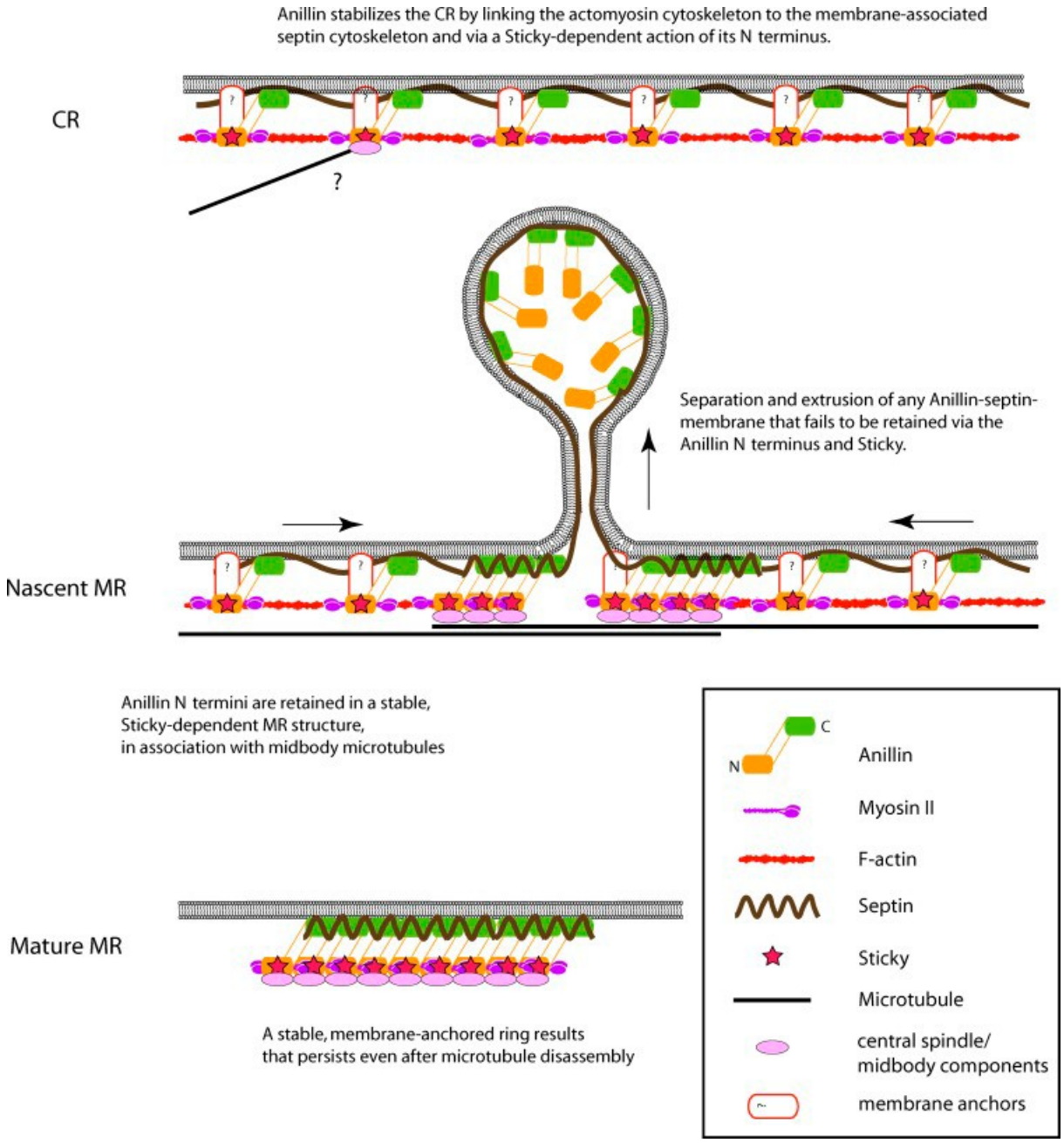
Anillin stabilizes the CR by linking the actomyosin cytoskeleton to the membrane-associated septin cytoskeleton and via a Sticky-dependent action of its N terminus.
CR
?
Separation and extrusion of any Anillin-septin-membrane that fails to be retained via the Anillin N terminus and Sticky.
Nascent MR
Anillin N termini are retained in a stable, Sticky-dependent MR structure, in association with midbody microtubules
C
N
Anillin
Myosin II
F-actin
Septin
Sticky
Microtubule
central spindle/ midbody components
membrane anchors
Mature MR
A stable, membrane-anchored ring results that persists even after microtubule disassembly

Figure 5.9: Model for the maturation of the CR and MR.

At the CR stage (top), Anillin links the plasma membrane-associated septin cytoskeleton to actomyosin, stabilizing the furrow. Anillin also stabilizes the furrow via a separate Sticky-dependent action of its N-terminus. At the nascent MR (middle), Sticky, myosin and the Anillin N-terminus are retained at the midbody where they will form a mature MR structure. Septins act on the C-terminus of Anillin to remove membrane-associated Anillin molecules whose N-termini are liberated upon disassembly of the F-actin ring. Note that this removal does not only occur at the center of the midbody, as depicted. Septins and the C-termini of Anillin molecules that are retained also act as membrane anchors for the mature MR that persists beyond ~1 h after furrowing (bottom).

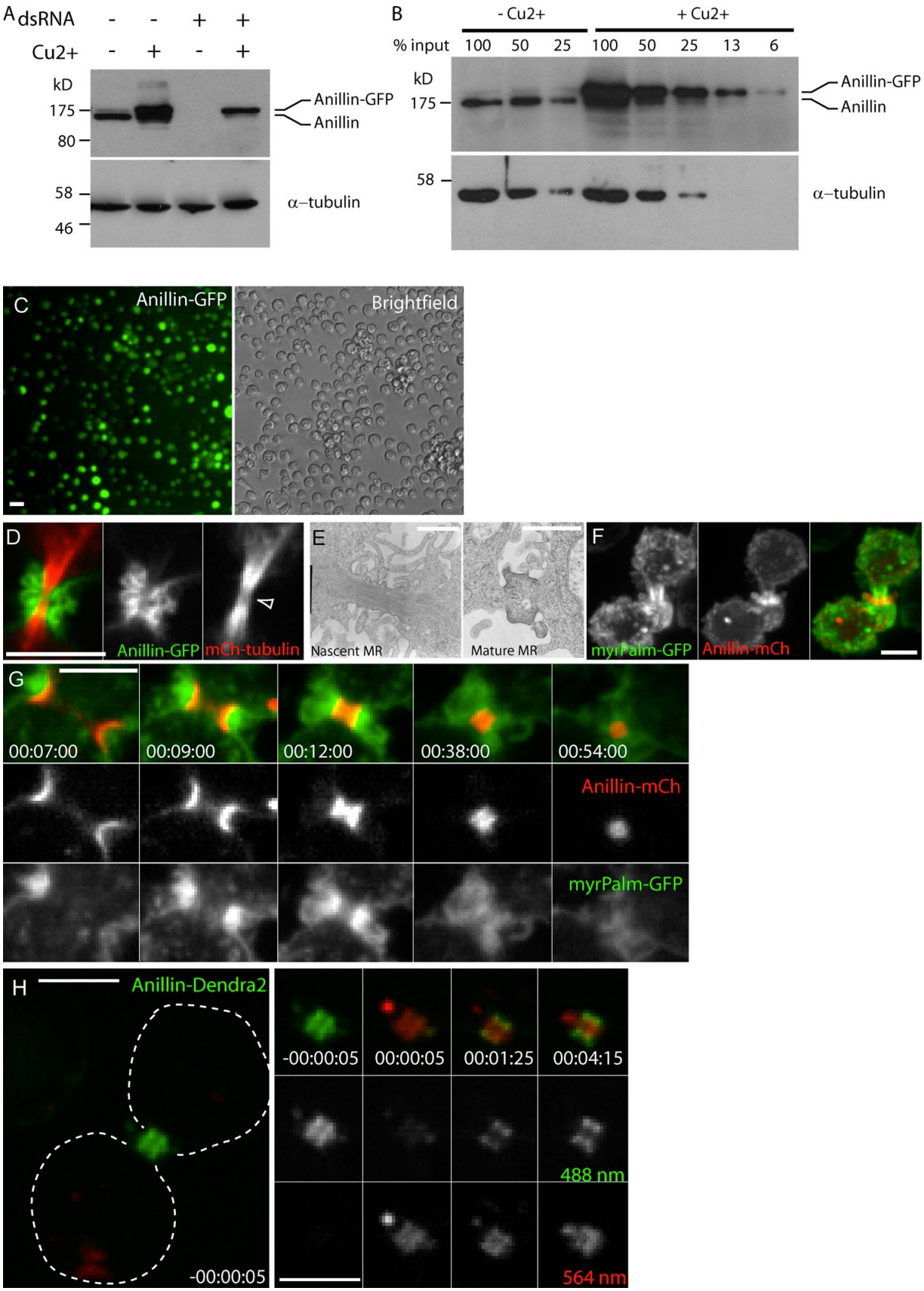
A
dsRNA - - + +
Cu2+ - + - +
kD
175
80
58
46
Anillin-GFP
Anillin
α–tubulin
B
- Cu2+
+ Cu2+
% input 100 50 25 100 50 25 13 6
kD
175
58
Anillin-GFP
Anillin
α–tubulin
C
Anillin-GFP
Brightfield
D
Anillin-GFP
mCh-tubulin
E
Nascent MR
Mature MR
F
myrPalm-GFP
Anillin-mCh
G
00:07:00
00:09:00
00:12:00
00:38:00
00:54:00
Anillin-mCh
myrPalm-GFP
H
Anillin-Dendra2
-00:00:05
-00:00:05
00:00:05
00:01:25
00:04:15
488 nm
564 nm

Figure S5.1: Anillin-FP expression and localization druing MR maturation.

A Anti-Anillin immunoblot analysis of cell lysates following 3-day treatment with or without Anillin dsRNAs, with or without $CuSO_4$ induction of Anillin-GFP. The same blot was cut and probed with anti-tubulin antibody as a loading control. **B** Serial dilutions of Anillin-GFP cell lysates with or without $CuSO_4$ induction, probed with anti-Anillin antibodies (top). The same blot was cut and probed with anti-tubulin antibody as a loading control (bottom). From this it can be estimated that Anillin-GFP is expressed at approximately four-fold higher levels than endogenous Anillin, although we note that this is likely an overestimate in mitotic cells since endogenous Anillin expression is cell-cycle regulated, accumulating in G2 (Field & Alberts, 1995), while Anillin-GFP expression is not. **C** Fluorescence and brightfield images of Anillin-GFP expression, showing that close to 100% of the cells express Anillin-GFP. **D** Single confocal sections of a nascent MR from a cell expressing Anillin-GFP and mCherry- tubulin. Arrowhead marks the midbody region. **E** Transmission electron micrographs of Anillin-GFP expressing S2 cells. **F-G** Single confocal sections of a nascent MR expressing Anillin-mCherry and myrPalm-GFP. **H** Single confocal sections of Anillin-Dendra2- expressing nascent MR before and after photoconversion, imaged using both 488nm and 564nm light. Separated channels of the MR region are shown at right (63x objective, 2x2 camera binning used throughout, except C, 20X objective). Time is h:min:s, scale bars, 5 µm, except in E, 1 µm.

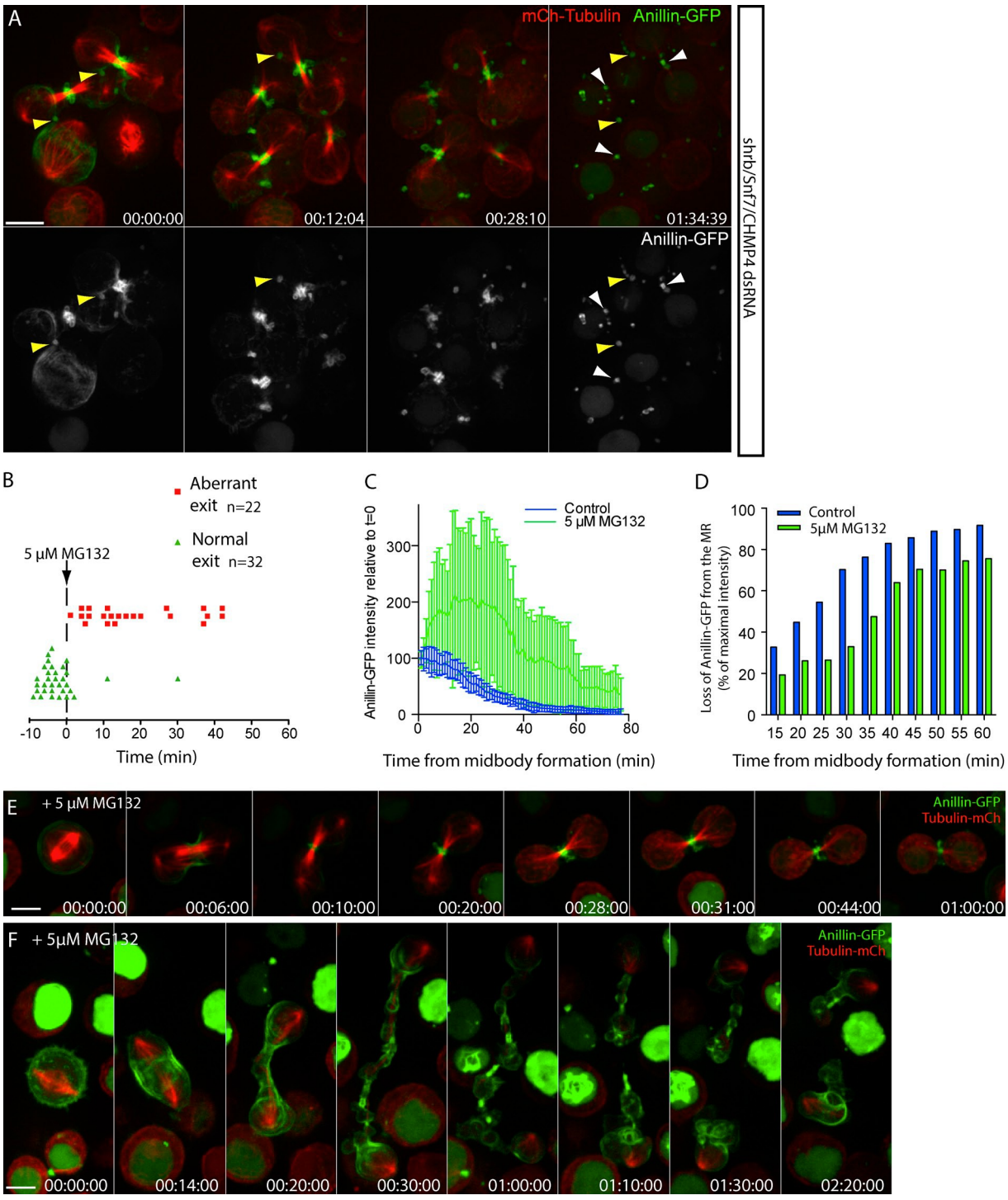
A
mCh-Tubulin Anillin-GFP
00:00:00
00:12:04
00:28:10
01:34:39
Anillin-GFP
shrb/Snf7/CHMP4 dsRNA
B
Aberrant exit n=22
Normal exit n=32
5 µM MG132
-10 0 10 20 30 40 50 60
Time (min)
C
Control
5 µM MG132
Anillin-GFP intensity relative to t=0
0 100 200 300
0 20 40 60 80
Time from midbody formation (min)
D
Control
5µM MG132
Loss of Anillin-GFP from the MR (% of maximal intensity)
0 20 40 60 80 100
15 20 25 30 35 40 45 50 55 60
Time from midbody formation (min)
E
+ 5 µM MG132
Anillin-GFP
Tubulin-mCh
00:00:00
00:06:00
00:10:00
00:20:00
00:28:00
00:31:00
00:44:00
01:00:00
F
+ 5µM MG132
Anillin-GFP
Tubulin-mCh
00:00:00
00:14:00
00:20:00
00:30:00
01:00:00
01:10:00
01:30:00
02:20:00

Figure S5.2: Additional cells treated with shrb/CHMP4 dsRNAs or MG132.

A Anillin-GFP expressing S2 cells incubated for 3 days with shrb/CHMP4 dsRNAs. Yellow arrowhead depicts MR from previous division that still connects sister cells. White arrowheads depict shedding from the nascent MRs of the current division. Same cells as shown in Fig. 3H. **B** Consequences of acute administration of 5 µM MG132 to mitotic cells expressing Anillin-GFP and mCh-tubulin. Points represent individual cells undergoing anaphase at the indicated times relative to MG132 addition. Data are from 3 independent experiments. **C** Changes in Anillin-GFP intensities at the MR in cells undergoing "normal" exit in the presence or absence of 5 µM MG132, relative to the time of midbody formation (t=0, mean values ± sd, n=14 and n=11, respectively). **D** Anillin-GFP sum intensity values at the MR are plotted at 5 min intervals relative to the maximal sum intensity value for each cell, regardless of when during MR maturation this occurred. Mean values are shown for cells in the presence (n=14) or absence (n=11) of 5 µM MG132. Data are from 3 independent experiments. **E** Selected frames from a time-lapse sequence of an Anillin-GFP cell in the presence of 5 µM MG132. **F** Example of Anillin-GFP expressing cell exhibiting aberrant mitotic exit and cytokinesis in the presence of 5µM MG132 added just prior to the metaphase/anaphase transition. Time is h:min:s, scale bar, 5 µm.

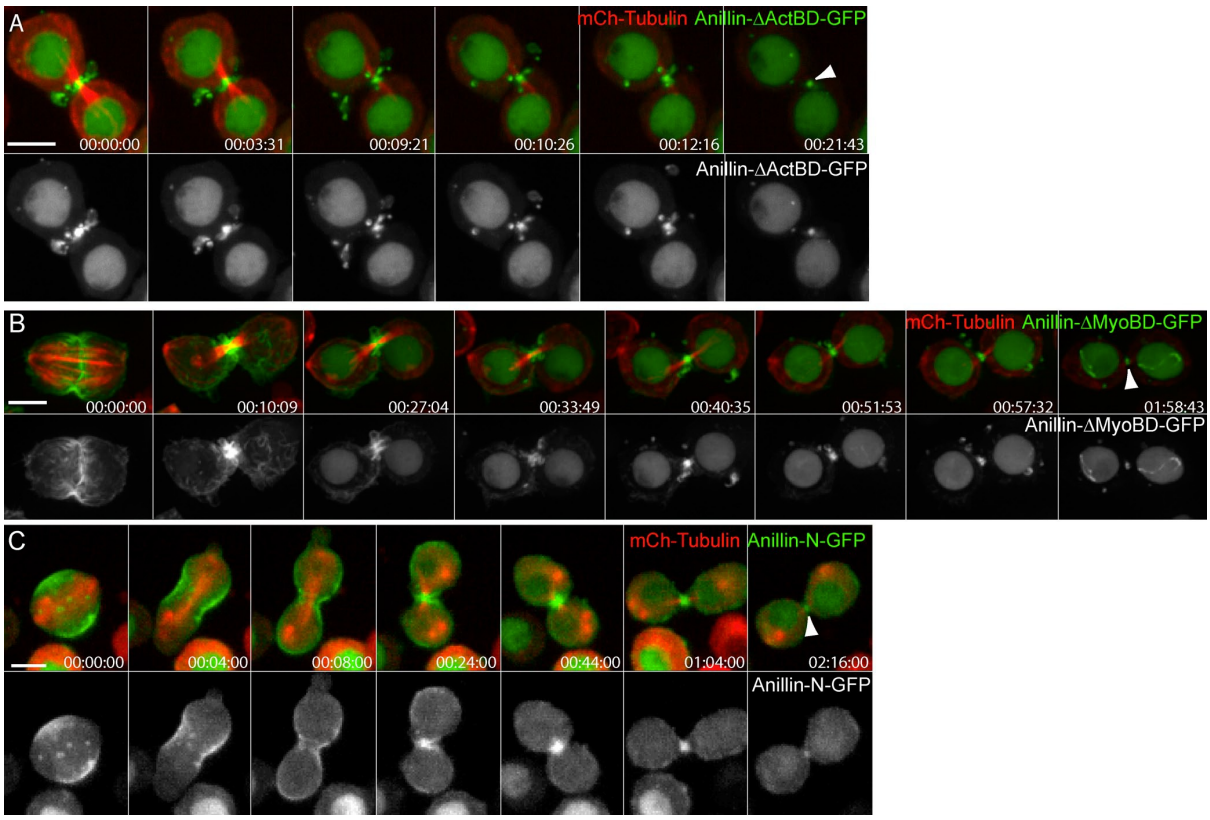
A
mCh-Tubulin Anillin-ΔActBD-GFP
00:00:00
00:03:31
00:09:21
00:10:26
00:12:16
00:21:43
Anillin-ΔActBD-GFP
B
mCh-Tubulin Anillin-ΔMyoBD-GFP
00:00:00
00:10:09
00:27:04
00:33:49
00:40:35
00:51:53
00:57:32
01:58:43
Anillin-ΔMyoBD-GFP
C
mCh-Tubulin Anillin-N-GFP
00:00:00
00:04:00
00:08:00
00:24:00
00:44:00
01:04:00
02:16:00
Anillin-N-GFP

Figure S5.3: Behaviors of additional Anillin truncations during MR maturation.

A Cell co-expressing Anillin-ΔActBD-GFP and mCh-tubulin. **B** Cell co-expressing Anillin-ΔMyoBD-GFP and mCh-tubulin. **C** Cell co-expressing Anillin-N-GFP and mCh-tubulin. Arrowheads point to the mature MR. Time is h:min:s, scale bar, 5 μm.

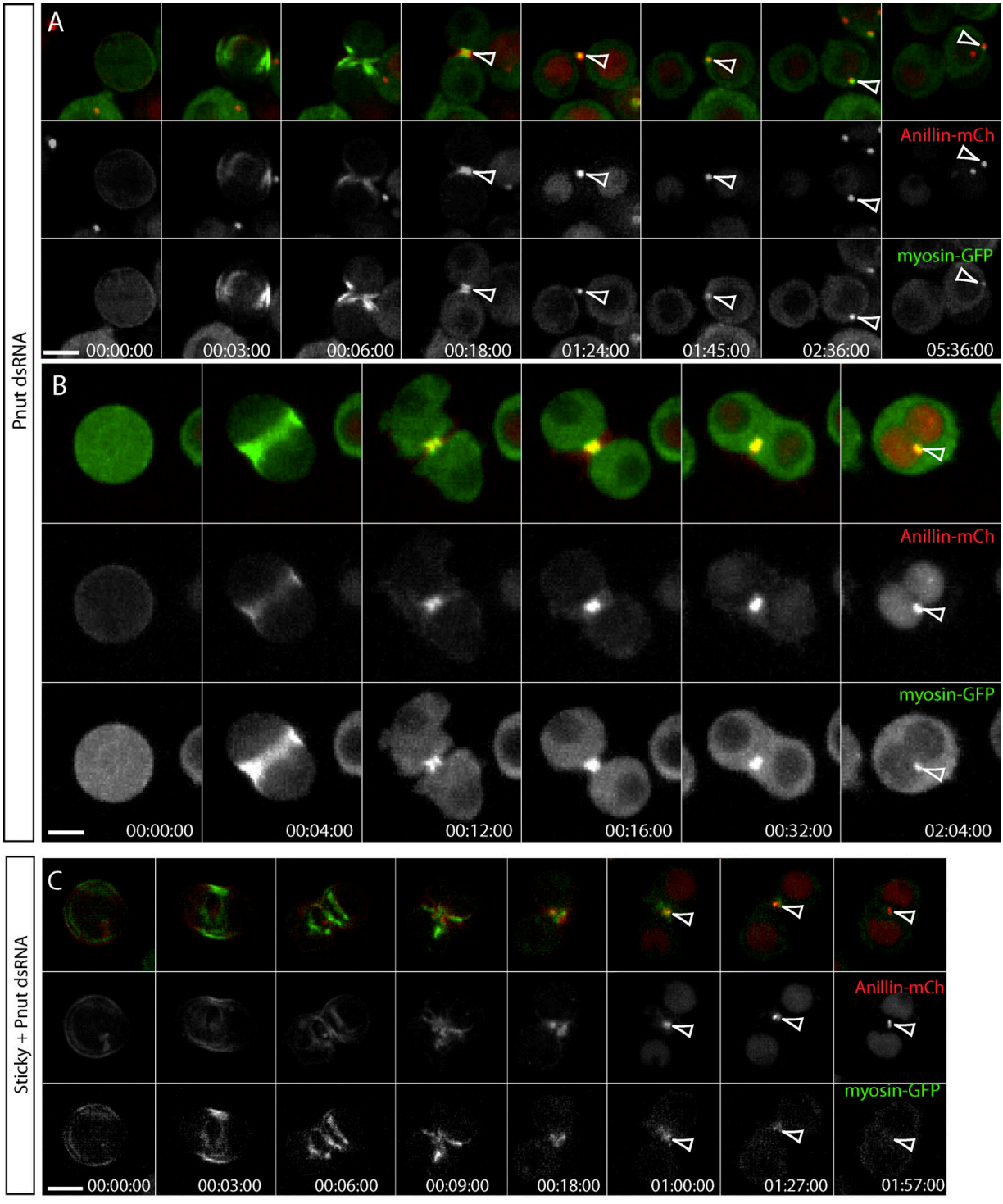
Pnut dsRNA
A
Anillin-mCh
myosin-GFP
00:00:00
00:03:00
00:06:00
00:18:00
01:24:00
01:45:00
02:36:00
05:36:00
B
Anillin-mCh
myosin-GFP
00:00:00
00:04:00
00:12:00
00:16:00
00:32:00
02:04:00
Sticky + Pnut dsRNA
C
Anillin-mCh
myosin-GFP
00:00:00
00:03:00
00:06:00
00:09:00
00:18:00
01:00:00
01:27:00
01:57:00

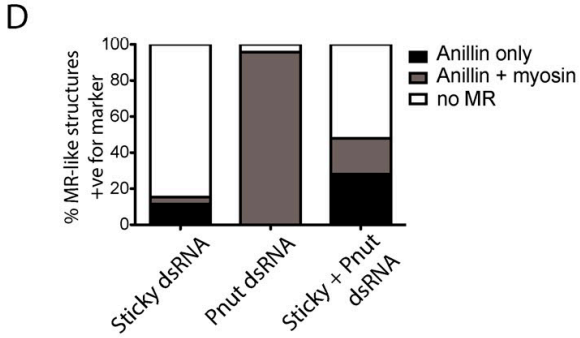
D
% MR-like structures +ve for marker
100
80
60
40
20
0
Anillin only
Anillin + myosin
no MR
Sticky dsRNA
Pnut dsRNA
Sticky + Pnut dsRNA

Figure S5.4: Co-depletion of Sticky and Pnut disrupts MR formation.

A-C Time-lapse sequences of cells co-expressing Anillin-mCh and myosin-GFP attempting cytokinesis following incubation with Pnut dsRNA (A-B) or Sticky and Pnut dsRNAs (C). Arrowheads mark the MR structures that result after successful (A) or failed (B-C) division attempts. **D** Quantification from time-lapse records (40x objective, 2x2 camera binning) of failed division attempts resulting in the presence or absence of internal MR-like structures positive for Anillin-mCh alone, or Anillin-mCh and myosin-GFP following depletion of Sticky (n=25), Pnut (n=28) or both (n=46). Data are from 1 experiment representative of 3 repeats. Time is h:min:s, scale bar, 5 μm.

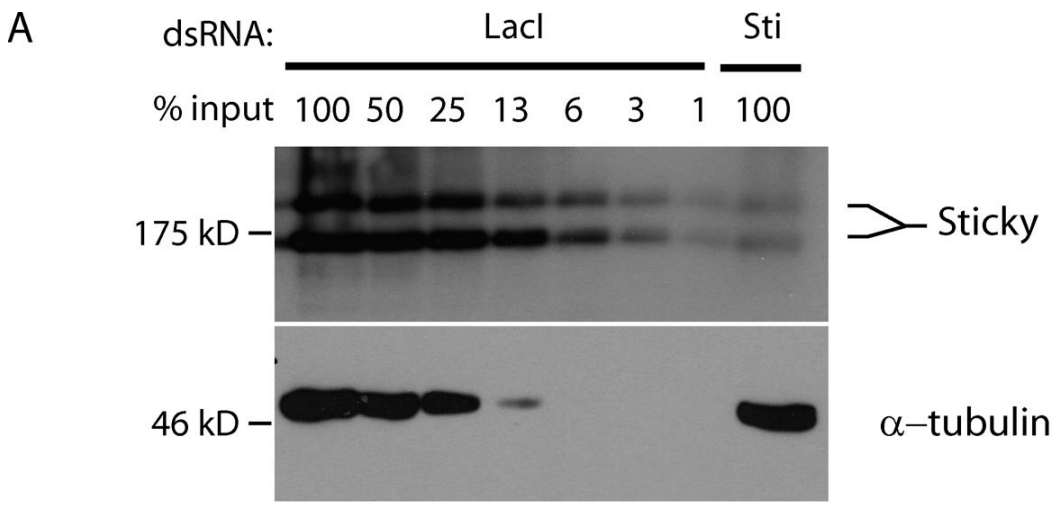
A
dsRNA:
LacI
Sti
% input 100 50 25 13 6 3 1 100
175 kD
Sticky
46 kD
α–tubulin

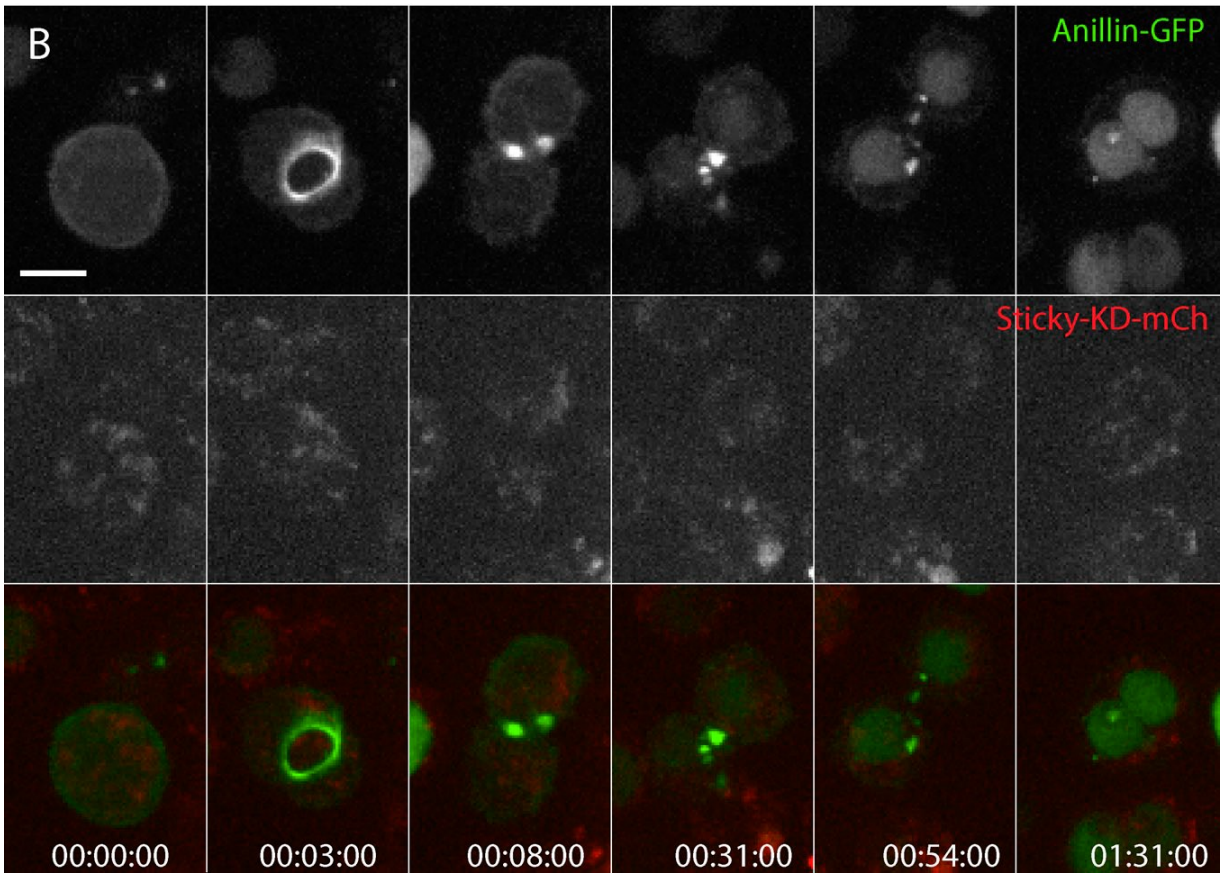
B
Anillin-GFP
Sticky-KD-mCh
00:00:00
00:03:00
00:08:00
00:31:00
00:54:00
01:31:00

Figure S5.5: Sticky immunoblot and example of cell Sticky-KD-mCh failure.

A Anti-Sticky immunoblot analysis of S2 cell lysates following 3-day treatment with LacI or Sti dsRNA. A serial dilution of the LacI lysate demonstrates the extreme sensitivity of detection of the antibody and the efficacy of the RNAi. The same blot was cut and probed with anti-tubulin antibody as a loading control (bottom). **B** Example of a cell expressing Anillin-GFP and Sticky-KD-mCh, depleted of endogenous Sticky, that failed to recruit any Sticky-KD-mCh and failed cytokinesis. Time is h:min:s, scale bar, 5 μm.

5.9 SUPPLEMENTAL DATA

http://jcb.rupress.org/content/203/3/487/tab-figures-data

Video S1 shows extrusion of Anillin-GFP from the nascent MR. Video S2 shows internalization of Anillin-GFP from the nascent MR. Video S3 shows the behavior of co-expressed Anillin-mCh and LifeAct-GFP at the nascent MR. Video S4 shows cells expressing Anillin-GFP undergoing cytokinesis following depletion of Shrb/CHMP4B. Video S5 shows a cell expressing Anillin-ΔN+CD-mCh and Anillin-ΔC-GFP undergoing cytokinesis. Video S6 shows a Sticky-depleted Anillin-GFP-expressing cell undergoing premature abscission. Video S7 shows a Sticky-depleted Anillin-GFP expressing cell failing cytokinesis. Video S8 shows an Anillin-GFP-expressing cell co-depleted of Sticky and Peanut attempting cytokinesis. Video S9 shows a cell expressing Anillin-GFP and Sticky-mCh undergoing cytokinesis following endogenous Sticky depletion. Video S10 shows a cell expressing Anillin-GFP and Sticky-KD-mCh undergoing cytokinesis following endogenous

6 A STRUCTURE-FUNCTION ANALYSIS OF TUM/RACGAP50C IN DROSOPHILA S2 CELLS HIGHLIGHTS FUNCTIONAL INTERPLAY WITH ANILLIN THROUGHOUT CYTOKINESIS.

Amel Kechad[1,2] **& Gilles R.X. Hickson**[1,2*]

1. *Département de pathologie et biologie cellulaire, Université de Montréal*.

2. Axe Maladies Immunitaires et Cancers, Centre de Recherche, *CHU-Sainte-Justine, 3175 Chemin de la Côte Sainte-Catherine, Montréal, Québec, H3T 1C5, Canada.*

* Corresponding author: gilles.hickson@umontreal.ca

Running title: Tum in cytokinesis

Keywords: Tumbleweed, Tum, RacGAP50C, Anillin, cytokinesis, Central spindle , contractile ring, midbody ring, midbody.

Manuscrit en préparation.

Contributions:

AK et GH ont conçu le projet

AK et GH ont rédigé l'article.

Les expériences ont été effectuées par AK.

Les figures ont été produites par AK.

6.1 ABSTRACT:

During cytokinesis, signals from the mitotic spindle drive assembly of a cortical acto-myosin contractile ring (CR) that constricts the cell at its equator. As the CR completes its closure, it matures into the midbody ring (MR), while the mitotic spindle midzone that it encircles matures into the midbody (MB). Together, the MR and MB form the intercellular bridge that serves as a platform for abscission. The relationships between the microtubule structures and cortical structures are very robust, yet their molecular bases remain poorly defined. CYK4/MgcRacGAP/Tum GTPase activating proteins (GAPs) are candidate microtubule-cortex linkers. They form part of the conserved centralspindlin complex and are required for central spindle formation, RhoGEF recruitment/activation for furrow initiation, and for anchorage of the MR/MB to the plasma membrane later. In *Drosophila*, Tumbleweed/RacGAP50C (Tum) has been shown to interact with Anillin, a scaffold protein required for the stability of the CR, formation of the MR and the maturation of the MB.

However, the function of the Tum-Anillin interaction is unknown. Furthermore, there is no consensus on the role of the GAP activity of Tum. We have performed a structure/function analysis of Tum in *Drosophila* Schneider's S2 cells. Live imaging of GFP-tagged, RNAi-resistant Tum truncation mutants in deplete-and-rescue experiments revealed that the GAP activity of Tum and its central domain are each required for CR formation and closure. Furthermore, deletion of sequences within the Anillin binding region of Tum impaired the cortical recruitment of Tum and MB/MR maturation later during cytokinesis, in an Anillin-dependent manner. Finally, Tum mutants that were able to support furrowing in the presence of Anillin, were unable to after Anillin depletion, indicating that Tum and Anillin act synergistically during furrow initiation. We propose a model in which interactions between Anillin and Tum link the CR\MR to the spindle/MB at multiple steps of cytokinesis.

6.2 INTRODUCTION

Cytokinesis is the robust and complex mechanism by which a cell physically separates in two. In animal cells, cytokinesis begins at anaphase when signalling between the central spindle (CS) and the cell cortex generates an equatorial zone of active RhoA. This triggers major remodelling events leading to the assembly and stabilization of a contractile ring (CR) at the cell equator. The CR contains, among others, RhoA itself, F-actin, myosin II, septin filaments and their crosslinking protein Anillin (Eggert et al., 2004; Glotzer, 2005; Green et al., 2012; Pollard, 2010). As the CR constricts, the zone of overlapping microtubule plus-ends within the CS compacts and matures to form the midbody (MB), a densely packed structure enriched in microtubule associated proteins such as Centralspindlin (Tum/CYK4/MgcRacGAP and the kinesin-6, Pavarotti/ MKLP1), Nebbish (KIF14), Fascetto (PRC1), and chromosome passenger proteins such as the Aurora B kinase (Ial) (Hu et al., 2012; Mullins and Biesele, 1973). The maturation of the CS to form the MB is accompanied by a transition of the dynamic CR to a more stable midbody ring (MR) that retains many of the CR components (El-Amine et al., 2013; Kechad et al., 2012). Together, the MB and associated MR form the intercellular bridge, which serves as a platform for abscission that completes cytokinesis (Green et al., 2012; Steigemann and Gerlich, 2009). Maturation of the microtubule-based and cortical structures appears to occur in parallel. In fact, disrupting CS/MB components alters CR positioning and closure (Gatti et al., 2000; Rappaport and Ebstein, 1965), and reciprocally, inhibition of CR closure blocks MB maturation (Hu et al., 2012; Straight et al., 2005). However, the mechanisms governing these transitions and their interdependence remain poorly understood.

At the level of the cortex, our previous work showed that the transition from the CR to the MR requires the scaffolding protein Anillin (El-Amine et al., 2013; Kechad et al., 2012) . Anillin is a conserved protein that localizes to the CR and that can bind many proteins including F-actin (Field and Alberts, 1995; Jananji et al., 2017), Myosin II (Straight et al., 2005) and Citron Kinase (Gai et al., 2011) through its N-terminus; and microtubules (Tse et al., 2011; van Oostende Triplet et al., 2014), Septins (Field et al., 2005; Liu et al., 2012; Oegema et al., 2000), RhoA (Piekny and Glotzer, 2008), as well as the plasma membrane through its C-terminus (Liu et al., 2012). Although Anillin depletion does not block CR

formation, it destabilizes the cleavage furrow, causing it to oscillate, and induces membrane blebbing (Goldbach et al., 2010; Hickson and O'Farrell, 2008a; Kechad et al., 2012; Piekny and Glotzer, 2008; Somma et al., 2002; Straight et al., 2005) . Importantly, even cells that managed to form a CR that almost completely closed ultimately failed to form a MR and failed cytokinesis (Echard et al., 2004; Kechad et al., 2012). Anillin also appears to be involved in CS maturation since Anillin depletion impaired the compaction of MTs and blocked midbody formation that normally accompanies MR formation (Kechad et al., 2012). The ability of Anillin to interact with the membrane, the cortical components and the spindle makes it a prime candidate as a coordinator of CR and CS maturation.

At the microtubule level, several studies that investigated signaling events between the cortex and the CS have highlighted Tum (Tumbleweed/ RacGAP50C in *Drosophila*, CYK-4 in *C. elegans*, and MgcRacGAP/CYK-4 in mammals) as a potential candidate for linking the CS to the CR. Tum interacts with the kinesin-6 motor protein Pavarotti (Pav) in Drosophila (ZEN-4 in *C. elegans*, and MKLP-1 in mammals) to form the evolutionarily conserved centralspindlin complex (Adams et al., 1998; Powers et al., 1998; Raich et al., 1998; Tao et al., 2016). Centralspindlin is required for CS formation and CR assembly and its depletion leads to rapid cytokinesis failure in all studied organisms and cell types (Mishima et al., 2002; Somers and Saint, 2003). In humans and flies, centralspindlin localizes to the CS and the cortex where the N-terminus of Tum/CYK-4 binds the Rho Guanine nucleotide exchange factor (RhoGEF) Pebble (flies) or ECT2 (mammals) and recruits it to the equatorial cortex. The RhoGEF accumulates at the plasma membrane and will locally activate RhoA to trigger CR assembly (Nishimura and Yonemura, 2006; Somers and Saint, 2003; Su et al., 2011; Yuce et al., 2005; Zhao and Fang, 2005). Thus, the N-terminus of CYK-4/TUM is essential for Rho activation.

Another important contribution of Tum in CR assembly involves its C-terminal GAP domain. Although all studies agree on a requirement for the GAP domain, the details are controversial. The GAP activity itself is required for cytokinesis in many systems including *Xenopus*, *C.elegans* and *Drosophila* embryos, as well as mammalian cells (Bastos et al., 2012; Loria et al., 2012; Miller and Bement, 2009; Zavortink et al., 2005; Zhang and Glotzer, 2015). However, the GAP activity was dispensable for cytokinesis in Chicken lymphocytes and

Drosophila neuroblasts (Goldstein et al., 2005; Yamada et al., 2006). Moreover, there are conflicting reports regarding the physiological target(s) of the GAP activity and its role in furrow formation. It is still debated as to whether Tum acts on Rho or Rac GTPases (Discussed in Basant and Glotzer, 2017). In support of RacGAP^{Cyk-4} acting on Rac1, its GAP domain has increased affinity and activity toward Rac1 and Cdc42 compared to RhoA *in vitro* (Bastos et al., 2012; Jantsch-Plunger et al., 2000; Toure et al., 1998), and genetic inhibition of Rac suppresses RacGAP^{Cyk-4} loss of function alleles (Canman et al., 2008; D'Avino et al., 2004). This led to a model where Rac inhibits CR closure and RacGAP^{Cyk-4} is needed to inactivate Rac at the cell equator to allow CR constriction (Canman et al., 2008; D'Avino et al., 2004; Zhuravlev et al., 2017) . On the other hand, other groups propose a role of RacGAP in the activation of Rho. Studies in *Xenopus* suggest that MgcRacGAP acts as RhoGAP to spatially constrain active Rho to a narrow equatorial zone. Expression of mutants lacking the GAP domain or harboring point mutations that inhibit the GAP activity in *Xenopu*s embryos caused an accumulation of RhoA in ectopic regions along the cortex and an increase in failure of cytokinesis (Miller and Bement, 2009). In this model, MgcRacGAP GAP activity would function throughout cytokinesis to balance the RhoGEF ^{ECT2} GEF activity of and prevent the spread of active RhoA along the cell cortex. In an alternative model specific to *C.elegans*, it was proposed that the main function of the GAP domain of RacGAP^{CYK-4} is to activate Rho non-canonically by promoting its activation by the RhoGEF ^{ECT2} (Loria et al., 2012; Zhang and Glotzer, 2015). An interaction between the GEF domain of ECT2 and the GAP domain of RacGAP^{CYK-4} has been reported (Zhang and Glotzer, 2015), but the mechanism by which this interaction would lead to the activation of Rho remains to be elucidated. The GAP domain could facilitate the relief of self-inhibition of RhoGEF^{ECT2} and participate in a ternary complex with RhoA to fully activate its GTPase activity.

In addition to its roles in the onset of cytokinesis, Tum has also been reported to act later during cytokinesis. In fact its human ortholog, MgcRacGAP, associates with the plasma membrane through its C1 domain, and this interaction is required for anchoring the plasma membrane to the MB/MR (Lekomtsev et al., 2012). Finally, studies in *Drosophila* reported direct interaction between Tum and Anillin *in vitro* and *in situ* (D'Avino et al., 2008; Gregory et al., 2008). Although the role of this interaction during cytokinesis remains unknown, it

highlights another potential role for Tum as a link between the CS and the CR.

To better characterize the roles of RacGAP^{Tum} during cytokinesis, and to shed light on the significance of the reported Tum-Anillin interaction, we have undertaken a structure/function analysis of Tum in *Drosophila* S2 cells.

6.3 RESULTS

6.3.1 Tum is required for cytokinesis

In order to track Tum localization in dividing S2 cells, we generated a stable cell line co-expressing full-length Tum (Fig. 1A) fused to GFP (Tum-GFP) along with mCherry-tubulin. Time-lapse spinning disc confocal microscopy revealed that Tum-GFP accumulated in the nucleus until nuclear envelope breakdown (data not shown) and localized weakly throughout the cortex at metaphase (Fig. 1B, t:-00:05, arrow). Upon anaphase onset, Tum-GFP strongly accumulated on the spindle midzone and became enriched at the equatorial cortex (Fig. 1B, t:00:02, arrow). Both cortical and CS pools were maintained as the CR constricted, although it became difficult to distinguish between them at the end of furrowing. Later, Tum-GFP accumulated at MB and MR structures and was retained in the MR-remnant even after abscission (Fig. 1B', arrow)

Several studies reported that Tum and its orthologs are required for furrow formation and ingression (Bastos et al., 2012; Loria et al., 2012; Miller and Bement, 2009; Mishima et al., 2002; Somers and Saint, 2003; Zavortink et al., 2005; Zhang and Glotzer,). To better characterize its the role during cytokinesis, we revisited Tum depletion phenotypes in *Drosophila* S2 cells expressing GFP-tubulin. In control cells (LacI dsRNA), a central spindle formed at the onset of anaphase, and cells completed furrowing 8-10 min after anaphase onset (Fig. 1C). From this time MB/MR formation can clearly be seen as a gap in the GFP-tubulin signal at the center of the intercellular bridge (Fig. 1B, t:00:20, arrow) and 92 % of the cells succeeded cytokinesis (N=3, n>75, Fig. 1F). Any of three long dsRNAs targeting different regions of the Tum mRNA (Fig. 1A) resulted in penetrant cytokinesis failure phenotypes after 3 days of incubation (Fig. 1F). In cells incubated with dsRNA1 or dsRNA2, which target distinct coding regions of the Tum mRNA, cells elongated slightly at anaphase onset, but

failed to form a central spindle (Fig. 1C) or initiate furrowing and the microtubules rapidly collapsed (Fig. 1C, t:00:08), resulting in cytokinesis failure and a terminal spherical binucleate cell phenotype 25±6 min after anaphase onset in >80 % of the cells that attempted division (Fig. 1D and 1F, red circles). A slightly weaker phenotype was observed with the dsRNA3 that targeted the 3'UTR. Although 75% of these cells failed cytokinesis, 50% of them were able to initiate furrowing and constrict slightly (Fig. 1E, 00:16) before regression, thereby delaying the terminal spherical binucleate cell phenotype (Fig. 1E and 1F, blue circles). This weaker phenotype is most likely due to a less complete depletion of Tum, as is commonly observed with dsRNAs that target 3'UTRs. Nevertheless, the results confirm that Tum is required for the early events of central spindle formation and furrow initiation in *Drosophila* S2 cells.

6.3.2 Structure /function analysis of Tum reveals multiple contributing activities

Although Tum depletion caused failure of cytokinesis at an early step, this does not preclude important roles for Tum at later stages. To address this issue and dissect the spatiotemporal requirements for Tum and its different conserved domains during cytokinesis, we developed an experimental system in *Drosophila* S2 cells that allows both genetic manipulation and real-time visualization throughout the successive stages of cytokinesis. We generated GFP-tagged truncation mutants of Tum that were rendered resistant to Tum dsRNA1 by inclusion of synonymous nucleotide changes in the targeted region (Fig. 2A). We then generated stable cell lines that inducibly express these constructs (under the control of the copper-inducible *metallothionein* promoter) and constitutively express mCherry-Tubulin (*act05C* promoter). This allowed for simultaneous depletion of endogenous Tum, and exogenous expression of Tum mutants, whose abilities to rescue cytokinesis progression could then be monitored by live microscopy.

In cells depleted of endogenous Tum using dsRNA1, full-length RNAi-resistant Tum-GFP (Tum-Res-GFP) localized identically to non-resistant Tum-GFP (compare Fig. 1B to Fig. 2B). While cells expressing mCherry-tubulin alone rampantly failed cytokinesis following 3-day incubation with Tum dsRNA1 (Fig. 1C,), copper-induced expression of Tum-R-GFP fully rescued the phenotype as 92% of the cells (N=3, n> 75 cells) furrowed with

normal kinetics and completed abscission (Fig. 2A and 2E). These results demonstrate that the GFP-tagged dsRNA-resistant form of Tum is fully functional and validates our experimental system for the structure/function analysis of Tum.

6.3.3 The N-terminus of Tum is necessary and sufficient for its recruitment to the central spindle, but is not sufficient to rescue furrowing.

Tum binds kinesin-6^{Pavarotti} to form the centralspindlin complex, and in turn recruits RhoGEF^{Pebble} to the cortex to activate Rho1. The kinesin-6^{Pavarotti}-interacting and RhoGEF^{Pebble}-interacting domains of Tum have been mapped to amino acids 1-65 and 66-103, respectively (Somers and saint, 2003; Tao et al., 2016). Because the molecular details of furrow initiation remain unclear, we wished to test whether or not a Tum mutant that encompasses only these regions (Tum$^{1-111}$) would be sufficient to localize to the cell equator, to activate Rho1 and to initiate furrowing. In the presence of endogenous Tum, Tum$^{1-111}$-R-GFP localized like full-length Tum throughout cytokinesis (Fig. S1-A). In cells where endogenous Tum was depleted using dsRNA1, Tum$^{1-111}$-R-GFP localized to the cortex in metaphase and became enriched at the spindle midzone during early anaphase, similar to Tum-GFP. However, as anaphase progressed, severe defects in the organization of the CS became apparent as the microtubules displayed compaction defects and rapidly collapsed (Fig 2C). Furrowing also failed to initiate in 85±6% (N=3, n> 75 cells) of the cells, leading to a terminal spherical binucleate cell phenotype 27±8 min after anaphase onset (Fig. 2C, quantified in 2E).

A reciprocal construct lacking the N-terminus, Tum$^{\Delta 1-111}$-GFP, was uniformly cytoplasmic and showed no evidence of recruitment to any structure at any stage of cytokinesis, whether in the presence or absence of Tum dsRNA1 (Fig. 2D, Fig. S1B). In cells depleted of endogenous Tum, 90±3% (N=3, n> 75 cells) of division attempts failed cytokinesis again resulting in a terminal binucleate phenotype within 30 min (35±12min) of anaphase onset (Fig. 2E). We conclude that the N terminal 111 amino acid residues of Tum, which harbour the kinesin-6^{Pavarotti}-interacting and RhoGEF^{Pebble}-interacting domains, are necessary and sufficient for the equatorial localization of Tum during cytokinesis; however, they are not sufficient for furrow initiation. Similarly, residues 112-625 are required for furrowing but are insufficient for localization.

6.3.4 The GAP activity of Tum is required for furrowing and maturation of the midbody

The C-terminus of CYK4/Tum orthologs contains a GAP domain that numerous studies in different systems have implicated in furrowing, either directly or indirectly through down-regulating adhesion complexes (Bastos et al., 2012; Loria et al., 2012; Miller and bement, 2009; Zavortink et al., 2005; Zhang and Glotzer, 2015). We wished to test the requirement for the Tum GAP domain in S2 cells, which are poorly adherent. We first examined a mutant lacking the C-terminus including the entire GAP domain, Tum^{1-378}-R-GFP. In presence of endogenous Tum, Tum^{1-378}-R-GFP localized like the full-length protein throughout cytokinesis (Fig. S1C). Following incubation with Tum dsRNA1, 88% of cells expressing Tum^{1-378}-R-GFP failed in their attempts at cytokinesis, and exhibited one of two main phenotypes. In 50% of the division attempts (N=3, n> 75 cells), Tum^{1-378}-R-GFP resembled Tum^{1-111}-R-GFP: it localized weakly at the cortex in metaphase, became enriched at the CS during early anaphase before MTs rapidly collapsed, furrows failed to initiate and a terminal binucleate phenotype resulted 22±06 min (mean±DS, N=3, n> 75 cells) after anaphase onset (Fig 3A). However, in 38% of scored division attempts, Tum^{1-378}-R-GFP was able to sustain some compaction of CS MTs and promote partial ingression of furrows that persisted until up to 20 min after anaphase. However, these furrows ultimately regressed without evidence of the gap in Tubulin fluorescence characteristic of MB/MR formation, and giving rise to a terminal binucleate phenotype 51±15 min after anaphase onset (Fig. 3B, Fig. 3E). We conclude that the C-terminus of Tum, which contains the GAP domain, is required for complete ingression of the furrow, even in poorly adherent S2 cells. The results also suggest that residues 112-378 confer some furrow initiating activity to the Tum N-terminus.

In order to discriminate between the requirement of the GAP domain and the GAP activity during cytokinesis, we generated a GAP dead mutant; $Tum^{\Delta YRL}$ which contains a targeted deletion of the catalytic arginine and one residue on either side ($Tum^{\Delta 416-418}$). This mutant has previously been tested in *Drosophila* embryos (Zavortnik et al., 2008) and analogous deletions in α-ChimerinGAP and Cdc42GAP have been shown to eliminate GAP activity while maintaining GTPase binding *in vitro* (Ahmed et al., 2004; Leonard et al, 1998). Following 3 days of Tum dsRNA1 treatment, $Tum^{\Delta YRL}$-R-GFP behaved similarly to Tum1-378-R-GFP although the former was more efficient at supporting

furrowing as 55% of dividing cells managed to ingress a cleavage furrow (Fig. 3C,D, Fig. 3E). Once again, however, even the cells that furrowed failed to form stable MB/MR and displayed a terminal binucleate phenotype 47min±7 min after anaphase (N=3, n> 75 cells). Taken together, these data demonstrate that, in *Drosophila* S2 cells, Tum's GAP activity is neither absolutely required, nor absolutely dispensable for furrowing and therefore it likely contributes to furrowing. However, GAP activity is clearly required for a faithful CR-to-MR transition.

6.3.5 The C1 domain of Tum anchors the MB/MR to the plasma membrane.

Given that Tum^{1-378} partially rescued furrowing, when compared to Tum^{1-111}, we sought to test whether the central region of Tum and/or its C1 domain also contributed to furrowing. C1 domains are involved in the recruitment of proteins to the membrane, and could link the CS to the membrane to stabilize ingressing furrows. To test this hypothesis, we generated two mutants compromising the C1 domain; a deletion mutant $Tum^{\Delta C1}$ ($Tum^{\Delta 320-366}$) and a point mutant of a conserved surface lysine in the C1 domain; Tum^{K324L}. $Tum^{\Delta C1}$-R-GFP localized to the cortex in metaphase and became enriched at the CS in anaphase. Remarkably, cells furrowed with normal kinetics and the CR closed fully within 10-15 min (Fig. 4A, t=00:15), before transitioning to stable MR structures (Fig. 4A 00:30). However, these MR-like structures failed to anchor the plasma membrane, which regressed around 50 min after anaphase onset in 70±8% (N=3, n> 75 cells) of division attempts, resulting in binucleate cells with persistent internal MR-like structures (Fig. 4A 00:40, Fig. 4C). Tum^{K324L} behaved in a similar fashion to $Tum^{\Delta C1}$ (Fig. 4B,C) although the former was more effective at supporting successful cytokinesis. In fact, after the usual 3 days incubation with Tum dsRNA1, expression of Tum^{K324L} fully rescued cytokinesis (Data not shown). It was only upon a prolonged 7 day RNAi schedule that 45 % of division attempts failed cytokinesis, again via late regression of the plasma membrane (Fig. 4B, C). Taken together these data show that the C1 domain of Tum is dispensable for furrowing but required for maintaining the anchoring of the MB\MR to the membrane at later stages of cytokinesis.

6.3.6 The central region of Tum is required for furrowing and MB/MR formation

Given that Tum$^{1-378}$ was more effective at promoting furrowing than Tum$^{1-111}$, and that the C1 domain (residues 320- 366) was dispensable for furrowing, we hypothesized that residues 112-319 (hereafter referred to as the central region) might contribute to furrowing. To test for putative activities within this central region, we first generated a cell line expressing Tum$^{112-319}$-GFP. This construct was nuclear-localized in interphase (not shown), uniformly cytoplasmic during metaphase and showed no evidence of localization to microtubules or the cortex at any stage of cytokinesis, whether in the presence of endogenous Tum (Fig. S1H), or following Tum RNAi (Fig. 5A). In cells depleted of endogenous Tum, 95±5% (N=3, n> 75 cells) of the cells expressing Tum$^{112-319}$-GFP rapidly failed cytokinesis, displaying the terminal binucleate phenotype 20±6 min after anaphase onset. Similar to cells depleted of all sources of Tum, anaphase microtubules were highly disorganized and rapidly collapsed and furrows failed to initiate (Fig. 5A,D). Meanwhile, Tum$^{112-319}$-GFP promptly returned to the nuclei as their envelopes reformed. Similar results were also observed in cells expressing Tum$^{112-378}$-GFP, comprising the central region together with the C1 domain (data not shown). Thus the Tum central region is not sufficient for equatorial localization during cytokinesis.

We next tested the requirement for the central region of Tum by generating a dsRNA-resistant Tum$^{\Delta 112-319}$-GFP. In the presence of endogenous Tum, Tum$^{\Delta 112-319}$-GFP localized similarly to the full-length Tum-GFP (Fig. S1I). However, upon depletion of endogenous Tum, Tum$^{\Delta 112-319}$-GFP localized unevenly to puncta during metaphase (Fig. 5B t:-00:04) before concentrating at the spindle midzone after anaphase onset (Fig. 5B t:00:02-00:04). Although the CS subsequently compacted, furrows failed to initiate and 90% of dividing cells (N=3, n> 75 cells) failed cytokinesis, displaying the terminal binucleate phenotype 30±8 min after anaphase onset (Fig. 5B-D). These data indicate that the central region of Tum is required for furrowing.

Interestingly, this central region contains a putative Anillin binding site that was identified independently by two groups (D'Avino et al., 2008, Gregory et al., 2008), one of which mapped the interaction to residues 245-311 using a yeast two-hybrid assay (Gregory et al., 2008). However, the importance of the interaction has never been tested. Clustal

alignments between *C. elegans*, *Drosophila* and human Tum orthologs revealed poor sequence conservation within this region (Fig. S2A). To probe the function of this region, we made two smaller deletion constructs each lacking 50 amino acids within this region: Tum$^{\Delta 236\text{-}285}$-GFP and Tum$^{\Delta 286\text{-}319}$-GFP. In the presence of endogenous Tum, both mutants localized in a similar manner to full-length Tum-GFP and cells successfully completed cytokinesis (Fig. S1J, K). Interestingly, Tum$^{\Delta 236\text{-}285}$-GFP and Tum$^{\Delta 286\text{-}319}$-GFP were both able to support successful cytokinesis following a 3-days incubation with Tum dsRNA1, unlike cells expressing Tum$^{\Delta 112\text{-}319}$-GFP, which lacked the entire central region and exhibited rampant failure at this time. However, extending the dsRNA treatment to 7 days caused 60% of cells expressing Tum$^{\Delta 236\text{-}285}$-GFP or Tum$^{\Delta 286\text{-}319}$-GFP to fail in their attempts at cytokinesis, unlike wild-type Tum-GFP, which rescued (Fig. S2B). Both Tum$^{\Delta 236\text{-}285}$-GFP (Fig. S2C) and Tum$^{\Delta 286\text{-}319}$-GFP (Fig. 5C,E,) concentrated at the spindle midzone throughout cytokinesis; however, the cortical pool observed with full-length Tum-GFP (Fig. 2A) was not detected at any point (Fig. 5C, E,. Nevertheless, cells furrowed within 15±4 min after anaphase onset but no maturation of the MB occurred (Fig. S3C, arrow) and the closed CR failed to transition to stable MR and collapsed, resulting in cytokinesis failures 45±10 min after anaphase (Fig. 5C, D). Taken together, these data suggest that the entire central region of Tum is required for furrowing while the reported Anillin binding domain is more specifically required for MB/MR ring formation.

6.3.7 The Anillin binding domain targets Tum to the cortex

Since Tum$^{\Delta 112\text{-}319}$ and the mutants with a defective Anillin binding region (Tum$^{\Delta 236\text{-}285}$-GFP and Tum$^{\Delta 286\text{-}319}$-GFP) failed to localize to the cortex, we wondered whether the Anillin–Tum interaction mediated cortical recruitment of Tum, which in turn would be required for MB/MR maturation. To scrutinize the localization of Tum and its recruitment to the cortex in live cells, we co-expressed the different dsRNA1-resistant Tum-GFP mutants with Anillin-mCherry, a prominent marker of the CR and MR. Co-expression of mCherry-Anillin did not appreciably change the behaviour of the mutants in dividing cells depleted of endogenous Tum and endogenous Anillin (data not shown).

During anaphase, the CR soon becomes juxtaposed with the CS, thus making it

difficult to distinguish any putative cortical pools of Tum from the very prominent pool of Tum that localizes to the CS via residues 1-111. As an alternative approach to examining cortical Tum, cells were pre-treated with the actin monomer-stabilizing drug LatrunculinA (LatA). In the presence of LatA, F-actin depolymerizes and the CR cannot form. Nevertheless, many cortical CR components are still recruited to the equatorial membrane, which remains distant from the CS. Indeed, our prior work revealed that, in LatA, Anillin assembles linear filamentous structures at the equatorial plasma membrane that also contain Rho1, myosin II and septins (Hickson and O'Farrell, 2008). Moreover, these linear structures form in association with astral microtubules directed toward the cell equator. Thus, we treated cells in metaphase with 1 µg/ml LatA and monitored formation of Anillin-mCherry-positive filamentous structures and recruitment of Tum mutants to them. Anillin-mCherry structures formed at the equator during anaphase and, similar to that reported in (D'Avino et al., 2008), Tum-FL-GFP was recruited to most of them (Fig. 6A, asterisks). Remarkably, Tum mutants that retained the central region, namely Tum^{1-378}, $Tum^{\Delta YRL}$ and $Tum^{\Delta C1}$ localized to some extent to Anillin structures (Fig. 6B-D). However, $Tum^{\Delta 112-319}$-GFP and $Tum^{\Delta 286-319}$-GFP, which lack the central region or part of the Anillin binding domain, respectively, failed to localize to the Anillin-positive structures at the plasma membrane, although strong signals persisted on the internal CS microtubules (Fig 6E-F). Thus the targeting of Tum to the equatorial plasma membrane, at least in the absence of F-actin, depends on its central region and more specifically on sequences previously shown to bind
Anillin.

6.3.8 Cortical retention of Tum during the CR-to-MR transition depends on Anillin.

To further test whether Anillin is required for Tum recruitment to the equatorial cortex, we analyzed the localization of Tum-GFP after co-depletion of endogenous Tum and Anillin. Depletion of Anillin did not affect the cortical pool of Tum-FL-GFP in metaphase and early anaphase (Fig. 7A, arrows. 13/15 cells that failed cytokinesis analyzed in high res had a cortical pool in metaphase). However, as furrows closed, Tum-GFP concentrated on the CS microtubules and failed to localize to the cortex. (Fig. 7A, compare with Fig.1B. Notice the bleb in Fig. 7A T=00:12 devoid of Tum). Cells exhibited slowed furrowing and displayed

defects in MR and MB maturation as expected after Anillin depletion (no tubulin gap was formed Fig. 7A, t:00:12-00:20). Oscillations of the compacted microtubules were also observed at the end of furrowing, again as expected upon Anillin depletion (Hickson & O'Farrell, 2008; Kechad et al., 2012). It is interesting to point out that the behaviour of Tum-FL-GFP in Anillin depleted cells phenocopies that of Tum mutants lacking the Anillin binding domain in the presence of Anillin (Fig. 5C). This supports the idea that Anillin is involved in the recruitment and/ or maintenance of Tum at the equatorial cortex.

6.3.9 Tum and Anillin act synergistically during furrow formation

We next tested the abilities of the different Tum mutants to promote furrowing after co-depletion of endogenous Tum and Anillin. Remarkably, regardless of the Tum mutant being expressed, Anillin and Tum co-depletion caused rapid cytokinesis failures before furrow initiation. Even mutants that fully supported furrowing in the presence of endogenous Anillin like $Tum^{\Delta C1}$, Tum^{K324L}, $Tum^{\Delta 235-285}$, $Tum^{\Delta 286-319}$ and to some extent $Tum^{\Delta YRL}$ failed to initiate furrowing in this context. All mutants localized to the CS but no cortical localization was detected either in metaphase or anaphase. Microtubules were disorganized, failed to compact, and rapidly collapsed resulting in penetrant cytokinesis failure within 30 min after anaphase onset (Fig. 7B,C).

The best characterized role for Tum in furrow initiation is through activation of Rho and Anillin has been proposed to stabilize active Rho at the equatorial cortex (Piekny et al, 2008). It is therefore reasonable to hypothesize that Anillin acts in concert with Tum to promote sustained activation of the Rho pathway. To further test this possibility, we analyzed the localization of the regulatory light chain of myosin II, Spaghetti Squash ($myosin^{Sqh}$), as an independent reporter of Rho activation, following single or double depletions of Tum and Anillin. In control cells (LacI dsRNA), $myosin^{Sqh}$-GFP was robustly recruited to the cell cortex during anaphase and was maintained in the CR and MR throughout cytokinesis (Fig. 8A). Depletion of the $RhoGEF^{Pebble}$ completely abrogated this recruitment, presumably by completely blocking Rho activation (Fig. 8B). Depletion of Anillin did not prevent $myosin^{Sqh}$ recruitment, although the $myosin^{Sqh}$-positive cortex was broader than in control cells (Fig. 8C), in accordance with previous studies (Hickson & O'Farrell, 2008; Kechad et al., 2012). Tum

depletion greatly reduced the accumulation of myosin^{Sqh} at the equatorial cortex; nonetheless, a transient recruitment was reproducibly detected at anaphase onset (Fig. 8D), suggesting the presence of a Tum-independent pool of active Rho at the cortex. Remarkably, co-depletion of Anillin and Tum phenocopied RhoGEF^{Pebble} depletion in that it attenuated all myosin^{Sqh} recrutment to the cortex (Fig. 8B,E). Collectively, these data suggest that Tum and Anillin act synergistically during furrow formation.

6.4 DISCUSSION

The relationship between the central spindle and the contractile ring has been established long ago by pioneer micromanipulation and functional studies in different experimental systems (Alsop and Zhang, 2004; D'Avino et al., 2005; Rappaport and Ebstein, 1965). Indeed, it is clear that the mitotic spindle dictates the formation and positioning of the cleavage furrow and that these two structures are interdependent throughout cytokinesis, although it remains poorly understood how. Our previous work in *Drosophila* S2 cells established the scaffolding protein Anillin as a key regulator for the stability of the CR, formation of the MR and anchoring to the plasma membrane (El-Amine et al., 2013; Kechad et al., 2012). Given that Tum orthologs are required for both central spindle integrity and cytokinetic furrow formation (Somers and Saint, 2003), and that Tum can interact with Anillin (D'Avino et al., 2008; Gregory et al., 2008), we postulated that Tum might be centrally involved in the maturation of the midbody and associated MR in *Drosophila* S2 cells. We therefore undertook a live-cell, structure-function analysis of Tum in this model system.

The best-characterized role for Tum orthologs in cytokinesis is thought to be the centralspindlin-RhoGEF$^{Ect2/Pebble}$ pathway. The N-termini of Tum orthologs are required for this function as they mediate dimerization and binding to kinesin-6 dimers to form the tetrameric centralspindlin complex (Mishima et al, 2002; Somers and Saint, 2003; Pavicic-Kaltenbrunner et al., 2007). For *Drosophila* Tum, this involves residues 1-65, which are sufficient to activate the kinesin-6^{Pavarotti} (Tao et al., 2016). Tum also recruits and activates the RhoGEF^{Pebble} through an adjacent binding domain that comprises residues 65-104 (Somers and Saint, 2003) an activity that is again conserved (Nishimura and Yonemura, 2006; Yuce et al., 2005), and that can explain the requirement for Tum in Rho activation and furrow initiation. However, it had

never been tested whether these sequences were sufficient to drive furrow formation. We performed such a test and found that although $Tum^{1\text{-}111}$ is necessary and sufficient for localization to the central-spindle, it is not sufficient to promote furrow formation, even though it contains the Pebble interaction domain.

Our results further show that both the central region and the GAP activity of Tum are required for furrowing. That the GAP activity is required is in agreement with previously published work in *Drosophila* embryos, where $Tum^{\Delta YRL}$ also failed to rescue cytokinesis in ectoderm cells (Zavortink et al., 2005). Analogous GAP-dead versions of Tum orthologs also fail to support cytokinesis in *Xenopus*, *C. elegans* and mammalian cells (Bastos et al., 2012; Canman et al., 2008; Loria et al., 2012; Miller and Bement, 2009; Tse et al., 1012, Zhang et al., 2015). Although both $Tum^{\Delta YRL}$ and $Tum^{\Delta GAP}$ mutants localized in a similar fashion, the latter was less able to support cytokinesis; as 50% of cells failed cytokinesis before furrow initiation compared to only 35% of cells expressing $Tum^{\Delta YRL}$. The difference in phenotypic penetrance between these two mutants could be due to many factors. First, it is possible that the different deletions do not cause the same level of inactivation of the GAP activity. It should be noted that the GAP activity of $Tum^{\Delta YRL}$ was not measured. It is assumed that the resulting protein is inactive because it lacks the catalytic arginine and adjacent residues and an analogous deletion blocked the GAP activity of α-ChimerinGAP (Ahmed et al., 1994; Leonard et al., 1998), but this remains to be tested for Tum. Another possibility is that deletion of Tum's C-terminus destabilizes other functions of the protein in addition to its GAP activity. Nevertheless, the fact that the specific and directed perturbation of the GAP activity allowed more cells to initiate furrowing but still caused them to fail to form a stable MB/MR suggests that there is an additional requirement for Tum's GAP activity at the transition from the CR to MR.

That being said, even though the GAP activity of Tum was important for furrow formation and closure, it was not sufficient for furrowing. Indeed, deletion of the central region of Tum caused more severe defects than deletion of the GAP domain. All cells expressing TumΔCD as their sole source of Tum failed to even initiate furrowing, the spindle appeared disconnected from the cortex, and the cortical localization of TumΔCD became punctate and disorganized. Although the possibility that deletion of the central region affected

the folding of the protein cannot be ruled out,. We are currently fine mapping this domain to better understand its role during furrowing. Collectively, these findings suggest that both the GAP activity and the central domain of Tum are required for furrowing.

The Anillin binding region of Tum is required for Tum's retention at the contractile ring and maturation of the MB/MR.

Two independent studies reported an interaction between Tum and Anillin in *Drosophila*, and proposed a model where this interaction would serve as a connection between the central spindle and the CR at the onset of furrowing (Gregory et al., 2008; D'avino et al., 2008). Here we tested Tum mutants with compromised Anillin binding domains. Although our attempts to purify soluble recombinant Tum to biochemically test binding to Anillin have thus far failed, several observations from our cell biological analysis provide support for the existence of such an interaction. First, mutants lacking portions of the Anillin binding region were restricted to the spindle midzone and strikingly excluded from the (Anillin-rich) cortex. Secondly, these same mutants lost the normal ability of Tum to co-localize with Anillin in the prominent septin-dependent cortical structures that form during anaphase following LatA treatment that we and others have previously described (Hickson and O'Farrell, 2008; D'Avino et al., 2008). Finally, Anillin depletion caused Tum-FL to behave in a similar fashion to TumΔ235-286 and TumΔ286-319, and only exhibit a transient cortical localization at anaphase onset, rather than a sustained cortical localization at later stages. Collectively, these observations suggest that Anillin recruits/retains a cortical pool of Tum and that this is important for maturation and stabilization of the MB/MR. Interestingly, loss of the Anillin–dependent cortical pool of Tum, either by deletion of Anillin-binding sequences or by depletion of Anillin, did not prevent furrow initiation. Rather, cells under these conditions failed to form a MR/MB and the furrow oscillated before collapsing. Taken together, these results are consistent with a model in which Anillin mediates the recruitment/retention of Tum at the cortex during furrowing and that this complex is important to coordinate the transition of the CR to MR with the maturation of the CS to a MB. Later both Anillin and Tum are independently required to anchor the MR to the plasma membrane, the latter via its C1 domain (Kechad et al., 2012; Lekomtsev et al., 2012; this study).

Synergy between Tum and Anillin during furrow initiation

One of the most interesting results in this study is that Tum mutants that can support furrowing in the presence of endogenous Anillin, no longer do when Anillin is depleted. Since Anillin depletion in the presence of endogenous Tum does not prevent furrowing, this clearly indicates synergy between Anillin and Tum during furrow initiation. Accordingly, cells singly depleted of Anillin or Tum retained some level of Rho activation, as evidenced by myosin-GFP recruitment. However, co-depletion of Anillin and Tum phenocopied depletion of $RhoGEF^{Pebble}$ and completely blocked myosin recruitment. This is not the first time that a redundancy between Anillin and a component of the centralspindlin complex is reported. Indeed, in human cells, Anillin is not necessary for the recruitment of actin or myosin at the equatorial cortex. However, it becomes crucial for their enrichment when the central spindle is disturbed by the depletion of kinesin-6/MKLP1 (Piekny and Glotzer, 2008; van Oostende Triplet et al., 2014). Similarly, in *C. elegans* zygotes, the canonical Anillin ortholog, ANI-1, which is normally dispensable for cytokinesis of this cell division, becomes necessary for complete ingression of the furrow when kinesin-6/ZEN-4 is depleted (Werner et al., 2007). Together, these results suggest that Anillin and centralspindlin operate redundantly in the equatorial specification or activation of Rho. Interestingly, in these contexts, the stabilization of the astral microtubules, in cells depleted of Anillin, restores the localization of Myosin to the equatorial cortex. These observations gave rise to a model that proposes that Anillin modulates the cortex through the astral pathway. In human cells, Anillin was shown to interact with the astral microtubules adjacent to the equatorial cortex and this interaction prevents its recruitment outside the equatorial cortex (van Oostende Triplet et al., 2014). In doing so, Anillin could refine the localization of cortical proteins near the equatorial cortex, thus allowing the activation of Rho and the recruitment of CR components to a discrete zone within the equatorial cortex. In addition to regulating the localization of equatorial proteins, Anillin also appears to be required for the localization of polar proteins. Indeed, NuMa and Arp1 proteins, which normally localize to the polar cortex where they regulate the position of the mitotic spindle, are relocated around the cellular cortex when Anillin is depleted (van Oostende Triplet et al., 2014). Thus, in this model, centralspindlin promotes the accumulation of RhoA at the equator while the association of Anillin with the astral microtubules restricts

the localization of RhoA out of the equator and contributes to the definition of polar and equatorial cortex (Lewellyn et al., 2010; van Oostende Triplet et al., 2014)

Interestingly, in *Drosophila* cells, we do not observe Anillin or any of the truncation mutants used in our studies directly on microtubules. However, in cells treated with Latrunculin A, Anillin produces filamentous structures at the plasma membrane that are often associated with the plus-ends of astral microtubules at the equatorial cortex and that also contain Tum (D'Avino et al., 2008; Hickson and O'Farrell, 2008b and this study). Anillin and Tum likely share many partners at the interface between the cortex and microtubules. Our results lead to a working model (Fig. 9) in which Tum organizes the signalling complexes responsible for the establishment of the cleavage furrow, while Anillin acts at the equatorial cortex as a major scaffolding protein that concentrates signals from different components of the machinery to maintain a robust cleavage furrow. The central spindle acts as sink for centralspindlin-RhoGEF^{Pebble} signalling complexes that allows for their controlled release towards the equatorial cortex where it mediates the activation of Rho1. In turn, RhoA triggers the recruitment of Anillin to the equatorial cortex. Thus, at the level of the cortex, one could imagine a complex grouping Tum, RhoGEF^{Pebble}, Rho1, and Anillin, which could serve to reinforce the GEF activity of RhoGEF^{Pebble} and /or limit the GAP activity of Tum and thereby increase Rho-GTP at the equatorial cortex. In human cells, Anillin does not interact with MgcRacGAP but has been shown to bind direcly to RhoGEF^{ECT2} (Frenette et al., 2012). An Anillin-RhoGEF^{ECT2}-RhoA complex is formed at the cortex and postulated to link the mitotic spindle to the cortex during cytokinesis. In *Drosophila*, Anillin does not interact directly with RhoGEF^{Pebble} but it does with Tum. These permutations in interacting partners would make it possible to form complexes grouping RhoGEF $^{ECT2/\ Pebble}$, RhoA, Tum and Anillin in order to maintain a discrete zone of active RhoA at the equator in addition to linking the spindle to the cortex. It is also known that at this stage, Anillin and RhoGEF^{ECT2}/^{Pebble} are independently bound to PIPs of the equatorial membrane via their respective PH domains (Goldbach et al., 2010; Logan and Mandato, 2006); and that these interactions are required for the establishment of a robust cleavage furrow and anchorage of the CR at the equator. Thus, by depleting Anillin in a context where Tum activity is partially disrupted, Rho recruitment/retention is reduced, affecting all downstream effectors necessary for CR

formation and anchorage.

In summary, this study shows that Tum acts as a key regulator throughout cytokinesis with different activities attributable to its different domains. The N-terminus of Tum mediates recruitment to the CS and is essential for all of Tum's functions. The central region of Tum is also essential for furrow initiation, whereas the C-terminal GAP activity of Tum contributes to furrow robustness and closure. Although Anillin is dispensable for furrowing, it acts synergistically with Tum during furrowing, in a manner that is consistent with previous reports of interaction between Tum and Anillin. This synergy is evident not only during furrow initiation but also at the close of furrowing where Anillin is required to retain Tum at the CR as it transitions into a more stable MR, a structure in which both Tum and Anillin are in turn required for plasma membrane anchoring (Figure 9).

6.5 ACKNOWLEDGEMENTS

We thank Drs. Alisa Piekny, Jean-Claude Labbé and all members of the Hickson lab for useful discussions. AK thanks the Fonds de Recherche Québec - Santé (FRQS) and the Dept. Pathologie et biologie cellulaire, Université de Montréal, for doctoral studentship awards. GH thanks the FRQS for research scholar awards. This work was supported by grants from the CIHR, the Cole Foundation and Canada Foundation for Innovation.

6.6 REFERENCES

Adams, R.R., A.A. Tavares, A. Salzberg, H.J. Bellen, and D.M. Glover. 1998. pavarotti encodes a kinesin-like protein required to organize the central spindle and contractile ring for cytokinesis. *Genes Dev*. 12:1483-1494.

Alsop, G.B., and D. Zhang. 2004. Microtubules continuously dictate distribution of actin filaments and positioning of cell cleavage in grasshopper spermatocytes. *J Cell Sci*. 117:1591-1602.

Basant, A., and M. Glotzer. 2017. A GAP that Divides. *F1000Res*. 6:1788.

Bastos, R.N., X. Penate, M. Bates, D. Hammond, and F.A. Barr. 2012. CYK4 inhibits Rac1-dependent PAK1 and ARHGEF7 effector pathways during cytokinesis. *J Cell Biol*. 198:865-880.

Canman, J.C., L. Lewellyn, K. Laband, S.J. Smerdon, A. Desai, B. Bowerman, and K. Oegema. 2008. Inhibition of Rac by the GAP activity of centralspindlin is essential for cytokinesis. *Science*. 322:1543-1546.

D'Avino, P., M.S. Savoian, and D.M. Glover. 2004. Mutations in sticky lead to defective organization of the contractile ring during cytokinesis and are enhanced by Rho and suppressed by Rac. *The Journal of Cell Biology*. 166:61-71.

D'Avino, P.P., M.S. Savoian, and D.M. Glover. 2005. Cleavage furrow formation and ingression during animal cytokinesis: a microtubule legacy. *J Cell Sci*. 118:1549-1558.

D'Avino, P.P., T. Takeda, L. Capalbo, W. Zhang, K.S. Lilley, E.D. Laue, and D.M. Glover. 2008. Interaction between Anillin and RacGAP50C connects the actomyosin contractile ring with spindle microtubules at the cell division site. *J Cell Sci*. 121:1151-1158.

Echard, A., G.R.X. Hickson, E. Foley, and P.H. O'Farrell. 2004. Terminal cytokinesis events uncovered after an RNAi screen. *Current biology : CB*. 14:1685-1693.

Eggert, U.S., A.A. Kiger, C. Richter, Z.E. Perlman, N. Perrimon, T.J. Mitchison, and C.M. Field. 2004. Parallel chemical genetic and genome-wide RNAi screens identify cytokinesis inhibitors and targets. *PLoS Biol*. 2:e379.

El-Amine, N., A. Kechad, S. Jananji, and G. Hickson. 2013. Opposing actions of septins and Sticky on Anillin promote the transition from contractile to midbody ring. *The Journal of Cell*

Biology. 203:487-504.

Field, C.M., and B.M. Alberts. 1995. Anillin, a contractile ring protein that cycles from the nucleus to the cell cortex. *J Cell Biol*. 131:165-178.

Field, C.M., M. Coughlin, S. Doberstein, T. Marty, and W. Sullivan. 2005. Characterization of anillin mutants reveals essential roles in septin localization and plasma membrane integrity. *Development*. 132:2849-2860.

Gai, M., P. Camera, A. Dema, F. Bianchi, G. Berto, E. Scarpa, G. Germena, and F. Cunto. 2011. Citron kinase controls abscission through RhoA and anillin. *Molecular biology of the cell*. 22:3768-3778.

Gatti, M., M.G. Giansanti, and S. Bonaccorsi. 2000. Relationships between the central spindle and the contractile ring during cytokinesis in animal cells. *Microsc Res Tech*. 49:202-208.

Glotzer, M. 2005. The molecular requirements for cytokinesis. *Science (New York, N.Y.)*. 307:1735-1739.

Goldbach, P., R. Wong, N. Beise, R. Sarpal, W.S. Trimble, and J.A. Brill. 2010. Stabilization of the actomyosin ring enables spermatocyte cytokinesis in Drosophila. *Mol Biol Cell*. 21:1482-1493.

Goldstein, A.Y., Y.N. Jan, and L. Luo. 2005. Function and regulation of Tumbleweed (RacGAP50C) in neuroblast proliferation and neuronal morphogenesis. *Proc Natl Acad Sci U S A*. 102:3834-3839.

Green, R.A., E. Paluch, and K. Oegema. 2012. Cytokinesis in animal cells. *Annual review of cell and developmental biology*. 28:29-58.

Gregory, S.L., S. Ebrahimi, J. Milverton, W.M. Jones, A. Bejsovec, and R. Saint. 2008. Cell division requires a direct link between microtubule-bound RacGAP and Anillin in the contractile ring. *Curr Biol*. 18:25-29.

Hickson, G., and P.H. O'Farrell. 2008a. Anillin: a pivotal organizer of the cytokinetic machinery. *Biochemical Society Transactions*. 36:439-441.

Hickson, G., and P.H. O'Farrell. 2008b. Rho-dependent control of anillin behavior during

cytokinesis. *The Journal of Cell Biology*. 180:285-294.

Hu, C.-K., M. Coughlin, and T.J. Mitchison. 2012. Midbody assembly and its regulation during cytokinesis. *Molecular Biology of the Cell*. 23:1024-1034.

Jananji, S., C. Risi, I.K.S. Lindamulage, L.P. Picard, R. Van Sciver, G. Laflamme, A. Albaghjati, G.R.X. Hickson, B.H. Kwok, and V.E. Galkin. 2017. Multimodal and Polymorphic Interactions between Anillin and Actin: Their Implications for Cytokinesis. *J Mol Biol*. 429:715-731.

Jantsch-Plunger, V., P. Gonczy, A. Romano, H. Schnabel, D. Hamill, R. Schnabel, A.A. Hyman, and M. Glotzer. 2000. CYK-4: A Rho family gtpase activating protein (GAP) required for central spindle formation and cytokinesis. *J Cell Biol*. 149:1391-1404.

Kechad, A., S. Jananji, Y. Ruella, and G.R. Hickson. 2012. Anillin acts as a bifunctional linker coordinating midbody ring biogenesis during cytokinesis. *Curr Biol*. 22:197-203.

Kim, H., F. Guo, S. Brahma, Y. Xing, and M.E. Burkard. 2014. Centralspindlin assembly and 2 phosphorylations on MgcRacGAP by Polo-like kinase 1 initiate Ect2 binding in early cytokinesis. *Cell Cycle*. 13:2952-2961.

Lekomtsev, S., K.C. Su, V.E. Pye, K. Blight, S. Sundaramoorthy, T. Takaki, L.M. Collinson, P. Cherepanov, N. Divecha, and M. Petronczki. 2012. Centralspindlin links the mitotic spindle to the plasma membrane during cytokinesis. *Nature*. 492:276-279.

Leonard, D.A., R. Lin, R.A. Cerione, and D. Manor. 1998. Biochemical studies of the mechanism of action of the Cdc42-GTPase-activating protein. *J Biol Chem*. 273:16210-16215.

Lewellyn, L., J. Dumont, A. Desai, and K. Oegema. 2010. Analyzing the effects of delaying aster separation on furrow formation during cytokinesis in the Caenorhabditis elegans embryo. *Mol Biol Cell*. 21:50-62.

Liu, J., G.D. Fairn, D.F. Ceccarelli, F. Sicheri, and A. Wilde. 2012. Cleavage furrow organization requires PIP(2)-mediated recruitment of anillin. *Curr Biol*. 22:64-69.

Logan, M.R., and C.A. Mandato. 2006. Regulation of the actin cytoskeleton by PIP2 in cytokinesis. *Biology of the Cell*. 98:377-388.

Loria, A., K.M. Longhini, and M. Glotzer. 2012. The RhoGAP domain of CYK-4 has an essential role

in RhoA activation. *Curr Biol*. 22:213-219.

Miller, A.L., and W.M. Bement. 2009. Regulation of cytokinesis by Rho GTPase flux. *Nat Cell Biol*. 11:71-77.

Mishima, M., S. Kaitna, and M. Glotzer. 2002. Central Spindle Assembly and Cytokinesis Require a Kinesin-like Protein/RhoGAP Complex with Microtubule Bundling Activity. *Developmental Cell*. 2:41-54.

Mullins, J.M., and J.J. Biesele. 1973. Cytokinetic activities in a human cell line: the midbody and intercellular bridge. *Tissue Cell*. 5:47-61.

Nishimura, Y., and S. Yonemura. 2006. Centralspindlin regulates ECT2 and RhoA accumulation at the equatorial cortex during cytokinesis. *J Cell Sci*. 119:104-114.

Oegema, K., M.S. Savoian, T.J. Mitchison, and C.M. Field. 2000. Functional analysis of a human homologue of the Drosophila actin binding protein anillin suggests a role in cytokinesis. *J Cell Biol*. 150:539-552.

Piekny, A.J., and M. Glotzer. 2008. Anillin is a scaffold protein that links RhoA, actin, and myosin during cytokinesis. *Curr Biol*. 18:30-36.

Pollard, T.D. 2010. Mechanics of cytokinesis in eukaryotes. *Curr Opin Cell Biol*. 22:50-56.

Powers, J., O. Bossinger, D. Rose, S. Strome, and W. Saxton. 1998. A nematode kinesin required for cleavage furrow advancement. *Curr Biol*. 8:1133-1136.

Raich, W.B., A.N. Moran, J.H. Rothman, and J. Hardin. 1998. Cytokinesis and midzone microtubule organization in Caenorhabditis elegans require the kinesin-like protein ZEN-4. *Mol Biol Cell*. 9:2037-2049.

Rappaport, R., and R.P. Ebstein. 1965. Duration of Stimulus and Latent Periods Preceding Furrow Formation in Sand Dollar Eggs. *J Exp Zool*. 158:373-382.

Somers, W.G., and R. Saint. 2003. A RhoGEF and Rho family GTPase-activating protein complex links the contractile ring to cortical microtubules at the onset of cytokinesis. *Dev Cell*. 4:29-39.

Somma, M.P., B. Fasulo, G. Cenci, E. Cundari, and M. Gatti. 2002. Molecular dissection of

cytokinesis by RNA interference in Drosophila cultured cells. *Mol Biol Cell*. 13:2448-2460.

Steigemann, P., and D.W. Gerlich. 2009. Cytokinetic abscission: cellular dynamics at the midbody. *Trends in Cell Biology*. 19:606-616.

Straight, A.F., C.M. Field, and T.J. Mitchison. 2005. Anillin Binds Nonmuscle Myosin II and Regulates the Contractile Ring. *Molecular Biology of the Cell*. 16:193-201.

Su, K.-C., T. Takaki, and M. Petronczki. 2011. Targeting of the RhoGEF Ect2 to the Equatorial Membrane Controls Cleavage Furrow Formation during Cytokinesis. *Developmental Cell*. 21:1104-1115.

Tao, L., B. Fasulo, B. Warecki, and W. Sullivan. 2016. Tum/RacGAP functions as a switch activating the Pav/kinesin-6 motor. *Nat Commun*. 7:11182.

Toure, A., O. Dorseuil, L. Morin, P. Timmons, B. Jegou, L. Reibel, and G. Gacon. 1998. MgcRacGAP, a new human GTPase-activating protein for Rac and Cdc42 similar to Drosophila rotundRacGAP gene product, is expressed in male germ cells. *J Biol Chem*. 273:6019-6023.

Tse, Y.C., A. Piekny, and M. Glotzer. 2011. Anillin promotes astral microtubule-directed cortical myosin polarization. *Mol Biol Cell*. 22:3165-3175.

van Oostende Triplet, C., M. Jaramillo Garcia, H. Haji Bik, D. Beaudet, and A. Piekny. 2014. Anillin interacts with microtubules and is part of the astral pathway that defines cortical domains. *J Cell Sci*. 127:3699-3710.

Werner, M., E. Munro, and M. Glotzer. 2007. Astral signals spatially bias cortical myosin recruitment to break symmetry and promote cytokinesis. *Curr Biol*. 17:1286-1297.

Yamada, T., M. Hikida, and T. Kurosaki. 2006. Regulation of cytokinesis by mgcRacGAP in B lymphocytes is independent of GAP activity. *Exp Cell Res*. 312:3517-3525.

Yuce, O., A. Piekny, and M. Glotzer. 2005. An ECT2-centralspindlin complex regulates the localization and function of RhoA. *J Cell Biol*. 170:571-582.

Zavortink, M., N. Contreras, T. Addy, A. Bejsovec, and R. Saint. 2005. Tum/RacGAP50C provides a critical link between anaphase microtubules and the assembly of the contractile ring in

Drosophila melanogaster. *J Cell Sci*. 118:5381-5392.

Zhang, D., and M. Glotzer. 2015. The RhoGAP activity of CYK-4/MgcRacGAP functions non-canonically by promoting RhoA activation during cytokinesis. *Elife*. 4.

Zhao, W.-m., and G. Fang. 2005. Anillin Is a Substrate of Anaphase-promoting Complex/Cyclosome (APC/C) That Controls Spatial Contractility of Myosin during Late Cytokinesis. *Journal of Biological Chemistry*. 280:33516-33524.

Zhuravlev, Y., S.M. Hirsch, S.N. Jordan, J. Dumont, M. Shirasu-Hiza, and J.C. Canman. 2017. CYK-4 regulates Rac, but not Rho, during cytokinesis. *Mol Biol Cell*. 28:1258-1270.

6.8 MATERIALS AND METHODS

Molecular biology

To generate a dsRNA-resistant allele of Tum the sequence TTGGCGTCCTTCGATGATCTGCGACGCTGCATGCAAGTGCTTACCGATGGAACTCC TGAGGAGGAGTTCCTGCGGTTCTTGCGCATGTTCGAGCAGTACCACGAAAAGTGC GCGGGCTACGCGGCCGAGACGGCCAGGATACAAAACGAGCTGGACAAGTCGTTG ACCAAAATGGGCGACCTGGAGGGCAAACTCTTTCACGCACGCCGCATCATCGACA TGGAGATCAAGGCGCGCCGCCAGGCGGAACACGAACGAGATGCCATGGAGAGCA AGATCATGGCTGTGGCAGATCTGCTGCGACACGAGCGCAAT (bp 15 -330 in Tum ORF sequence) was changed to TTaGCcTCgTTtGAcGAcCTcCGtCGaTGtAT GCAgGTcCTaACgGAcGGtACaCCaGAaGAaGAaTTtCTcCGcTTtTTaCGgATGTTtGAaCA aTAtCAtGAgAAaTGtGCaGGaTAtGCaGCaGAaACcGCgAGaATcCAgAAtGAaCTaGAtAA aTCcTTaACgAAgATGGGtGAtCTaGAaGGaAAgCTgTTcCAtGCcCGaCGaATtATtGAtAT GGAaATtAAaGCcCGaCGaCAaGCcGAgCAtGAgCGtGAcGCgATGGAaAGtAAaATtATG GCaGTa by inclusion of synonymous nucleotide changes. The resulting construct was used as a template to generate Tum deletion and point mutants by PCR by overlap extension and site directed mutagenesis using the primers described below. PCR products were then cloned into pENTR-D-TOPO (Invitrogen), Thermo Fisher Scientific, cat# k2400-20) and sequence-verified. Constructs were recombined using LR Clonase into the copper inducible expression vectors pMT-WGFP and pMT-WCherry, to generate fusions to the 5' ends of GFP and mCherry, respectively. Anillin-GFP, myosin^{Sqh}-GFP and mCherry-Tubulin were previously described (Hickson et al., 2008).

Primers list

Tum ORF F: CACC `ATG GCG CTC TCC GCA TTG GCG`

Tum ORF R: TTT CTT GTG CGC AGA TGC CGG

Tum 111 R: CAG ATT GCG CTC GTG TCG CAG

Tum112 F: CACC ATG AAC AAC GAG ACC CGC GAC

Tum 319 R: GTG GTT CCT CAT CAG TGG ACG

Tum 378 R: TGCAAAGTCCGTTACATAGCC

Tum Δ 112-319 F: GAG CGC AAT CTG GCC GTG CGG GAG GAC AAG TCC

Tum Δ 112-319 R: CTG ACT GAA GGT CAG ATT GCG CTC GTG TCG CAG

Tum Δ 236-285 F: CAA GGC GCT GAG GAG GCC ACC GCA CCG CCG CTG

Tum Δ 236-285 R: TGC GGT GGC CTC CTC AGC GCC TTG ACC CAC GTC

Tum Δ 286-319 F: CAA GGC GCT GAG GAG GCC ACC GCA CCG CCG CTG

Tum Δ 286-319 R: CTG ACT GAA GGT TTT AAG CAC CGA TCG CCG TGG

Tum ΔC1 F: ATG AGG AAC CAC GTG CCG CAA ACG GGA ACA CCG

Tum ΔC1 R: CGT TTG CGG CAC GTG GTT CCT CAT CAG TGG AGC

Tum K324L F: CAC ACC TTC AGT CAG CTG ACA TTC TTG CGT GGC

Tum K324L R: GCC ACG CAA GAA TGT CAG CTG ACT GAA GGT GTG

Cell lines and cell culture

Plasmids were transfected into *Drosophila* Schneider's S2 cells using Cellfectin II reagent (Invitrogen) or Fugene (Promega), together with pCoHygro, and stable cell lines were selected using 400 µg/ml hygromycin B (Thermo Fisher Scientific, Cat #10687-010), supplemented to the growth media for 4 weeks.

S2 cells were cultured in Schneider's *Drosophila* medium (Life Technologies/Thermo Fisher Scientific, cat#21720-001), supplemented with 10% heat-inactivated foetal calf serum (Invitrogen/Thermo Fisher Scientific, US origin cat#16140-071) and penicillin/streptomycin (Invitrogen/Thermo Fisher Scientific, cat#15140-122) and maintained under normal ambient

temperature (20-25°C) and atmospheric conditions.

RNAi experiments:

Double-stranded RNAs (dsRNAs) were designed as described (Kechad et al., 2017) and generated using Ribomax kits (Promega), following a two-step PCR amplification of template DNA, the first with gene-specific primers containing 5' 8 bp anchors (GGGCGGGT), the second with a T7 linker primer that anneals with the anchor sequence (5′[TAATACGACTCACTATAGGG]3′). Anillin dsRNAs were previously described (Kechad et al., 2012). Tum and pebble dsRNAs were generated using the following gene-specific primer sequences:

Tum dsRNA 1F: GGGCGGGTGCGCTCTCCGCATTGGCGTCC

Tum dsRNA 1R: GGGCGGGTGCCACAGCCATGATCTTGCTC

Tum dsRNA 2F: GGGCGGGTGACTTTGCACCATCTATT

Tum dsRNA 2F: GGGCGGGTTTTCTTGTGCGCAGATGCCGG

Tum 3'UTR dsRNA F: GGGCGGGTCAAGAAATAACGAGACTTTCC

Tum 3'UTR dsRNA R: GGGCGGGTTTGTTATATTCTTTTATCGT

Pebble dsRNA F: GGGCGGGTATGGAAATGGAGACCATTGAA

Pebble dsRNA R: GGGCGGGTCAGATAGTCCATCTCATTGGC

For RNAi experiments, cells were plated in 96 well dishes and incubated with ~1 µg/ml dsRNA. Live imaging was performed after 72 hours for Anillin and pebble dsRNAs, and between 3 and 7 days for Tum dsRNA, in which case cells were split and fresh dsRNA added at day 4 (see Kechad et al., 2017 for a detailed protocol). Expression of fluorescent proteins fusions under the control of the metallothionien promoter (pMT plasmids) was induced with 250 µM $CuSO_4$ at the time of dsRNA addition for rescue experiments or 12-24 h prior to the start of imaging for other experiments. 12-24 h prior to imaging or fixation, cells were transferred to 8 wells chambered coverglass dishes (Lab-tek II, Nunc, cat.

#CA43300774) or 96 well glass bottomed plates (Whatman, cat#306180-030) and imaged.

Live cell microscopy

Live cell imaging of *Drosophila* S2 cells was performed in 8-well chambered coverglass dishes (Labtek, Nunc) or 96 well glass bottomed plates (Whatman, cat#306180-030) at room temperature (20-23°C) using an Ultraview Vox spinning disc confocal system (Perkin Elmer), employing a CSU-X1 scanning unit (Yokogawa) and an Orca-R2 CCD camera (Hamamatsu) fitted to a Leica DMI6000B inverted microscope equipped with a motorized piezo-electric stage (Applied Scientific Instrumentation). Image acquisition and quantitation was performed using Volocity 5 software (Improvision/PerkinElmer). Routine and long time-course imaging was performed using Plan Apo 40x (0.85 NA) air objectives with camera binning set to 2x2, high-resolution imaging was performed using Plan Apo 63x or 100x oil immersion objectives (NA 1.4) with either 1x1 or 2x2 binning as described in the figure legends.

Latrunculin A treatment:

The actin monomer stabilizing drug Latrunculin A (EMD) was used at 1µg/ml final concentration diluted in S2 cells growth media. For live imaging, Lat A was added to the imaging dish during acquisition. For immunofluorescence, Lat A was added 30 min prior to fixation.

Image analysis

Quantitation of 4D datasets (x,y,z, time) was performed using Volocity 6 analysis. Intensity measurements of myosin-GFP (Fig. 8) were performed using the measure line profile tool in the Volocity analysis module as follows. A line of 1um thickness was drawn across the equator of a single optical section. Raw data were given by the software as mean intensity values along the line and then expressed as percentages relative to the highest value within the line for each cell. Graphs present mean % intensity ±STDEV. Images were processed for publication using Adobe Photoshop and assembled as figures using Adobe Illustrator. Movie files were exported from Volocity as QuickTime movies.

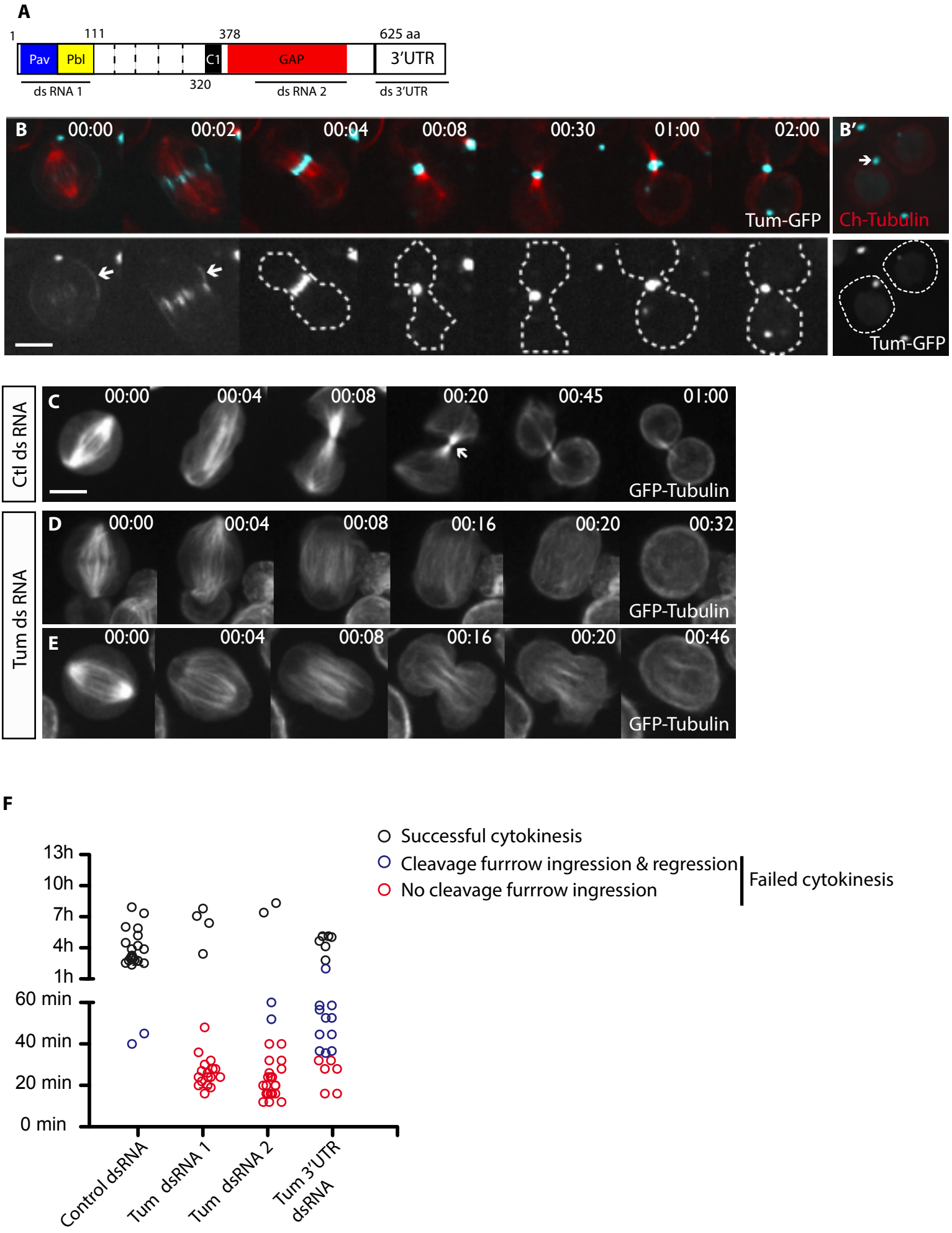
A
1
111
378
625 aa
Pav
Pbl
C1
GAP
3'UTR
ds RNA 1
320
ds RNA 2
ds 3'UTR
B
00:00
00:02
00:04
00:08
00:30
01:00
02:00
Tum-GFP
B'
Ch-Tubulin
Tum-GFP
Ctl ds RNA
C
00:00
00:04
00:08
00:20
00:45
01:00
GFP-Tubulin
Tum ds RNA
D
00:00
00:04
00:08
00:16
00:20
00:32
GFP-Tubulin
E
00:00
00:04
00:08
00:16
00:20
00:46
GFP-Tubulin
F
Time after anaphase onset
13h
10h
7h
4h
1h
60 min
40 min
20 min
0 min
Control dsRNA
Tum dsRNA 1
Tum dsRNA 2
Tum 3'UTR dsRNA
Successful cytokinesis
Cleavage furrrow ingression & regression
No cleavage furrrow ingression
Failed cytokinesis

6.9 FIGURES AND LEGENDS

Figure 6.1: Tum is required for cytokinesis

(A) Domain organization of Tum. Pav: Pavarotti binding domain, Pbl: Pebble binding domain, C1: C1 domain, GAP: GAP domain, aa: Amino acid. **(B)** Time-lapse sequence of S2 cells expressing GFP-tagged Tum. Arrows point to the cortical pool of Tum. Images at time 00:00 and 00:02 were contrasted differently to show the cortical pool of Tum **(B')** A distinct cell showing localization of Tum to the MR remnant after abscission (Arrow). **(C-E)** Time-lapse sequence of S2 cells expressing GFP-tagged Tubulin, treated with control LacI ds RNA **(C)**, Tum dsRNA1or 2 **(D)** and Tum dsRNA 3'UTR **(E)** for 3 days. Maximum intensity projections acquired using a 63X oil-immersion objective (1.4 NA), with camera binning set to 2x2 are shown, Times are h:min. Scale bars, 5 µm. **(E)** Timing of abscission or cytokinesis failure of cells expressing GFP-Tubulin treated for 3–5 days with described dsRNAs. Each circle represents a single cell. Data are from a single representative experiment out of three repeats. N=3, n= 25 cells /condition/ experiment.

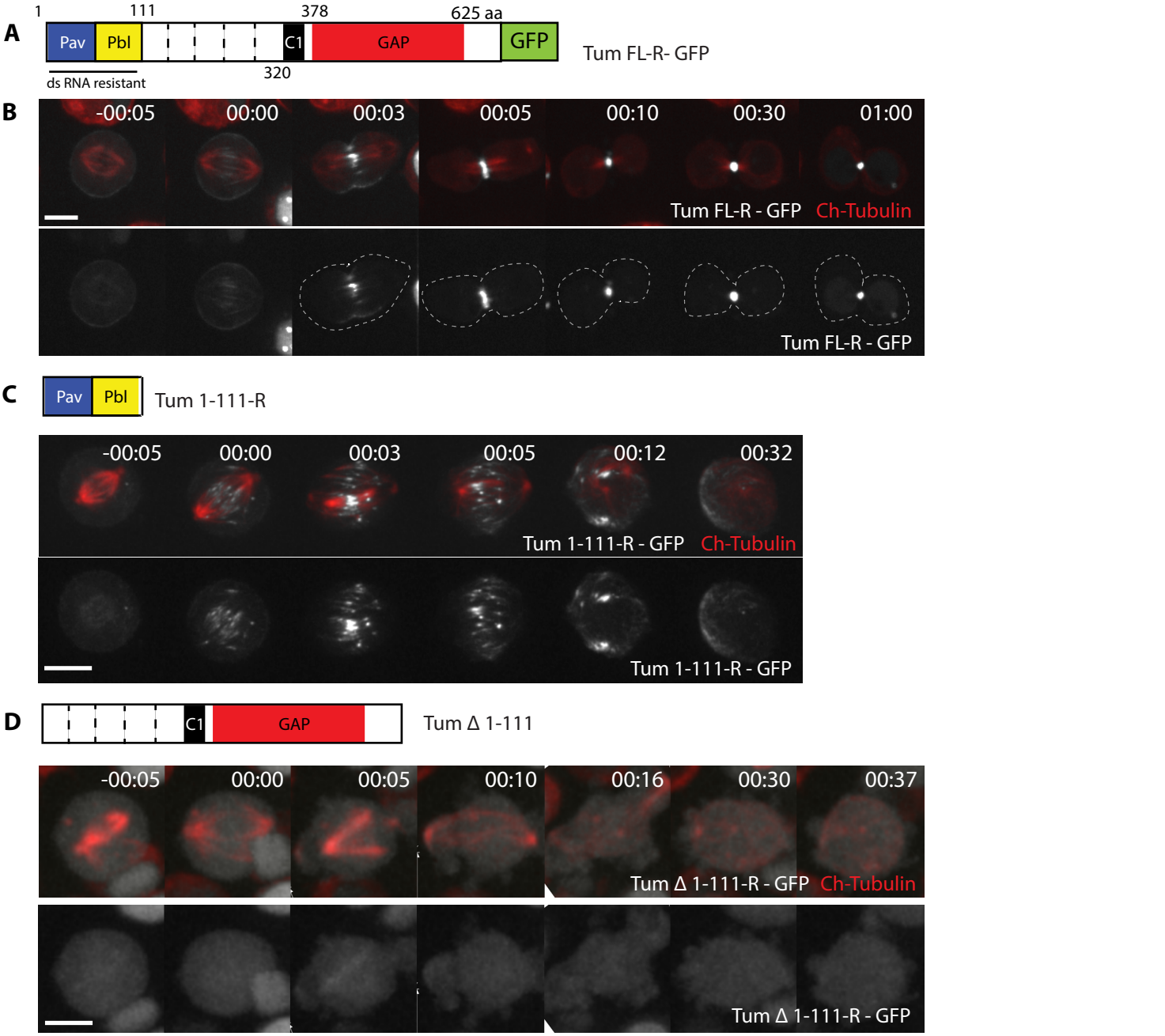
A
1
111
378
625 aa
Pav
Pbl
C1
GAP
GFP
320
ds RNA resistant
Tum FL-R- GFP
B
-00:05
00:00
00:03
00:05
00:10
00:30
01:00
Tum FL-R - GFP
Ch-Tubulin
Tum FL-R - GFP
C
Pav
Pbl
Tum 1-111-R
-00:05
00:00
00:03
00:05
00:12
00:32
Tum 1-111-R - GFP
Ch-Tubulin
Tum 1-111-R - GFP
D
C1
GAP
Tum Δ 1-111
-00:05
00:00
00:05
00:10
00:16
00:30
00:37
Tum Δ 1-111-R - GFP
Ch-Tubulin
Tum Δ 1-111-R - GFP
E
Successful cytokinesis
Cleavage furrrow ingression & regression
No cleavage furrrow ingression
Failed cytokinesis
Time after anaphase onset
13h
10h
7h
4h
1h
60 min
40 min
20 min
0 min
Tum-FL-R
Tum 1-111-R
Tum Δ1-111

Figure 6.2: The N-terminus of Tum is necessary and sufficient for its recruitment to the central spindle, but is not sufficient to rescue furrowing

(A) Domain organization of GFP-tagged, dsRNA-resistant Tum (Tum FL-R-GFP) **(B-D)** Time-lapse sequences of S2 cells co-expressing dsRNA-resistant GFP-tagged Tum mutants and mCherry-Tubulin **(B)** Tum^{FL}-R-GFP, 63X, Z stack **(C)** Tum^{1-111}-R-GFP, 63X Zstack **(D)** $Tum^{\Delta 1-111}$-GFP, treated with Tum dsRNA1 for 3 days. Maximum intensity projections acquired using a 40X air objective (0.85 NA), with camera binning set to 2x2 are shown. Times are h:min. Scale bars 5 µm. (D) Timing of abscission or cytokinesis failure of cells co-expressing dsRNA-resistant GFP-tagged Tum mutants and mCherry-Tubulin treated for 3–5 days with Tum dsRNA1. Each circle represents a single cell. Data are from a single representative experiment out of three repeats. N=3, n= 25 cells /condition/ experiment.

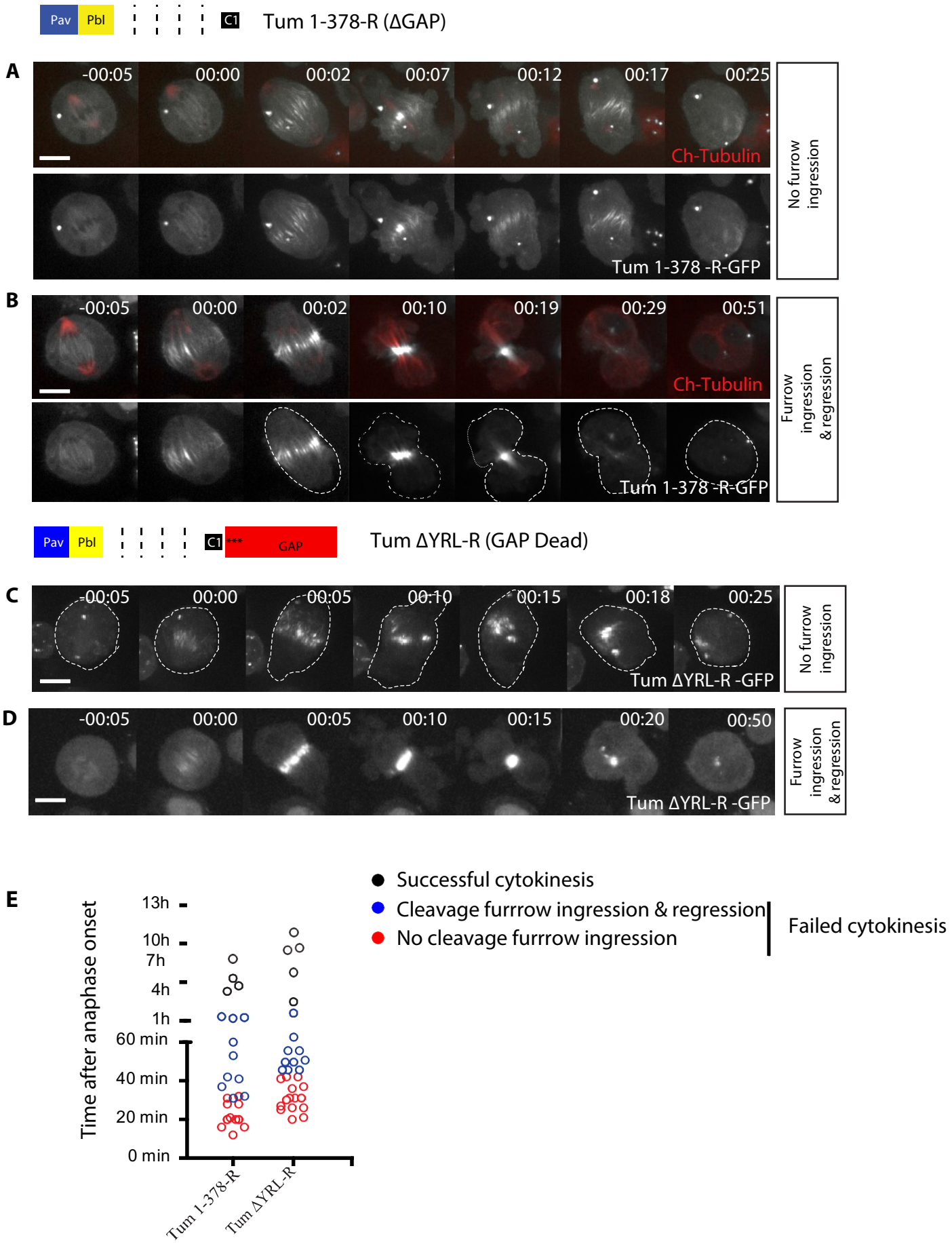
Pav
Pbl
C1
Tum 1-378-R (ΔGAP)
A
-00:05
00:00
00:02
00:07
00:12
00:17
00:25
Ch-Tubulin
Tum 1-378 -R-GFP
No furrow ingression
B
-00:05
00:00
00:02
00:10
00:19
00:29
00:51
Ch-Tubulin
Tum 1-378 -R-GFP
Furrow ingression & regression
Pav
Pbl
C1
***
GAP
Tum ΔYRL-R (GAP Dead)
C
-00:05
00:00
00:05
00:10
00:15
00:18
00:25
Tum ΔYRL-R -GFP
No furrow ingression
D
-00:05
00:00
00:05
00:10
00:15
00:20
00:50
Tum ΔYRL-R -GFP
Furrow ingression & regression
E
Time after anaphase onset
13h
10h
7h
4h
1h
60 min
40 min
20 min
0 min
Tum 1-378-R
Tum ΔYRL-R
Successful cytokinesis
Cleavage furrrow ingression & regression
No cleavage furrrow ingression
Failed cytokinesis

Figure 6.3: The GAP activity of Tum is required for furrowing and maturation of the MB/MR

Time-lapse sequences of S2 cells co-expressing dsRNA-resistant GFP-tagged Tum mutants and mCherry-Tubulin treated with Tum dsRNA1 for 3 days. **(A-B)** Tum^{1-378}-R-GFP, single confocal sections acquired using 63X objective, with camera binning set to 2x2 are shown. **(C-D)** $Tum^{\Delta YRL}$-R-GFP, maximum intensity projections acquired using 40X objective are shown. Times are h:min. Scale bars 5 µm. **(E)** Timing of abscission or cytokinesis failure of cells co-expressing dsRNA-resistant GFP-tagged Tum mutants and mCherry-Tubulin treated for 3–5 days with Tum dsRNA1. Each circle represents a single cell; data are from a single representative experiment out of three repeats. N=3, n= 25 cells /condition/ experiment.

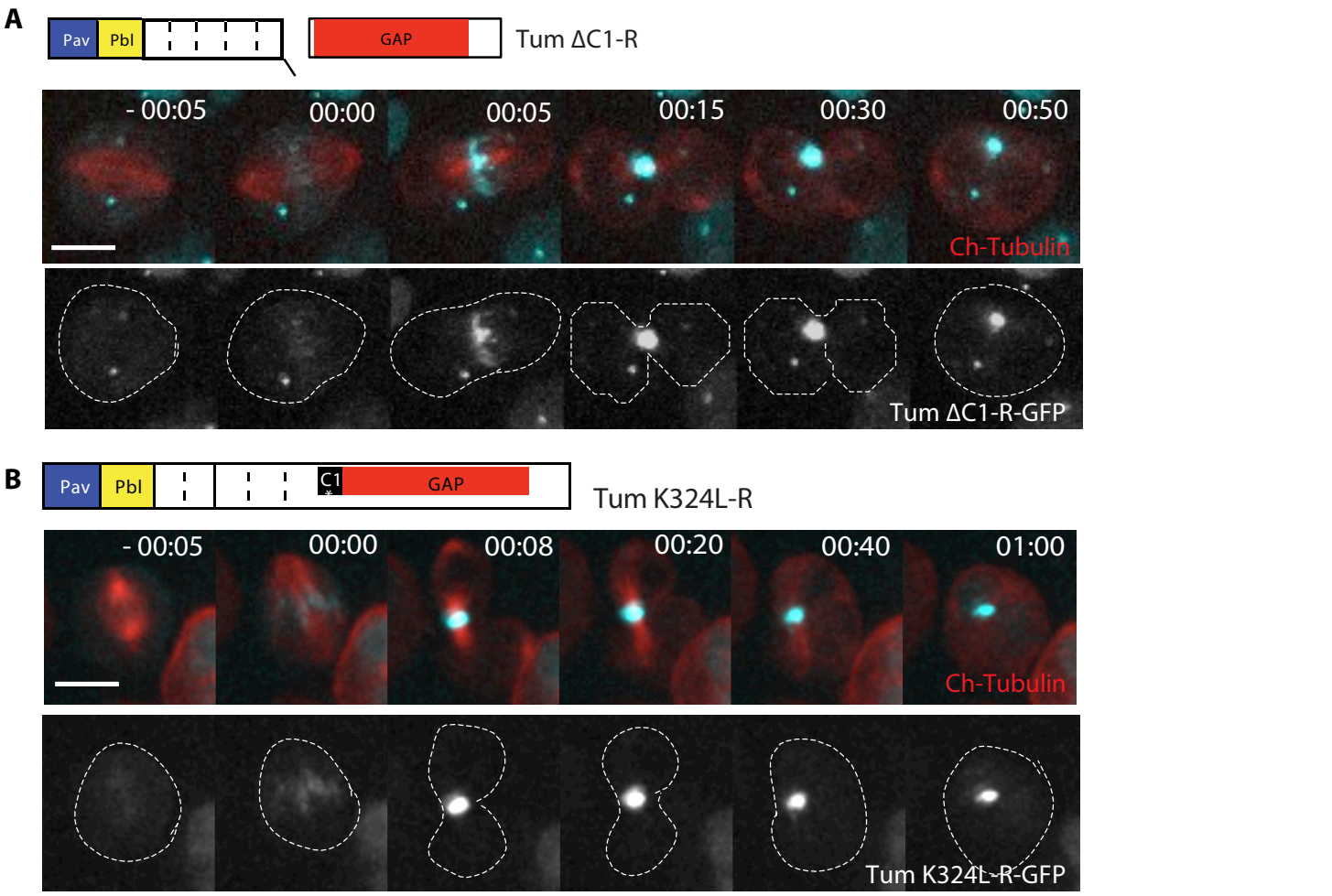
A
Pav
Pbl
GAP
Tum ΔC1-R
- 00:05
00:00
00:05
00:15
00:30
00:50
Ch-Tubulin
Tum ΔC1-R-GFP
B
Pav
Pbl
C1
GAP
Tum K324L-R
- 00:05
00:00
00:08
00:20
00:40
01:00
Ch-Tubulin
Tum K324L-R-GFP
C
Time after anaphase onset
13h
10h
7h
4h
1h
60 min
40 min
20 min
0 min
Tum ΔC1-R
Tum K324L-R
3days
7days
Successful cytokinesis
Cleavage furrrow ingression & regression
No cleavage furrrow ingression
Failed cytokinesis

Figure 6.4: The C1 domain of Tum anchors the MB/MR to the plasma membrane

(A-B) Time-lapse sequences of S2 cells co-expressing dsRNA-resistant GFP-tagged Tum mutants and mCherry-Tubulin **(A)** $Tum^{\Delta C1}$-R-GFP **(B)** Tum^{F289G}-R-GFP, treated with Tum dsRNA1 for 3-5 days and 7-8 days respectively. Maximum intensity projections acquired using a 40X objective, with camera binning set to 2x2, are shown. Times are h:min. Scale bars 5 µm. **(C)** Timing of abscission or cytokinesis failure of cells co-expressing dsRNA-resistant GFP-tagged Tum mutants and Tubulin-mCherry treated for 3–5 or 7-8 days with Tum dsRNA1. Each circle represents a single cell; data are from a single representative experiment out of three repeats. N=3, n= 25 cells /condition/ experiment.

A Tum-112-319 (Tum CD)

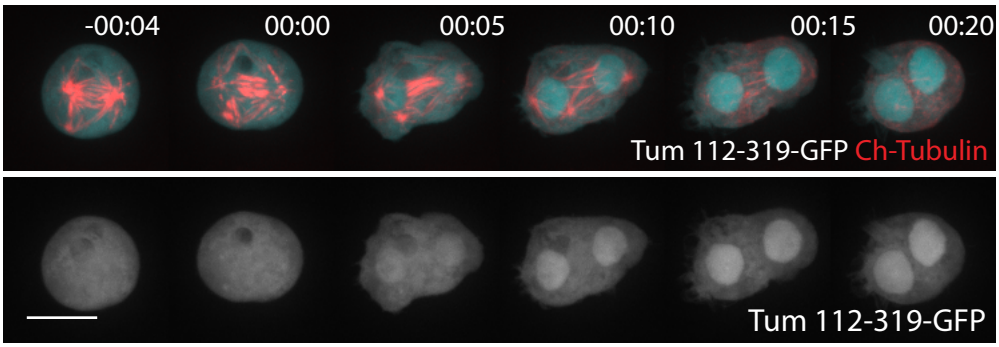

B Pav Pbl C1 GAP Tum-Δ111-319 (Tum ΔCD)

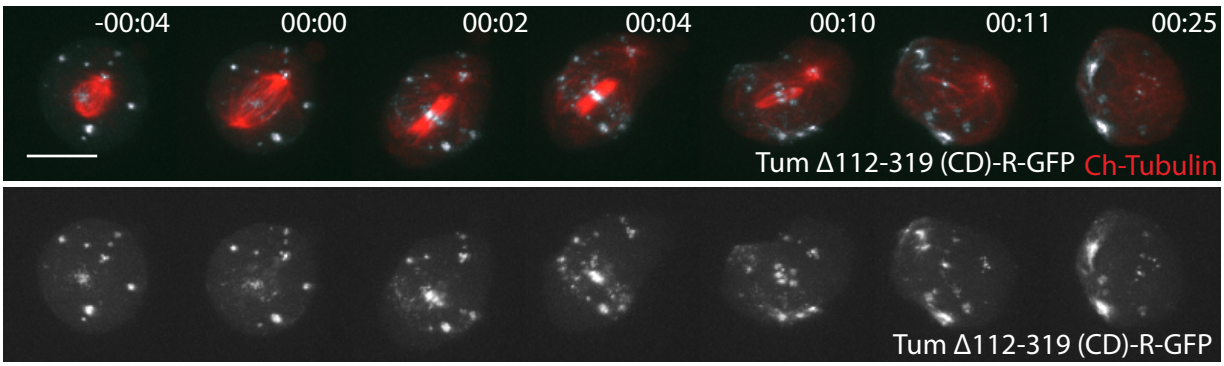

C Pav Pbl C1 GAP Tum Δ286-319-R

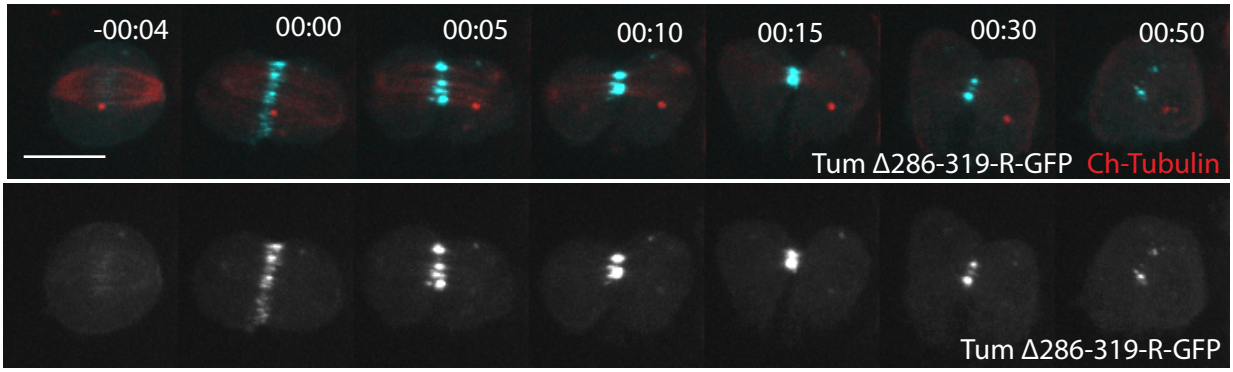

D

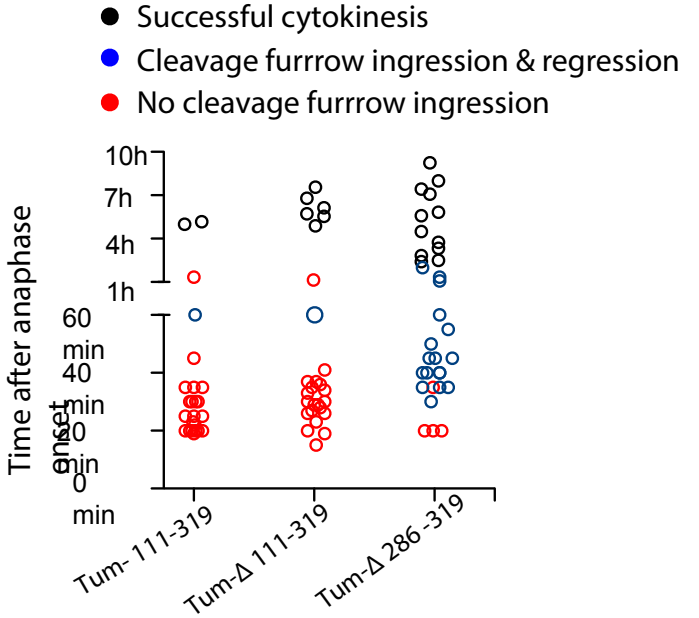

E Cells depleted of endogenous Tum

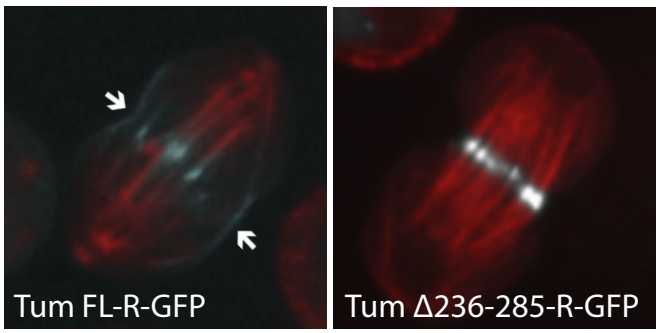

Figure 6.5: The central region of Tum is required for furrowing and MB/MR formation

(A-C) Time-lapse sequences of S2 cells co-expressing dsRNA-resistant GFP-tagged Tum mutants and mCherry-Tubulin **(A)** $Tum^{112-319}$-R-GFP **(B)** $Tum^{\Delta 112-319}$-R-GFP, treated with Tum dsRNA1 for 3-5 days. **(C)** $Tum^{\Delta 286-319}$-R-GFP, treated with Tum dsRNA1 for 7-8 days. Maximum intensity projections acquired using a 63X objective, with camera binning set to 2x2, are shown.. Times are h:min. Scale bars 5 µm. **(D)** Timing of abscission or cytokinesis failure of cells co-expressing dsRNA-resistant GFP-tagged Tum mutants and Tubulin-mCherry treated for 3–5 or 7-8 days with Tum dsRNA1. Each circle represents a single cell; data are from a single representative experiment out of three repeats. N=3, n= 25 cells /condition/ experiment. **(E)** S2 cells expressing Tum-^{FL}-R-GFP or Tum $^{\Delta 235-286}$- R-GFP treated with Tum dsRNA1 for 7-8 days. Arrows depict the cortical pool of Tum-^{FL}-R-GFP that is lost in cells expressing Tum $^{\Delta 235-286}$- R-GFP.

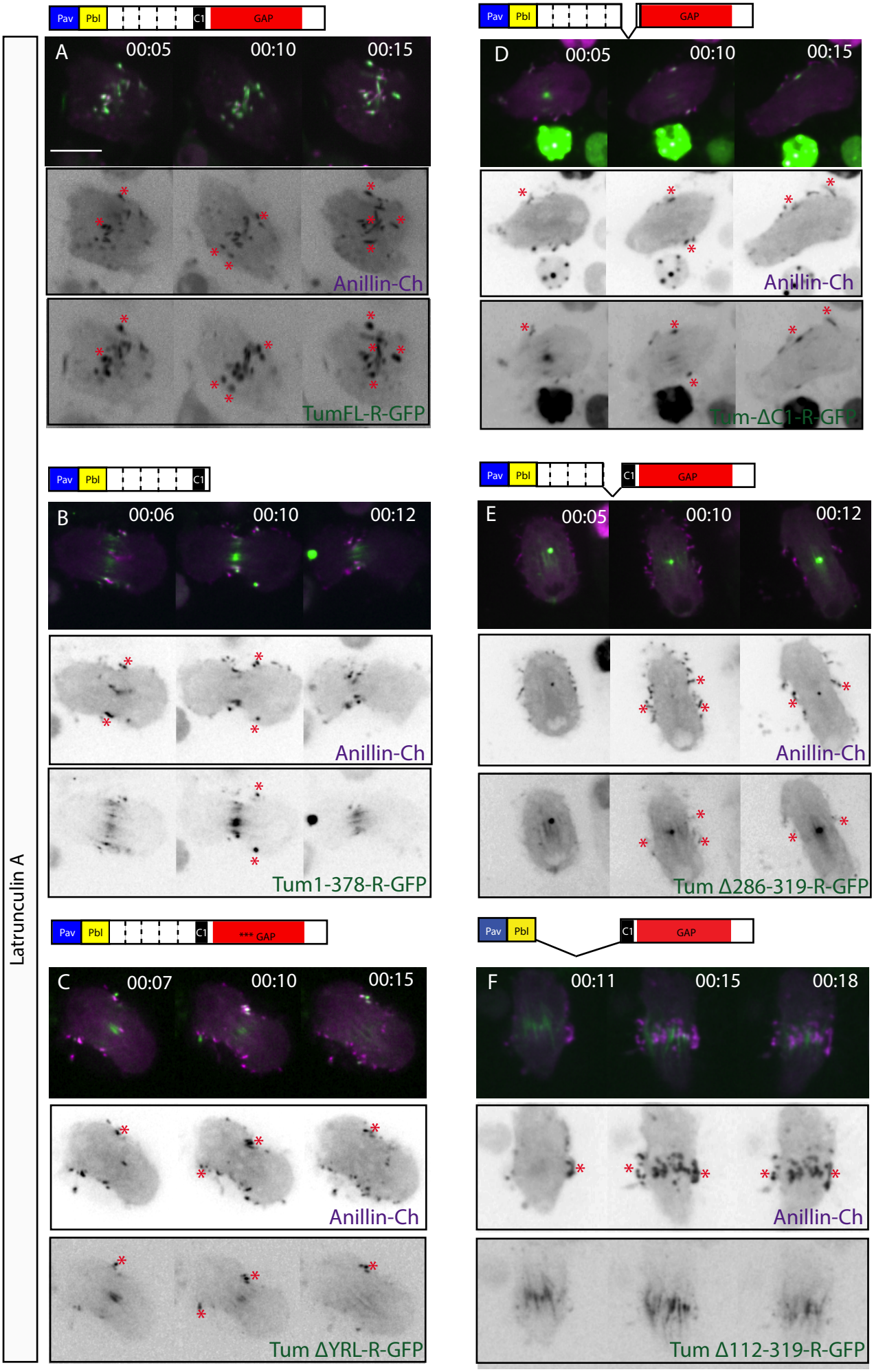
Latrunculin A
Pav
Pbl
C1
GAP
*** GAP
A
00:05
00:10
00:15
Anillin-Ch
TumFL-R-GFP
D
Tum-ΔC1-R-GFP
B
00:06
00:12
Tum1-378-R-GFP
E
Tum Δ286-319-R-GFP
C
00:07
Tum ΔYRL-R-GFP
F
00:11
00:18
Tum Δ112-319-R-GFP

Figure 6.6: The putative Anillin binding domain targets Tum to the cortex

Time-lapse sequences of S2 cells co-expressing dsRNA-resistant GFP-tagged Tum mutants and Anillin-mCherry treated with Tum dsRNA and 1µg/ml of Latrunculin A, an actin monomer stabilizing drug in metaphase. Asterisks point to LatA induced Anillin filaments. Times are h:min. Mutants containing the putative Anillin binding domain: **(A)** Tum-^{FL}-R-GFP, **(B)** Tum$^{1\text{-}378}$-R-GFP, **(C)** Tum$^{\Delta YRL}$-R-GFP, **(D)** Tum$^{\Delta C1}$-R-GFP, which co-localize with Anillin in the cortical filaments, whereas mutants lacking the Anillin binding region do not: **(E)** Tum$^{\Delta 286\text{-}319}$-R-GFP, **(F)** Tum$^{\Delta 112\text{-}319}$-R-GFP. Single confocal sections acquired using a 63X objective, with camera binning set to 2x2, are shown.. Data shown are of representative cells from at least 10 cells analyzed per condition.

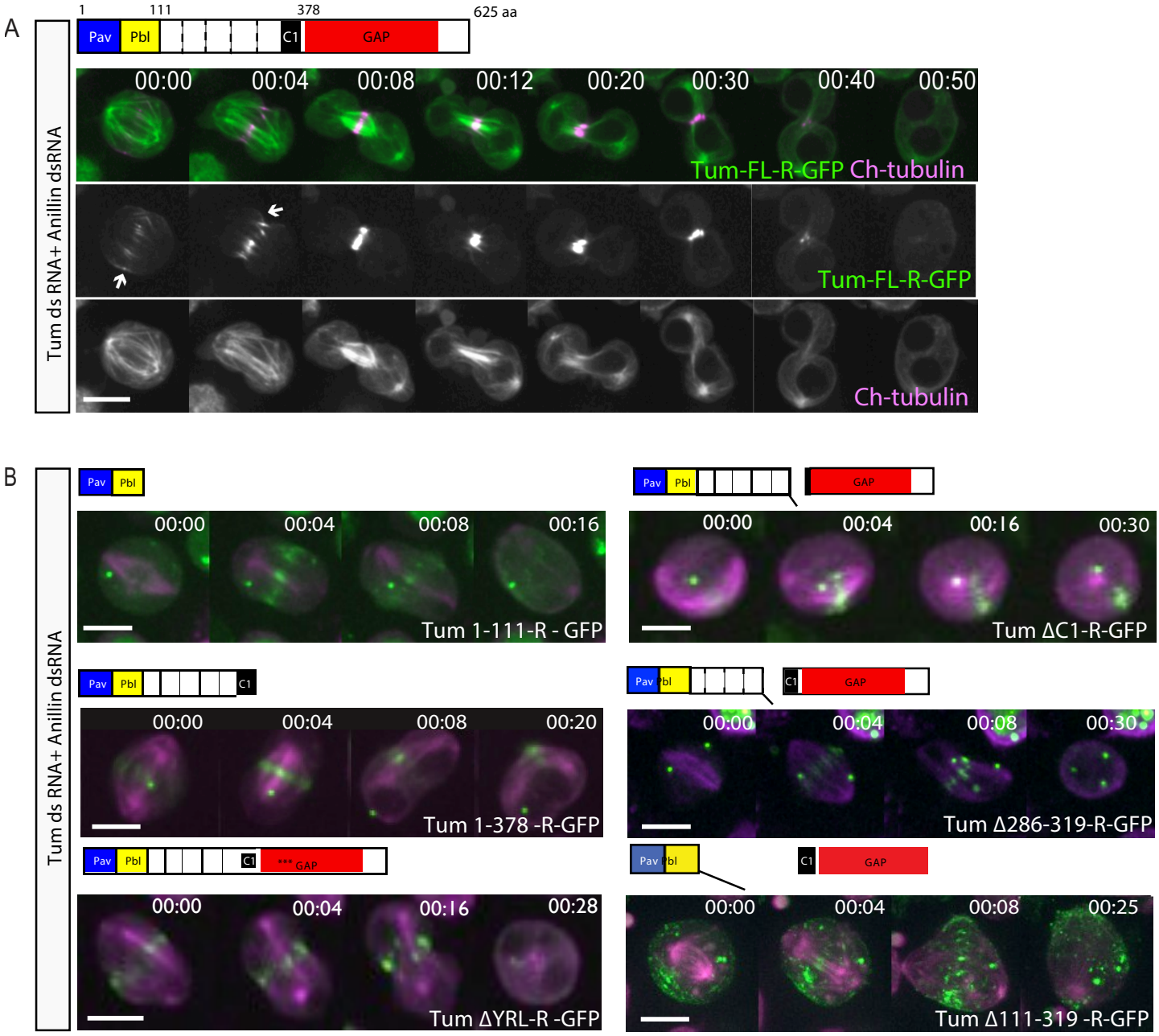
A
1
111
378
625 aa
Pav
Pbl
C1
GAP
Tum ds RNA+ Anillin dsRNA
00:00
00:04
00:08
00:12
00:20
00:30
00:40
00:50
Tum-FL-R-GFP Ch-tubulin
Tum-FL-R-GFP
Ch-tubulin
B
Tum ds RNA+ Anillin dsRNA
00:00
00:04
00:08
00:16
Tum 1-111-R - GFP
00:00
00:04
00:16
00:30
Tum ΔC1-R-GFP
00:00
00:04
00:08
00:20
Tum 1-378 -R-GFP
00:00
00:04
00:08
00:30
Tum Δ286-319-R-GFP
*** GAP
00:00
00:04
00:16
00:28
Tum ΔYRL-R -GFP
00:00
00:04
00:08
00:25
Tum Δ111-319 -R-GFP
C
% Division attempts
100
80
60
40
20
0
Successful cytokinesis
Cleavage furrrow ingression & regression
No cleavage furrrow ingression
Ch-Tubulin
Tum-FL
Tum- 1-111
Tum- 1-378
Tum-ΔYRL
Tum-ΔC1
Tum Δ285-319
Tum-ΔCD
Tum dsRNA1+Anillin dsRNA

Figure 6.7: Genetic interactions between Tum and Anillin are required for furrowing

(A) Time-lapse sequence of an S2 cell co-expressing Tum-^{FL}-R-GFP and mCherry-Tubulin treated for 3 days with Tum dsRNA1 and Anillin dsRNA. Arrows point to a cortical pool of Tum. Single confocal sections acquired using a 63X objective, with camera binning set to 2x2, are shown. Times are h:min **(B)** Time-lapse sequences of S2 cells co-expressing ds-resistant tum mutants and mCherry-Tubulin treated for 3 days with Tum dsRNA1 and Anillin dsRNA. Maximum intensity projections acquired using a 40X objective, with camera binning set to 2x2, are shown., Times are h:min. **(C)** quantification of cytokinesis outcomes in cells co-expressing dsRNA-resistant GFP-tagged Tum mutants and Tubulin-mCherry treated for 3–5 days with Tum dsRNA1 and Anillin dsRNA. Data are from a single representative experiment out of three repeats. N=3, n= 50 cells /condition/ experiment.

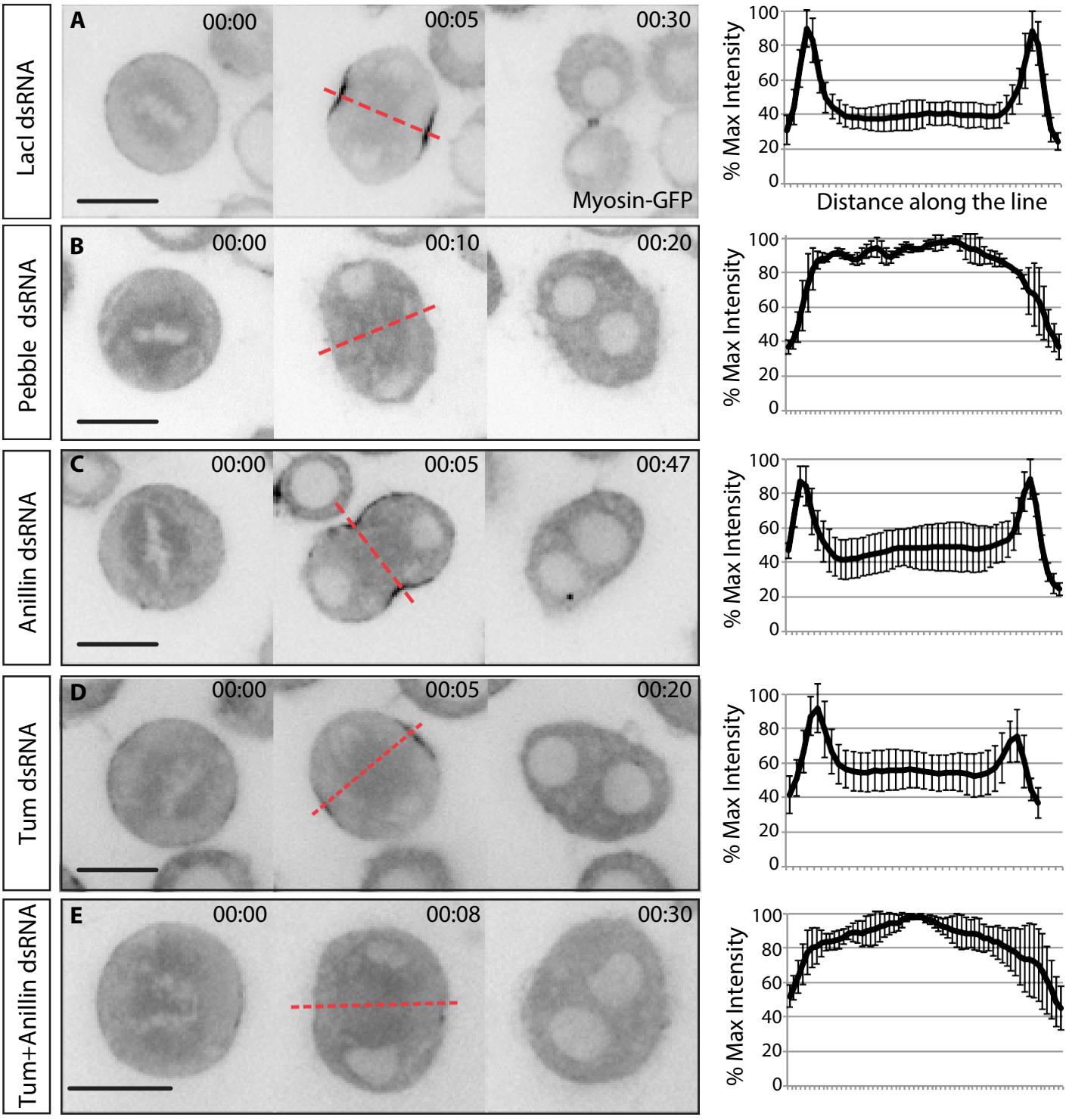
LacI dsRNA
A
00:00
00:05
00:30
Myosin-GFP
Pebble dsRNA
B
00:00
00:10
00:20
Anillin dsRNA
C
00:00
00:05
00:47
Tum dsRNA
D
00:00
00:05
00:20
Tum+Anillin dsRNA
E
00:00
00:08
00:30
% Max Intensity
100
80
60
40
20
0
Distance along the line

Figure 6.8: Co-depletion of Anillin and Tum impairs Rho activation at the equatorial cortex

Time-lapse sequences of S2 cells expressing GFP-tagged Myosin^{Sqh} treated for 3 days with **(A)** Control LacI dsRNA **(B)** Pebble dsRNA**(C)** Anillin dsRNA **(D)** Tum dsRNA1 **(E)** Anillin and Tum dsRNAs. Single confocal sections acquired using a 63X objective, with camera binning set to 2x2, are shown. Times are h:min. Scale bars, 5 µm. Graphs represent % maximum myosin-GFP along a line drawn across the cell equator (Red dotted line, n=10 cells /condition). Data shown is a representative cell from 10 cells analyzed /condition.

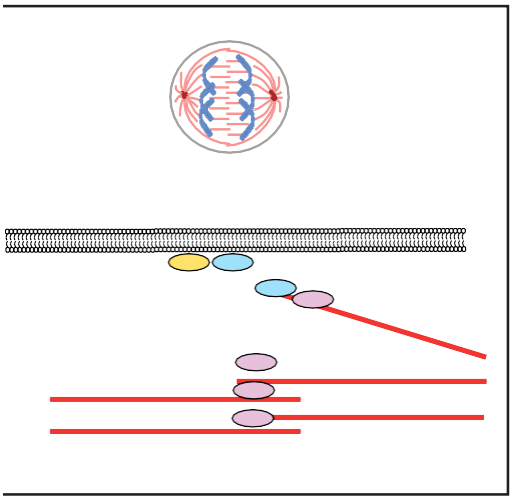

Furrow initiation

- Tum is recruited to the spindle through its N-terminus where it forms Centralspindlin. Centralspindlin recruits RhoGEF/Pebble to the membrane.

- Pebble activates Rho at the Equator and triggers furrow formation.

- The GAP domain and the central region of Tum are required for furrow formation and closure.

- Genetic interaction between Anillin and Tum is required for Furrow formation.

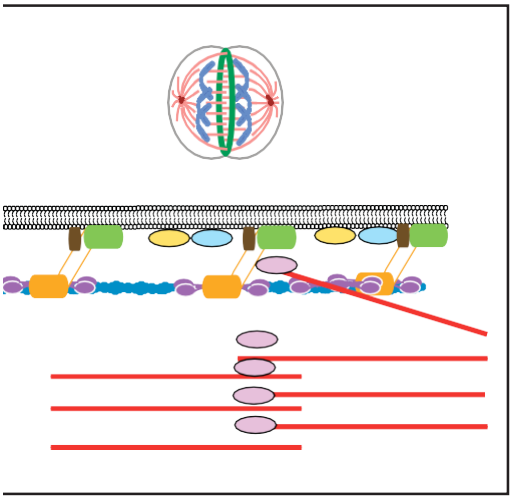

CR formation and closure

- Active RhoA recruits Anillin, Myosin II, Actin, and triggers formation of the CR.

- Anillin-PiP2 binding is essential to anchor the CR to the plasma membra

- An Anillin -Tum interaction is required for retention of Tum at the cortex

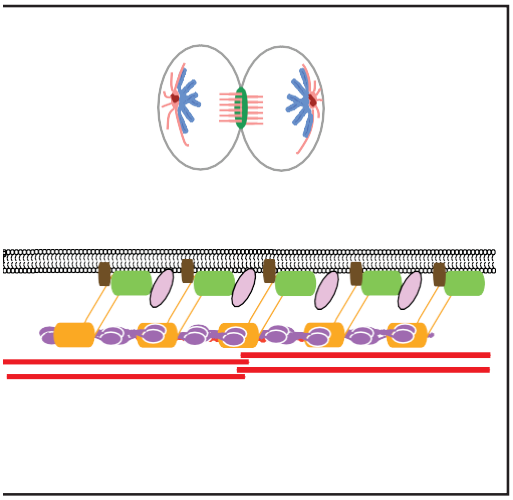

MR/MB formation

- An Anillin -Tum interaction is required for maturation of the MB/MR

- Anillin and Septins are required for anchoring the MR to the membrane

- Cortical Tum mediates anchoring of the MB/MR to the membrane through its C1 domain .

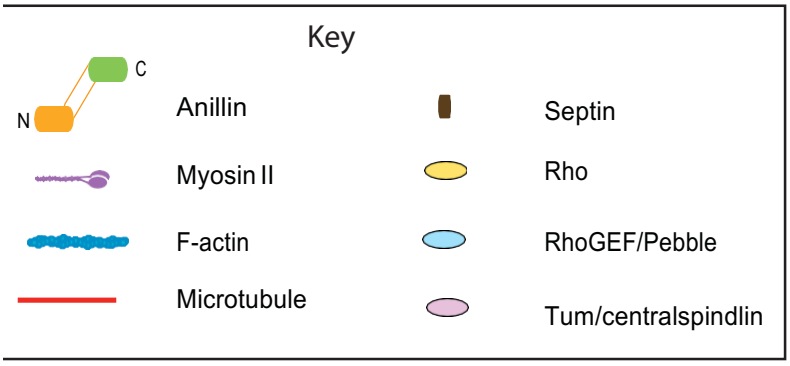

Figure 6.9: Model of the functional interplay between Anillin and Tum throughout cytokinesis

Cartoon summary of results and model for Anillin and tum roles during furrow initiation and the transition from CR to MR.

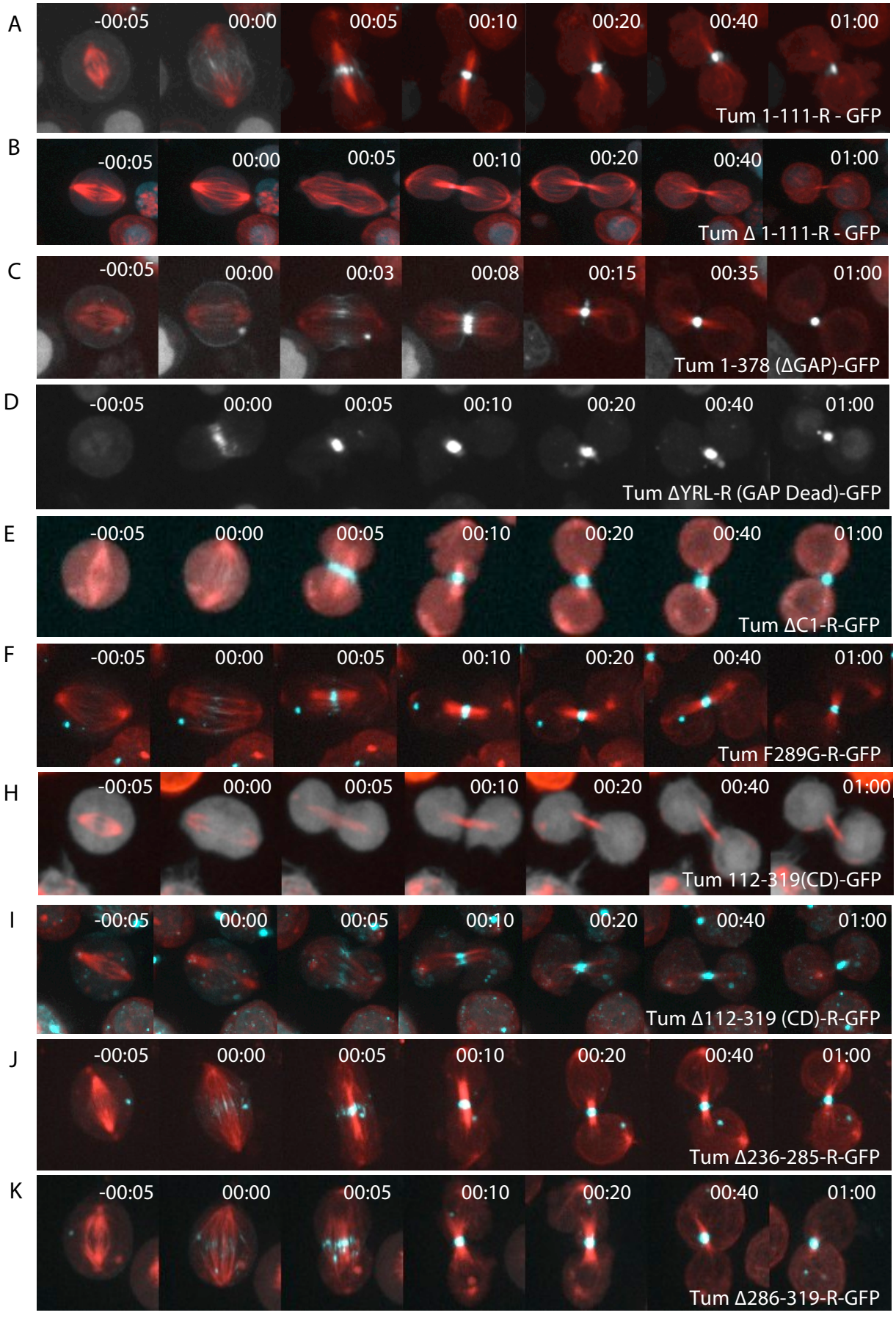
A
-00:05
00:00
00:05
00:10
00:20
00:40
01:00
Tum 1-111-R - GFP
B
-00:05
00:00
00:05
00:10
00:20
00:40
01:00
Tum Δ 1-111-R - GFP
C
-00:05
00:00
00:03
00:08
00:15
00:35
01:00
Tum 1-378 (ΔGAP)-GFP
D
-00:05
00:00
00:05
00:10
00:20
00:40
01:00
Tum ΔYRL-R (GAP Dead)-GFP
E
-00:05
00:00
00:05
00:10
00:20
00:40
01:00
Tum ΔC1-R-GFP
F
-00:05
00:00
00:05
00:10
00:20
00:40
01:00
Tum F289G-R-GFP
H
-00:05
00:00
00:05
00:10
00:20
00:40
01:00
Tum 112-319(CD)-GFP
I
-00:05
00:00
00:05
00:10
00:20
00:40
01:00
Tum Δ112-319 (CD)-R-GFP
J
-00:05
00:00
00:05
00:10
00:20
00:40
01:00
Tum Δ236-285-R-GFP
K
-00:05
00:00
00:05
00:10
00:20
00:40
01:00
Tum Δ286-319-R-GFP

Figure S6.1: Localization of GFP-tagged ds-resistant tum mutants in control conditions

Time-lapse sequences of S2 cells co-expressing GFP-tagged ds-resistant tum mutants (As labelled) and mCherry-Tubulin (Red) treated for 3 days with Control LacI dsRNA. Maximum intensity projections acquired using a 40X objective, with camera binning set to 2x2, are shown. Times are h:min. Scale bars, 5 µm.

A

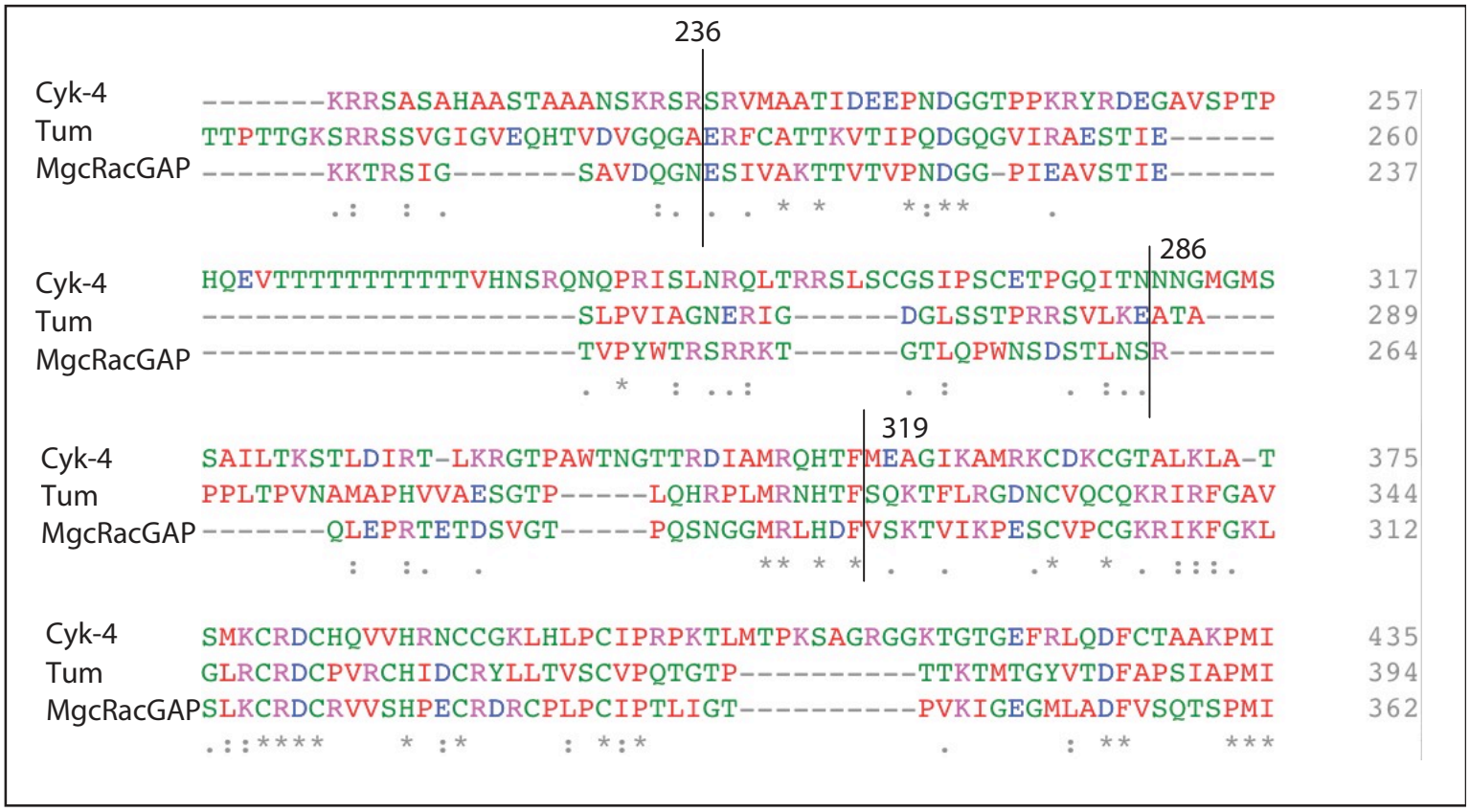
236
286
319
Cyk-4 -------KRRSASAHAASTAAANSKRSRSRVMAATIDEEPNDGGTPPKRYRDEGAVSPTP 257
Tum TTPTTGKSRRSSVGIGVEQHTVDVGQGAERFCATTKVTIPQDGQGVIRAESTIE------ 260
MgcRacGAP -------KKTRSIG-------SAVDQGNESIVAKTTVTVPNDGG-PIEAVSTIE------ 237
Cyk-4 HQEVTTTTTTTTTTTVHNSRQNQPRISLNRQLTRRSLSCGSIPSCETPGQITNNNGMGMS 317
Tum ----------SLPVIAGNERIG------DGLSSTPRRSVLKEATA---- 289
MgcRacGAP ----------TVPYWTRSRRKT------GTLQPWNSDSTLNSR------ 264
Cyk-4 SAILTKSTLDIRT-LKRGTPAWTNGTTRDIAMRQHTFMEAGIKAMRKCDKCGTALKLA-T 375
Tum PPLTPVNAMAPHVVAESGTP-----LQHRPLMRNHTFSQKTFLRGDNCVQCQKRIRFGAV 344
MgcRacGAP -------QLEPRTETDSVGT-----PQSNGGMRLHDFVSKTVIKPESCVPCGKRIKFGKL 312
Cyk-4 SMKCRDCHQVVHRNCCGKLHLPCIPRPKTLMTPKSAGRGGKTGTGEFRLQDFCTAAKPMI 435
Tum GLRCRDCPVRCHIDCRYLLTVSCVPQTGTP----------TTKTMTGYVTDFAPSIAPMI 394
MgcRacGAP SLKCRDCRVVSHPECRDRCPLPCIPTLIGT----------PVKIGEGMLADFVSQTSPMI 362

B

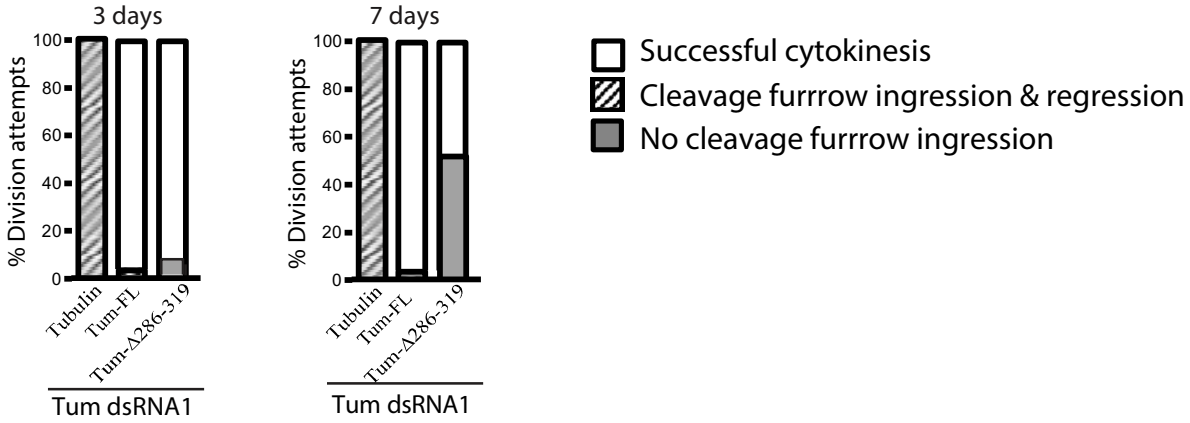
3 days
7 days
% Division attempts
100
80
60
40
20
0
Tubulin
Tum-FL
Tum-Δ286-319
Tum dsRNA1
Successful cytokinesis
Cleavage furrrow ingression & regression
No cleavage furrrow ingression

C

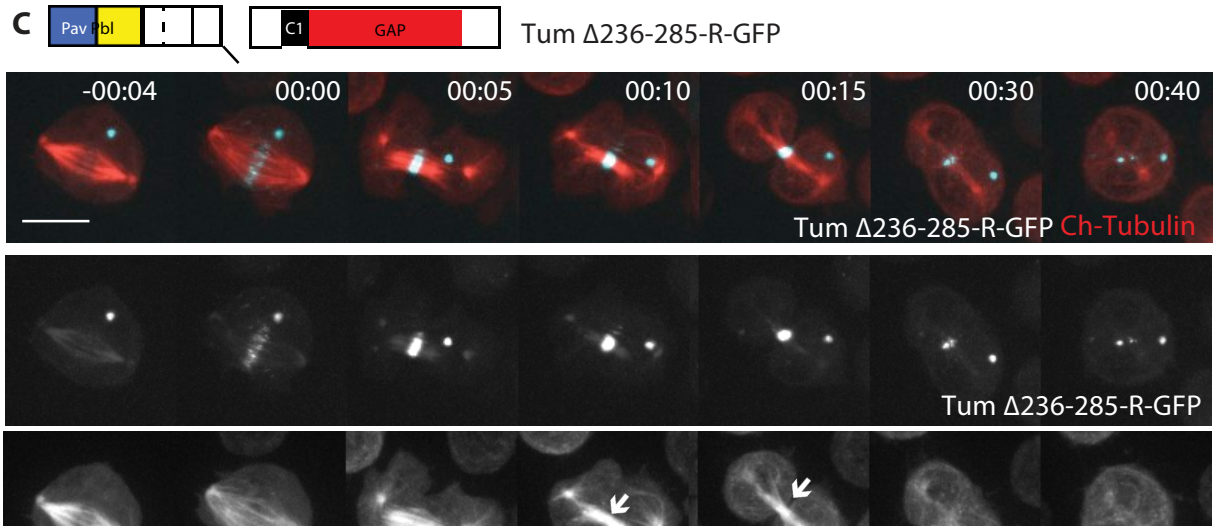
Pav
Pbl
C1
GAP
Tum Δ236-285-R-GFP
-00:04
00:00
00:05
00:10
00:15
00:30
00:40
Tum Δ236-285-R-GFP Ch-Tubulin
Tum Δ236-285-R-GFP

Figure S6.2: The putative Anillin binding domain of Tum is required for maturation of the MB/MR

(A) Clustal protein sequence alignment of the putative Anillin binding domain of *C. elegans* CYK-4, *Drosophila* Tum and human MgcRacGAP. Asterisks mark identical amino acids. **(B)** Quantification of cytokinesis outcome in cells expressing mCherry-Tubulin alone, Tum-^{FL}-R-GFP and mCherry-tubulin or Tum$^{-\Delta 286\text{-}319}$-R-GFP and mCherry-Tubulin treated for 3–4 days or 7-8 days with Tum dsRNA1. Data are from a single representative experiment out of three repeats. N=3, n= 30 cells /condition/ experiment. **(C)** Time-lapse sequence of an S2 cell co-expressing mCherry-Tubulin **and** Tum$^{\Delta 236\text{-}285}$-R-GFP, treated with Tum dsRNA1 for 7-8 days. Maximum intensity projections acquired using a 40X objective, with camera binning set to 2x2, are shown. Times are h:min. Scale bars 5 µm. Arrows highlight the absence of the gap in tubulin fluorescence at the zone of overlapping MT plus ends that usually accompanies MB formation.

7 DISCUSSION

La cytokinèse considérée initialement comme un processus mécanique simple, s'est avérée être un processus complexe, robuste et hautement régulé. Les recherches menées au cours des 20 dernières années ont permis d'identifier un ensemble de molécules de base qui forment la machinerie de la cytokinèse. Cependant, lorsqu'on s'intéresse à un processus aussi complexe et dynamique que la cytokinèse où chaque composante de la machinerie interagit avec et dépend de plusieurs autres composantes, il est important de pouvoir suivre les différentes composantes dans le temps et l'espace afin d'avoir une compréhension globale de la complexité du processus et des mécanismes qui le régissent. Dans le cadre de cette thèse, nos travaux sur la cytokinèse par des études fonctionnelles couplées à l'imagerie en temps réel nous ont permis d'identifier et de caractériser de nouvelles étapes clés au cours de la cytokinèse.

Dans ce modèle de cytokinèse que nous avons mis à jour, l'Anilline est un facteur crucial tout au long de la cytokinèse. En effet, elle se distingue par son interaction avec un grand nombre de protéines clés composant la machinerie de la cytokinèse et qui regroupent le cortex, la membrane et les microtubules. Bien que les recherches actives menées au cours des quinze dernières années aient établi que l'Anilline joue un rôle central dans la cytokinèse, sa contribution fonctionnelle à la cytokinèse et à sa régulation dans le temps et l'espace restaient mal comprises. Les données présentées dans le cadre de cette thèse ont permis de mieux définir le rôle de l'Anilline durant la cytokinèse et révèlent de nouvelles fonctions tout au long de la cytokinèse ; incluant l'établissement du sillon de clivage, la stabilisation de l'AC, la formation de l'AM et sa maturation, et finalement l'ancrage de cet anneau à la membrane plasmique.

7.1 LA TRANSITION DE L'ANNEAU CONTRACTILE A L'ANNEAU DU MIDBODY

Dès les premières études fonctionnelles sur l'Anilline, il semblait clair qu'elle jouait un rôle crucial dans la stabilisation de l'anneau contractile (AC). Bien que sa déplétion n'empêche pas le recrutement de l'actine et de la myosine ni la formation de l'AC, elle cause

une instabilité de l'AC et des oscillations qui mènent ultimement à un échec de la cytokinèse (Goldbach et al., 2010; Hickson and O'Farrell, 2008a; Kechad et al., 2012; Piekny and Glotzer, 2008; Somma et al., 2002; Straight et al., 2005). En plus de ce phénotype, notre étude par imagerie en temps réel a également permis de caractériser un nouveau phénotype qui résulte de la déplétion de l'Anilline. Chez certaines cellules, un AC se forme et se ferme au delà de 50% avant de régresser ; mais nous n'avons observé aucun anneau du midbody (AM) (Chapitre 4 ; Kechad et al., 2012). Historiquement l'AC et l'AM ont été considérés comme deux structures distinctes composées de différentes protéines. Les travaux s'intéressaient soit à la formation et la fermeture de l'AC, soit à la composition de l'AM et aux mécanismes de l'abscission, mais peu d'intérêt a été porté aux évènements entre ces deux phases. Dans le cadre de cette thèse, nous avons démontré que l'AC et l'AM sont la même structure à différents stades de sa maturation et nous avons nommé cette étape la transition de l'AC à l'AM. En effet, l'expression de l'extrémité N-terminale de l'Anilline qui contient les domaines de liaisons à l'actine et la myosine supporte la formation d'un AC stable, sa fermeture et la formation de structures semblables à l'AM. Ainsi, l'extrémité N-terminale de l'Anilline se localise à l'AC et guide la transformation de l'AC dynamique en AM stable. Collectivement, ces données montrent que l'AM découle de l'AC et que l'Anilline coordonne cette transition (Kechad et al, 2012 ; Chapitre 4).

Bien que l'extrémité N-terminale de l'Anilline soit suffisante pour la formation de l'AC et sa maturation en AM, ces anneaux étaient incapables d'ancrer la membrane plasmique, qui finissait par régresser produisant des cellules avec des vestiges d'AMs. Par ailleurs, l'extrémité C-terminale bien qu'incapable de se localiser à l'AC ou l'AM naissant, se localise indépendamment au cortex équatorial où elle forme des structures associées à la membrane. De façon similaire, la déplétion des septines, ne prévient pas le recrutement de l'Anilline ni la formation des AMs, mais empêche également l'ancrage de ces anneaux à la membrane plasmique. À la lumière de ces données, nous avons proposé un modèle ou l'extrémité N-terminale soutient la formation de l'AC et la formation de l'AM alors que l'extrémité C-terminale permet un recrutement robuste de l'Anilline au sillon de clivage où elle organise avec les septines, une ancre stable entre l'AM et la membrane (Chapitre 4 ; Kechad et al., 2012).

7.2 L'ANILLINE, UNE PROTEINE D'ANCRAGE TOUT AU LONG DE LA CYTOKINESE

Les premières études fonctionnelles sur l'Anilline avaient suggéré un rôle dans l'ancrage de l'AC vu les oscillations observées suite à sa déplétion (Field et al., 1995). Nos travaux sont en accord avec cette idée, et nous avons proposé la présence de mécanismes d'ancrage distincts pour l'AC et l'AM, puisque la déplétion des septines n'affecte pas l'ancrage de l'AC mais uniquement l'ancrage de l'AM (Chapitre 4 ; Kechad et al., 2012). Depuis, plusieurs études ont permis d'identifier plus précisément les mécanismes d'ancrage de l'Anilline à la membrane et ont mis en évidence son rôle comme protéine d'ancrage tout au long de la cytokinèse.

Dans une élégante étude, Liu et al ont démontré qu'en plus des septines, l'Anilline lie les phosphoinositides phosphates (PIPs) à la membrane à travers son domaine PH. Ainsi, des mutations qui bloquent spécifiquement la liaison de l'Anilline au PIPs bloquent également sa localisation au sillon de clivage et causent un échec de la cytokinèse (Liu et al, 2012). Ensuite, afin de séparer la liaison aux septines de la liaison à la membrane, les auteurs ont généré une protéine chimère où le domaine PH de l'Anilline à été remplacé par le domaine PH de la phospholipase C-δ1, qui lie également les PIPs. Dans les cellules appauvries en Anilline endogène, l'Anilline chimère a restauré la localisation de l'Anilline au cortex équatorial et a restauré la formation de sillons de clivage et stabilisé leur ingression. Cependant, ces sillons étaient incapables de supporter la cytokinèse, suggérant que l'interaction entre l'Anilline et les PIPs est requise pour le recrutement de l'Anilline au sillon de clivage alors que l'interaction du domaine PH est requise également à un stade ultérieur de la cytokinèse. Ces données sont en accord avec nos résultats et supportent un modèle où le domaine PH de l'Anilline a au moins deux fonctions: d'une part, il permet la liaison aux PIPs qui est nécessaire pour cibler l'Anilline au sillon de clivage au début de la cytokinèse et fournir l'ancrage nécessaire pour éviter que le sillon oscille dans le plan de la membrane (Liu et al, 2012). D'autre part, il régit le recrutement des septines afin de former une ancre stable de l'AM à la membrane plasmique. Ceci dit, bien que l'Anilline soit nécessaire au recrutement des septines, la déplétion des septines cause une réduction du recrutement de l'extrémité C-terminale à la membrane plasmique (Kechad et al, 2012). Ainsi, il existe une boucle de renforcement positif entre

l'Anilline et les septines afin d'assurer un ancrage robuste de l'AM à la membrane.

Récemment, une étude par cristallographie a permis de compléter le tableau et révélé qu'en plus du domaine PH, deux éléments cryptiques au niveau du domaine AHD de l'Anilline humaine permettent également son association à la membrane, soit le domaine de liaison à Rho et un domaine cryptique C2 adjacent. Une mutation ou une délétion d'un de ces domaines cause des défauts de localisation de l'Anilline au sillon de clivage dans les cellules humaines, suggérant une coopération pour l'ancrage stable de l'Anilline au plan de division (Sun et al., 2015). Ainsi, au lieu de s'associer à la membrane plasmique par un seul domaine, l'Anilline est ancrée au plan de division par des actions synergiques d'au moins trois éléments de liaison à la membrane soit le domaine PH, le domaine C2 et le domaine de liaison à Rho. Nous proposons qu'à travers ces éléments, l'Anilline régit l'ancrage de l'AC à la membrane plasmique. Plus tard, une fois que l'AC s'est transformé en AM, l'Anilline recrute des septines et ensemble ils organisent l'ancrage de l'AM.

7.3 UN EQUILIBRE ENTRE LA RETENTION ET L'EXCRETION DE LA MEMBRANE REGIT LA MATURATION DE L'ANNEAU DU MIDBODY

Après avoir montré que l'AM découle de l'AC, la question logique qui a suivi était de comprendre comment? Alors que plusieurs études indiquent que l'AC se désassemble pendant sa fermeture (Schroeder, 1972; Carvalho et al, 2009), peu d'intérêt a été porté au devenir de la membrane qui y est associée. Les travaux décris dans le cadre de cette thèse montrent que l'AC donne lieu à l'AM via un processus de maturation non caractérisé précédemment. Au cours de la formation de l'AM, nous avons observé un amincissement progressif de la structure de l'AM par un processus de maturation qui dure ~ 1 h par lequel la membrane ainsi que les protéines qui y sont associées sont éliminées du cortex équatorial. En effet, nous observons des excrétions membranaires riches en Aniline qui contiennent également plusieurs autres composantes de la machinerie de la cytokinèse comme la septine Peanut, Rho, la kinase Citron, les composantes du complexe centralspindlin RacGAP50C/Tumbleweed et la kinésine-6 Pavarotti ainsi que la kinase Aurora B. Remarquablement, nous avons observé très peu de myosine ou d'actine dans ces extrusions (El Amine et al., 2013, Chapitre 5).

La perte de la membrane, un mécanisme universel pour la fermeture de l'AC?

Bien qu'inattendu, ce phénomène d'élimination de la membrane a été observé auparavant. En effet, des phénomènes similaires avaient été décris dans des études par microscopie électronique lors de la division de zygotes de l'oursin de mer (Shroeder, 1972) et dans les cellules humaines D985 (Mullins et Biesle, 1976). Plus récemment, il a été démontré que les progéniteurs neuronaux de souris éjectent, via leur midbody apical, des particules membranaires qui contiennent de l'Anilline et la prominine-1/CD133 (Dubreuil et al., 2007). Suite à nos travaux, d'autres évènements d'extrusion ont été décrits notamment chez les cellules humaines où des tubules de membranes enrichies en Anilline et septines ont également été observés au midbody (Renshaw et al, 2014) et les zygotes de *C.elegans* ou d'autres évènements d'extrusion, de topologie différente, régulent l'abscission (Green et al, 2013). Ces observations provenant de différents organismes suggèrent que l'extrusion de membrane pendant la maturation de l'AC en anneau du midbody est un phénomène conservé qui mérite des études plus approfondies.

Des actions opposées de la kinase Citron et des Septines sur l'Anilline régulent les extrusions de membrane.

Nos résultats suggèrent que l'Anilline est nécessaire à la maturation de l'AM et que ce processus implique une compétition moléculaire entre la rétention et l'élimination de l'Anilline par des actions opposées mais complémentaires de la kinase Citron et des septines. D'une part, la kinase Citron interagit avec l'extrémité N-terminale de l'Anilline et assure sa rétention au niveau de l'AC et de l'AM. La déplétion de Citron augmente considérablement le nombre et la durée des extrusions et prévient la formation de l'AM. D'autre part, les septines agissent avec le domaine PH à l'extrémité C-terminale de l'Anilline et favorisent l'amincissement de l'AM en éliminant localement la membrane plasmique et les protéines associées. La déplétion des septines ou du domaine PH de l'Anilline bloque cette perte locale de la membrane et produit des AMs volumineux incapables de soutenir la cytokinèse. Pour ce qui est de la membrane, nous savons que ce processus est distinct de l'abscission puisqu'il ne requiert pas la formation des complexes ESCRT III et est insensible à une déplétion de CHMP4B/Shrub (El Amine et al, 2013; Chapitre 5). L'organisation exacte de la membrane ainsi que la machinerie nécessaire

à l'élimination de la membrane lors de ce processus restent à être déterminés.

Quel serait le rôle de ce processus durant la cytokinèse ?

Les modèles actuels de fermeture de l'AC se concentrent sur les protéines du cytosquelette et accordent peu d'attention à la membrane plasmique à laquelle ces éléments sont ancrés. Bien que l'ajout net de membranes soit peut-être nécessaire pendant la fermeture du sillon (Albertson et al., 2005, McKay et al., 2011; Neto et al., 2011), nos résultats mettent en évidence un besoin d'une perte locale de la membrane au niveau de l'équateur pour permettre la fermeture totale de l'AC et la maturation de l'AM. Point intéressant, les protrusions formées à la membrane durant ce processus sont semblables aux structures tubulaires que l'on observe à l'équateur lorsque l'Anilline est déconnecté du réseau d'actine. Par exemple, lorsqu'on exprime l'extrémité C-terminale de l'Anilline, ou lorsqu'on perturbe le cytosquelette d'actine avec la Latrunculine A, on induit la relocalisation de l'Anilline à des structures filamenteuse à l'équateur qui rappellent celles formées lors du processus d'extrusion. Ces observations soutiennent un modèle où le désassemblage de l'actine lors de la fermeture de l'AC libère l'extrémité N-terminale de l'Anilline, permettant à l'extrémité C-terminale et aux septines de former ces protrusions membranaires et leur élimination. Comme l'AM devient de plus en plus dense au fur et à mesure qu'il se ferme, on peut imaginer que ça soit difficile pour la cellule d'éliminer la membrane par endocytose alors que la tubulation de la membrane plasmique vers l'extérieur et son extrusion permettrait d'éliminer rapidement et spécifiquement la membrane excédentaire, tout en serrant la membrane restante autour des microtubules du midbody.

Par ailleurs, plusieurs observations soutiennent l'idée que l'extrusion de la membrane soit un prérequis à l'abscission. En effet, dans les conditions où l'élimination de la membrane était bloquée soit par la déplétion des septines, ou du domaine PH de l'Anilline, nous avons observées des anneaux du midbody larges, qui étaient incapables de supporter la cytokinèse. Inversement, la déplétion de la kinase citron qui cause une augmentation des évènements d'extrusion, cause une abscission précoce (El- Amine et al., 2013 ; Chapitre 5). Dans les cellules humaines où les extrusions médiées par les septines et l'Anilline sont bloquées**,** aucun site de constriction n'est formé au niveau du pont intercellulaire et la relocalisation du

composant ESCRT III Chmp4B ne se produit pas (Renshaw et al., 2014). De telles observations suggèrent que l'élimination de la membrane participe à la biogénèse d'un pont intercellulaire stable, et la définition du site d'abscission.

7.4 UNE INTERACTION ENTRE TUM ET L'ANILLINE REGULE-T-ELLE LA TRANSITION DE L'AC A L'AM ?

Deux études indépendantes ont rapporté une interaction entre RacGAP^{Tum} et l'Anilline chez *Drosophila* (D'avino et al., 2008; Gregory et al., 2008), et ont proposé un modèle où cette interaction servirait de lien entre le fuseau central et l'AC. Les travaux présentés dans cette thèse suggèrent plutôt que cette interaction est requise plus tard lors de la transition de l'AC à l'AM et la maturation du midbody. D'une part, nous avions démontré dans le cadre de notre étude de structure/ fonction de l'Anilline, qu'en plus de son rôle au niveau de l'organisation des structures corticales lors de la transition de l'AC à l'AM, l'Anilline est également impliquée dans la maturation du midbody. En effet, les cellules appauvries en Anilline présentent des défauts dans la compaction des microtubules (MTs) de la zone médiane (Echard et al., 2004 ; Kechad et al., 2012; Somma et al., 2002). De plus, cette fonction nécessite l'extrémité C-terminale qui interagit, entre autres, avec RacGAP^{Tum} (D'avino et al., 2008; Gregory et al., 2008) et chez l'humain, les MTs (Tse et al., 2011; Van Oostende Triplet et al., 2014). D'autre part, la déplétion de l'Anilline n'affecte pas le recrutement de RacGAP^{Tum} au cortex en métaphase ou au début de l'anaphase. Cependant, la localisation de RacGAP^{Tum} au cortex équatorial après l'ingression du sillon de clivage est grandement perturbée (Chapitre 6). Finalement, les mutants de RacGAP^{Tum} qui ne contiennent pas le domaine de liaison à l'Anilline sont incapables de se localiser au cortex équatorial après l'initiation du sillon de clivage et ne sont pas recrutées aux structures membranaires formées par l'Anilline en présence de la Latrunculine A. Dans ce contexte, les cellules sont capables de former un AC et d'initier sa constriction, mais la transition de l'AC à l'AM et la maturation du fuseau central en un midbody sont toutes deux bloquées, bien que l'Anilline soit présente. Ces résultats soutiennent un modèle où l'interaction entre l'Anilline et RacGAP^{Tum} est requise pour coordonner la formation de l'AM et le midbody (Chapitre 6). Au cours de la maturation du

midbody, on observe une relocalisation d'un pool de RacGAP^{Tum} des MTs vers l'AM. Il est possible que cette relocalisation nécessite l'Anilline qui servirait à stabiliser le pool de RacGAP^{Tum}. Ensemble, l'Anilline et RacGAP^{Tum} agiraient comme protéines d'échafaudages entre les microtubules, le cortex et la membrane afin de stabiliser le pont intercellulaire jusqu'à l'abscision. Bien que la validité de ce modèle reste à prouver par des études biochimiques, notre étude a permis de caractériser une fonction potentielle pour l'interaction de RacGAP^{Tum} et l'Anilline durant la cytokinèse.

7.5 L'ACTIVITE GAP DE RACGAP^{TUM} EST NECESSAIRE POUR L'INGRESSION DU SILLON DE CLIVAGE

La découverte d'une interaction directe entre la sous-unité RacGAP^{Tum} de centralspindlin et de la RhoGEF$^{ECT2/Pebble}$, essentielle pour l'assemblage du sillon de clivage représente une des grandes percées dans le domaine de la cytokinèse (Somers and Saint, 2003). Cette interaction a donné naissance à une voie linéaire d'induction du sillon par laquelle RacGAP^{Tum} provenant du fuseau central recrute et active RhoGEF$^{ECT2/Pebble}$ au cortex équatorial, laquelle à son tour active Rho pour induire la formation du sillon de clivage. Ainsi la fonction de RacGAP^{Tum} comme le régulateur principal de l'induction du sillon de clivage à travers la voie RhoGEF$^{ECT2\ /Pebble}$ est bien caractérisé. Cependant, un des points qui reste moins clair est le rôle du domaine GAP de RacGAP^{Tum}. Des résultats contradictoires ont été rapportés en ce qui concerne l'exigence de l'activité GAP qui semble être dispensable dans certains types de cellules (Goldstein et al., 2005; Yamada et al., 2006) mais pas dans d'autres (Bastos et al., 2012; Canman et al., 2008; Loria et al., 2012; Miller et al., 2009; Tse et al., 2012; Zavortnik et al., 2005; Zhang and Glotzer, 2015). Dans le cadre de cette étude, nous avons montré que l'activité GAP est nécessaire à l'induction du sillon dans les cellules S2 de *Drosophiles*. En effet, bien que les mutants de RacGAP^{Tum} contenant les domaines de liaison à la Kinésine-6^{Pavarotti} et la RhoGEF^{Pebble} aient été recrutés au fuseau central, ils étaient incapables de déclencher la formation du sillon. De plus, les deux mutants déficients en activité GAP, Tum 1-378 et TumΔYRL, utilisés dans notre étude étaient incapables de sauver la cytokinèse dans les cellules S2. Ces résultats sont en accord avec le travail précédemment publié sur des embryons de *Drosophila* où TumΔYRL n'a pas réussi à sauver la cytokinèse dans les cellules d'ectoderme (Zavortink et al., 2005). Ceci dit, les cellules qui ont réussi à initier un sillon de

clivage, ont quand même échoué à former un AM stable, suggérant qu'il y ai une seconde phase critique pour l'activité GAP au cours de la cytokinèse, dans ce cas pendant la transition de l'AC à l'AM. Nos résultats montrent également que le domaine central de RacGAP^{Tum} contribue à l'initiation du sillon de clivage. En effet, les cellules exprimant le mutant TumΔCD étaient incapables d'initier un sillon de clivage, bien qu'elles contenaient le domaine GAP. Il reste néanmoins à déterminer si ce phénotype est dû à des défauts au niveau de la structure de la protéine suite a la délétion de ce domaine, ou alternativement reflètent une fonction de ce domaine dans l'initiation du sillon.

L'autre question qui demeure non résolue est comment l'activité GAP contribue à l'activation de Rho lors de la cytokinèse. Les études publiées à ce jour proposent un rôle de RacGAP^{Tum} dans l'activation (plutôt que l'inactivation) de Rho, soit en facilitant le flux de cycle de la GTPase Rho (Miller et al., 2009), ce qui serait bénéfique pour établir une zone étroite de Rho-GTP, ou en stimulant l'activité GEF de la RhoGEF ^{ECT2} (Loria et al., 2012; Tse et al., 2012; Zhang et al., 2015; pour plus de détails voir Chapitre 1). Récemment une interaction directe entre le domaine GEF de la RhoGEF^{ECT2} et le domaine GAP de RacGAP^{CYK-4} a été rapportée chez *C. elegans*. La conservation de ce complexe et son mécanisme d'action pour l'activation de Rho restent des questions à adresser dans les études à venir (Zhang and Glotzer, 2015).

7.6 L'ANILLINE CONTRIBUE A L'ETABLISSEMENT DU SILLON DE CLIVAGE

En plus de son rôle comme protéine d'échafaudage et d'ancrage lors de la transition de l'AC à l'AM, les résultats décrits dans le cadre de cette thèse révèlent un rôle pour l'Anilline dans l'établissement du sillon de clivage. À elle seule, la déplétion de l'Anilline n'abolit pas la formation du sillon de clivage et l'assemblage de l'AC mais déstabilise le sillon de clivage, ce qui se manifeste par des bourgeonnements membranaires à l'équateur et des oscillations latérales du sillon de clivage. Cependant, la déplétion de l'Anilline dans les cellules où la fonction de RacGAP^{Tum} est sensibilisée bloque l'initiation du sillon, suggérant une redondance ou une synergie entre l'Anilline et RacGAP^{Tum} dans l'initiation du sillon. De plus, il semble que cette régulation se fasse via l'activation de Rho. En effet, en utilisant la myosine comme

rapporteur de l'activation de Rho, nous observons que les cellules appauvries en Anilline ou en RacGAP^{Tum} conservent un certain niveau d'activation de Rho. Cependant, la co-déplétion d'Anilline et de RacGAP^{Tum} bloque complètement l'activation de Rho, un phénotype similaire à celui qu'on observe après la déplétion de RhoGEF^{ECT2} (Chapitre 6).

Ce n'est pas la première fois que cette redondance entre l'Anilline et le complexe centralspinslin est observée. En effet, dans les cellules humaines, l'Anilline n'est pas nécessaire au recrutement de l'actine et de la myosine à l'équateur. Cependant, elle devient cruciale pour leur enrichissement lorsque le fuseau central est perturbé par la déplétion de MKLP1 (Piekny and Glotzer, 2008; Van Oostende Triplet et al., 2014). Chez *C. elegans*, ANI-1, normalement dispensable pour la cytokinèse du zygote, devient nécessaire pour l'insertion complète du sillon lorsque la kinésine-6, ZEN-4, est déplétée (Werner and Glotzer, 2008). Ensembles ces résultats suggèrent que l'Anilline et centralspindlin fonctionnent de manière redondante dans la spécification équatoriale ou l'activation de Rho. Comment ces deux composantes agissent ensembles pour favoriser l'activation de Rho reste à élucider, cependant plusieurs modèles non exclusifs peuvent être proposés.

Dans les cellules humaines, l'Anilline n'interagit pas avec MgcRacGAP mais se lie directement à RhoGEF^{ECT2}. Un complexe Anilline-RhoGEF^{ECT2}-Rho est formé au niveau du cortex et postulé pour lier le fuseau mitotique au cortex pendant la cytokinèse. Fait intéressant, c'est le contraire chez *Drosophila*. L'Anilline interagit directement avec RacGAP^{Tum} mais pas avec la RhoGEF^{Pebble}. Bien que nos résultats suggèrent qu'une interaction directe entre RacGAP^{Tum} et l'Anilline ne soit pas nécessaire à l'initiation du sillon de clivage. Un complexe contenant l'Anilline et Tum pourrait améliorer l'activation de Rho directement ou par l'intermédiaire de la RhoGEF^{Pebble} afin de maintenir l'activation de Rho à une zone discrète au niveau du cortex équatorial.

Par ailleurs, bien que l'Anilline soit un marqueur proéminent du cortex, plusieurs études ont également rapporté des interactions entre l'Anilline et les microtubules. En effet, l'Anilline interagit avec les MTs dans les embryons de *C. elegans* et est enrichie sur les MTs associées à des invaginations membranaires (Tse et al., 2011). Une interaction entre l'Anilline et les MTs a également été rapportée dans les cellules humaines et une liaison directe peut être

reconstituée *in vitro* (Triplet et al, 2014). Chez *Drosophila*, l'Anilline a été purifiée grâce à son affinité pour les MTs stabilisés au taxol (Sisson et al., 2000). Dans les cellules de *Drosophila* traitées avec la Latrunculine A, une drogue qui mène à la perte des filaments d'actine, l'Anilline produit des structures filamenteuses qui sont souvent associées aux extrémités positives des MTs astraux stabilisés au niveau du cortex équatorial (D'Avino et al., 2008; Hickson and O'Farrell, 2008). Ainsi, par son interaction avec $RacGAP^{Tum}$ et les MTs, l'Anilline pourrait lier le sillon naissant aux MTs au niveau de l'équateur permettant ainsi de former un sillon robuste et stable (non-oscillatoire) et favoriser son ingression.

Chez *C. elegans* et les cellules humaines, l'Anilline semble également agir de façon redondante avec le fuseau central pour la spécification du sillon de clivage. En effet, la co-déplétion de MKLP1 et de l'Anilline bloque l'initiation du sillon de clivage et cause une relocalisation de la myosine autour de l'ensemble du cortex. Par ailleurs, la stabilisation des MTs astraux, dans les cellules où l'Anilline est déplétée restaure la localisation de la myosine au cortex équatorial. Ces observations ont donné naissance à un modèle qui propose que l'Anilline module le cortex à travers une voie astrale. Dans ces systèmes, il est proposé que l'Anilline interagisse avec les MTs astraux adjacents au cortex équatorial et cette interaction prévient son recrutement au cortex et son interaction avec Rho (van Oostende Triplet et al., 2014). Ce faisant, l'Anilline pourrait affiner la localisation des protéines corticales près du cortex équatorial permettant ainsi l'activation de Rho et le recrutement des composantes de l'AC à une zone discrète au sein du cortex équatorial. Ainsi, dans ce modèle, centralspindlin au niveau du fuseau central favorise l'accumulation de Rho dans une région précise à l'équateur alors que l'association de l'Anilline aux MTs astraux restreint la localisation de Rho hors de l'équateur et contribue à la définition des cortex polaire et équatorial. La collaboration de ces deux voies permettrait la formation du sillon de clivage et d'un AC robuste en anaphase (Lewellyn et al., 2010; van Oostende Triplet et al., 2014). Ainsi, en appauvrissant les cellules en Anilline et en sensibilisant le fuseau central, on affaiblirait les deux voies nécessaires à l'établissement d'une zone active de Rho, ce qui empêcherait la formation du sillon.

7.7 MODELE RECAPITULATIF

La relation d'interdépendance entre le fuseau central et l'AC a été établie il y a longtemps par des études de micromanipulation et des études fonctionnelles dans différents systèmes expérimentaux (Alsop et al., 2004; Rappaport et al., 1985 ; revue dans D'Avino, 2005). En effet, il est clair que le fuseau mitotique dicte la formation et le positionnement du sillon de clivage et que ces deux structures sont interdépendantes tout au long de la cytokinèse, cependant, il reste mal compris comment. Nos travaux ont permis d'établir que la protéine d'échafaudage Anilline est le principal régulateur de la transition de l'AC à l'AM (El-Amine et al. 2013; Kechad et al., 2012) et nous postulons que RacGAP^{Tum} a un rôle équivalent dans la transition du fuseau central au midbody. L'Anilline et RacGAP^{Tum} partagent de nombreux partenaires d'interactions que ce soit au niveau du cortex ou au niveau des MTs. À travers ces interactions ils forment différents complexes qui connectent et régulent un réseau moléculaire composé de protéines associées au microtubules, au cortex et à la membrane et permettent d'établir un sillon de clivage robuste et lient la transition de l'AC à l'AM avec la maturation du fuseau central en midbody **(Figure 7.1)**.

Nous proposons un modèle où RacGAP^{Tum} localise et agit principalement à partir du fuseau central et organise les complexes de signalisation responsables de l'établissement du sillon de clivage; alors que l'Anilline localise et agit majoritairement au niveau du cortex comme protéine d'échafaudage majeure qui concentre les signaux provenant de différents éléments de la machinerie au niveau du cortex équatorial afin de maintenir un sillon de clivage robuste et assurer la transition de l'AC à l'AM.

Formation du fuseau central et Initiation du sillon de clivage

RacGAP^{Tum} en complexe avec kinésine-6^{Pav} forment centralspindlin qui permet la formation du fuseau central et le recrutement de la RhoGEF^{Pebble} **(Figure 7.1A)**. Le fuseau central agit comme un bassin d'entreposage de ce complexe de signalisation et permet sa propagation vers le cortex équatorial où il permet l'activation de Rho. À son tour, Rho va permettre le recrutement de l'Anilline au cortex équatorial. Ainsi, au niveau du cortex, on pourrait imaginer un complexe regroupant la RhoGEF^{pebble}, Rho, RacGAP^{Tum} et l'Anilline qui servirait a renforcer l'activité GEF de RhoGEF^{pebble} où réduire l'activité GAP de RacGAP^{Tum}

et augmenter le bassin de Rho au cortex. En soutien à cette idée, on sait par exemple que le recrutement de l'Anilline nécessite l'activation de Rho mais la déplétion de l'Anilline cause un étalement de la zone équatoriale où Rho est active (Piekny and Glotzer, 2008). On sait également qu'à cette étape, l'Anilline et RhoGEF^{ECT2} sont indépendamment liées au PIPs de la membrane équatoriale via leur domaine PH respectifs (Liu et al., 2012; Su et al., 2011) et que ces liaisons sont requises pour l'établissement d'un sillon de clivage robuste et l'ancrage de l'AC au niveau de l'équateur **(Figure 7.1B)**.

LA transition de l'AC à l'AM

Une fois l'AC formé, il commence à se fermer afin de donner naissance à l'AM. Cette transition est accompagnée par une maturation du fuseau central en un midbody. Ces deux processus sont interdépendants et nécessitent des interactions coopératives entre les composantes de l'AC et du fuseau central tout au long de la transition. Au niveau de l'AC, l'extrémité N-terminale de l'Anilline qui lie la myosine et l'actine est nécessaire est suffisante à la formation de l'AC et sa transition vers un AM. L'extrémité C-terminale est quand à elle nécessaire pour la maturation du midbody. Une interaction potentielle entre l'Anilline et RacGAP^{Tum} qui renforce le recrutement robuste de RacGAP^{Tum} au cortex est également nécessaire à la transition de l'AC à l'AM et à la maturation du midbody. Un tel complexe pourrait servir à lier l'AC aux MTs tout au long de la fermeture de l'anneau **(Figure 7.1C)**. La fermeture de l'AC se fait par désassemblage de l'actine et de la myosine à l'intérieur de la cellule. En parallèle, la kinase Citron et les septines régissent respectivement la rétention et l'élimination de la membrane excédentaire et des protéines associées comme l'Anilline, les septines et RacGAP^{Tum} hors du cortex équatorial.

Formation et ancrage du pont intercellulaire

Au niveau des microtubules, la kinase Citron organise la formation du midbody en régulant un réseau moléculaire de composantes de l'anneau contractile et de protéines associées aux microtubules. Ainsi, Citron, interagit directement avec deux kinésines, KIF-14 et kinésine-6$^{MKLP1/Pav}$, qui à leur tour interagissent entre elles et avec une autre protéine du fuseau central, PRC1. Citron recrute KIF-4 au sillon de clivage, et les deux protéines sont nécessaires pour la formation du midbody (Bassi et al., 2013). Le midbody, l'AM mature et

les MTs restants forment finalement le pont intercellulaire (**Figure 7.1D**). Cette structure doit rester ancrée à la membrane jusqu'à l'abscission qui finalisera le processus de cytokinèse. L'ancrage de l'AM à la membrane est régi par le domaine PH de l'Anilline et les septines (Kechad et al., 2012). McgRacGAP est également essentiel pour l'ancrage du midbody/AM à la membrane via son domaine C1 (Lekomtsev et al., 2012; Chapitre 6 de cette thèse). Toutes ces étapes doivent être réussies afin que les cellules procèdent à l'ultime étape de la cytokinèse qu'est l'abscission.

Bien que ce modèle reste incomplet et n'adresse pas toute la complexité de la cytokinèse, il met en évidence la coopération entre les trois éléments majeurs de la machinerie de la cytokinèse : la membrane, le cortex et les microtubules. Des complexes hétérogènes contenants des composantes de chacun de ces éléments sont formés tout au long de la cytokinèse et sont nécessaires à son succès. Il souligne également deux caractéristiques remarquables de la machinerie de la cytokinèse. D'une part, on constate que les mêmes complexes protéiques agissent de façon redondante lors d'une même étape. Cette combinaison permet à la cellule d'employer un nombre restreint de protéines pour effectuer un processus très complexe tout en assurant une grande robustesse. On devra tenir compte de ces caractéristiques lors de futures études et interpréter les résultats de perte de fonction en conséquence. Les déplétions de gènes nous ont permis d'identifier les composantes clés de la machinerie mais à l'avenir, il faudrait favoriser des approches de mutagénèse ciblée, afin de disséquer les différentes fonctions de chaque protéine à différents temps au cours de la cytokinèse. Il serait également intéressant d'exploiter les nouvelles techniques de microscopies par super-résolution afin de raffiner la caractérisation des composantes déjà connues, leur localisation, l'identification de nouveaux partenaires d'interactions, etc. Ces approches, couplées à de nouvelles approches telles que la reconstitution *in vitro* ou la modélisation informatique fourniront de nouvelles voies pour améliorer notre compréhension de ce processus complexe.

Par ailleurs, bien que les études sur les lignées cellulaires aient mis en évidence la plupart des éléments décris dans ce modèle, des études plus approfondies sont nécessaires pour comprendre comment ces modèles se rapportent à la division des cellules dans les tissus *in vivo*, et comment l'environnement extracellulaire et les cellules voisines influencent la

cytokinèse. Il est nécessaire de comprendre ce processus dans un contexte normal afin de comprendre comment son dérèglement peut causer des maladies, tel que le cancer, et exploiter les composantes de la machinerie comme cible potentielles pour les traiter.

A) **Formation du fuseau central**

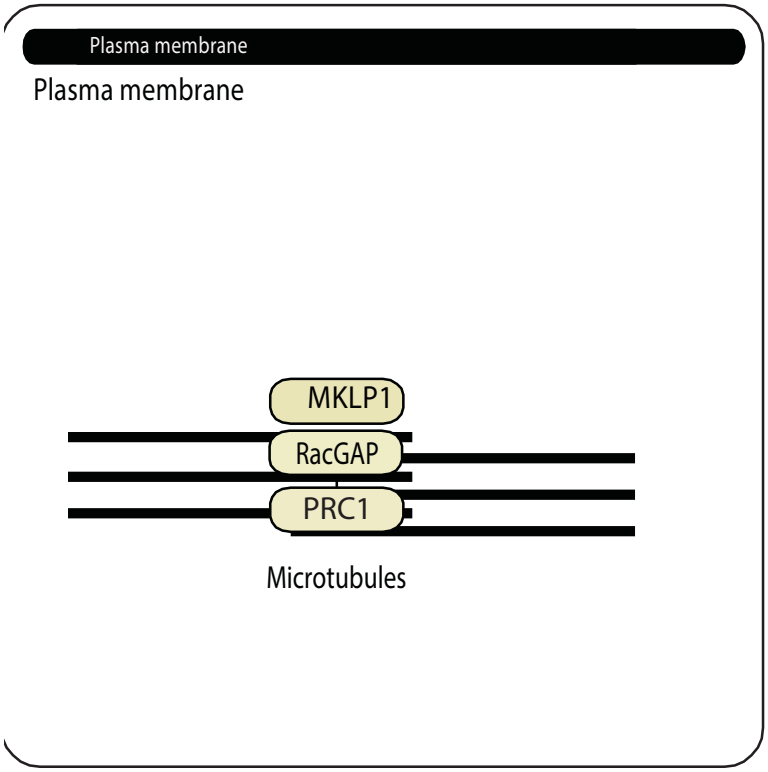

B) **Initiation du sillon de clivage**

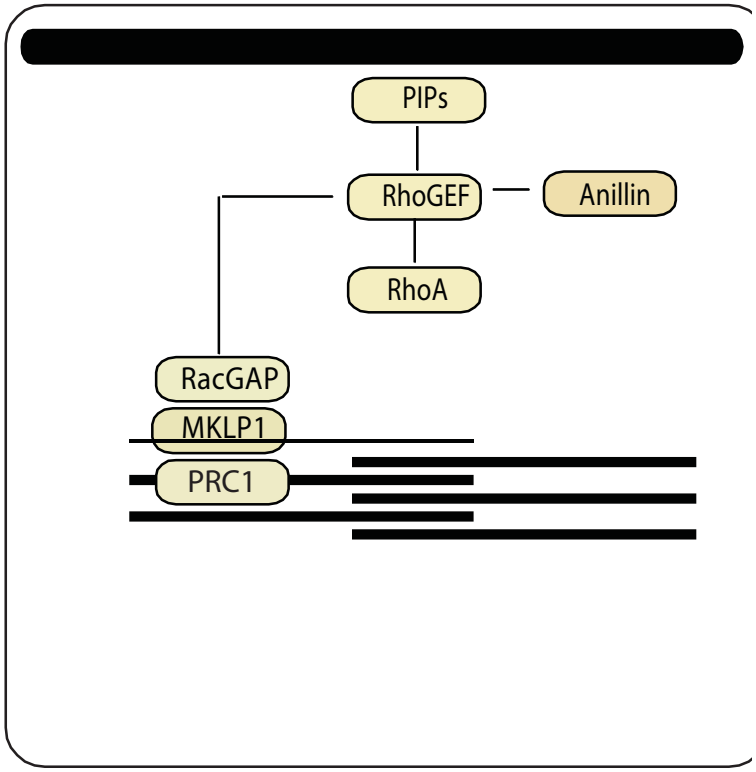

C) **Transition de l'AC à l'AM**

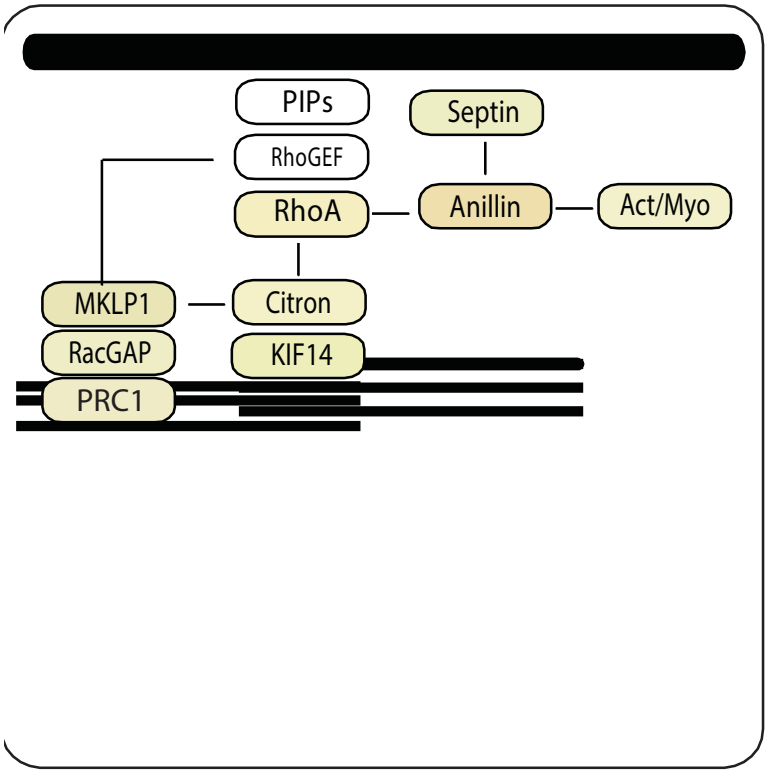

D) **Ancrage du pont intercellulaire**

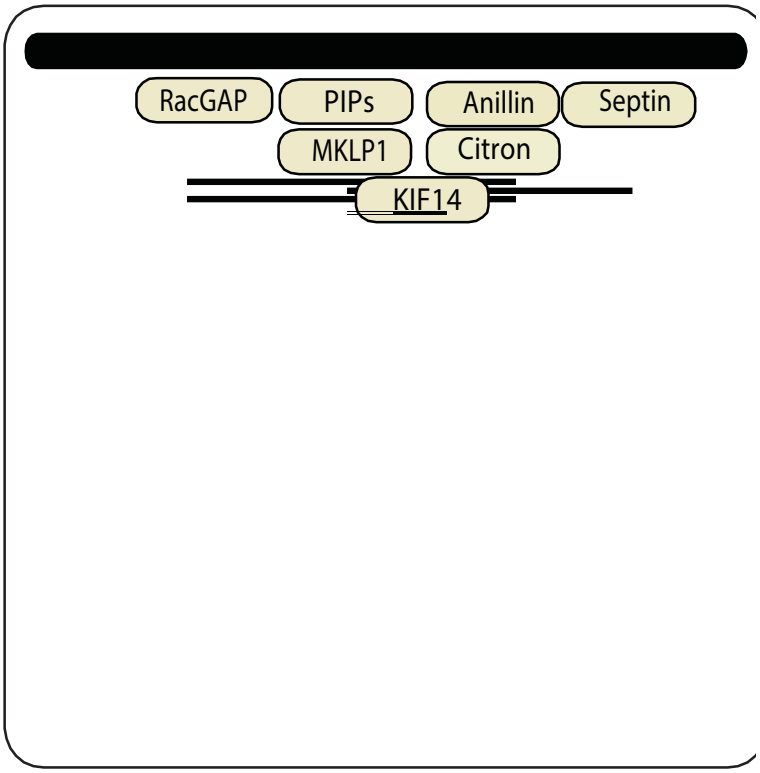

Figure 7.1 Modèle recapitulatif

Représentation des complexes qui connectent et régulent un réseau moléculaire composé de protéines associées aux microtubules, au cortex et à la membrane et permettent d'établir un sillon de clivage robuste et lient la transition de l'AC à l'AM avec la maturation du fuseau central en midbody.

8 BIBLIOGRAPHIE

Adam, J.C., J.R. Pringle, and M. Peifer. 2000. Evidence for functional differentiation among Drosophila septins in cytokinesis and cellularization. *Mol Biol Cell*. 11:3123-3135.

Adams, R.R., A.A. Tavares, A. Salzberg, H.J. Bellen, and D.M. Glover. 1998. pavarotti encodes a kinesin-like protein required to organize the central spindle and contractile ring for cytokinesis. *Genes Dev*. 12:1483-1494.

Alberts, A.S. 2001. Identification of a carboxyl-terminal diaphanous-related formin homology protein autoregulatory domain. *J Biol Chem*. 276:2824-2830.

Albertson, R., B. Riggs, and W. Sullivan. 2005. Membrane traffic: a driving force in cytokinesis. *Trends Cell Biol*. 15:92-101.

Amano, M., M. Ito, K. Kimura, Y. Fukata, K. Chihara, T. Nakano, Y. Matsuura, and K. Kaibuchi. 1996. Phosphorylation and activation of myosin by Rho-associated kinase (Rho-kinase). *J Biol Chem*. 271:20246-20249.

Barr, F.A., and U. Gruneberg. 2007. Cytokinesis: placing and making the final cut. *Cell*. 131:847-860.

Basant, A., and M. Glotzer. 2017. A GAP that Divides. *F1000Res*. 6:1788.

Basit, S., K.M. Al-Harbi, S.A. Alhijji, A.M. Albalawi, E. Alharby, A. Eldardear, and M.I. Samman. 2016. CIT, a gene involved in neurogenic cytokinesis, is mutated in human primary microcephaly. *Hum Genet*. 135:1199-1207.

Bassi, Z.I., M. Audusseau, M.G. Riparbelli, G. Callaini, and P.P. D'Avino. 2013. Citron kinase controls a molecular network required for midbody formation in cytokinesis. *Proc Natl Acad Sci U S A*. 110:9782-9787.

Bassi, Z.I., K.J. Verbrugghe, L. Capalbo, S. Gregory, E. Montembault, D.M. Glover, and P. D'Avino. 2011. Sticky/Citron kinase maintains proper RhoA localization at the cleavage site during cytokinesis. *The Journal of Cell Biology*. 195:595-603.

Bastos, R.N., and F.A. Barr. 2010. Plk1 negatively regulates Cep55 recruitment to the midbody to ensure orderly abscission. *J Cell Biol*. 191:751-760.

Bastos, R.N., X. Penate, M. Bates, D. Hammond, and F.A. Barr. 2012. CYK4 inhibits Rac1-dependent PAK1 and ARHGEF7 effector pathways during cytokinesis. *J Cell Biol*. 198:865-880.

Bement, W.M., H.A. Benink, and G. von Dassow. 2005. A microtubule-dependent zone of active RhoA during cleavage plane specification. *The Journal of Cell Biology*. 170:91-101.

Ben El Kadhi, K., C. Roubinet, S. Solinet, G. Emery, and S. Carreno. 2011. The inositol 5-phosphatase dOCRL controls PI(4,5)P2 homeostasis and is necessary for cytokinesis. *Curr Biol*. 21:1074-1079.

Bonaccorsi, S., M.G. Giansanti, and M. Gatti. 1998. Spindle self-organization and cytokinesis during male meiosis in asterless mutants of Drosophila melanogaster. *J Cell Biol*. 142:751-761.

Brennan, I.M., U. Peters, T.M. Kapoor, and A.F. Straight. 2007. Polo-like kinase controls vertebrate spindle elongation and cytokinesis. *PLoS One*. 2:e409.

Brill, J.A., G.R. Hime, M. Scharer-Schuksz, and M.T. Fuller. 2000. A phospholipid kinase regulates actin organization and intercellular bridge formation during germline cytokinesis. *Development*. 127:3855-3864.

Brill, J.A., R. Wong, and A. Wilde. 2011. Phosphoinositide function in cytokinesis. *Curr Biol*. 21:R930-934.

Bringmann, H., and A.A. Hyman. 2005. A cytokinesis furrow is positioned by two consecutive signals. *Nature*. 436:731-734.

Burgess, D.R., and F. Chang. 2005. Site selection for the cleavage furrow at cytokinesis. *Trends in Cell Biology*. 15:156-162.

Cai, K.Q., C. Caslini, C.D. Capo-chichi, C. Slater, E.R. Smith, H. Wu, A.J. Klein-Szanto, A.K. Godwin, and X.X. Xu. 2009. Loss of GATA4 and GATA6 expression specifies ovarian cancer histological subtypes and precedes neoplastic transformation of ovarian surface epithelia. *PLoS One*. 4:e6454.

Canman, J.C., L.A. Cameron, P.S. Maddox, A. Straight, J.S. Tirnauer, T.J. Mitchison, G. Fang, T.M. Kapoor, and E.D. Salmon. 2003. Determining the position of the cell division plane. *Nature*. 424:1074-1078.

Canman, J.C., L. Lewellyn, K. Laband, S.J. Smerdon, A. Desai, B. Bowerman, and K. Oegema. 2008. Inhibition of Rac by the GAP activity of centralspindlin is essential for cytokinesis. *Science*. 322:1543-1546.

Carlton, J.G., A. Caballe, M. Agromayor, M. Kloc, and J. Martin-Serrano. 2012. ESCRT-III governs the Aurora B-mediated abscission checkpoint through CHMP4C. *Science*. 336:220-225.

Carlton, J.G., and J. Martin-Serrano. 2007. Parallels between cytokinesis and retroviral budding: a role for the ESCRT machinery. *Science*. 316:1908-1912.

Carvalho, A., A. Desai, and K. Oegema. 2009. Structural memory in the contractile ring makes the duration of cytokinesis independent of cell size. *Cell*. 137:926-937.

Castrillon, D.H., and S.A. Wasserman. 1994. Diaphanous is required for cytokinesis in Drosophila and shares domains of similarity with the products of the limb deformity gene. *Development*. 120:3367-3377.

Cauvin, C., and A. Echard. 2015. Phosphoinositides: Lipids with informative heads and mastermind functions in cell division. *Biochim Biophys Acta*. 1851:832-843.

Chalamalasetty, R.B., S. Hümmer, E.A. Nigg, and H.H.W. Silljé. 2006. Influence of human Ect2 depletion and overexpression on cleavage furrow formation and abscission. *Journal of cell science*. 119:3008-3019.

Chen, C.T., A.W. Ettinger, W.B. Huttner, and S.J. Doxsey. 2013. Resurrecting remnants: the lives of post-mitotic midbodies. *Trends Cell Biol*. 23:118-128.

Crowell, E.F., A.L. Gaffuri, B. Gayraud-Morel, S. Tajbakhsh, and A. Echard. 2014. Engulfment of the midbody remnant after cytokinesis in mammalian cells. *J Cell Sci*. 127:3840-3851.

D'Avino, P., M.S. Savoian, and D.M. Glover. 2004. Mutations in sticky lead to defective organization of the contractile ring during cytokinesis and are enhanced by Rho and suppressed by Rac. *The Journal of Cell Biology*. 166:61-71.

D'Avino, P.P. 2009. How to scaffold the contractile ring for a safe cytokinesis - lessons from Anillin-related proteins. *J Cell Sci*. 122:1071-1079.

D'Avino, P.P. 2017. Citron kinase - renaissance of a neglected mitotic kinase. *J Cell Sci*. 130:1701-1708.

D'Avino, P.P., and L. Capalbo. 2016. Regulation of midbody formation and function by mitotic kinases. *Semin Cell Dev Biol*. 53:57-63.

D'Avino, P.P., M.S. Savoian, and D.M. Glover. 2005. Cleavage furrow formation and ingression during animal cytokinesis: a microtubule legacy. *J Cell Sci*. 118:1549-1558.

D'Avino, P.P., T. Takeda, L. Capalbo, W. Zhang, K.S. Lilley, E.D. Laue, and D.M. Glover. 2008. Interaction between Anillin and RacGAP50C connects the actomyosin contractile ring with spindle microtubules at the cell division site. *J Cell Sci*. 121:1151-1158.

Dambournet, D., M. Machicoane, L. Chesneau, M. Sachse, M. Rocancourt, A. El Marjou, E. Formstecher, R. Salomon, B. Goud, and A. Echard. 2011. Rab35 GTPase and OCRL phosphatase remodel lipids and F-actin for successful cytokinesis. *Nat Cell Biol*. 13:981-988.

Davoli, T., and T. de Lange. 2012. Telomere-driven tetraploidization occurs in human cells undergoing crisis and promotes transformation of mouse cells. *Cancer Cell*. 21:765-776.

DeBiasio, R.L., G.M. LaRocca, P.L. Post, and D.L. Taylor. 1996. Myosin II transport, organization,

and phosphorylation: evidence for cortical flow/solation-contraction coupling during cytokinesis and cell locomotion. *Mol Biol Cell*. 7:1259-1282.
Dechant, R., and M. Glotzer. 2003. Centrosome separation and central spindle assembly act in redundant pathways that regulate microtubule density and trigger cleavage furrow formation. *Dev Cell*. 4:333-344.
Douglas, M.E., T. Davies, N. Joseph, and M. Mishima. 2010. Aurora B and 14-3-3 Coordinately Regulate Clustering of Centralspindlin during Cytokinesis. *Current Biology*. 20:927-933.
Dubreuil, V., A.M. Marzesco, D. Corbeil, W.B. Huttner, and M. Wilsch-Brauninger. 2007. Midbody and primary cilium of neural progenitors release extracellular membrane particles enriched in the stem cell marker prominin-1. *J Cell Biol*. 176:483-495.
Echard, A., G.R.X. Hickson, E. Foley, and P.H. O'Farrell. 2004. Terminal cytokinesis events uncovered after an RNAi screen. *Current biology : CB*. 14:1685-1693.
Eda, M., S. Yonemura, T. Kato, N. Watanabe, T. Ishizaki, P. Madaule, and S. Narumiya. 2001. Rho-dependent transfer of Citron-kinase to the cleavage furrow of dividing cells. *Journal of cell science*. 114:3273-3284.
Eggert, U.S., A.A. Kiger, C. Richter, Z.E. Perlman, N. Perrimon, T.J. Mitchison, and C.M. Field. 2004. Parallel chemical genetic and genome-wide RNAi screens identify cytokinesis inhibitors and targets. *PLoS Biol*. 2:e379.
Eggert, U.S., T.J. Mitchison, and C.M. Field. 2006. Animal Cytokinesis: From Parts List to Mechanisms. *Biochemistry*. 75:543-566.
Elia, N., G. Fabrikant, M.M. Kozlov, and J. Lippincott-Schwartz. 2012. Computational model of cytokinetic abscission driven by ESCRT-III polymerization and remodeling. *Biophys J*. 102:2309-2320.
Elia, N., R. Sougrat, T.A. Spurlin, J.H. Hurley, and J. Lippincott-Schwartz. 2011. Dynamics of endosomal sorting complex required for transport (ESCRT) machinery during cytokinesis and its role in abscission. *Proc Natl Acad Sci U S A*. 108:4846-4851.
Engel, F.B., M. Schebesta, and M.T. Keating. 2006. Anillin localization defect in cardiomyocyte binucleation. *J Mol Cell Cardiol*. 41:601-612.
Estey, M.P., C. Ciano-Oliveira, C.D. Froese, M.T. Bejide, and W.S. Trimble. 2010. Distinct roles of septins in cytokinesis: SEPT9 mediates midbody abscission. *The Journal of Cell Biology*. 191:741-749.
Ettinger, A.W., M. Wilsch-Brauninger, A.M. Marzesco, M. Bickle, A. Lohmann, Z. Maliga, J. Karbanova, D. Corbeil, A.A. Hyman, and W.B. Huttner. 2011. Proliferating versus differentiating stem and cancer cells exhibit distinct midbody-release behaviour. *Nat Commun*. 2:503.
Fares, H., M. Peifer, and J.R. Pringle. 1995. Localization and possible functions of Drosophila septins. *Mol Biol Cell*. 6:1843-1859.
Field, C.M., and B.M. Alberts. 1995. Anillin, a contractile ring protein that cycles from the nucleus to the cell cortex. *J Cell Biol*. 131:165-178.
Field, C.M., M. Coughlin, S. Doberstein, T. Marty, and W. Sullivan. 2005a. Characterization of anillin mutants reveals essential roles in septin localization and plasma membrane integrity. *Development*. 132:2849-2860.
Field, C.M., M. Coughlin, S. Doberstein, T. Marty, and W. Sullivan. 2005b. Characterization of anillin mutants reveals essential roles in septin localization and plasma membrane integrity. *Development*. 132:2849-2860.
Field, S.J., N. Madson, M.L. Kerr, K.A. Galbraith, C.E. Kennedy, M. Tahiliani, A. Wilkins, and L.C. Cantley. 2005c. PtdIns(4,5)P2 functions at the cleavage furrow during cytokinesis. *Curr Biol*. 15:1407-1412.
Flemming, W. 1965. Contributions to the Knowledge of the Cell and Its Vital Processes. *J Cell Biol*.

25:3-69.
Frenette, P., E. Haines, M. Loloyan, M. Kinal, P. Pakarian, and A. Piekny. 2012. An anillin-Ect2 complex stabilizes central spindle microtubules at the cortex during cytokinesis. *PLoS One*. 7:e34888.
Fujiwara, T., M. Bandi, M. Nitta, E.V. Ivanova, R.T. Bronson, and D. Pellman. 2005. Cytokinesis failure generating tetraploids promotes tumorigenesis in p53-null cells. *Nature*. 437:1043-1047.
Gai, M., P. Camera, A. Dema, F. Bianchi, G. Berto, E. Scarpa, G. Germena, and F. Cunto. 2011. Citron kinase controls abscission through RhoA and anillin. *Molecular biology of the cell*. 22:3768-3778.
Gai, M., and F. Di Cunto. 2016. Citron kinase in spindle orientation and primary microcephaly. *Cell Cycle*:1-2.
Gatt, M.K., and D.M. Glover. 2006. The Drosophila phosphatidylinositol transfer protein encoded by vibrator is essential to maintain cleavage-furrow ingression in cytokinesis. *J Cell Sci*. 119:2225-2235.
Gbadegesin, R.A., G. Hall, A. Adeyemo, N. Hanke, I. Tossidou, J. Burchette, G. Wu, A. Homstad, M.A. Sparks, J. Gomez, R. Jiang, A. Alonso, P. Lavin, P. Conlon, R. Korstanje, M.C. Stander, G. Shamsan, M. Barua, R. Spurney, P.C. Singhal, J.B. Kopp, H. Haller, D. Howell, M.R. Pollak, A.S. Shaw, M. Schiffer, and M.P. Winn. 2014. Mutations in the gene that encodes the F-actin binding protein anillin cause FSGS. *J Am Soc Nephrol*. 25:1991-2002.
Gentric, G., C. Desdouets, and S. Celton-Morizur. 2012. Hepatocytes polyploidization and cell cycle control in liver physiopathology. *Int J Hepatol*. 2012:282430.
Giansanti, M.G., S. Bonaccorsi, and M. Gatti. 1999. The role of anillin in meiotic cytokinesis of Drosophila males. *J Cell Sci*. 112 (Pt 14):2323-2334.
Giansanti, M.G., S. Bonaccorsi, R. Kurek, R.M. Farkas, P. Dimitri, M.T. Fuller, and M. Gatti. 2006. The class I PITP giotto is required for Drosophila cytokinesis. *Curr Biol*. 16:195-201.
Gilden, J., and M.F. Krummel. 2010. Control of cortical rigidity by the cytoskeleton: emerging roles for septins. *Cytoskeleton (Hoboken)*. 67:477-486.
Glotzer, M. 2005. The molecular requirements for cytokinesis. *Science (New York, N.Y.)*. 307:1735-1739.
Glotzer, M. 2009. The 3Ms of central spindle assembly: microtubules, motors and MAPs. *Nature reviews. Molecular cell biology*. 10:9-20.
Goldbach, P., R. Wong, N. Beise, R. Sarpal, W.S. Trimble, and J.A. Brill. 2010. Stabilization of the actomyosin ring enables spermatocyte cytokinesis in Drosophila. *Mol Biol Cell*. 21:1482-1493.
Goldstein, A.Y., Y.N. Jan, and L. Luo. 2005. Function and regulation of Tumbleweed (RacGAP50C) in neuroblast proliferation and neuronal morphogenesis. *Proc Natl Acad Sci U S A*. 102:3834-3839.
Green, R.A., E. Paluch, and K. Oegema. 2012. Cytokinesis in animal cells. *Annual review of cell and developmental biology*. 28:29-58.
Greenbaum, M.P., L. Ma, and M.M. Matzuk. 2007. Conversion of midbodies into germ cell intercellular bridges. *Dev Biol*. 305:389-396.
Gregory, S.L., S. Ebrahimi, J. Milverton, W.M. Jones, A. Bejsovec, and R. Saint. 2008. Cell division requires a direct link between microtubule-bound RacGAP and Anillin in the contractile ring. *Curr Biol*. 18:25-29.
Gromley, A., C. Yeaman, J. Rosa, S. Redick, C.T. Chen, S. Mirabelle, M. Guha, J. Sillibourne, and S.J. Doxsey. 2005. Centriolin anchoring of exocyst and SNARE complexes at the midbody is required for secretory-vesicle-mediated abscission. *Cell*. 123:75-87.
Gruneberg, U., R. Neef, X. Li, E. Chan, R.B. Chalamalasetty, E.A. Nigg, and F.A. Barr. 2006a. KIF14

and citron kinase act together to promote efficient cytokinesis. *The Journal of Cell Biology*. 172:363-372.

Gruneberg, U., R. Neef, X. Li, E.H. Chan, R.B. Chalamalasetty, E.A. Nigg, and F.A. Barr. 2006b. KIF14 and citron kinase act together to promote efficient cytokinesis. *J Cell Biol*. 172:363-372.

Guizetti, J., and D.W. Gerlich. 2010. Cytokinetic abscission in animal cells. *Seminars in cell & developmental biology*. 21:909-916.

Guizetti, J., L. Schermelleh, J. Mantler, S. Maar, I. Poser, H. Leonhardt, T. Muller-Reichert, and D.W. Gerlich. 2011. Cortical constriction during abscission involves helices of ESCRT-III-dependent filaments. *Science*. 331:1616-1620.

Haglund, K., I.P. Nezis, D. Lemus, C. Grabbe, J. Wesche, K. Liestol, I. Dikic, R. Palmer, and H. Stenmark. 2010. Cindr interacts with anillin to control cytokinesis in Drosophila melanogaster. *Curr Biol*. 20:944-950.

Hall, P.A., C.B. Todd, P.L. Hyland, S.S. McDade, H. Grabsch, M. Dattani, K.J. Hillan, and S.E. Russell. 2005. The septin-binding protein anillin is overexpressed in diverse human tumors. *Clin Cancer Res*. 11:6780-6786.

Harding, B.N., A. Moccia, S. Drunat, O. Soukarieh, H. Tubeuf, L.S. Chitty, A. Verloes, P. Gressens, V. El Ghouzzi, S. Joriot, F. Di Cunto, A. Martins, S. Passemard, and S.L. Bielas. 2016. Mutations in Citron Kinase Cause Recessive Microlissencephaly with Multinucleated Neurons. *Am J Hum Genet*. 99:511-520.

Henne, W.M., N.J. Buchkovich, Y. Zhao, and S.D. Emr. 2012. The endosomal sorting complex ESCRT-II mediates the assembly and architecture of ESCRT-III helices. *Cell*. 151:356-371.

Hickson, G., and P.H. O'Farrell. 2008. Rho-dependent control of anillin behavior during cytokinesis. *The Journal of Cell Biology*. 180:285-294.

Hu, C.-K., M. Coughlin, and T.J. Mitchison. 2012. Midbody assembly and its regulation during cytokinesis. *Molecular Biology of the Cell*. 23:1024-1034.

Hu, C.K., M. Coughlin, C.M. Field, and T.J. Mitchison. 2011. KIF4 regulates midzone length during cytokinesis. *Curr Biol*. 21:815-824.

Hurley, J.H., and P.I. Hanson. 2010. Membrane budding and scission by the ESCRT machinery: it's all in the neck. *Nat Rev Mol Cell Biol*. 11:556-566.

Iwamori, T., N. Iwamori, L. Ma, M.A. Edson, M.P. Greenbaum, and M.M. Matzuk. 2010. TEX14 interacts with CEP55 to block cell abscission. *Mol Cell Biol*. 30:2280-2292.

Jananji, S., C. Risi, I.K.S. Lindamulage, L.P. Picard, R. Van Sciver, G. Laflamme, A. Albaghjati, G.R.X. Hickson, B.H. Kwok, and V.E. Galkin. 2017. Multimodal and Polymorphic Interactions between Anillin and Actin: Their Implications for Cytokinesis. *J Mol Biol*. 429:715-731.

Janetopoulos, C., and P. Devreotes. 2006. Phosphoinositide signaling plays a key role in cytokinesis. *J Cell Biol*. 174:485-490.

Jantsch-Plunger, V., P. Gonczy, A. Romano, H. Schnabel, D. Hamill, R. Schnabel, A.A. Hyman, and M. Glotzer. 2000. CYK-4: A Rho family gtpase activating protein (GAP) required for central spindle formation and cytokinesis. *J Cell Biol*. 149:1391-1404.

Joo, E., M.C. Surka, and W.S. Trimble. 2007. Mammalian SEPT2 Is Required for Scaffolding Nonmuscle Myosin II and Its Kinases. *Developmental Cell*. 13:677-690.

Jordan, P., and R. Karess. 1997. Myosin light chain-activating phosphorylation sites are required for oogenesis in Drosophila. *J Cell Biol*. 139:1805-1819.

Kamasaki, T., M. Osumi, and I. Mabuchi. 2007. Three-dimensional arrangement of F-actin in the contractile ring of fission yeast. *J Cell Biol*. 178:765-771.

Kanada, M., A. Nagasaki, and T.Q. Uyeda. 2005. Adhesion-dependent and contractile ring-independent equatorial furrowing during cytokinesis in mammalian cells. *Mol Biol Cell*. 16:3865-3872.

Kechad, A., and G.R. Hickson. 2017. Imaging cytokinesis of Drosophila S2 cells. *Methods Cell Biol*.

137:47-72.
Kimura, K., M. Ito, M. Amano, K. Chihara, Y. Fukata, M. Nakafuku, B. Yamamori, J. Feng, T. Nakano, K. Okawa, A. Iwamatsu, and K. Kaibuchi. 1996. Regulation of myosin phosphatase by Rho and Rho-associated kinase (Rho-kinase). *Science*. 273:245-248.
Kinoshita, M., S. Kumar, A. Mizoguchi, C. Ide, A. Kinoshita, T. Haraguchi, Y. Hiraoka, and M. Noda. 1997. Nedd5, a mammalian septin, is a novel cytoskeletal component interacting with actin-based structures. *Genes Dev*. 11:1535-1547.
Kitazawa, D., T. Matsuo, K. Kaizuka, C. Miyauchi, D. Hayashi, and Y.H. Inoue. 2014. Orbit/CLASP is required for myosin accumulation at the cleavage furrow in Drosophila male meiosis. *PLoS One*. 9:e93669.
Komatsu, S., T. Yano, M. Shibata, R.A. Tuft, and M. Ikebe. 2000. Effects of the regulatory light chain phosphorylation of myosin II on mitosis and cytokinesis of mammalian cells. *J Biol Chem*. 275:34512-34520.
Kouranti, I., M. Sachse, N. Arouche, B. Goud, and A. Echard. 2006. Rab35 regulates an endocytic recycling pathway essential for the terminal steps of cytokinesis. *Curr Biol*. 16:1719-1725.
Kovar, D.R., and T.D. Pollard. 2004. Insertional assembly of actin filament barbed ends in association with formins produces piconewton forces. *Proc Natl Acad Sci U S A*. 101:14725-14730.
Kunda, P., N.T. Rodrigues, E. Moeendarbary, T. Liu, A. Ivetic, G. Charras, and B. Baum. 2012. PP1-mediated moesin dephosphorylation couples polar relaxation to mitotic exit. *Curr Biol*. 22:231-236.
Kuo, T.C., C.T. Chen, D. Baron, T.T. Onder, S. Loewer, S. Almeida, C.M. Weismann, P. Xu, J.M. Houghton, F.B. Gao, G.Q. Daley, and S. Doxsey. 2011. Midbody accumulation through evasion of autophagy contributes to cellular reprogramming and tumorigenicity. *Nat Cell Biol*. 13:1214-1223.
Lacroix, B., and A. Maddox. 2012. Cytokinesis, ploidy and aneuploidy. *The Journal of Pathology*. 226:338-351.
Lafaurie-Janvore, J., P. Maiuri, I. Wang, M. Pinot, J.B. Manneville, T. Betz, M. Balland, and M. Piel. 2013. ESCRT-III assembly and cytokinetic abscission are induced by tension release in the intercellular bridge. *Science*. 339:1625-1629.
LaFlamme, S.E., B. Nieves, D. Colello, and C.G. Reverte. 2008. Integrins as regulators of the mitotic machinery. *Curr Opin Cell Biol*. 20:576-582.
Liu, J., G.D. Fairn, D.F. Ceccarelli, F. Sicheri, and A. Wilde. 2012. Cleavage furrow organization requires PIP(2)-mediated recruitment of anillin. *Curr Biol*. 22:64-69.
Liu, M., S. Shen, F. Chen, W. Yu, and L. Yu. 2010. Linking the septin expression with carcinogenesis. *Mol Biol Rep*. 37:3601-3608.
Loria, A., K.M. Longhini, and M. Glotzer. 2012. The RhoGAP domain of CYK-4 has an essential role in RhoA activation. *Curr Biol*. 22:213-219.
Madaule, P., M. Eda, N. Watanabe, K. Fujisawa, T. Matsuoka, H. Bito, T. Ishizaki, and S. Narumiya. 1998. Role of citron kinase as a target of the small GTPase Rho in cytokinesis. *Nature*. 394:491-494.
Madaule, P., T. Furuyashiki, M. Eda, H. Bito, T. Ishizaki, and S. Narumiya. 2000. Citron, a Rho target that affects contractility during cytokinesis. *Microscopy research and technique*. 49:123-126.
Maddox, A.S., B. Habermann, A. Desai, and K. Oegema. 2005. Distinct roles for two C. elegans anillins in the gonad and early embryo. *Development*. 132:2837-2848.
Maddox, A.S., L. Lewellyn, A. Desai, and K. Oegema. 2007. Anillin and the septins promote asymmetric ingression of the cytokinetic furrow. *Dev Cell*. 12:827-835.

Madhavan, J., M. Mitra, K. Mallikarjuna, O. Pranav, R. Srinivasan, A. Nagpal, P. Venkatesan, and G. Kumaramanickavel. 2009. KIF14 and E2F3 mRNA expression in human retinoblastoma and its phenotype association. *Mol Vis*. 15:235-240.

Magnusson, K., G. Gremel, L. Ryden, V. Ponten, M. Uhlen, A. Dimberg, K. Jirstrom, and F. Ponten. 2016. ANLN is a prognostic biomarker independent of Ki-67 and essential for cell cycle progression in primary breast cancer. *BMC Cancer*. 16:904.

Maiato, H., and M. Lince-Faria. 2010. The perpetual movements of anaphase. *Cell Mol Life Sci*. 67:2251-2269.

Manukyan, A., K. Ludwig, S. Sanchez-Manchinelly, S.J. Parsons, and P.T. Stukenberg. 2015. A complex of p190RhoGAP-A and anillin modulates RhoA-GTP and the cytokinetic furrow in human cells. *J Cell Sci*. 128:50-60.

Mathe, E., Y.H. Inoue, W. Palframan, G. Brown, and D.M. Glover. 2003. Orbit/Mast, the CLASP orthologue of Drosophila, is required for asymmetric stem cell and cystocyte divisions and development of the polarised microtubule network that interconnects oocyte and nurse cells during oogenesis. *Development*. 130:901-915.

Matsumura, F., G. Totsukawa, Y. Yamakita, and S. Yamashiro. 2001. Role of myosin light chain phosphorylation in the regulation of cytokinesis. *Cell structure and function*. 26:639-644.

Mavrakis, M., Y. Azou-Gros, F.C. Tsai, J. Alvarado, A. Bertin, F. Iv, A. Kress, S. Brasselet, G.H. Koenderink, and T. Lecuit. 2014. Septins promote F-actin ring formation by crosslinking actin filaments into curved bundles. *Nat Cell Biol*. 16:322-334.

Mazumdar, A., and M. Mazumdar. 2002. How one becomes many: blastoderm cellularization in Drosophila melanogaster. *Bioessays*. 24:1012-1022.

McIntosh, J.R., and S.C. Landis. 1971. The distribution of spindle microtubules during mitosis in cultured human cells. *J Cell Biol*. 49:468-497.

McKenzie, C., Z.I. Bassi, J. Debski, M. Gottardo, G. Callaini, M. Dadlez, and P.P. D'Avino. 2016. Cross-regulation between Aurora B and Citron kinase controls midbody architecture in cytokinesis. *Open Biol*. 6.

McKenzie, C., and P.P. D'Avino. 2016. Investigating cytokinesis failure as a strategy in cancer therapy. *Oncotarget*.

Menon, M.B., and M. Gaestel. 2015. Sep(t)arate or not – how some cells take septin-independent routes through cytokinesis. *Journal of cell science*. 128:1877-1886.

Mierzwa, B., and D.W. Gerlich. 2014. Cytokinetic abscission: molecular mechanisms and temporal control. *Dev Cell*. 31:525-538.

Miller, A.L. 2011. The contractile ring. *Curr Biol*. 21:R976-978.

Miller, A.L., and W.M. Bement. 2009. Regulation of cytokinesis by Rho GTPase flux. *Nat Cell Biol*. 11:71-77.

Miller, K.G., C.M. Field, and B.M. Alberts. 1989. Actin-binding proteins from Drosophila embryos: a complex network of interacting proteins detected by F-actin affinity chromatography. *J Cell Biol*. 109:2963-2975.

Mishima, M. 2016. Centralspindlin in Rappaport's cleavage signaling. *Seminars in Cell & Developmental Biology*. 53:45-56.

Mishima, M., S. Kaitna, and M. Glotzer. 2002. Central Spindle Assembly and Cytokinesis Require a Kinesin-like Protein/RhoGAP Complex with Microtubule Bundling Activity. *Developmental Cell*. 2:41-54.

Mishima, M., V. Pavicic, U. Grüneberg, E.A. Nigg, and M. Glotzer. 2004. Cell cycle regulation of central spindle assembly. *Nature*. 430:908-913.

Mitchison, T.J., and E.D. Salmon. 2001. Mitosis: a history of division. *Nat Cell Biol*. 3:E17-21.

Miyauchi, C., D. Kitazawa, I. Ando, D. Hayashi, and Y.H. Inoue. 2013. Orbit/CLASP is required for germline cyst formation through its developmental control of fusomes and ring canals in

Drosophila males. *PLoS One*. 8:e58220.
Mollinari, C., J.-P. Kleman, W. Jiang, G. Schoehn, T. Hunter, and R.L. Margolis. 2002. PRC1 is a microtubule binding and bundling protein essential to maintain the mitotic spindle midzone. *The Journal of cell biology*. 157:1175-1186.
Monzo, P., N.C. Gauthier, F. Keslair, A. Loubat, C.M. Field, Y. Le Marchand-Brustel, and M. Cormont. 2005. Clues to CD2-associated protein involvement in cytokinesis. *Mol Biol Cell*. 16:2891-2902.
Motegi, F., N.V. Velarde, F. Piano, and A. Sugimoto. 2006. Two phases of astral microtubule activity during cytokinesis in C. elegans embryos. *Dev Cell*. 10:509-520.
Mullins, J.M., and J.J. Biesele. 1973. Cytokinetic activities in a human cell line: the midbody and intercellular bridge. *Tissue Cell*. 5:47-61.
Nagata, Y., M.R. Jones, H.G. Nguyen, D.J. McCrann, C. St Hilaire, B.M. Schreiber, A. Hashimoto, M. Inagaki, W.C. Earnshaw, K. Todokoro, and K. Ravid. 2005. Vascular smooth muscle cell polyploidization involves changes in chromosome passenger proteins and an endomitotic cell cycle. *Exp Cell Res*. 305:277-291.
Naim, V., S. Imarisio, F. Di Cunto, M. Gatti, and S. Bonaccorsi. 2004. Drosophila citron kinase is required for the final steps of cytokinesis. *Mol Biol Cell*. 15:5053-5063.
Neto, H., L.L. Collins, and G.W. Gould. 2011. Vesicle trafficking and membrane remodelling in cytokinesis. *Biochemical Journal*. 437:13-24.
Neufeld, T.P., and G.M. Rubin. 1994. The Drosophila peanut gene is required for cytokinesis and encodes a protein similar to yeast putative bud neck filament proteins. *Cell*. 77:371-379.
Ng, M.M., F. Chang, and D.R. Burgess. 2005. Movement of membrane domains and requirement of membrane signaling molecules for cytokinesis. *Dev Cell*. 9:781-790.
Nguyen, T.Q., H. Sawa, H. Okano, and J.G. White. 2000. The C. elegans septin genes, unc-59 and unc-61, are required for normal postembryonic cytokineses and morphogenesis but have no essential function in embryogenesis. *J Cell Sci*. 113 Pt 21:3825-3837.
Oegema, K., and T.J. Mitchison. 1997. Rappaport rules: cleavage furrow induction in animal cells. *Proc Natl Acad Sci U S A*. 94:4817-4820.
Oegema, K., M.S. Savoian, T.J. Mitchison, and C.M. Field. 2000. Functional analysis of a human homologue of the Drosophila actin binding protein anillin suggests a role in cytokinesis. *J Cell Biol*. 150:539-552.
Olakowski, M., T. Tyszkiewicz, M. Jarzab, R. Krol, M. Oczko-Wojciechowska, M. Kowalska, M. Kowal, G.M. Gala, M. Kajor, D. Lange, E. Chmielik, E. Gubala, P. Lampe, and B. Jarzab. 2009. NBL1 and anillin (ANLN) genes over-expression in pancreatic carcinoma. *Folia Histochem Cytobiol*. 47:249-255.
Ou, G., C. Gentili, and P. Gonczy. 2014. Stereotyped distribution of midbody remnants in early C. elegans embryos requires cell death genes and is dispensable for development. *Cell Res*. 24:251-253.
Paoletti, A., and F. Chang. 2000. Analysis of mid1p, a protein required for placement of the cell division site, reveals a link between the nucleus and the cell surface in fission yeast. *Mol Biol Cell*. 11:2757-2773.
Paolini, A., A.L. Duchemin, S. Albadri, E. Patzel, D. Bornhorst, P. Gonzalez Avalos, S. Lemke, A. Machate, M. Brand, S. Sel, V. Di Donato, F. Del Bene, F.R. Zolessi, M. Ramialison, and L. Poggi. 2015. Asymmetric inheritance of the apical domain and self-renewal of retinal ganglion cell progenitors depend on Anillin function. *Development*. 142:832-839.
Pavicic-Kaltenbrunner, V., M. Mishima, and M. Glotzer. 2007. Cooperative assembly of CYK-4/MgcRacGAP and ZEN-4/MKLP1 to form the centralspindlin complex. *Mol Biol Cell*. 18:4992-5003.
Petronczki, M., M. Glotzer, N. Kraut, and J.-M. Peters. 2007. Polo-like Kinase 1 Triggers the

Initiation of Cytokinesis in Human Cells by Promoting Recruitment of the RhoGEF Ect2 to the Central Spindle. *Developmental Cell*. 12:713-725.
Piekny, A.J., and M. Glotzer. 2007. Anillin is a scaffold protein that links RhoA, actin, and myosin during cytokinesis. *Current biology : CB*. 18:30-36.
Piekny, A.J., and M. Glotzer. 2008. Anillin is a scaffold protein that links RhoA, actin, and myosin during cytokinesis. *Curr Biol*. 18:30-36.
Piekny, A.J., and A. Maddox. 2010. The myriad roles of Anillin during cytokinesis. *Seminars in Cell & Developmental Biology*. 21:881-891.
Pohl, C., and S. Jentsch. 2009. Midbody ring disposal by autophagy is a post-abscission event of cytokinesis. *Nat Cell Biol*. 11:65-70.
Pruyne, D., M. Evangelista, C. Yang, E. Bi, S. Zigmond, A. Bretscher, and C. Boone. 2002. Role of formins in actin assembly: nucleation and barbed-end association. *Science*. 297:612-615.
Rappaport, R., and R.P. Ebstein. 1965. Duration of Stimulus and Latent Periods Preceding Furrow Formation in Sand Dollar Eggs. *J Exp Zool*. 158:373-382.
Renshaw, M.J., J. Liu, B.D. Lavoie, and A. Wilde. 2014. Anillin-dependent organization of septin filaments promotes intercellular bridge elongation and Chmp4B targeting to the abscission site. *Open Biol*. 4:130190.
Reyes, C.C., M. Jin, E.B. Breznau, R. Espino, R. Delgado-Gonzalo, A.B. Goryachev, and A.L. Miller. 2014. Anillin regulates cell-cell junction integrity by organizing junctional accumulation of Rho-GTP and actomyosin. *Curr Biol*. 24:1263-1270.
Salzmann, V., C. Chen, C.Y. Chiang, A. Tiyaboonchai, M. Mayer, and Y.M. Yamashita. 2014. Centrosome-dependent asymmetric inheritance of the midbody ring in Drosophila germline stem cell division. *Mol Biol Cell*. 25:267-275.
Saul, D., L. Fabian, A. Forer, and J.A. Brill. 2004. Continuous phosphatidylinositol metabolism is required for cleavage of crane fly spermatocytes. *J Cell Sci*. 117:3887-3896.
Schiel, J.A., and R. Prekeris. 2012. Membrane dynamics during cytokinesis. *Current Opinion in Cell Biology*. 25:92-98.
Schupbach, T., and E. Wieschaus. 1989. Female sterile mutations on the second chromosome of Drosophila melanogaster. I. Maternal effect mutations. *Genetics*. 121:101-117.
Severson, A.F., D.L. Baillie, and B. Bowerman. 2002. A Formin Homology protein and a profilin are required for cytokinesis and Arp2/3-independent assembly of cortical microfilaments in C. elegans. *Curr Biol*. 12:2066-2075.
Shaheen, R., A. Hashem, G.M. Abdel-Salam, F. Al-Fadhli, N. Ewida, and F.S. Alkuraya. 2016. Mutations in CIT, encoding citron rho-interacting serine/threonine kinase, cause severe primary microcephaly in humans. *Hum Genet*. 135:1191-1197.
Shandala, T., S.L. Gregory, H.E. Dalton, M. Smallhorn, and R. Saint. 2004. Citron Kinase is an essential effector of the Pbl-activated Rho signalling pathway in Drosophila melanogaster. *Development*. 131:5053-5063.
Silverman-Gavrila, R.V., K.G. Hales, and A. Wilde. 2008. Anillin-mediated targeting of peanut to pseudocleavage furrows is regulated by the GTPase Ran. *Mol Biol Cell*. 19:3735-3744.
Skop, A.R., D. Bergmann, W.A. Mohler, and J.G. White. 2001. Completion of cytokinesis in C. elegans requires a brefeldin A-sensitive membrane accumulation at the cleavage furrow apex. *Curr Biol*. 11:735-746.
Skop, A.R., H. Liu, J. Yates, 3rd, B.J. Meyer, and R. Heald. 2004. Dissection of the mammalian midbody proteome reveals conserved cytokinesis mechanisms. *Science*. 305:61-66.
Somers, W.G., and R. Saint. 2003. A RhoGEF and Rho family GTPase-activating protein complex links the contractile ring to cortical microtubules at the onset of cytokinesis. *Dev Cell*. 4:29-39.
Stock, A., M.O. Steinmetz, P.A. Janmey, U. Aebi, G. Gerisch, R.A. Kammerer, I. Weber, and J. Faix.

1999. Domain analysis of cortexillin I: actin-bundling, PIP(2)-binding and the rescue of cytokinesis. *EMBO J*. 18:5274-5284.

Straight, A.F., C.M. Field, and T.J. Mitchison. 2005. Anillin Binds Nonmuscle Myosin II and Regulates the Contractile Ring. *Molecular Biology of the Cell*. 16:193-201.

Su, K.-C., T. Takaki, and M. Petronczki. 2011. Targeting of the RhoGEF Ect2 to the Equatorial Membrane Controls Cleavage Furrow Formation during Cytokinesis. *Developmental Cell*. 21:1104-1115.

Sun, L., R. Guan, I.J. Lee, Y. Liu, M. Chen, J. Wang, J.Q. Wu, and Z. Chen. 2015. Mechanistic insights into the anchorage of the contractile ring by anillin and Mid1. *Dev Cell*. 33:413-426.

Takiguchi, K., A. Yamada, M. Negishi, M. Honda, Y. Tanaka-Takiguchi, and K. Yoshikawa. 2009. Chapter 3 - Construction of cell-sized liposomes encapsulating actin and actin-cross-linking proteins. *Methods Enzymol*. 464:31-53.

Tasto, J.J., J.L. Morrell, and K.L. Gould. 2003. An anillin homologue, Mid2p, acts during fission yeast cytokinesis to organize the septin ring and promote cell separation. *J Cell Biol*. 160:1093-1103.

Telentschak, S., M. Soliwoda, K. Nohroudi, K. Addicks, and F.J. Klinz. 2015. Cytokinesis failure and successful multipolar mitoses drive aneuploidy in glioblastoma cells. *Oncol Rep*. 33:2001-2008.

Thompson, S.L., S.F. Bakhoum, and D.A. Compton. 2010. Mechanisms of chromosomal instability. *Curr Biol*. 20:R285-295.

Tian, D., M. Diao, Y. Jiang, L. Sun, Y. Zhang, Z. Chen, S. Huang, and G. Ou. 2015. Anillin Regulates Neuronal Migration and Neurite Growth by Linking RhoG to the Actin Cytoskeleton. *Curr Biol*. 25:1135-1145.

Tormos, A.M., R. Taléns-Visconti, and J. Sastre. 2015. Regulation of cytokinesis and its clinical significance. *Critical Reviews in Clinical Laboratory Sciences*. 52:159-167.

Toure, A., O. Dorseuil, L. Morin, P. Timmons, B. Jegou, L. Reibel, and G. Gacon. 1998. MgcRacGAP, a new human GTPase-activating protein for Rac and Cdc42 similar to Drosophila rotundRacGAP gene product, is expressed in male germ cells. *J Biol Chem*. 273:6019-6023.

Tse, Y., M. Werner, K.M. Longhini, J.-C. Labbe, B. Goldstein, and M. Glotzer. 2012. RhoA activation during polarization and cytokinesis of the early Caenorhabditis elegans embryo is differentially dependent on NOP-1 and CYK-4. *Molecular Biology of the Cell*. 23:4020-4031.

Tse, Y.C., A. Piekny, and M. Glotzer. 2011. Anillin promotes astral microtubule-directed cortical myosin polarization. *Mol Biol Cell*. 22:3165-3175.

Uehara, R., and G. Goshima. 2009. [Mitotic spindle formation mediated by augmin protein complex]. *Tanpakushitsu Kakusan Koso*. 54:1850-1855.

Uehara, R., G. Goshima, I. Mabuchi, R.D. Vale, J.A. Spudich, and E.R. Griffis. 2010. Determinants of myosin II cortical localization during cytokinesis. *Current biology : CB*. 20:1080-1085.

Uehara, R., R.S. Nozawa, A. Tomioka, S. Petry, R.D. Vale, C. Obuse, and G. Goshima. 2009. The augmin complex plays a critical role in spindle microtubule generation for mitotic progression and cytokinesis in human cells. *Proc Natl Acad Sci U S A*. 106:6998-7003.

van Oostende Triplet, C., M. Jaramillo Garcia, H. Haji Bik, D. Beaudet, and A. Piekny. 2014. Anillin interacts with microtubules and is part of the astral pathway that defines cortical domains. *J Cell Sci*. 127:3699-3710.

Verbrugghe, K.J., and J.G. White. 2004. SPD-1 is required for the formation of the spindle midzone but is not essential for the completion of cytokinesis in C. elegans embryos. *Curr Biol*. 14:1755-1760.

Versele, M., and J. Thorner. 2004. Septin collar formation in budding yeast requires GTP binding

and direct phosphorylation by the PAK, Cla4. *J Cell Biol*. 164:701-715.
von Dassow, G. 2009. Concurrent cues for cytokinetic furrow induction in animal cells. *Trends in Cell Biology*. 19:165-173.
Wagner, E., and M. Glotzer. 2016. Local RhoA activation induces cytokinetic furrows independent of spindle position and cell cycle stage. *The Journal of Cell Biology*. 213:641-649.
Wang, D., G.K. Chadha, A. Feygin, and A.I. Ivanov. 2015. F-actin binding protein, anillin, regulates integrity of intercellular junctions in human epithelial cells. *Cell Mol Life Sci*. 72:3185-3200.
Watanabe, S., T. De Zan, T. Ishizaki, and S. Narumiya. 2013. Citron kinase mediates transition from constriction to abscission through its coiled-coil domain. *J Cell Sci*. 126:1773-1784.
Watanabe, S., K. Okawa, T. Miki, S. Sakamoto, T. Morinaga, K. Segawa, T. Arakawa, M. Kinoshita, T. Ishizaki, and S. Narumiya. 2010. Rho and anillin-dependent control of mDia2 localization and function in cytokinesis. *Mol Biol Cell*. 21:3193-3204.
Werner, M., E. Munro, and M. Glotzer. 2007. Astral signals spatially bias cortical myosin recruitment to break symmetry and promote cytokinesis. *Curr Biol*. 17:1286-1297.
White, E.A., and M. Glotzer. 2012. Centralspindlin: At the heart of cytokinesis. *Cytoskeleton*. 69:882-892.
Wolfe, B.A., T. Takaki, M. Petronczki, and M. Glotzer. 2009. Polo-Like Kinase 1 Directs Assembly of the HsCyk-4 RhoGAP/Ect2 RhoGEF Complex to Initiate Cleavage Furrow Formation. *PLoS Biology*. 7.
Wong, R., I. Hadjiyanni, H.C. Wei, G. Polevoy, R. McBride, K.P. Sem, and J.A. Brill. 2005. PIP2 hydrolysis and calcium release are required for cytokinesis in Drosophila spermatocytes. *Curr Biol*. 15:1401-1406.
Wunderlich, V. 2002. JMM---past and present. Chromosomes and cancer: Theodor Boveri's predictions 100 years later. *J Mol Med (Berl)*. 80:545-548.
Yamada, T., M. Hikida, and T. Kurosaki. 2006. Regulation of cytokinesis by mgcRacGAP in B lymphocytes is independent of GAP activity. *Exp Cell Res*. 312:3517-3525.
Yamakita, Y., S. Yamashiro, and F. Matsumura. 1994. In vivo phosphorylation of regulatory light chain of myosin II during mitosis of cultured cells. *J Cell Biol*. 124:129-137.
Yamashiro, S., G. Totsukawa, Y. Yamakita, Y. Sasaki, P. Madaule, T. Ishizaki, S. Narumiya, and F. Matsumura. 2003. Citron kinase, a Rho-dependent kinase, induces di-phosphorylation of regulatory light chain of myosin II. *Mol Biol Cell*. 14:1745-1756.
Yuce, O., A. Piekny, and M. Glotzer. 2005. An ECT2-centralspindlin complex regulates the localization and function of RhoA. *J Cell Biol*. 170:571-582.
Zavortink, M., N. Contreras, T. Addy, A. Bejsovec, and R. Saint. 2005. Tum/RacGAP50C provides a critical link between anaphase microtubules and the assembly of the contractile ring in Drosophila melanogaster. *J Cell Sci*. 118:5381-5392.
Zhang, D., and M. Glotzer. 2015. The RhoGAP activity of CYK-4/MgcRacGAP functions non-canonically by promoting RhoA activation during cytokinesis. *Elife*. 4.
Zhang, J., C. Kong, H. Xie, P.S. McPherson, S. Grinstein, and W.S. Trimble. 1999. Phosphatidylinositol polyphosphate binding to the mammalian septin H5 is modulated by GTP. *Curr Biol*. 9:1458-1467.
Zhang, L., and A.S. Maddox. 2010. Anillin. *Curr Biol*. 20:R135-136.
Zhao, W.-m., and G. Fang. 2005. Anillin Is a Substrate of Anaphase-promoting Complex/Cyclosome (APC/C) That Controls Spatial Contractility of Myosin during Late Cytokinesis. *Journal of Biological Chemistry*. 280:33516-33524.
Zhu, C., and W. Jiang. 2005. Cell cycle-dependent translocation of PRC1 on the spindle by Kif4 is essential for midzone formation and cytokinesis. *Proceedings of the National Academy of Sciences of the United States of America*. 102:343-348.

Zhuravlev, Y., S.M. Hirsch, S.N. Jordan, J. Dumont, M. Shirasu-Hiza, and J.C. Canman. 2017. CYK-4 regulates Rac, but not Rho, during cytokinesis. *Mol Biol Cell*. 28:1258-1270.